Identification of novel N-MYC interacting proteins reveals N-MYC interaction with TFIIIC

Identifizierung von neuen N-MYC interagierenden Proteinen offenbart N-MYC´s Interaktion mit TFIIIC

Doctoral thesis

for a doctoral degree
at the Graduate School of Life Sciences,
Julius-Maximilians-Universität Würzburg,
Section Biomedicine

submitted by

Anne Carola Carstensen

from Henstedt-Ulzburg

Würzburg 2016

Submitted on:

Members of the Thesis Committee

Chairperson: Prof. Manfred Gessler

Primary Supervisor: Prof. Martin Eilers
Second Supervisor: Prof. Hermann Schindelin
Third Supervisor: Prof. Alexander Buchberger

PhD Submitted on:

Date of Public Defence:

Date of Receipt of Certificates:

Contents

Summary

N-MYC is a member of the human MYC proto-oncogene family, which comprises three transcription factors (C-, N- and L-MYC) that function in multiple biological processes. Deregulated expression of MYC proteins is linked to tumour initiation, maintenance and progression. For example, a large fraction of neuroblastoma displays high N-MYC levels due to an amplification of the N-MYC encoding gene. *MYCN*-amplified neuroblastoma depend on high N-MYC protein levels, which are maintained by Aurora-A kinase. Aurora-A interaction with N-MYC interferes with degradation of N-MYC via the E3 ubiquitin ligase SCF$^{\text{FBXW7}}$. However, the underlying mechanism of Aurora-A-mediated stabilisation of N-MYC remains to be elucidated.

To identify novel N-MYC interacting proteins, which could be involved in N-MYC stabilisation by Aurora-A, a proteomic analysis of purified N-MYC protein complexes was conducted. Since two alanine mutations in MBI of N-MYC, T58A and S62A (N-MYC mut), disable Aurora-A-mediated stabilisation of N-MYC, N-MYC protein complexes from cells expressing either N-MYC wt or mut were analysed. Proteomic analysis revealed that N-MYC interacts with two deubiquitinating enzymes, USP7 and USP11, which catalyse the removal of ubiquitin chains from target proteins, preventing recognition by the proteasome and subsequent degradation. Although N-MYC interaction with USP7 and USP11 was confirmed in subsequent immunoprecipitation experiments, neither USP7, nor USP11 was shown to be involved in the regulation of N-MYC stability. Besides USP7/11, proteomic analyses identified numerous additional N-MYC interacting proteins that were not described to interact with MYC transcription factors previously. Interestingly, many of the identified N-MYC interaction partners displayed a preference for the interaction with N-MYC wt, suggesting a MBI-dependent interaction. Among these were several proteins, which are involved in three-dimensional organisation of chromatin domains and transcriptional elongation by POL II. Not only the interaction of N-MYC with proteins functioning in elongation, such as the DSIF component SPT5 and the PAF1C components CDC73 and CTR9, was validated in immunoprecipitation experiments, but also with the POL III transcription factor TFIIIC and topoisomerases TOP2A/B. ChIP-sequencing analysis of N-MYC and TFIIIC subunit 5 (TFIIIC5) revealed a large number of joint binding sites in POL II promoters and intergenic regions, which are characterised by the presence of a specific motif that is highly similar to the CTCF motif. Additionally, N-MYC was shown to interact with the ring-shaped cohesin complex that is known to bind to CTCF motifs and to assist the insulator protein CTCF. Importantly, individual ChIP experiments demonstrated that N-MYC, TFIIIC5 and cohesin subunit RAD21 occupy joint binding sites comprising a CTCF motif.

Collectively, the results indicate that N-MYC functions in two biological processes that have not been linked to MYC biology previously. Furthermore, the identification of joint binding sites of N-MYC, TFIIIC and cohesin and the confirmation of their interaction with each other suggests a novel function of MYC transcription factors in three-dimensional organisation of chromatin.

Zusammenfassung

N-MYC ist ein Mitglied der humanen MYC proto-Onkogen Familie, welche drei Transkriptionsfaktoren umfasst (C-,N- und L-MYC), die in zahlreichen biologischen Prozessen fungieren. Deregulierte Expression der MYC Proteine ist mit Tumorinitiierung, -erhalt und -progression verbunden. Zum Beispiel zeigt ein großer Anteil an Neuroblastomen aufgrund einer Amplifizierung des N-MYC kodierenden Gens hohe N-MYC Level. *MYCN*-amplifizierte Neuroblastome hängen von den hohen N-MYC Protein Leveln ab, die durch die Aurora-A Kinase erhalten werden. Die Interaktion von Aurora-A mit N-MYC behindert den Abbau von N-MYC durch die E3 Ubiquitin Ligase SCF^{FBXW7}. Allerdings muss der zugrunde liegende Mechanismus der Aurora-A vermittelten Stabilisierung von N-MYC noch aufgedeckt werden.

Um neue N-MYC interagierende Proteine zu identifizieren, welche in der N-MYC Stabilisierung durch Aurora-A involviert sind, wurde eine Proteom Analyse der aufgereinigten N-MYC Proteinkomplexe durchgeführt. Da zwei Alanin-Mutationen in MBI von N-MYC, T58A und S62A (N-MYC mut), die Aurora-A vermittelte Stabilisierung von N-MYC verhindern, wurden N-MYC Protein-Komplexe von Zellen, die entweder N-MYC wt oder mut exprimieren analysiert. Die Proteom Analyse offenbarte, dass N-MYC mit zwei Deubiquitinierenden Enzymen, USP7 und USP11, interagiert, welche das Entfernen von Ubiquitinketten von Zielproteinen katalysieren und dadurch die Erkennung durch das Proteasom und den darauf folgenden Abbau verhindern. Obwohl die Interaktion von N-MYC mit USP7 und USP11 in darauf folgenden Immunpräzipitationsexperimenten bestätigt wurde, konnnte weder für USP7, noch für USP11 gezeigt werden, dass es in die Regulierung der Stabilität von N-MYC involviert ist. Neben USP7/11 wurden in der Proteom Analyse zusätzlich zahlreiche mit N-MYC interagierende Proteine identifiziert, die zuvor noch nicht beschrieben wurden mit MYC Transkriptionsfaktoren zu interagieren. Interessanterweise zeigten viele der identifizierten N-MYC Interaktionspartner eine Präferenz für die Interaktion mit N-MYC wt, was eine MBI-abhängige Interaktion suggeriert. Unter diesen waren einige Proteine, die in die drei-dimensionale Organisation von Chromatindomänen und transkriptioneller Elongation durch POL II involviert sind. Nicht nur die Interaktion von N-MYC mit Proteinen, die in der Elongation agieren, wie die DSIF Komponente SPT5 und die PAF1C Komponenten CDC73 und CTR9, wurden in Immunpräzipitationsexperimenten bestätigt, sondern auch mit dem POL III Transkriptionsfaktor TFIIIC und den Topoisomerasen TOP2A/B. Analyse von ChIP-Sequenzierungsexperimenten für N-MYC und TFIIIC Untereinheit 5 (TFIIIC5) offenbarte eine große Anzahl von gemeinsamen Bindungsstellen in POL II Promotoren und intergenen Regionen, welche durch das Vorkommen eines speziellen Motivs gekennzeichent waren, das dem CTCF Motiv sehr ähnlich ist. Zusätzlich wurde gezeigt, dass N-MYC mit dem ringförmigen Cohesin Komplex interagiert, der dafür bekannt ist an CTCF Motive zu binden und dem Insulator Protein CTCF zu assistieren. Entscheidender Weise zeigten individuelle ChIP Experimente, dass N-MYC, TFIIIC5 und die Cohesin Untereinheit RAD21 gemeinsame Bindungstellen haben, die ein CTCF Motiv enthalten.

Zusammenfassend weisen die Ergebnisse darauf hin, dass N-MYC in zwei biologischen Prozessen fungiert, die zuvor nicht mit der Biologie von MYC verbunden wurden. Zudem suggeriert die Identifizierung von gemeinsamen Bindungstellen von N-MYC, TFIIIC und Cohesin und die Bestätigung der Interaktion untereinander eine neue Funktion von MYC Transkriptionsfaktoren in der drei-dimensionalen Organisation von Chromatin.

1   Introduction

1.1   The MYC protein family

The MYC proto-oncogene family is one of the most studied protein families in tumour biology. The name of the protein family originates from the discovery of the retroviral *v-Myc* gene, which was identified to cause myelocytomatosis in chickens [Sheiness et al., 1978]. The cellular homologue of *v-Myc*, *c-Myc*, was discovered shortly afterwards and it was found to be expressed in all vertebrates, *Drosophila melanogaster* and the *Northern sea star Asterias vulgaris* [Vennstrom et al., 1982, Gallant et al., 1996, Walker et al., 1992]. In human, three proteins belong to the family of MYC proteins, besides the human C-MYC protein two additional homologues were described: N-MYC was identified in human neuroblastoma cell lines and tumours and L-MYC in human small cell lung cancer (SCLC) [Schwab et al., 1983, Kohl et al., 1983, Nau et al., 1985]. The discovery of C-MYC homologues in different kinds of tumours highlights the strong association of *MYC* expression and tumourigenesis. *MYC* is a *bona fide* oncogene and various mechanisms can induce high MYC protein levels, which play a role in tumour initiation and progression across many human cancer types [Dang, 2012] (Fig. 1.2). High expression levels of the three different human homologues are specific for certain tumours. C-MYC is one of the most highly amplified oncogenes among numerous tumour entities [Beroukhim et al., 2010]. One example are Burkitt lymphoma, which consistently display a balanced translocation of the C-MYC encoding gene to one of the immunoglobulin enhancer loci leading to elevated C-MYC expression levels [Taub et al., 1982]. Also for N-MYC there are several cancer types known to carry an amplification of the N-MYC encoding gene, *MYCN*, such as subgroups of neuroendocrine prostate cancers (NEPCs) and neuroblastoma [Beltran et al., 2011, Schwab et al., 1983, Kohl et al., 1983]. The L-MYC encoding gene is mainly known for its amplification and expression in SCLC [Nau et al., 1985]. Besides gene amplification there are several other mechanisms, which induce overexpression of MYC proteins, for example deregulation of the phosphoinositide-3-kinase (PI3K) and sonic hedgehog (SHH) signaling pathway (see introduction, section 1.4).

One reason why different MYC homologues are drivers for certain kinds of tumours is presumably that the originating tissues display differences in MYC expression. While C-, N-, and L-MYC are highly similar in regard of protein structure and function (Fig. 1.1 and see introduction, section 1.2), they differ in their expression pattern. Whereas C-MYC is ubiquitously expressed, N-MYC is only essential in embryogenesis, within which it is highly expressed in the central nervous system (CNS) and the renal glands [Zimmerman et al., 1986]. After birth N-MYC is redundant with C-MYC and high expression levels are restricted to stem cells and some tumour entities [Huang and Weiss, 2013]. L-MYC expression occurs in the developing kidney and lung, as well as in some parts of the brain and neural tube, but was shown to be dispensable for embryonic development [Hatton et al., 1996].
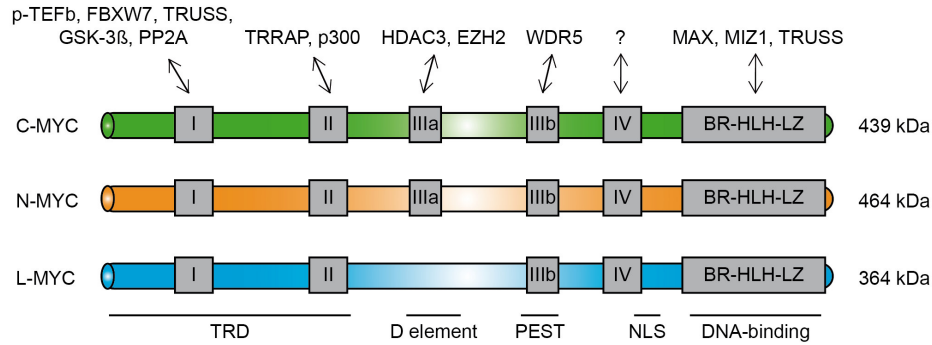
Figure 1.1
Protein structure and interacting proteins of the human MYC protein family
Schematic representation of the human MYC proteins. All MYC proteins comprise highly conserved domains, named MYC-boxes (MB), which are shown here as grey rectangles and numbered with the Latin numbers I-IV. Examples of proteins known to interact with a certain MB are indicated on top. Localisation of functional elements is indicated on the bottom. The transregulatory domain (TRD) is located in the N-terminus, the PEST sequence and D element are in the central part, followed by a nuclear localisation signal (NLS), and the C-terminal basic region helix-loop-helix leucine zipper domain (BR-HLH-LZ), which mediates DNA-binding.

MYC proteins are transcription factors and share a well conserved protein structure among all species [Conacci-Sorrell, McFerrin, and Eisenman, 2014]. All MYC proteins comprise highly conserved sequences, which are called MYC-boxes (MB) and are numbered consecutively in Latin starting in the N-terminus (Fig. 1.1). Human MYC proteins have 4 MBs and MBIII is divided in two parts, MBIIIa and MBIIIb. While C-MYC and N-MYC share all MB sequences, L-MYC lacks MBIIIa (Fig. 1.1). MYC transcription factors exert their function via protein-protein interactions, which mostly occur via the MBs, whereas DNA-binding is mediated via the basic region helix-loop-helix-leucine zipper (BR-HLH-LZ) domain in the C-terminus (Fig. 1.1). The transregulatory domain (TRD) in the N-terminus of MYC proteins mediates transcriptional activation and repression via interaction with different kinds of proteins [Kato et al., 1990, Lee et al., 1996] (see introduction, section 1.3). The central part comprises a D element and a PEST sequence, which are both important for MYC degradation (see introduction, section 1.4). Downstream of MBVI is a canonical lysine-rich nuclear localisation signal (NLS), which ensures nuclear localisation of MYC proteins, a prerequisite for transcription factor function [Dang and Lee, 1988].

1.2   Biological functions of MYC proteins

Since MYC proteins are not able to bind to DNA as a monomer or homodimer, MYC´s function as a transcription factor depends on its dimerisation with MAX proteins via the HLH-LZ motif [Blackwood and Eisenman, 1991] (Fig. 1.1). The MYC/MAX heterodimer was shown to activate a large number of target genes, which are involved a broad range of biological functions, such as proliferation, metabolism and cell cycle regulation [Eilers and Eisenman, 2008]. More recently, it was proposed that MYC functions as a "general amplifier" of transcription that globally enhances transcription instead of inducing specific cellular processes [Lin et al., 2012, Nie et al., 2012]. Besides its function in transcriptional

activation, MYC can also function as a repressor of transcription. Repression of MYC target genes is mostly mediated by antagonism of other activating transcription factors, such as SP1/SP3 and MIZ1 [Gartel et al., 2001, Staller et al., 2001]. Interestingly, some MYC effects were shown to be independent of MAX-mediated DNA-binding and were not linked to its transcriptional activity [Cole and Cowling, 2008, Dominguez-Sola et al., 2007, Steiger et al., 2008].

MYC/MAX dimers bind to E-box elements within the DNA, which comprise either the palindromic canonical sequence "CACGTG" or a so-called non-canonical E-box sequence "CANNTG" (where N can be any nucleotide) [Blackwell et al., 1993]. More recent publications utilising high-throughput screening methods to study MYC binding to DNA have revealed that MYC occupies many regions, which lack canonical and non-canonical E-box sequences, but were shown to be enriched for histone marks of open chromatin (H3K4me^3, H3K27ac) and to coincidence with RNA polymerase (POL) II binding and binding of proteins involved in transcription [Guccione et al., 2006, Guo et al., 2014, Zeller et al., 2003]. Interestingly, high MYC expression levels change MYC´s behaviour in regard of binding to DNA: sequence-specificity gets less important and the number of MYC binding sites increases until almost all accessible genomic regions are occupied ("invasion") [Fernandez et al., 2003, Lin et al., 2012, Nie et al., 2012]. However, MYC binding does not necessarily directly translate into specific cellular responses, instead effects of MYC target genes are further modulated by cell type- and context-specific interactions [Sabo et al., 2014, Walz et al., 2014]. Importantly, MYC/MAX dimers are also able to regulate target gene transcription indirectly, via protein-protein interactions with other transcription factors, as it was shown for repression of MIZ1 and SP1/SP3 activated target genes [Gartel et al., 2001, Staller et al., 2001]. Furthermore, a recent publication identified MYC´s interaction with WDR5 via MBIIIb as an important determinant for MYC target gene recognition [Thomas et al., 2015] (Fig. 1.1).

Despite a lot of effort, high-throughput sequencing methods have not yet revealed a complete picture of common MYC target genes that are the same across different mammalian cell types. A large sequencing study aiming to identify cell type-independent core MYC target gene signatures identified one core target gene set of MYC, which is shared among murine and human embryonic stem cells (ESCs) and 4 human cancer cell types. This core MYC target gene set comprises genes encoding for proteins involved in ribosome biogenesis, RNA processing and biomass accumulation [Ji et al., 2011]. MYC´s role in the ribosome biogenesis and function is conserved between different species. In *Drosophila melanogaster* it was shown that diminished dMyc function and mutations affecting ribosomal proteins genes induce the same phenotype, resulting in smaller cells and body size [Johnston et al., 1999]. Since there is only one MYC homologue in *Drosophila melanogaster*, it makes it easier to evaluate functional studies on MYC in this model organism. Concluding from these studies conserved MYC functions encompass regulation of cell growth, proliferation and differentiation [Gallant, 2013]. However, the complete set of MYC target genes that are not

cell type-specific remains to be determined. What is clear is that MYC functions are the key to the oncogenic potential of MYC proteins. High (oncogenic) MYC levels play an important role in tumour development and progression. Key tumour-relevant functions include MYC-mediated induction of cell cycle progression and growth, regulation of metabolism in order to induce faster energy supply, as well as inhibition of apoptosis induction and promotion of angiogenesis and metastasis (Fig. 1.2). Furthermore, MYC induces mutations and genome instability by disconnecting the cell cycle from growth factor stimuli, leading to an override of cell cycle checkpoints and a shortening of G1 and G2 phase of the cell cycle [Tansey, 2014]. All of these functions of MYC can initiate tumour development and induce fast and unrestricted tumour growth. But the identical MYC functions are also important for normal development, which requires tight regulation in order to keep the balance between physiological and oncogenic MYC levels.
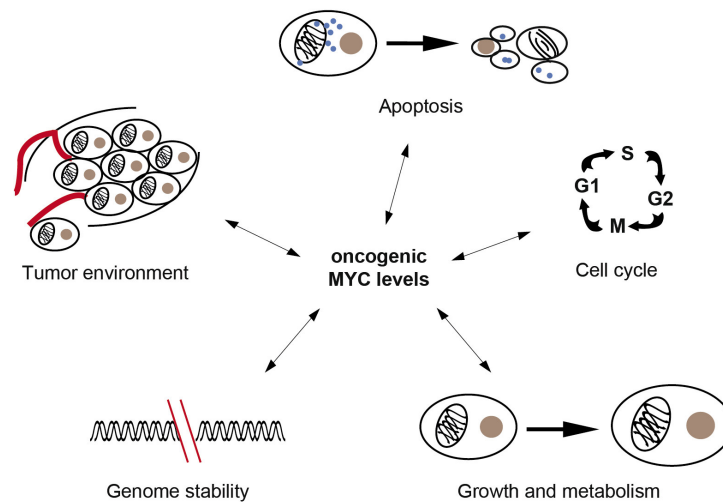
Figure 1.2
Key tumour-relevant functions of MYC proteins
Scheme illustrating 5 of the most tumour-relevant processes that are influenced by high MYC levels. Adapted from Tansey [2014].

MYC functions are essential in murine development, since C- and N-MYC knockout (k.o.) mice are not viable and die early during embryogenesis (*MYC* k.o.: E9,5-10,5; *MYCN* k.o.: E10,5-11,5) [Charron et al., 1992, Davis et al., 1993]. Strikingly, reconstitution of the N-MYC encoding gene into the *MYC* locus of C-MYC k.o. mice demonstrated that N-MYC is able to substitute nearly all C-MYC functions [Malynn et al., 2000]. This shows that C- and N-MYC functions are highly similar, although there are temporal and spatial differences in expression, which could account for embryonic lethality upon k.o. of one of the two genes (see introduction, section 1.1). Importantly, k.o. of both, *MYC* and *MYCN*, was demonstrated to completely abolish embryonic development. Murine ESCs depleted of C- and N-MYC encoding genes exhibited severely disrupted self-renewal, pluripotency and

survival and displayed enhanced differentiation, showing that C- and N-MYC expression is essential for mESC pluripotency and self-renewal [Varlakhanova et al., 2010]. In agreement with their important role in maintenance of pluripotency, C- and N-MYC are among the factors, which are needed in order to reprogram fibroblasts into induced pluripotent stem (iPS) cells [Nakagawa and Yamanaka, 2010].

1.3 Mechanisms of transcriptional regulation by MYC

Transcription of nuclear and nucleolar human genes is mediated via three different types of RNA polymerases (POL I-III), while transcription of mitochondrial DNA occurs by a specialised RNA polymerase. Genomic sequences encoding for ribosomal RNA (rRNA) are localised in the nucleolus and transcribed by POL I, except for 5S rRNA, which is transcribed by POL III [Grummt, 1999, Russell and Zomerdijk, 2006]. Apart from 5S rRNA, POL III transcribes transfer RNAs (tRNAs) and other small RNAs, including short interspersed repetitive elements (SINEs) and U6 small nucleolar RNAs (snoRNAs) [Dieci et al., 2013]. Transcription of protein encoding messenger RNAs (mRNAs) and most micro RNAs (miRNAs) and snoRNAs is mediated by POL II. MYC´s function as a transcription factor is not restricted to one polymerase, but plays a role for transcription by all three POLs [Dang, 2012].

1.3.1 Regulation of transcription by POL II

The function of MYC proteins in transcription is best studied for POL II-mediated transcription. In mammalian cells, the mechanisms of MYC-mediated transcriptional activation and repression of POL II target genes are best studied for C-MYC and will be described in the following, but most findings were reproduced for N-MYC.

C-MYC-mediated activation of transcription

Activation of transcription by C-MYC involves several steps of transcriptional regulation. In a first step, MYC/MAX dimers bind to promotor-close DNA elements, for example E-boxes, recognising target genes by the existence of open chromatin marks (H3K4me^3) or other determinants, such as WDR5 binding [Guccione et al., 2006, Thomas et al., 2015] (Fig. 1.3). Subsequently, C-MYC mediates recruitment of chromatin remodeling complexes, which enhance opening of the chromatin structure, mainly by acetylation of histones. Known histone acetyltransferases (HATs) recruited by C-MYC are for example TIP60 and GCN5 [Frank et al., 2003, McMahon et al., 2000] (Fig. 1.3). Recruited HATs are a part of large cofactor complexes that comprise adaptor proteins, such as the MBII-interacting multidomain protein TRRAP and ATPases, like p400, which induce nucleosome remodeling and assist HATs in their function [Fuchs et al., 2001, McMahon et al., 1998, Martinato et al., 2008] (Fig. 1.1, 1.3).
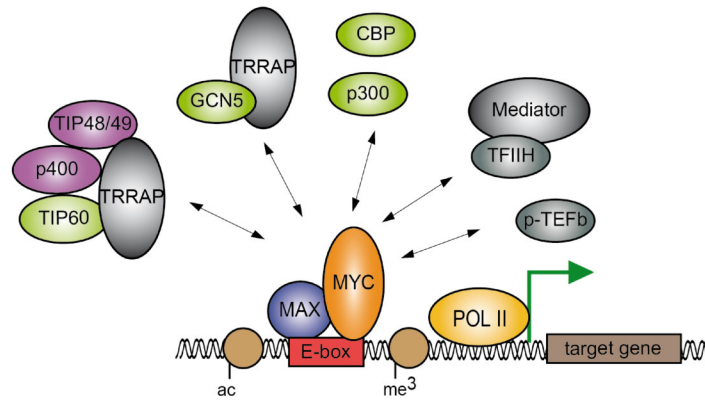
Figure 1.3
C-MYC-mediated activation of transcription
Scheme illustrating mechanisms of transcriptional activation by MYC proteins. C-MYC binds as a heterodimer with MAX to DNA elements, for example E-boxes, within open promoters of its target genes that are characterised by trimethylated (me^3) histones (brown circles). Bound MYC/MAX dimers recruit co-activator complexes comprising histone acetyltransferases (HATs) and ATPases, which induce histone acetylation (ac) and remodeling of the chromatin structure. Additionally, C-MYC induces recruitment of POL II and the two multi-protein complexes TFIIH and p-TEFb. Examples of recruited HATs are shown in green and examples of ATPases in purple.

An open chromatin structure with highly acetylated histones enables recruitment of POL II and binding of general transcription factors (GTFs). Formation of this pre-initiation complex is the first step in POL II transcription and it is followed by initiation of transcription, promoter clearance, transcriptional elongation and subsequent termination of transcription [Shandilya and Roberts, 2012, Weake and Workman, 2010]. Importantly, C-MYC can stimulate POL II binding to promoters and recruits the Mediator/TFIIH complex, which induces POL II phosphorylation at S5 residues in its highly repetitive carboxy-terminal domain (CTD), promoting release of POL II from promoters [Bouchard et al., 2004, Walz et al., 2014] (Fig. 1.3). After promoter clearance, POL II transcription is often attenuated close to the promoter and re-initiation of transcription into productive elongation requires phosphorylation of S2 residues within the POL II CTD, which is primarily mediated by the positive elongation factor p-TEFb [Shandilya and Roberts, 2012, Weake and Workman, 2010]. Since C-MYC interacts with p-TEFb via MBI and is able to recruit p-TEFb to promoter-proximal paused POL II, C-MYC also plays an important role during this step of transcription [Eberhardy and Farnham, 2002, Rahl et al., 2010] (Fig. 1.1, 1.3). Among its numerous roles in activation of transcription, this C-MYC function in pause release of POL II into productive elongation is thought to be a key mechanism for C-MYC-mediated transactivation [Rahl and Young, 2014, Walz et al., 2014].

C-MYC-mediated repression of transcription

How C-MYC induces repression of transcription is less clear compared to its role in transcriptional activation. However, there are several reports on direct and indirect repression of transcription by C-MYC. Direct repression can be mediated either via recruitment of histone deacetylases (HDACs) and DNA methyltransferases (DNMTs), or via displacement of

co-activator complexes (Fig. 1.4). For example C-MYC interacts with HDAC3 via MBIIIa and induces HDAC3 recruitment to promoters, where HDAC3 deacetylates histone H3 and H4, inducing a closed chromatin structure [Kurland and Tansey, 2008] (Fig. 1.1, 1.4). Furthermore, it was shown that C-MYC represses transcription via its interaction with other transcription factors, such as MIZ1 (Fig. 1.4). C-MYC interacts with MIZ1 via its C-terminal HLH domain and represses expression of MIZ1 activated target genes, such as the tumour suppressors *CDKN1A* and *CDKN2B* [Herold et al., 2002, Peukert et al., 1997] (Fig. 1.4). On the one hand side, C-MYC interaction with MIZ1 leads to displacement of MIZ1-associated co-activator complexes (p300 and nucleophosmin (NPM) 1), on the other hand side, C-MYC stimulates recruitment of HDACs and DNMT3a, which induce deacetylation of histones and methylation of the DNA, respectively, resulting in a closed chromatin structure [Brenner et al., 2005, Staller et al., 2001, Wanzel et al., 2008] (Fig. 1.4). In contrast to direct repression of transcriptional activation, one way of indirect repression of transcription is the C-MYC-mediated positive transcriptional regulation of specific miRNAs. For example, C-MYC induces expression of the miRNA miR-17-92, which represses translation of proteins important for induction of senescence or apoptosis, supporting C-MYC-mediated induction of autonomous proliferation [Li et al., 2014].
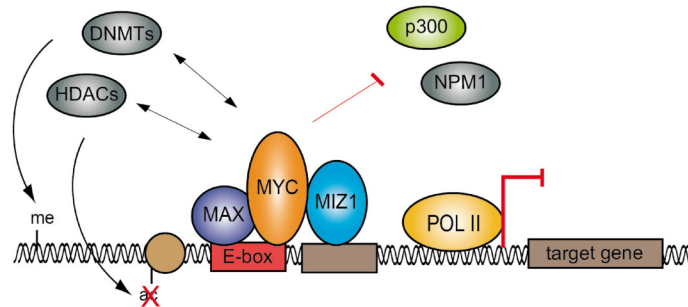
Figure 1.4
C-MYC-mediated repression of transcription
Scheme illustrating transcriptional repression of MIZ1 target genes by MYC proteins. C-MYC interacts with MIZ1 as a heterodimer with MAX and displaces MIZ1 co-activator complexes (NPM1 and the HAT p300). C-MYC mediates removal of open chromatin marks and induces a closed chromatin structure via recruitment of histone deacetylases (HDACs) and DNA methyltransferases (DNMTs), which induce deacetylation of histones and methylation of the DNA (me), respectively.

1.3.2   Regulation of transcription by POL I and POL III

Products of transcription by POL I and POL III are essential for cellular growth, since they comprise the components that enable transcription and translation of protein encoding mRNAs transcribed by POL II. Oncogenes, such as MYC proteins, enhance POL I- and POL III-mediated transcription at multiple levels in order to stimulate protein synthesis and cellular growth [Hannan et al., 2013, White, 2008].

Expression of POL I itself, as well as POL I GTFs is induced by direct binding of MYC transcription factors to the promoters of the encoding POL II genes, which was demonstrated by ChIP experiments [Grewal et al., 2005, Ji et al., 2011, Poortinga et al., 2011].

Importantly, mammalian MYC proteins can also localise to the nucleolus where they bind to non-canonical E-boxes in the promoter of rRNA encoding DNA sequences (rDNAs) [Arabi et al., 2005, Grandori et al., 2005, Lin et al., 2012]. Human C-MYC was shown to enhance loading of POL I and the GTF complex SL1 and to induce histone acetylation, as well as recruitment of co-activator complexes, promoting POL I-mediated transcription [Grandori et al., 2005]. In contrast, in *Drosophila melanogaster* no binding of dMyc to rDNA sequences was detected [Grewal et al., 2005]. The localisation of MYC proteins to the nucleolus is stimulated by NPM1, which is also a direct MYC target gene [Li and Hann, 2013]. An additional mechanism that is thought to lead to an induction of POL I transcription by MYC transcription factors is the MYC-mediated formation of gene loop structures of rDNA, which link promoter and terminator sequences, bearing the potential to enhance re-initiation of transcription [Shiue et al., 2009]. Furthermore, MYC proteins enhance processing of the POL I transcription products into their mature form, since MYC target genes encode proteins involved in rRNA processing and maturation in the nucleolus, for example fibrillarin and nucleolin [Schlosser et al., 2003].

Transcription by POL III is induced by MYC proteins in a similar way as POL I-mediated transcription. Based on their promoter structure POL III transcribed genes are classified into three distinct classes, which differ in regard of the mechanism of transcription and involved GTFs. The 5S rRNA is a type I gene, type II genes are mainly tRNA genes and type III genes encode a large variety of different small RNAs, including for example the 7SK RNA, U6 snoRNAs and Y RNAs [Dieci et al., 2007, Geiduschek and Kassavetis, 2001, Schramm and Hernandez, 2002, Willis, 1993]. As it was shown for the POL I transcription machinery, genes encoding POL III and several POL III GTFs are direct MYC target genes [Gomez-Roman et al., 2003, Felton-Edkins et al., 2003, Lin et al., 2012, Raha et al., 2010]. In addition, MYC proteins also co-localise with POL III target genes and induce histone acetylation and transcription by POL III [Kenneth et al., 2007, Raha et al., 2010]. Since there are no canonical or non-canonical sequences in the vicinity of most POL III target genes and it was shown in *Drosophila melanogaster* that dMyc can enhance POL III transcription in the absence of MAX, MYC proteins are thought to localise to POL III target genes via protein-protein interactions [Campbell and White, 2014, Steiger et al., 2008]. TFIIIB, a POL III GTF, was shown to interact with MYC proteins in different organisms and is thought to recruit MYC transcription factors to POL III target genes [Ernens et al., 2006, Gomez-Roman et al., 2003, Steiger et al., 2008]. In contrast to POL I target genes, it is not known, if MYC binding to POL III target genes can induce loop formation of chromatin in order to enhance transcription [Campbell and White, 2014]. However, tRNA encoding tDNAs usually form clusters in the nucleus and their interaction can induce loop formation of chromatin and modulate transcription of POL II target genes [Raab et al., 2012]. Interestingly, several studies suggest that transcription of POL III target genes is induced upon co-localisation with actively transcribed POL II genes and POL II transcription factors, such as MYC [Alla and Cairns, 2014, Barski et al., 2010, Moqtaderi

et al., 2010, Oler et al., 2010, Raha et al., 2010].

1.4 Regulation of the transcription factor N-MYC

Since MYC proteins play a role in numerous processes, most importantly in the regulation of cellular proliferation, transcription of MYC encoding genes, as well as translation of MYC mRNA and protein stability must be tightly regulated. From what is known in literature, human C- and N-MYC differ in regard of regulatory mechanisms and much less is known about regulation of N-MYC. Giving that N-MYC is the subject of this study, the following descriptions focus on N-MYC.

In contrast to the immediate-early gene C-MYC, N-MYC is an E2F target gene and transcribed later in the cell cycle [Strieder and Lutz, 2003]. E2F and SP1/SP3 transcription factors were shown to cooperate in the induction of *MYCN* expression [Kramps et al., 2004]. However, E2F proteins, which can bind to E2F responsive elements in the *MYCN* promoter, are also involved in negative regulation of *MYCN* transcription, assisting TGF-beta- and retinoic acid (RA)-mediated repression [Kramps et al., 2004, Lutz and Schwab, 1997, Strieder and Lutz, 2003]. While TGF-beta signaling reduces steady-state levels of *MYCN* mRNA [Serra et al., 1994], the vitamin A analogue RA, as well as the neuronal growth factor (NGF) were demonstrated to decrease *MYCN* expression and induce differentiation of neuronal cells [Matsushima and Bogenmann, 1993, Thiele et al., 1985, Wada et al., 1992]. In agreement with these findings, N-MYC was shown to block neuronal differentiation via repression of differentiation pathways [Kang et al., 2006, Nara et al., 2007]. Importantly, *MYCN* is a direct target of the SHH signaling pathway, which plays an important role in neuronal differentiation [Kenney et al., 2003]. Accordingly, a tight balance between RA/NGF-signaling and the SHH pathway are required to regulate differentiation and proliferation of the nervous system, depending on *MYCN* expression levels [Hurlin, 2005, Kenney et al., 2004].

On a post-transcriptional level, different factors were shown to regulate the stability of *MYCN* mRNA. For example, translation of *MYCN* mRNA is negatively regulated by miR-34a, which is encoded in a region (chromosome 1p36) that is commonly lost in neuroblastoma carrying an amplification of the N-MYC encoding gene [Wei et al., 2008]. In contrast, HuD proteins enhance the stability of *MYCN* mRNA via binding to cis-acting destabilising elements in the 3'-untranslated region (UTR) of *MYCN* [Manohar et al., 2002].

Post-translational regulation of N-MYC is mediated via a large variety of signaling pathways, which induce different kinds of modifications on N-MYC. Modifications include phosphorylation, acetylation and ubiquitinylation, which translate into distinct mechanisms, such as regulation of protein stability [Vervoorts et al., 2006]. Degradation of N-MYC occurs via the ubiquitin-system or via an ubiquitin-independent mechanism. The D element and the PEST sequence, which is enriched for the amino acids proline (P), glutamic acid (E), serine (S) and threonine (T), are located in the central part of MYC proteins and regulate ubiquitin-independent proteolysis [Gregory and Hann, 2000, Herbst et al., 2004]. Ubiquitin-dependent

degradation is mediated via the ubiquitin-system and involves a cascade of three different kinds of enzymes, ubiquitin-activating enzymes (E1), ubiquitin-conjugating enzymes (E2) and ubiquitin ligases (E3), that induce ubiquitination of a target protein. Ubiquitin is a small protein of 8 kDa and comprises 7 lysine (K) residues, which are involved in ubiquitin chain formation on a target protein, inducing different cellular processes, for example K48-linked ubiquitin chains signal proteasomal degradation of a target protein [Haglund and Dikic, 2005, Pickart and Eddins, 2004]. Different E3 ligases are known to target N-MYC for proteasomal degradation: HUWE1 [Zhao et al., 2008], DBB1-CUL4 [Choi et al., 2010] and SCF^{FBXW7}[Sjostrom et al., 2005]. Degradation of MYC proteins via the E3 ligase complex SCF^{FBXW7} was described first for C-MYC and is triggered by phosphorylation at two highly conserved residues in MBI, T58 and S62 [Alvarez et al., 1991, Henriksson et al., 1993] (Fig. 1.5). These phosphorylation sites are among the best characterised modifications on MYC proteins and were shown to be not only involved in degradation, but also in regulation of apoptosis and transformation by MYC [Chang et al., 2000, Henriksson et al., 1993, Noguchi et al., 1999, Pulverer et al., 1994].
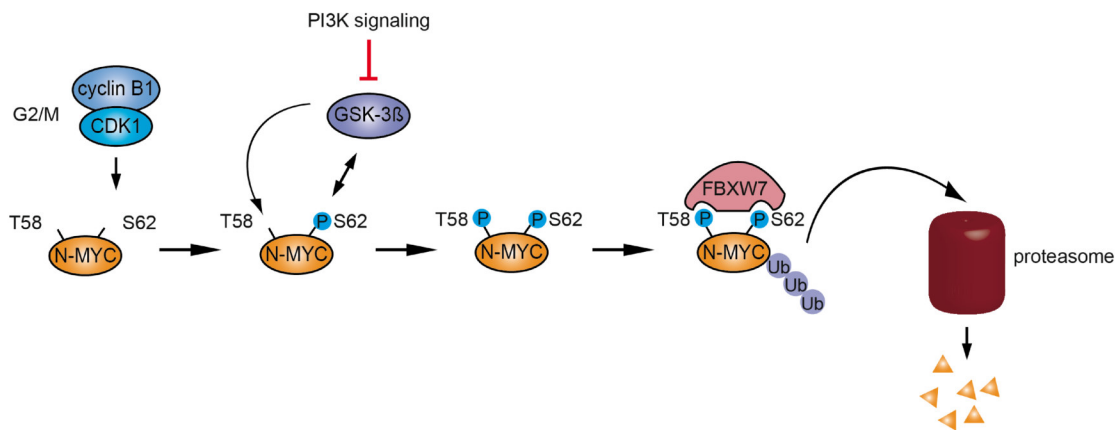
Figure 1.5
N-MYC degradation
Scheme illustrating N-MYC degradation via FBXW7. At the G2/M phase boundary of the cell cycle cyclin B1 is expressed and forms a complex with CDK1. Complex formation with cyclin B1 activates CDK1 kinase activity and enables CDK1-mediated phosphorylation of N-MYC at S62. N-MYC phosphorylation at S62 primes its phosphorylation at T58 by GSK-3ß, a kinase that is negatively regulated by the PI3K signaling pathway. When N-MYC is phosphorylated at T58 and S62 residues it is recognised by FBXW7, a part of the E3 ubiquitin ligase SCF^{FBXW7} , which mediates ubiquitination of N-MYC leading to proteasomal degradation.

While C-MYC phosphorylation at S62 is mediated via different kinases (c-Jun, CDK2, Ras-activated mitogen activated protein kinases (MAPKs) Alvarez et al., 1991, Hydbring et al., 2010, Noguchi et al., 1999), so far only one kinase, CDK1, was described to phosphorylate N-MYC at S62 [Sjostrom et al., 2005] (Fig. 1.5). CDK1 is a cyclin-dependent kinase, which is kinetically active in a complex with cyclin B1 that is selectively expressed in G2/M phase of the cell cycle [Lindqvist, Rodriguez-Bravo, and Medema, 2009]. The cyclin B1/CDK1-dependent phosphorylation of N-MYC links its degradation to a certain phase of the cell cycle, in contrast to C-MYC, which can be degraded via SCF^{FBXW7} throughout the cell

cycle. N- and C-MYC phosphorylation at S62 primes phosphorylation at T58 by glycogen synthase kinase 3 beta (GSK-3ß) [Gregory et al., 2003, Lutterbach and Hann, 1994, Sjostrom et al., 2005] (Fig. 1.5). GSK-3ß is negatively regulated by the PI3K signaling pathway via an inhibitory phosphorylation at S9 by the serine/threonine-protein kinase AKT, which is activated upon mitogen-stimulation of the PI3K signaling, linking MYC protein degradation with growth signals [Cohen and Frame, 2001, Lutterbach and Hann, 1994, Parisi et al., 2011] (Fig. 1.5). For N-MYC it was shown that there is a synergy of PI3K and SHH signaling in N-MYC regulation, controlling cell cycle progression of neuronal precursor cells [Kenney et al., 2004]. Phosphorylation at T58 enables recognition by the F-box protein FBXW7, a part of the SCF^{FBXW7} E3 ligase complex, and subsequent ubiquitination of C- and N-MYC with K48-linked ubiquitin chains, which target the proteasome [Otto et al., 2009, Popov et al., 2010, Welcker et al., 2004, Yada et al., 2004] (Fig. 1.5).

Disruption of the tightly balanced regulation of N-MYC expression and stability leads to transformation and tumour development (see introduction, section 1.1). High N-MYC levels can induce repression of anti-tumourigenic functions, such as apoptosis, immune surveillance and differentiation, and maintain a stem cell-like de-differentiated state, as it was shown for neuronal progenitor cells [Huang and Weiss, 2013, Knoepfler et al., 2002].

1.5   Deregulation of N-MYC in a subgroup of neuroblastoma

Deregulated *MYCN* expression plays an important role in a subgroup of neuroblastoma, a tumour that arises from neuronal progenitor cells of the peripheral nervous system [Huang and Weiss, 2013]. Amplification of the N-MYC encoding gene leads to high N-MYC protein levels and correlates with high-risk diseases and a poor prognosis for neuroblastoma patients [Brodeur et al., 1984, Seeger et al., 1985]. Neuroblastoma is the most common extracranial solid tumour of children and *MYCN*-amplification is one of several markers used to stratify tumour stage [Mueller and Matthay, 2009]. The clinical course of neuroblastoma is strongly heterogeneous and the clinical outcome varies from spontaneous regression to relentless growth and development of metastasis [Brodeur and Bagatell, 2014]. Metastasis occur mainly in bone marrow, bone, lymph nodes and liver, while the primary tumour arises in paraspinal ganglia in the chest or abdomen and in the adrenal glands [DuBois et al., 1999]. Taking into account the observations that *MYCN*-amplified neuroblastoma patients are usually young children, that N-MYC is normally not expressed in neuronal tissues after embryonic development and that N-MYC levels play an important role in neuronal differentiation, a lack of differentiation appears to be a reasonable explanation for neuroblastoma development [Brodeur and Bagatell, 2014, Huang and Weiss, 2013, Knoepfler et al., 2002] (Fig. 1.6). Importantly, induction of differentiation is a mechanism that can lead to spontaneous regression of neuroblastoma, for example, via activation of the Tyrosine-kinase A (TrkA)/NGF-signaling pathway [Matsushima and Bogenmann, 1993, Nakagawara et al., 1993, Nakagawara and Brodeur, 1997] (Fig. 1.6). Furthermore, administration of the differentiation-inducing ligand RA is successfully exploited as a therapeutic approach for

neuroblastoma patients [Matthay et al., 2009]. The knowledge that high N-MYC protein levels can interfere with differentiation of neuroblastoma, has classified N-MYC as a potential target for therapy of *MYCN*-amplified neuroblastoma [Beltran et al., 2011, Pession and Tonelli, 2005]. But since N-MYC is a transcription factor, it is difficult to develop a drug, which directly targets its function, and the predominant treatment of patients with *MYCN*-amplified neuroblastoma remains chemotherapy [Tonini et al., 2012].
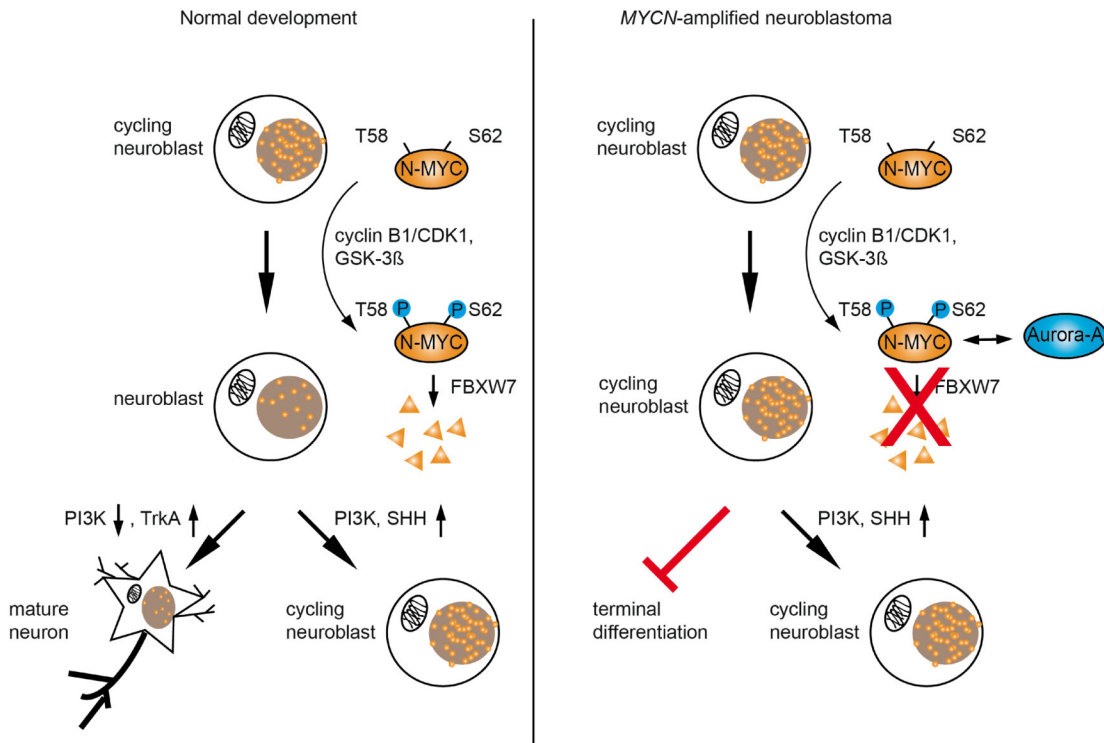
Figure 1.6
Aurora-A stabilises N-MYC in *MYCN*-amplified neuroblastoma
Scheme illustrating Aurora-A-mediated stabilisation of N-MYC. In normal development cycling neuroblasts have high N-MYC protein levels. In order to differentiate N-MYC levels are decreased in neuroblasts and this can be mediated via SCF^{FBXW7}-mediated ubiquitination and degradation via the proteasome (Fig. 1.4). The decrease in N-MYC levels is dependent on different factors, for example PI3K/SHH signaling and TrkA expression. *MYCN*-amplified neuroblastoma have high N-MYC levels and Aurora-A interferes with N-MYC degradation via SCF^{FBXW7}. Accordingly, N-MYC levels stay high and disable terminal differentiation of neuroblasts into mature neurons. Adapted from Otto et al., 2009.

The discovery of Aurora-A-mediated stabilisation of N-MYC in *MYCN*-amplified neuroblastoma represented a breakthrough in research on potential indirect targets for therapy of *MYCN*-amplified neuroblastoma patients [Brockmann et al., 2013, Otto et al., 2009]. Aurora-A was identified in an small hairpin RNA (shRNA) screen for genes, which are synthetic lethal with an amplification of *MYCN* upon shRNA-mediated knockdown [Otto et al., 2009]. In the shRNA screen effects on proliferation of *MYCN*-amplified versus non-*MYCN*-amplified neuroblastoma cell lines were assessed upon knockdown of 194 genes, which were either shown to be expressed in a N-MYC-dependent manner, or which were known direct C-MYC target genes. Depletion of Aurora-A resulted in decreased proliferation of *MYCN*-amplified neuroblastoma cell lines, but did not affect non-*MYCN*-amplified

cells [Otto et al., 2009]. Since a previous study detected high Aurora-A expression levels specifically in *MYCN*-amplified neuroblastoma, the functional relationship of N-MYC and Aurora-A was further investigated [Berwanger et al., 2002, Otto et al., 2009]. Detailed analyses revealed that Aurora-A interaction with N-MYC rescues N-MYC from proteasomal degradation via the E3 ligase SCF^{FBXW7} [Otto et al., 2009] (Fig. 1.6). Importantly, the Aurora-A encoding gene, *AURKA*, is a direct target of N-MYC and its expression is strongly induced in *MYCN*-amplified neuroblastoma [Berwanger et al., 2002].

Aurora-A is a serine/threonine kinase, whose kinase activity is highly relevant for cells to progress through mitosis. In mitosis Aurora-A phosphorylates several targets, that are involved in different processes, among others Aurora-A plays a role in centrosomal maturation, bipolar alignment of microtubles of the mitotic spindle and cytokinesis [Nikonova et al., 2013]. The functions of Aurora-A in mitosis are highly relevant, since Aurora-A k.o. mice are not viable and die early during embryonic development before the 16-cell stage, displaying severe defects in mitosis, particularly in spindle assembly [Lu et al., 2008, Sasai et al., 2008]. Interestingly, Aurora-A is not only essential for early embryonic development, but also for tumour suppression, as Aurora-A heterozygosity led to a significant increase in tumour incidences in mice [Lu et al., 2008]. More recently, mitosis-independent functions of Aurora-A were described, including a function in ciliogenesis, microtubuli dynamics and regulation of the activity of the tumour suppressor p53 [Chen et al., 2002, Katayama et al., 2004, Lorenzo et al., 2009, Pugacheva et al., 2007]. Aurora-A-mediated phosphorylation of p53 induces its degradation via the E3 ubiquitin-protein ligase MDM2, interfering with p53 function in tumour surveillance and facilitating oncogenic transformation [Katayama et al., 2004]. This mechanism represents one of the Aurora-A functions, which stratify Aurora-A as an oncogene. Cancer susceptibility is increased upon overexpression, gain of function, and/or loss of function of Aurora-A and there are numerous solid tumours that display deregulated Aurora-A expression and function, for example breast, ovarian and colon cancer entities [Karthigeyan et al., 2011]. Neuroblastoma is not the only tumour, which displays both, *AURKA* and *MYCN* overexpression, also for NEPCs an amplification of both genes was demonstrated [Terry and Beltran, 2014]. In addition, a study was published recently, which showed that also high C-MYC and Aurora-A expression levels are inter-linked in hepatocellular carcinoma (HCC) and that like N-MYC, C-MYC can be stabilised by Aurora-A in HCC cells [Dauch et al., 2016]. Due to the large panel of tumour entities, which show deregulated Aurora-A expression, several Aurora-A inhibitors have been developed, using the knowledge from the crystal structure of the C-terminal Aurora-A kinase domain [Cheetham et al., 2002]. Aurora-A inhibitors were designed as small molecules binding to the ATP-binding site in the kinase domain and leading either to a blockage of protein–protein interactions between Aurora-A and a co-factor or substrate (type I inhibitors), or to an inhibition of the activity of the serine/threonine kinase (type II inhibitors) [Karthigeyan et al., 2011]. The first reported Aurora-A inhibitor, being specific for Aurora-A and not affecting the Aurora-A homologues Aurora-B and Aurora-C, was MLN8054, which was de-

veloped by the company Millenium Pharmaceuticals [Karthigeyan et al., 2011, Manfredi et al., 2007]. Strikingly, MLN8054 and an improved variant, MLN8237, were demonstrated to not only inhibit Aurora-A kinase activity, but also to disrupt the interaction of Aurora-A and N-MYC, inducing N-MYC degradation via the proteasome [Brockmann et al., 2013]. Accordingly, MLN8054/8237 would have a dual role in therapy of tumours with high N-MYC and Aurora-A levels, such as *MYCN*-amplified neuroblastoma overexpressing Aurora-A. For this reason, MLN8237, also known as "Alisertib", is currently used in clinical trials phase II, as a single agent or in combination with other drugs, to treat for example neuroblastoma, SCLC and NEPC patients [Niu et al., 2015].

1.6   Objectives of this thesis

Deregulated expression of the N-MYC transcription factor drives tumour initiation and progression in multiple cancer entities. More profound knowledge about functional interactions, regulation of expression and protein stability of N-MYC is required in order to make strides in the battle against these specific tumours.

Amplification of the N-MYC encoding gene occurs for example in a subgroup of neuroblastoma and is linked to a poor prognosis for the patients. Importantly, neuroblastoma proliferation depends on the maintenance of high N-MYC protein levels, turning N-MYC into a highly relevant therapeutic target at hand. Previous studies have uncovered the interaction of N-MYC with Aurora-A kinase as a weak spot of N-MYC stability in *MYCN*-amplified neuroblastoma. N-MYC interaction with Aurora-A prevents its degradation via a specific E3 ubiquitin ligase, SCF$^{\text{FBXW7}}$, which attaches ubiquitin chains to N-MYC that target it to the proteasome. However, it is not known, how complex formation with Aurora-A can interfere with proteasomal degradation of N-MYC.

Uncovering the mechanism of Aurora-A-mediated stabilisation of N-MYC does not only allow the development of specific inhibitors that target N-MYC stability, but also leads to a better understanding of regulatory pathways evolving on N-MYC. Therefore, this thesis aimed to identify novel N-MYC interacting proteins that could be involved in the regulation of N-MYC stability, specifically by Aurora-A interaction.

A proteomic analysis of purified N-MYC protein complexes should be performed to reveal previously unknown interactions. Additionally, complex components of an N-MYC mutant, which is known to be deficient in stabilisation by Aurora-A, should be analysed, in order to identify N-MYC interaction partners that are specific for Aurora-A stabilisation of N-MYC wt. Finally, the functional relationship of N-MYC and novel N-MYC interacting proteins should be uncovered and their mechanistic function together with Aurora-A should be elucidated.

2   Materials

2.1   Strains and cell lines

2.1.1   Bacterial strains

DH5α

Escherichia coli F-, Φ80dlacZΔM15 Δ(lacZYA-argF)U169 deoR recA1 endA1 hsdR17 (rk-,mk+) phoA supE44 λ- thi-1 gyrA96 relA1; for amplification of plasmids

XL1 blue

Escherichia   coli,   recA1   endA1   gyrA96,   thi-1   hsdR17   supE44   relA1   lac [F'proAB lacIqZΔM15Tn10(Tetr)]; for generation and amplification of plasmids

BL21

Escherichia coli F-, ompT gal dcm lon hsdSB(rB- mB-) λDE3 lacI lacUV5-T7 gene 1 ind1 sam7 nin5; for expression of GST fusion proteins

2.1.2   Human cell lines

HEK293TN

Human embryonic kidney cell line,

purchased from ATCC

IMR-32

Human *MYCN*-amplified neuroblastoma cell line, stable transfected with the murine eco-
tropic receptor and Hygromycin resistance gene,

provided by Manfred Schwab

IMR-5

Human *MYCN*-amplified neuroblastoma cell line, stable transfected with the murine eco-
tropic receptor and Hygromycin resistance gene,

provided by Angelika Eggert

Plat-E

Platinum-E cell line, potent retroviral packaging cell line,

provided by Björn von Eyss

SH-EP

Human *MYCN*-non-amplified neuroblastoma cell line, stable transfected with the murine
ecotropic receptor and Hygromycin resistance gene,

provided by Manfred Schwab

2.2   Cultivation media and supplements

2.2.1   Media for mammalian cell culture

Basal medium DMEM and RPMI-1640 containing L-glutamine (584 mg/ml) was purchased
by Sigma. Fetal bovine serum (FBS; from Biochrom) was heat inactivated for 30 min at 56
°C before use.

Basal medium for neuroblastoma cell lines
RPMI-1640 with 10% (v/v) FBS and 1% (v/v) penicillin/ streptomycin (100.000 U/ml; from Sigma)
Basal medium for HEK293TN and Plat-E cell lines
DMEM with 10% (v/v) FBS and 1% (v/v) penicillin/ streptomycin (100.000 U/ml; from Sigma)
Freezing medium
70% (v/v) Basal medium, according to the cell line, with 20% (v/v) FBS and 10% (v/v) DMSO

2.2.2   Antibiotics and compounds for mammalian cell culture

For selection of successfully transfected or infected cells, if not indicated otherwise, all cell lines were treated with the antibiotic concentrations given below. A resistance to Neomycin was selected with G418.

Blasticidin S (InvivoGen)	3.03 µg/ml
CD532 (provided by R. Bayliss)	1000 nM in DMSO
G418 (PAA)	100 µg/ml in aqua bidest
Hygromycin B (Merck)	100 µg/ml in aqua bidest
MG-132 (Calbiochem)	20 µM in EtOH
MLN8237 (Selleckchem)	250-1000 nM in DMSO
MK-5108 (Selleckchem)	1000 nM in DMSO
Puromycin (InvivoGen)	1-2 µg/ml
Polybrene (Sigma)	4 µg/ml in aqua bidest

2.2.3   Media and antibiotics for bacterial cell culture

Media

LB-medium
10% (w/v) bacto tryptone
0.5% (w/v) yeast extract
1% (w/v) NaCl
LB-agar
LB-medium
1.2% (w/v) Bacto-Agar
The solution was autoclaved and then cooled down to 50 °C before antibiotics
were added, 20 ml was poured into each 10 cm dish.

Antibiotics

Depending on the resistance marker encoded on the DNA plasmid, the following antibiotics were added to the LB-medium or LB-agar:

Ampicillin 100 mg/ml

Kanamycin 100 mg/ml

2.3 Nucleic acids

2.3.1 DNA oligonucleotides

DNA-primers were synthesised by Sigma and target human DNA/mRNA, if not indicated otherwise. Primers for quantitative qRT-PCR were designed with the open source software Primer3 and are all intron-spanning to avoid amplification of genomic DNA.

name	application	sequence
AURKA fwd	qRT-PCR	GGAGAAAGCCGGAGTGGAGCATC
AURKA rev	qRT-PCR	TTCAATCATTTCAGGGGGCAGGTA
B2M fwd	qRT-PCR	GTGCTCGCGCTACTCTCTC
B2M rev	qRT-PCR	GTCAACTTCAATGTCGGAT
FL 195 FASN TSS 1 fwd	ChIP	CCAAGCTGTCAGCCCATGT
FL 196 FASN TSS 1 rev	ChIP	CGTCTCTCTGGCTCCCTCTA
GALNT14 PP1 fwd	ChIP	AATGTGCTCGTCCTACCACA
GALNT14 PP1 rev	ChIP	AGTAGCCAGGCAAGTGAACC
GALNT14 PP2 fwd	ChIP	CTAGACCCAGGATCCGGTTG
GALNT14 PP2 rev	ChIP	CAGGCTCGCTTCTCTTCGA
GALNT14 neg.region fwd	ChIP	GCACAGGTCAGAGGGTAGTT
GALNT14 neg.region rev	ChIP	CAGAGGCTGGAGGAAGGAAT
MYCN fwd	qRT-PCR	CCACAAGGCCCTCAGTACC
MYCN rev	qRT-PCR	TCTTCCTCTTCATCATCTTCATCA
MYCN NT HA EcoRI fwd	cloning	CGGAATTCATGTACCCTTACGACG TGCCCGACTACGCCGGGCCGAGCT GCTCCACGT
MYCN CT XbaI rev	cloning	GCTCTAGACTAGCAAGTCCGAGC GTGTT

name	application	sequence
MYCN NTdelta110 HA EcoRI fwd neu	cloning	CGGAATTCATGTACCCTTACGACG TGCCCGACTACGCCGGGGTCATCC TCCAGGACT
MYCN NTdelta44 HA EcoRI fwd	cloning	CGGAATTCATGTACCCTTACGACG TGCCCGACTACGCCGGGCCGGGGG AGGACATCT
MYCN V339 stop fwd	mutagenesis	CTCTCCCTACGTGTAGAGTGAGGA TGC
MYCN V339 stop rev	mutagenesis	GCATCCTCACTCTACACGTAGGGA GAG
MYCN L318 stop fwd	mutagenesis	CAGTCCAGCGAGCTGTAGCTCAAA CGATGCCTTC
MYCN L318 stop rev	mutagenesis	GAAGGCATCGTTTGAGCTACAGCT CGCTGGACTG
MYCN V197 stop fwd	mutagenesis	CCCCTTTCCCGTGTAGAAGCGCGA GCCAG
MYCN V197 stop rev	mutagenesis	CTGGCTCGCGCTTCTACACGGGAA AGGGG
MYCN E185 stop fwd	mutagenesis	CGGCCGCCGAGTAAGTGGATCCC GC
MYCN E185 stop rev	mutagenesis	GCGGGATCCACTTACTCGGCGGC CG
MYCN L126 stop fwd	mutagenesis	CCGCGAGAAGCTGTAACGCGCCG TGAGCG
MYCN L126 stop rev	mutagenesis	CGCTCACGGCGCGTTACAGCTTC TCGCGG
MYCN P109 stop fwd	mutagenesis	CTCACCCCCAACCCGTAAATCCT CCAGGACTG
MYCN P109 stop rev	mutagenesis	CAGTCCTGGAGGATTTACGGGTT GGGGGTGAG
Site-Directed Mutagenesis pWZLblast MYCN (mut*) fwd	mutagenesis	GAACACGCTCGGACTTGCAGATC TTTCGAAATCACC
Site-Directed Mutagenesis pWZLblast MYCN (mut*) rev	mutagenesis	GGTGATTTCGAAAGATCTGCAAG TCCGAGCGTGTTC
Site-Directed Mutagenesis MYCN mut* zu MYCN wt fwd	mutagenesis	TTTGAGCTGCTGCCCACGCCCCC GCTGTCGCCCAGCCGTGGCTTC

name	application	sequence
Site-Directed Mutagenesis MYCN mut* zu MYCN wt rev	mutagenesis	GAAGCCACGGCTGGGCGACAGCG GGGGCGTGGGCAGCAGCTCAAA
Site-Directed Mutagenesis pWZLblast MYCN (mut*) fwd	mutagenesis	GAACACGCTCGGACTTGCTAGTC TTTCGAAATCACCATGG
Site-Directed Mutagenesis pWZLblast MYCN (mut*) rev	mutagenesis	CCATGGTGATTTCGAAAGACTAG CAAGTCCGAGCGTGTTC
Site-Directed Mutagenesis MYCN wt zu MYCN mut* fwd	mutagenesis	TTTGAGCTGCTGCCCGCGCCCCC GCTGGCGCCCAGCCGTGGCTTC
Site-Directed Mutagenesis MYCN wt zu MYCN mut* rev	mutagenesis	GAAGCCACGGCTGGGCGCCAGCG GGGGCGCGGGCAGCAGCTCAAA
NCL LJ307 fwd	ChIP	CTACCACCCTCATCTGAATCC
NCL LJ308 fwd	ChIP	TTGTCTCGCTGGGAAAGG
NME1 fwd (site 3; chr17 (49.230.711-49.230.913))	ChIP	GGGGTGGAGAGAAGAAAGCA
NME1 rev (site 3; chr17 (49.230.711-49.230.913))	ChIP	TGGGAGTAGGCAGTCATTCT
SW ChIP negChr1 fwd	ChIP	GCAGTTCAACCTACAAGCCAATAG AC
SW ChIP negChr1 rev	ChIP	CACAAATTAGCGCATTGCCTGA
SW ChIP negChr2 fwd	ChIP	TGTCACAGGCTCACAGGAAC
SW ChIP negChr2 rev	ChIP	ACCTGCTGACTAAAGAGCCC
EW9-ch11-80MB-fwd	ChIP	TTTTCTCACATTGCCCCTGT
EW10-ch11-80MB-rev	ChIP	TCAATGCTGTACCAGGCAAA
NPM LJ305 fwd	ChIP	TTCACCGGGAAGCATGG
NPM LJ306 fwd	ChIP	CACGCGAGGTAAGTCTACG
AC RAD21 RT fwd	qRT-PCR	ACCATGAGAGAAGAAGTTGGGA
AC RAD21 RT rev	qRT-PCR	TCCTCAAAAGCACTGCCTTC
SP ODC1 fwd	qRT-PCR	AAAGTTGGTTTTGCGGATTG
SP ODC1 rev	qRT-PCR	CGAAGGTCTCAGGATCGGTA

name	application	sequence
PP1 intergenic fwd (site 1; chr16 (51.796.107-51.796.338))	ChIP	CACACGAGGGTCCATAACGT
PP1 intergenic rev (site 1; chr16 (51.796.107-51.796.338))	ChIP	GTGGATTTCAGAGCCATCCG
PP2 intergenic fwd (site 2; chr2 (232.316.737-232.316.978))	ChIP	ACTGGTCTGGAATCTGAGGC
PP2 intergenic rev (site 2; chr2 (232.316.737-232.316.978))	ChIP	GGCAGCATAAGTCCACAAGG
PPRC1 PP1 fwd	ChIP	GTGAGGATTAGCGCTTGGAG
PPRC1 PP1 rev	ChIP	TGCTGACGTTCCTTTCACC
PPRC1 PP2 fwd	ChIP	GAAGGCTGAGACCTCCATGT
PPRC1 PP2 rev	ChIP	GTTCTCCCGGGAAAATTGCT
PPRC1 neg.region fwd	ChIP	GGAAAGGGGAAGGGAAGAGG
PPRC1 neg.region rev	ChIP	CGGTTCTAGGAGTTGGGACA
TFIIIC5 RT fwd (left) PP1	qRT-PCR	GATGTGGCTAAGATGCTGCC
TFIIIC5 RT rev (right) PP1	qRT-PCR	AGGCCAATCAGATTCTCACCT
TFIIIC5 RT fwd (left) PP2	qRT-PCR	GGAAGCTGTTTGACATCCGT
TFIIIC5 RT rev (right) PP2	qRT-PCR	AGACCTTGAGCTTGTCTGGG
trna7Leu fwd	ChIP	ATGTAGCATAAGCGCGTCAG
trna7Leu rev	ChIP	ACTGTCAGGAGTGGGATTCG
trna119Ala fwd	ChIP	ACTTGTGCCAGGGGATGTAG
trna119Ala rev	ChIP	AATCTACGTGATCGCCTTGG
USP7 fwd	qRT-PCR	AGGCTCAGAAGCGGAAGG
USP7 rev	qRT-PCR	AAACTGGTCCTCTGCGACTATC
hUSP11 fwd	qRT-PCR	ATAGAAAACGGCGAGAGTGG
hUSP11 rev	qRT-PCR	GTGCTTCTCCACAAGGAACC

name	application	sequence
Site-Directed Mutagenesis hUSP11 wt zu hUSP11 C318S fwd	mutagenesis	CTGGGCAACACGTCCTTCATGAA CTCG
Site-Directed Mutagenesis hUSP11 wt zu hUSP11 C318S rev	mutagenesis	CGAGTTCATGAAGGACGTGTTGC CCAG
Site-Directed Mutagenesis hUSP11 wt zu hUSP11 C318A fwd	mutagenesis	CAATCTGGGCAACACGGCCTTCA TGAACTCGGC
Site-Directed Mutagenesis hUSP11 wt zu hUSP11 C318A rev	mutagenesis	GCCGAGTTCATGAAGGCCGTGTT GCCCAGATTG

fwd: forward; rev: reverse;

: introduces a frameshift, which was corrected with "Site-Directed Mutagenesis pWZL Blast MYCN (mut) fwd/rev" primers

2.3.2 RNA oligonucleotides

RNA-primers for shRNA oligonucleotides were designed using sequences published in Cellecta DECIPHER shRNA Library Human Module 1 for pRSI12 plasmids and target sequences for pLKO.1 puro plasmids were designed and cloned by Helem Ribeiro. Scrambled shRNA and shLuc2 in pLKO.1 puro were provided by Jiajia Xu. All oligos were synthesised by Sigma and purified via HPLC.

shRNAs in pRSI12

Fwd oligo (5'->3'): ACCG-sense(21nt-GT*)-GTTAATATTCATAGC-antisense-TTTTTT
Rev oligo (5'->3'): CGAA-AAAAAA-sense(21nt)-GCTATGAATATTAAC-antisense

name	targeting sequence (sense (21nt-GT*))
shLuc2	CTTCGAAATGTTCGTTTGGTT
shMYCN-1 (Barcode ID 36252)	GCAGCAGCAGTTGTTAAAGAAA
shMYCN-2 (Barcode ID 36253)	GCGGACGAAGATGATTTCTATT
shMYCN-3 (Barcode ID 36254)	GGCGTCGCAGAAATCACAATAT
shUSP11-1 (Barcode ID 33315)	CCGTGATGATATCTTTGTCTA
shUSP11-2 (Barcode ID 33316)	CCGATTCTATTGGCTTAGTAT
shUSP11-3 (cloned from pLKO.1 puro)	ACCTGAACACAGAGTGTATTT

*GT: mismatches introduced in targeting sequence, cytosine -> thymidine, creates GT-mismatch in stem loop structure

shRNAs in pLKO.1 puro

Fwd oligo (5'->3'): CCGG-Sense(19 nt)-CTCGAG-Antisense-TTTTTG
Rev oligo (5'->3'): AATTCAAAAA-sense(19nt)-CTCGAG-Antisense

name	targeting sequence (sense (19nt))
shLuc2	TAGCGCGGTGTATTATAC
shUSP7-1	GATTGAGCTCAGTGATAAT
shUSP7-2	CAGAGAAAGGTGTGAAATT
shUSP7-3	CCCTAATGATCCTGGATTT

siRNAs

Pools of 4 siRNA oligonucleotides against target human mRNAs were purchased from Dharmacon (ON-TARGETplus SMARTpool) and as a control siCONTROL (ON-TARGETplus Non-targeting Pool) was used. For siRNA screening the following siRNA library was used: "Dharmacon ON-TARGETplus® Set of Four siRNA Library - Human Deubiquitinating Enzymes" (GU-104705 Lot 10102).

target mRNA	sequences in SMARTpool
human AURKA	UCGAAGAGAGUUAUUCAUA, CGGUAGGCCUGAUUGGGUU, UUCUUAGAUGUAUGGUUA, AAUAGGAACACGUGCUCUA
human MYCN	CCUCCAUGACAGCGCUAAA, GGACAGUGAGCGUCGCAGA, GAACCCAGACCUCGAGUUU, CGAGCUGGGUCACGGAGAU
human RAD21	GCUCAGCCUUUGUGGAAUA, GGGAGUAGUUCGAAUCUAU, GACCAAGGUUCCAUAUUAU, GCAUUGGAGCCUAUUGAUA
human TFIIIC5	GCAGAUGUUCUACCAGUUA, CCGAAUCCGUUGUGGAAUG, ACCCAGAUGCCAAGAUUUA, ACUCCGAGGUCACAUUUGA
human USP11	GAAGAAGCGUUACUAUGAC, GGACCGUGAUGAUAUCUUC, GAGAAGCACUGGUAUAAGC, GCGCACAGCUGCAUGUCAU

2.4 Plasmids

2.4.1 Empty vectors

name	description
pcDNA3	Eucaryotic expression vector with CMV (cytomegalovirus)- promoter (Invitrogen)
pCMV-Sport 6	Eucaryotic expression vector with CMV (cytomegalovirus)- promoter for higher expression levels (Deutsche Ressourcenzentrum für Genomforschung)
pGEX-4T-1	Bacterial expression vector with tac-promoter for expression of GST-tagged recombinant proteins (GE Healthcare)
pGEX-6P-1	Bacterial expression vector with tac-promoter for expression of GST-tagged recombinant proteins (GE Healthcare)
pJET1.2/blunt	Bacterial expression vector with T7 promoter for cloning (CloneJET PCR Cloning Kit)
pLKO.1 puro	Eucaryotic lentiviral expression vector for constutive U6 promoter driven shRNA expression and puromycin restistance gene (TRC Consortium)
pRSI12	Eucaryotic lentiviral expression vector for constutive U6 promoter driven shRNA expression and with constutitive UbiC (Ubiquitin C) driven TagRFP marker expression (CELLECTA)
pWZLblast	Eucaryotic retroviral expression vector with LTR (long terminal repeat) promoter and blasticidin resistance gene
pWZLneo	Eucaryotic retroviral expression vector with LTR (long terminal repeat) promoter and neomycin resistance gene (Cell Biolabs)

2.4.2 Expression vectors

name	description
pcDNA3 AURKA	pcDNA3 with CDS of human AURKA wt
pCMV-Sport 6 AURKA wt	pCMV-Sport 6 with CDS of human AURKA wt
pGEX-4T-1 GST Aurora-A	pGEX-4T-1 with CDS of human AURKA
pcDNA3 ELP3 NT HA	pcDNA3 with CDS of human N-terminal HA-tagged ELP3 (cloned by Steffi Herold)
pcDNA3 MYCN wt	pcDNA3 with CDS of human MYCN wt
pcDNA3 MYCN T58/S62A	pcDNA3 with CDS of human MYCN T58/S62A

name	description
pcDNA3 MYCN wt NT HA	pcDNA3 with CDS of human N-terminal HA-tagged MYCN wt
pcDNA3 MYCN T58/S62A NT HA	pcDNA3 with CDS of human N-terminal HA-tagged MYCN T58/S62A
pcDNA3 MYCN aa339 stop NT HA	pcDNA3 with CDS of human N-terminal HA-tagged MYCN aa339 stop C-terminal deletion mutant
pcDNA3 MYCN aa318 stop NT HA	pcDNA3 with CDS of human N-terminal HA-tagged MYCN aa318 stop C-terminal deletion mutant
pcDNA3 MYCN aa197 stop NT HA	pcDNA3 with CDS of human N-terminal HA-tagged MYCN aa197 stop C-terminal deletion mutant
pcDNA3 MYCN aa185 stop NT HA	pcDNA3 with CDS of human N-terminal HA-tagged MYCN aa185 stop C-terminal deletion mutant
pcDNA3 MYCN aa126 stop NT HA	pcDNA3 with CDS of human N-terminal HA-tagged MYCN aa126 stop C-terminal deletion mutant
pcDNA3 MYCN aa109 stop NT HA	pcDNA3 with CDS of human N-terminal HA-tagged MYCN aa109 stop C-terminal deletion mutant
pcDNA3 MYCN deltaN1 NT HA	pcDNA3 with CDS of human N-terminal HA-tagged MYCN deltaN1 N-terminal deletion mutant
pcDNA3 MYCN deltaN2 NT HA	pcDNA3 with CDS of human N-terminal HA-tagged MYCN deltaN2 N-terminal deletion mutant
pWZLblast MYCN wt NT HA	pWZLblast with CDS of human N-terminal HA-tagged MYCN wt
pWZLblast MYCN T58/S62A NT HA	pWZLblast with CDS of human N-terminal HA-tagged MYCN T58/S62A
pGEX-6P-1 GST MYCN wt	pGEX-6P-1 with CDS of human MYCN wt
pcDNA3 USP7 wt NT Myc	pcDNA3 with CDS of human USP7 wt (provided by Stefanie Peter)
pcDNA3 USP7 C223S NT Myc	pcDNA3 with CDS of human USP7 C223S (provided by Stefanie Peter)
pcDNA3 USP11 wt	pcDNA3 with CDS of human USP11 wt
pcDNA3 USP11 C318A	pcDNA3 with CDS of human USP11 C318A
pcDNA3 USP11 C318S	pcDNA3 with CDS of human USP11 C318S

2.4.3 Lentiviral packaging vectors

psPAX2

plasmid coding for the lentiviral virion packaging system (HIV gag, pol, rev)

pMD2.g

plasmid coding for the lentiviral envelope (VSV-G env)

2.5 Antibodies

2.5.1 Primary Antibodies

protein	type	application	name
Actin beta	m, mono IgG1	WB	AC15 (Sigma)
Aurora-A	rb, poly	WB	3092 (Cell Signaling)
Aurora-A	goat, poly	IP	N-20 (Santa Cruz)
pT288 Aurora-A	rb, mono	WB	2914 (Cell Signaling)
CDC73	rb, poly	WB	A300-171A (Bethyl)
CDK2	m, mono IgG1	WB	M-2 (Santa Cruz)
Cleaved PARP	m, mono IgG1	WB	F21-852 (BD Pharmingen)
CTCF	rb, poly	WB	07-729 (Millipore)
CTR9	rb, poly	WB	A301-395A (Bethyl)
GST	goat, poly	WB	27-4577-50 (GE Healthcare)
HA	m, mono IgG1	WB	16B12 (Covance)
MAX	rb, poly	WB	C-17 (Santa Cruz)
pT58 MYC	rb, poly	WB	ab28842 (Abcam)
pS62 MYC	rb, poly	WB	ab51156 (Abcam)
N-MYC	m, mono IgG2a	WB, ChIP	B8.4.B (Santa Cruz)
N-MYC	m, mono IgG1	IF	NCM II 100 (Santa Cruz)
RAD21	rb, poly"	WB, ChIP	A300-080A (Bethyl)
SPT5	m, mono	WB	A-3 (Santa Cruz)
TUBULIN alpha	rb, poly	WB	E-19 (Santa Cruz)
TFIIIC1	m, mono	WB, ChIP	F-12 (Santa Cruz)
TFIIIC2	m, poly	WB	ab89113 (Abcam)

protein	type	application	name
TFIIIC4	rb, poly	WB	A301-239A (Bethyl)
TFIIIC5	rb, poly	WB, ChIP	A301-242A (Bethyl)
TOP2A	rb, poly	WB	A300-054A (Bethyl)
TOP2B	rb, poly	WB	A300-949A (Bethyl)
TOP1	rb, poly	WB	A302-589A (Bethyl)
USP7	rb, poly	WB	A300-033A (Bethyl)
USP11	rb, poly	WB, ChIP	A301-613A (Bethyl)
Vinculin	m, mono IgG1	WB	hVin-1 (Sigma)

ChIP: chromatin immunoprecipitation; IP: immunoprecipitation; WB: Western blot
mono: monoclonal; poly: polyclonal; m: mouse; rb: rabbit

2.5.2   Secondary Antibodies

name	application	description
Anti-rabbit-HRP	WB	donkey-anti-rabbit-immunoglobulin coupled with horseradish peroxidase (Amersham, NA 934)
Anti-mouse-HRP	WB	donkey-anti-mouse-immunoglobulin coupled with horseradish peroxidase (Amersham, NA 931)
Rabbit TrueBlot	WB of IPs	mouse-anti-rabbit immunoglobulin coupled with horseradish peroxidase, clone eB182 (Rockland, 18-8816-33)
Mouse TrueBlot ULTRA	WB of IPs	rat-anti-mouse immunoglobulin coupled with horseradish peroxidase, clone eB144 (Rockland, 18-8817-33)
Anti-goat-HRP	WB	donkey-anti-goat-immunoglobulin coupled with horseradish peroxidase (Santa Cruz, sc-2020)
Streptavidin-HRP	WB	streptavidin horseradish peroxidase conjugate (Invitrogen, 43-4323)

2.6   Chemicals

All chemicals were purchased from the companies Sigma, Merck, Roth, Invitrogen and Applichem and used without further purification.

2.7 Enzymes, standards, beads/sepharose for purification and kits

2.7.1 Enzymes

DNase-free RNaseA	Qiagen
M-MLV reverse transcriptase	Promega
Restriction endonucleases	NEB
T4-DNA-Ligase	Fermentas
Pfu Polymerase	Fermentas
Phusion Hot Start II Polymerase®	Fermentas

2.7.2 Standards

PageRuler Pre-Stained Protein Ladder	Fermentas
HiMark™ Pre-Stained HMW Protein Standard	Invitrogen
1kb DNA Ladder	Invitrogen

2.7.3 Beads/sepharose for purification

Glutathione Sepharose™ 4B	GE Healthcare
Dynabeads® MyOne™ Streptavidin C1	Invitrogen
Dynabeads® Protein A/G	Life Technologies
Pierce® Anti-HA Agarose and HA Peptide	Thermo Scientific
Protein A Sepharose® 4B	Invitrogen
Protein G Sepharose® Fast Flow	Sigma

2.7.4 Kits

ABsolute qPCR SYBR Green Mix	
(Cat.No.: AB-1158/B)	Thermo Scientific
CloneJET PCR Cloning Kit	
(Cat.No.: K1236)	Thermo Scientific
Experion DNA Analysis kit 1k	
(Cat.No.: 700-7107)	BioRad

Experion RNA HighSense kit

(Cat.No.: 700-7105)   BioRad

Experion RNA StdSense kit

(Cat.No.: 700-7103)   BioRad

GeneJET Gel Extraction Kit

(Cat.No.: K0692)   Thermo Scientific

MinElute® PCR Purification Kit

(Cat.No.: 28004)   Qiagen

NEBNext® Poly(A) mRNA magnetic

isolation module (Cat.No.: E7490)   NEB

NEBNext® ChIP-Seq Library

(Cat.No.: E6240)   NEB

NEBNext® mRNA-Seq Library

(Cat.No.: E6110)   NEB

NEBNext® Multiplex Oligos

Index Set 1 and 2 (Cat.No.: E7335)   NEB

PureLink® HiPure Plasmid DNA Purification

Kit for MAXiprep (Cat.No.: K210007)   Invitrogen

QIAquick® PCR Purification Kit

(Cat.No.: 28104)   Qiagen

Qiagen Gel extraction Kit

(Cat.No.: 28704)   Qiagen

Quant-iT™ PicoGreen®

dsDNA Kit (Cat.No.: P7589)   Invitrogen

RNEasy kit

(Cat.No.: 74106)   Qiagen

RNase-free DNase kit

(Cat.No.: 79254)   Qiagen

TNT® Quick Coupled Transcription/Translation

Systems (Cat.No.: L1170)   Promega

2.8 Buffers and solutions

Annealing buffer 2x
   100 mM HEPES NaOH pH 7.4
   200 mM pottassium acetate
   4 mM magnesium acetate

Bis-Tris blot buffer 20x

   25 mM Bicine

   25 mM Bis-Tris

   1 mM EDTA

   adjusted to pH 7.2

Bis-Tris blot buffer 1x

   25% (v/v) methanol

   0.1% (v/v) Sodium Bisulfite (of 1 M stock solution)

   prepared by diluting Bis-Tris blot buffer 20x

Bis-Tris HCl buffer 3.5x

   1.25 M Bis-Tris HCl

   adjusted to pH 6.8

Bis-Tris separating gel

   8 - 15% (v/v) Acrylamide/Bisacrylamide

   28.57% (v/v) Bis-Tris HCl buffer 3.5x pH 6.8

   0.05% (w/v) APS

   0.05% (v/v) TEMED

Bis-Tris stacking gel

   4% (v/v) Acrylamide/Bisacrylamide

   28.57% (v/v) Bis-Tris HCl buffer 3.5x pH 6.8

   0.05% (w/v) APS

   0.05% (v/v) TEMED

Blocking solution milk

   5% (w/v) skimmed milk in TBS-T

   stirred about 60 min and filtered with filter paper

Blocking solution BSA

   3-5% (w/v) BSA in TBS-T

   stirred about 60 min and filtered with filter paper

Bradford solution

   8.5% (v/v) ortho-phosphoric acid

4.75% (v/v) ethanol

0.01% (w/v) Coomassie Brilliant Blue G

stirred O/N and filtered with filter paper

and stored at 4 °C wrapped into aluminium foil

BSA PBS

0.5% (w/v) BSA in PBS

ChIP elution buffer

1% (v/v) SDS

0.1 M NaHCO$_3$

prepared fresh in aqua dest

ChIP lysis buffer I

5 mM PIPES pH 8.0

85 mM KCl

0.5% (v/v) NP40

freshly added protease inhibitor mix (Sigma) at 1:1000 dilution

ChIP lysis buffer II

50 mM HEPES pH 7.9

140 mM NaCl

1 mM EDTA

1% (v/v)TritonX-100

0,1% (w/v) deoxycholic acid sodium salt

0,1% (v/v) SDS

freshly added protease inhibitor mix (Sigma) at 1:1000 dilution

ChIP wash buffer I

20 mM Tris HCl pH 8.1

150 mM NaCl

2 mM EDTA

0.1% (v/v) SDS

1% (v/v) TritonX-100

ChIP wash buffer II

20 mM Tris HCl pH 8.1

500 mM NaCl

2 mM EDTA

0.1% (v/v) SDS

1% (v/v) TritonX-100

ChIP wash buffer III

10 mM Tris HCl pH 8.1

250 mM LiCl

1 mM EDTA

1% (v/v) NP40

1% (v/v) deoxycholic acid sodium salt

Coomassie solution

50% (v/v) methanol

10% (v/v) acetic acid

0,5% (w/v) Coomassie Brilliant Blue R-250

Coomassie destain

20% (v/v) methanol

10% (v/v) acetic acid

Crystal violet solution

0.1% (w/v) crystal violet

20% (v/v) ethanol

DNA loading buffer 6x

40% (w/v) sucrose

0.2% (w/v) Bromphenol Blue

0.2% (w/v) xylene cyanol

10 mM EDTA pH 8.0

EDTA 0.5 M

0.5 M EDTA

adjusted to pH 8.0 using 10 M NaOH

autoclaved

GST sonification buffer

50 mM Tris pH 8.0

50 mM NaCl

1 mM DTT

0.25 mM PMSF

freshly added protease inhibitor mix (Sigma) at 1:1000 dilution

HBS 2x

280 mM NaCl

1.5 mM Na_2HPO_4

50 mM HEPES adjusted to pH 7.05 using 1 M NaOH (at 24 °C)

filtered sterile (0.2 µm) and stored at 4 °C

HEGN lysis buffer 2x

40 mM HEPES KOH pH 7.8

20% (v/v) glycerol

0.4 mM EDTA

0.2% (v/v) NP40

2 mM Na-ß-glycerophosphat

20 mM NaF

20 mM $Na_4P_2O_7$

filtered sterile (0.2 µm) and stored at 4 °C

freshly added 0 - 450 mM KCl and aqua dest ad 1x

and freshly added protease inhibitor mix (Sigma) at 1:100 dilution

and phosphatase inhibitors I and II each at 1:1000 dilution

MES running buffer 20x

4 M Tris

4 M MES

100 mM EDTA

10% (v/v) SDS

MES running buffer 1x

prepared by diluting MES running buffer 20x

with 5 mM sodium bisulfite

stored at 4 °C and heated before use (30 min 56 °C)

NP40 lysis buffer

150 mM NaCl

1% (v/v) NP40

50 mM Tris-HCl pH 8.0

10 mM $Na_4P_2O_7$ (decahydrate)

100 mM NaF

2 mM Na_3VO_4

filtered sterile (0.2 µm) and stored at 4 °C

freshly added protease inhibitor mix (Sigma) at 1:1000 dilution

PBS

137 mM NaCl

2.7 mM KCl

10.1 mM Na_2HPO_4

1.76 mM KH_2PO_4

autoclaved

Plasmid prep buffer 1

TE with RNaseA at 1:1000 dilution

Plasmid prep buffer 2

200 mM NaOH

1% (w/v) SDS

Plasmid prep buffer 3

3.1 M potassium acetate (trihydrate)

adjusted to pH 4.8 using acetic acid

SDS running buffer

25 mM Tris base

250 mM glycine

0.1% (v/v) SDS

SDS sample buffer 3x

187.5 mM Tris HCl pH 6.8

30% (v/v) glycerine

6% (v/v) SDS

0.03% (w/v) Bromphenol Blue

2 M β-mercaptoethanol

SDS separating gel

7.5 - 12.5% (v/v) acrylamide/bisacrylamide

375 mM Tris HCl pH 8.8

0.1% (w/v) SDS

0.1% (w/v) APS

0.1% (v/v) TEMED

SDS stacking gel

4% (v/v) acrylamide/bisacrylamide

125 mM Tris HCl pH 6.8

0.1% (w/v) SDS

0.1% (w/v) APS

0.1% (v/v) TEMED

Sodium bisulfite

1 M sodium bisulfite

Stripping buffer

62.5 mM Tris HCl pH 6.8

2% (v/v) SDS

100 mM β-mercaptoethanol (add freshly)

TAE 50x

2 M Tris base

5.7% (v/v) acetic acid

50 mM EDTA pH 8.0

TAE 1x

prepared by diluting TAE 50x

40 mM Tris-acetate pH 8.0

1 mM EDTA

Tank blot buffer SDS 10x

250 mM Tris base

1.5 M glycine

Tank blot buffer SDS 1x

prepared by diluting Tank blot buffer SDS 10x

with 15% (v/v) methanol

TBS 20x

500 mM Tris base

2.8 M NaCl

adjusted to pH 7.4 using concentrated HCl

TBS-T

prepared by diluting TBS 20x

0.2% (v/v) Tween-20

25 mM Tris pH 7.4

140 mM NaCl

TE

10 mM Tris pH 8.0

1 mM EDTA pH 8.0

autoclaved

TNN lysis buffer

50 mM Tris-HCl pH 7.4

120 mM NaCl

5 mM EDTA

0.5% (v/v) NP40

10 mM $Na_4P_2O_7$ (decahydrate)

100 mM NaF

2 mM Na_3VO_4

filtered sterile (0.2 µm) and stored at 4 °C

freshly added protease inhibitor mix (Sigma) at 1:100 dilution

and phosphatase inhibitors I and II each at 1:1000 dilution

Trypsin solution

0.25% trypsin

5 mM EDTA

22.3 mM Tris pH 7.4

125 mM NaCl

Water

sterile injection water from Ampuwa®

2.9 Consumables and equipment

Consumables such as reaction tubes, cell culture and other plastic products were purchased from Applied Biosystems, Eppendorf, Greiner, Kimberley-Clark, Nunc, Sarstedt, B. Braun, Schleicher und Schüll, Millipore and VWR international.

2.9.1 Equipment

Chemiluminescence imaging	LAS-4000 mini (Fujifilm)
Cell culture incubator	BBD 6220 (Heraeus)
Cell counter	CASY cell counter (Innovatis)

Centrifuges	Galaxy MiniStar (VWR International), Avanti J-26 XP (Beckman Coulter), Multifuge 1S-R (Heraeus), Eppendorf 542 and 5417R (Eppendorf)
Heating block	Dry Bath System (STARLAB)
Incubator shaker	Model G25 (New Brunswick Scientific)
Microscope for cell culture	Axiovert 40CFL (Zeiss)
Microscope for siRNA screen	Operetta High Content Imaging System (Perkin Elmer)
PCR thermal cycler	Mastercycler pro S (Eppendorf)
Photometer	Ultrospec™ 3100 pro UV/Visible (Amersham Biosciences), Spectrofluorometer NanoDrop 3000 (Thermo Scientific)
Power supply	PowerPac HC (Bio-Rad)
Quantitation of RNA	Experion Automated Electrophoresis System (Bio-Rad), StdSens Experion RNA Chip
Quantitative real-time PCR machine	MXp3000P qPCR system (Stratagene), StepOne™ Realtime Cycler (Applied Biosystems)
SDS-PAGE system	Mini-PROTEAN Tetra Cell (Bio-Rad)
Sterile bench	HeraSafe (Heraeus)
Ultrasonifier	W-250 D (Heinemann)
Universal shaker	SM-30 (Edmund Bühler GmbH)
Vortex mixer	Vortex-Genie 2 (Scientific Industries)
Waterbath	ED-5M heating bath (Julabo)
Western blot transfer chamber	PeQlab

2.10   Software

Acrobat™ 9 Pro v9.5.5	Adobe Inc.
Ape plasmid editor v1.17	M. Wayne Davis
Bedtools v2.11.2	Quinlan and Hall, 2010

Bowtie v0.12.7   Langmead, 2010

CLC Sequence Viewer 6   CLC bio

GraphPad Prism v4.0   GraphPad Software

Illustrator™ v14.0.0   Adobe Inc.

Integrated Genome Browser v8.1   Nicol et al., 2009

Mac OS X v10.6.8   Apple Inc.

MACS v1.4.2   Zhang et al., 2008

Microsoft Office 2008 Mac   Microsoft Inc.

Multi Gauge v3.2   Fujifilm

MxPro qPCR Software   Stratagene

Photoshop™v11.0.2   Adobe Inc.

R v2.15.2   R Foundation

Samtools v1.4   Li et al., 2009

Scaffold Viewer 4.0   Proteome Software

SerialCloner 2-6-1   SerialBasics

SeqMiner v1.3.3   Ye et al., 2011

StepOne™ Software v2.3   Applied Biosystems

2.11   Online programs and databases

DAVID   Huang et al. 2009a,b

                      http://david.abcc.ncifcrf.gov/

                      https://main.g2.bx.psu.edu/

GEO   Edgar et al., 2002

                      http://www.ncbi.nlm.nih.gov/geo/

JASPAR   http://jaspar.genereg.net

                      pubmed ID: 17512414 (MA0139.1)

                      and 10497269 (MA0003.2)

MEME Suite	Bailey et al., 2009
	http://meme-suite.org
MSigDB v5.1	Subramanian et al., 2005
	http://www.broadinstitute.org/gsea/msigdb/index.jsp
Primer3 v0.4.0	Rozen and Skaletsky, 2000
	http://frodo.wi.mit.edu/
pubmed	http://www.ncbi.nlm.nih.gov/pubmed
UCSC Table Browser	Karolchik et al., 2004
	http://genome.ucsc.edu/cgi-bin/hgTables?command=start

3   Methods

3.1   Molecular biology methods

3.1.1   Transfection of bacteria with plasmid DNA and plasmid amplification

To transform circular DNA into bacteria for plasmid amplification, competent bacteria were thawed on ice and mixed with 100 µg plasmid DNA or 5 µl ligation mix. After 30 min of incubation on ice, heat shock was performed for 90 s at 42 °C. The bacteria were placed back on ice for one minute. Then 900 µl LB-medium without any antibiotics was added and after one hour of shaking (450 rpm) at 37 °C bacteria were plated on LB agar plates and incubated upside down over night at 37 °C. In the morning the next day plates were stored at 4 °C until clones were picked, either for Mini preparation in 3 ml of LB-medium or for MAXi-preparation in 200 ml of LB-medium using the appropriate antibiotic to select for bacteria that had been successfully transformed. Cultures were incubated shaking 12-24 h at 30 or 37 °C depending on the plasmid backbone.

3.1.2   Isolation of plasmid DNA from bacteria

A large scale MAXi-preparation of plasmid DNA was performed with the JETSTAR 2.0 Plasmid Purification MAXi Kit according to the manufacturer's instructions. The purified plasmid was dissolved in Ampuwa water, diluted to a concentration of 1 mg/ml and stored at -20 °C. For Mini-preparation, the 3 ml of cultivated bacteria were transferred to a reaction tube (2x 1.5 ml), spun down (13,000 rpm, 5 min, RT) and resuspended in 200 µl plasmid prep buffer 1. To lyse the cells 200 µl plasmid prep buffer 2 was added, samples were mixed by inverting and incubated for 5 min at room temperature (RT). Afterwards 200 µl plasmid prep buffer 3 was added for neutralisation. Samples were mixed by inverting the tubes and spun down subsequently (13,000 rpm, 5 min, 4 °C). The supernatant was transferred to a fresh tube and mixed with 420 µl isopropanol to precipitate the DNA, which was then pelleted by centrifugation (13,000 rpm, 15 min, 4 °C). The DNA was washed once with 1 ml of 70% Ethanol, then dried and resuspended in 30 µl Ampuwa water.

3.1.3   Nucleic acid quantitation

The concentration of DNA and RNA in solution was determined with Peqlab's NanoDrop 1000. Purity was determined by assessing the ratio of absorbance at 260 and 280 nm. For pure DNA, A260/280 is ~1.8, for RNA ~2.

3.1.4   Restriction of plasmid DNA Plasmid

DNA from Mini- or MAXi-preparation (5-10 µl or 1 µg for test-digestions and 5 µg for cloning reactions) was hydrolysed in a sequence-specific manner with restriction endonucleases from New England Biolabs (1 µl per 1 µg plasmid DNA) using the recommended reaction buffers

and Ampuwa water. The digestions were incubated at 37 °C, one hour for sequence-specific test-digestions and 3 h for plasmid cloning reactions.

3.1.5   Separation of DNA fragments via gel electrophoresis

DNA fragments of different sizes were separated by agarose gel electrophoresis. Depending on the fragment size, a solution of 0.8-2% agarose was boiled in TAE buffer. 1 mg/ml ethidium bromide was added and the molten agarose was poured into a gel chamber with combs to form sample wells in the gel. DNA samples supplemented with DNA loading buffer were loaded into the wells of the polymerised agarose gel. The size of the nucleotide fragments was determined using 15 µl of the 1 kb DNA Ladder from Invitrogen which was separated next to the samples. Gels were run at 120 V for 1.5 h, afterwards DNA fragments were visualised using a UV transilluminator detecting the DNA via the intercalated ethidium bromide.

3.1.6   DNA extraction and purification from agarose gels

After separating the DNA by gel electrophoresis the fragment of interest was cut out of the gel using a scalpel. The DNA was extracted from the gel using the GeneJET Gel Extraction Kit from Thermo Scientific following the manufacturer's protocol. Purified DNA was eluted using 30 µl Ampuwa water.

3.1.7   Ligation of digested purified DNA fragments into digested vector

Digested purified DNA fragments were covalently attached with the accordingly digested and purified plasmid by means of ligation. Insert and plasmid were incubated in a molar ration of 3:1 or 1:7 in the ligation mix. Ligation was performed in a volume of 10 µl adjusted with Ampuwa water and using the T4 DNA ligase from Fermentas. Samples were incubated over night at 16 °C and at room temperature until transformation into competent bacteria was performed in the afternoon.

3.1.8   Sequencing of plasmids (LGC)

For full-service sequencing of a plasmid, first the ordering sheet was filled in online on the LGC homepage (https://shop.lgcgenomics.com/). Then for each sequencing reaction 1 µg of plasmid was pipetted into an according to the ordering LGC barcode labelled reaction tube, and 2 µl of the appropriate primer (10 pmol/µl) or nothing, if a primer from the list of LGC primers was picked during ordering. Sample volumes were adjusted to 14 or 12 µl of total volume using Ampuwa water and send for sequencing in an LGC envelope.

3.1.9   DNA-Extraction out of Whatman Paper

To extract DNA out of Whatman Paper, the spot with DNA was cut out and put in a reaction tube with 500 µl TE buffer. After an incubation for one hour at 22 °C and 450 rpm

in a Thermo-block, the extracted DNA can be frozen at –20 °C or directly subjected to retransformation in competent bacteria (see methods, section 3.1.1).

3.1.10   Isolation of RNA

For the isolation of total RNA from cultured cells TriFast reagent from Peqlab was used. Cells were harvested as described in section 3.3.1 and pellets were resuspended in 1 ml TriFast. Samples were stored at -80 °C or RNA isolation was continued. Samples were incubated 5 min at room temperature before 200 µl chloroform was added to each sample and the mixture was vortexed thoroughly for 15 s. After 3 more min of incubation the solution was separated into aqueous and organic phase by centrifugation (10 min, 14,000 rpm, 4 °C). The upper, aqueous phase was transferred into a fresh reaction tube and the RNA was precipitated by adding 500 µl of isopropanol, 1 µl glycogen was added to make the pellet non-transparent and clearly visible. Samples were vortexed for 15 s and incubated for at least 20 min on ice. Afterwards the precipitated RNA was pelleted (10 min, 14,000 rpm, 4 °C) and washed twice with 1 ml of 75% ethanol. The final pellet was dried, resuspended in 30 µl Ampuwa water, and the RNA concentration was determined by NanoDrop measurement. Immediately afterwards the RNA was used for cDNA synthesis and the remainder stored at -80 °C.

3.1.11   cDNA synthesis

To quantify specific mRNAs, the RNA was transcribed into complementary DNA (cDNA) by reverse transcription, using random hexanucleotide primers. For that, 2 µg total RNA in a volume of 10 or 20 µl were heated up to 65 °C to dissolve any secondary structures. The cDNA synthesis mix listed below was added and incubated for 10 min at RT, 60 min at 37 °C and 15 min at 70 °C. After cooling the samples down to 4 °C, 450 µl Ampuwa water was added to each generated cDNA sample. Subsequently cDNA was used for qRT-PCR (see methods, section 3.1.12) and stored at -20 °C.

cDNA synthesis mix

10 µl   5x M-MLV (Promega)

5 µl   dNTPs (2.5 mM, Roth)

2 µl   random primer p(dN)6 (2 mg/ml)

0.2 µl   Ribolock (Fermentas)

1 µl   M-MLV reverse transcriptase (200 U/ml, Promega)

             ad 40 or 30 µl Ampuwa water

3.1.12   Polymerase chain reaction (PCR)

The polymerase chain reaction [Mullis et al., 1986] was used to amplify specific regions of DNA for different purposes as described below.

PCR to amplify cDNA for cloning

To generate new expression vectors the gene of interest was amplified based on existing expression vectors. The utilisation of specifically designed primers enabled the addition of new restriction sites and tag-encoding sequences.

Standard PCR setup

5 µl	10x Pfu buffer (Stratagene)
(4 µl	of 25 mM MgSO$_4$ stock solution for Pfu buffer without MgSO$_4$)
1 µl	Pfu polymerase (Stratagene)
100 ng	cDNA template
10 pmol	fwd primer
10 pmol	rev primer
3-5 µl	DMSO
1 µl	dNTPs (10 mM)
	ad 50 µl Ampuwa water

Standard PCR thermal cycling profile

temperature	time	number of cycles
95 °C	2 min	1
95 °C	30 s	
53 - 65 °C*	30 s	30
72 °C	2 min/kb amplicon	
72 °C	10 min	1
4 °C	∞	

* dependent on GC-content of primers used (Tm − 5 °C)

PCR based site directed mutagenesis

To mutate single bases in a target DNA construct 5' and 3' PCR template primers were chosen encoding the desired target sequence. PCR samples were pipetted according to the standard PCR setup and amplified using the mutagenesis PCR thermal cycling profile. As such, a product mostly containing the modified bases was generated. To remove residual wild type template DNA, the PCR product was digested with the enzyme *DpnI* (1 h, 37 °C), which hydrolyses only methylated DNA. 5 µl sample with 1 µl 6x Loading Buffer were loaded on an 0.8% agarose gel to check, if the PCR worked. Successfully amplified PCR products were transformed into competent bacteria and amplified and purified in Mini-preparations as usual. Minis were sequenced with the appropriate primers to check for correct mutagenesis.

Mutagenesis PCR thermal cycling profile

temperature	time	number of cycles
95 °C	30 s	1
95 °C	30 s	
55 °C	1 min	30
72 °C	2 min/kb amplicon	
72 °C	10 min	1
4 °C	∞	

Quantitative reverse transcriptase PCR (qRT-PCR)

To quantify specific mRNA levels the cDNA synthesised by reverse transcription (see methods, section 3.1.11) was amplified by qRT-PCR. The measurement was carried out with the Mx3000P qPCR system (Stratagene) or the StepOne™ Realtime Cycler (Applied Biosystems). The basis of qRT-PCR is fluorescent monitoring of DNA amplification, from which target DNA concentrations can be determined from the fractional cycle at which a threshold amount of amplicon DNA is produced. The calculation of the relative cycle threshold (CT) value was performed by the software supplied by the manufacturer. For normalisation the housekeeping gene beta-2-microglobulin was used. All qRT-PCR reactions were performed in triplicates to calculate the standard deviation according to the Gaussian law of error. For each reaction 10 µl of ChIP DNA or 1:10 diluted cDNA were pipetted into the wells of 96-well qRT-PCR plates. Afterwards a mix of 7 µl of ABsolute qRT-PCR SYBR Green Mix from Thermo Scientific, 2 µl of forward and reverse qRT-PCR primer mix (each 10 pmol/µl) and 1 µl of Ampuwa water was added into each well.

qRT-PCR thermal cycling profile with meltcurve

temperature	time	number of cycles
95 °C	15 min	1
95 °C	15 s	
60 °C	20 s	40
72 °C	15 s	
95 °C	15 s	1
60 °C	1 min	1
60 - 95 °C; stepwise	15 s	0.3 °C steps
95 °C	15 s	1

3.1.13 pRSI12-DECIPHER shRNA cloning

The shRNA sequences cloned in pRSI12 are listed in section 2.3.2. For annealing of the
oligonucleotides to get double stranded DNA with the appropriate overhangs 25 µl of 2x
Annealing buffer was mixed with 5 µl of each oligonucleotide, forward and reverse (100 µM
stock solution), and 15 µl Ampuwa water. In the PCR Thermo Cycler samples were first
denatured at 95 °C and then the temperature was step-wise decreased in 3 °C-steps from
95 °C to 87 °C with 3 min of incubation each, followed by a 10 min incubation at 85 °C.
Afterwards the temperature was again step-wise decreased in 3 °C-steps from 82 °C to 25 °C
with 2 min of incubation each, ending with a 12 °C step lasting forever. Annealed oligonuc-
leotides were ligated into the pRSI12-DECIPHER plasmid digested with *BbsI*. For ligation
the protocol described in section 3.1.7 was conducted using 2 µl of annealed oligonucleotides.

3.1.14 Phenol/chloroform extraction of DNA

To extract DNA 1 volume of phenol/chloroform/isoamylalcohol (25:24:1) was added to each
sample and samples were vortexed vigorously. After 5 min of centrifugation at 14,000 rpm
and RT two phases were separated, the upper phase was transferred into a fresh reaction
tube and 1 µl glycogene (Glycoblue), 50 µl of 3 M NaAc pH 5.2 and 1 ml of ice cold 100%
ethanol were added. Samples were vortexed and incubated at least 30 min at -20 °C and
centrifuged at 14,000 rpm and 4 °C for 30 min. Pelleted DNA was washed once with 500
µl ice cold 70% ethanol (14,000 rpm, 10 min, 4 °C) and then dried for 5 min at RT before
resuspension in TE buffer or Ampuwa water according to the protocol.

3.1.15 RNA-Seq. Library preparation

For RNA-Seq. another protocol was used to harvest and extract RNA than the one described
in section 3.1.10. To extract RNA the RNEasy kit from Qiagen (Cat.No.: 74106) was used

following the manufacturers instructions. Importantly cells plated on 10 cm dishes were scraped in RLT buffer with ß-mercaptoethanol without washing with PBS, shock frozen in liquid nitrogen and stored at -80 °C. The day of RNA extraction the cells frozen in RLT buffer were thawed and homogenised using a syringe with a 20 G needle (6x passages). A DNaseI on column digestion was performed as described in the manual. After RNA extraction concentrations were measured by Nandrop and cDNA was prepared as described in section 3.1.11. Selected targets were investigated by qRT-PCR or Western Blot and if the experiment worked as expected, an Experion RNA StdSense chip was performed using the kit from BioRad (Cat.No.:700-7103) to assess the purity of the samples. If the purity was good (RQI 9-10), RNA-Seq. library preparation was performed following the NEBNext® Ultra™ RNA Library Prep Kit for Illumina® protocol. The purity of the prepared samples was accessed using a DNA 1k Experion Chip according to the manufacturers instructions. Samples for sequencing were adjusted to an equimolare concentration and denatured before loading on an Illumina flow cell according to the manufacturers instructions.

3.2   Cell biology methods

All cell culture work was performed at a sterile workbench. Cells were cultivated in CO_2 incubators at 37 °C, 95% relative humidity and 5% CO_2.

3.2.1   Thawing cells

Frozen cells were stored in cryo vials at -80 °C (short storage) or in liquid nitrogen (long-term storage). Cells were thawed in the evening by placing the cryo vials into a 37 °C water bath. As soon as there was only small clump of frozen cell suspension visible, cells were resuspended with ~700 µl warm (37 °C) Basal medium and transferred onto a 15 cm dish with 35 ml warm Basal medium (previously prepared and placed in the incubator for ~20 min). In the morning the next day, medium was changed. Cells were passaged twice in Basal medium before using them in experiments.

3.2.2   Passaging cells

Cells were passaged when culture dishes were nearly confluent. The cultivation medium was removed and cells were washed with PBS. An appropriate amount of trypsin solution was added (e.g. 1 ml on a 10 cm dish) and the dishes were incubated for ~5 min in the incubator to enhance the trypsin-activity. By tilting the dishes the cell detachment was checked before resuspending the cells in fresh Basal medium stopping the enzymatic activity of trypsin. Singularised cells were splitted (1/4–1/20 v/v) onto a new dish with fresh medium or transferred into a 50 ml Falcon tube for counting. For S1 cells counting was performed using the CASY cell counter following the manufacturer's protocol. S2 cells were counted manually with a Neubauer counting chamber. After counting the cells were seeded for experiments according to their size and proliferation rate in relation to the length

of the experiment.

3.2.3   Freezing cells

For freezing cells were detached with trypsin solution as described above, resuspended in fresh medium and then pelleted (5 min, 1200 rpm, 21 °C). The cells were resuspended in 1 ml freezing medium containing DMSO, transferred to a cryo vial and then slowly frozen at -80 °C using a MrFROSTY freezing container. After 24 h the cells were stored in a liquid nitrogen storage tank.

3.2.4   Transfection of plasmid DNA

Calcium phosphate method

24 h prior to transfection cells were plated at specific density (SH-EP: 0.3 million; SK-N-BE: 0.5 million; IMR-5, IMR-32: 1.5-2 million per 10 cm dish). Some h ($\sim$4 h) before transfection neuroblastoma cells cultured in RPMI-based medium were washed with PBS and medium was changed to DMEM-based medium (less medium than usual, e.g. 8 ml on a 10 cm dish). The reason for changing the medium to DMEM is that RPMI medium interferes with calcium phosphate mediated transfection. For each transfection two 50 ml Falcon tubes were prepared, tube A containing 500 µl HBS 2x (pH 7.05) and tube B containing 50 µl CaCl$_2$ of sterile 2.5 M stock solution and up to 30 µg plasmid DNA of 1 µg/µl MAXi preparation adjusted to 500 µl total volume using sterile Ampuwa water. After preparation of the tubes, solution B was slowly dropped into solution A while vortexing it in the sterile workbench. The transfection solution was vortexed with closed lid for another 15 s. Immediately afterwards the dish for transfection was taken from the incubator and the solution was dropped carefully onto the cells. After 14–16 h cells were washed twice with PBS before changing the medium back to RPMI-based medium and transfection efficiency, monitored by GFP-encoding plasmid DNA, was checked 24–48 h post transfection. Transfected cells were harvested 48 h post transfection.

Polyethylenimine (PEI) method

24 h prior to transfection cells were plated at specific density (SH-EP: 0.3 million; SK-N-BE: 0.5 million; IMR-5, IMR-32: 1.5-2 million per 10 cm dish). Shortly before transfection cells were washed with PBS and medium was changed to medium with low serum (2%) and without antibiotics (less medium than usual, e.g. 6 ml on a 10 cm dish). Transfections were carried out in the afternoon. For each transfection two 1.5 ml reaction tubes were prepared, tube A containing up to 25 µg plasmid DNA of 1 µg/µl MAXi preparation in 700 µl Opti-MEM® I and tube B containing PEI transfection reagent in 700 µl Opti-MEM® I (DNA:PEI ratio of 5:4, 1:1 or 1:3). After incubating the PEI- Opti-MEM® I dilution for 5 min at RT, solutions from tube A and B were combined by dropping solution from tube B in tube A. Combined solutions were mixed by inverting the tubes several times and

incubated for 20 min at RT before dropping the transfection solutions onto the cells. 4 h later cells were washed once with PBS before changing the medium back to Basal medium with antibiotics and transfection efficiency, monitored by GFP-encoding plasmid DNA, was checked 24–48 h post transfection. Transfected cells were harvested 48 h post transfection.

Lipofectamine™ 2000 method

48 h prior to transfection cells were plated at specific density (SH-EP: 0.3 million; SK-N-BE: 0.5 million; IMR-5, IMR-32: 1.5-2 million per 10 cm dish). 24 h prior to transfection cells were washed with PBS and medium was changed to medium without antibiotics (less medium than usual, e.g. 8 ml on a 10 cm dish). Transfections were carried out in the afternoon. For each transfection two 2 ml reaction tubes were prepared, tube A containing 16 µg plasmid DNA of 1 µg/µl MAXi preparation in 1 ml Opti-MEM® I and tube B containing 40 µl Lipofectamine™ 2000 in 1 ml Opti-MEM® I. Lipofectamine™ 2000 was gently mixed before usage and after carefully mixing it with Opti-MEM® I, the mix was incubated 5 min at RT before dropping 1 ml of it in tube A. The combined DNA-Lipofectamine™ 2000 transfection solution was mixed by inverting the tube several times and incubated for 20 min at RT. Afterwards the transfection solution was carefully dropped onto the cells. After 14–16 h cells were washed once with PBS before changing the medium back to Basal medium with antibiotics and transfection efficiency, monitored by GFP-encoding plasmid DNA, was checked 24–48 h post transfection. Selection of transfected cells was started 48–72 h post transfection using the appropriate cytostatic.

siRNA transfection with RNAiMAX

24 h prior to transfection cells were plated at specific density (SH-EP: 0.3 million; SK-N-BE: 0.5 million; IMR-5, IMR-32: 1.5-2 million per 10 cm dish). On the day of transfection cells were washed with PBS and medium was changed to medium without antibiotics (less medium than usual, e.g. 8 ml on a 10 cm dish). Transfections were carried out in the afternoon. For each transfection two 2 ml reaction tubes were prepared, tube A containing 10 µl siRNA of 20 µM stock solution in 1 ml Opti-MEM® I and tube B containing 20 µl RNAiMAX in 1 ml Opti-MEM® I. RNAiMAX was gently mixed before usage and after carefully mixing it with Opti-MEM® I, the mix was incubated 5 min at RT before dropping 1 ml of it in tube A. The combined RNAiMAX transfection solution was mixed by inverting the tube several times and incubated for 20 min at RT. Afterwards the transfection solution was carefully dropped onto the cells. After 14–16 h cells were washed once with PBS before changing the medium back to Basal medium with antibiotics. Transfected cells were harvested 48 or 72 h post transfection.

3.2.5   Viruspreparation and Infection of adherent cells

Retrovirus production

24 h prior to transfection Phoenix/PlatE cells were plated at 4-5 million per 10 cm dish. Cells were transfected following the protocol for the calcium phosphate method described above and using 40 µg of the desired plasmid DNA for each transfection. After 14 – 16 h cells were washed twice with PBS before changing the medium back to 7 ml of DMEM-based medium and transfection efficiency, monitored by GFP-encoding plasmid DNA, was checked 24-48 h post transfection. 48 h post transfection first viral supernatant was harvested by taking the 7 ml of medium into a 15 ml Falcon tube. The virus was first frozen in liquid nitrogen and then stored at -80 °C until infection. Afterwards 7 ml of fresh DMEM-based medium were carefully added. 66 h post transfection second viral supernatant was harvested by taking the 7 ml of medium into a 15 ml Falcon tube. The virus was first frozen in liquid nitrogen and then stored at -80 °C until infection. The dishes were discarded.

Retroviral infection

24 h prior to infection cells were plated at specific density (SH-EP: 0.3 million; SK-N-BE: 0.5 million; IMR-5, IMR-32: 1.5-2 million per 10 cm dish). Before infection the frozen retroviral supernatant was thawed by putting the 15 ml Falcon tubes into a 37 °C water bath ($\sim$5 min). Subsequently the thawed virus was centrifuged at 1500 rpm for 5 min to pellet cell debris and filtered sterile in the workbench (0.45 µm filter). After removing the medium from the dishes for infection, one Falcon tube of sterile filtered viral supernatant (preferentially first harvest) was poured onto each dish and 4 µg/ml polybrene (5 µl of 4 mg/ml stock solution) were added. After 14–16 h 5 ml of Basal medium were added per 10 cm dish. Selection of infected cells was started 48–72 h post infection using the appropriate cytostatic.

Lentivirus production

24 h prior to transfection HEK293TN cells were plated at 4.5-5 million per 10 cm dish. Cells were transfected following the protocol for the PEI method described above using 2.8 µg psPAX2, 1.4 µg pMD2.g of packaging plasmids and 11.1 µg of the desired plasmid DNA together with 30 µl of PEI for each transfection. After transfection cells were S2 and accordingly incubated and handled in S2 cell culture. After 14–16 h the medium was changed to 6 ml of DMEM-based medium with antibiotics and normal serum (5%). 38–40 h post transfection first viral supernatant was collected in a 50 ml Falcon tube and 6 ml medium was added. The collected virus was stored at 4 °C. 42–48 h post transfection second viral supernatant was collected in the same 50 ml Falcon tube as 8 h before and 6 ml medium was added. 56–58 h post transfection third viral supernatant was collected in a 50 ml Falcon tube and the dishes were discarded. The collected virus filtered sterile (0.45 µm filter), aliquoted in cryo vials, frozen in liquid nitrogen and stored at -80 °C.

Lentiviral infection

24 h prior to infection cells were plated at specific density (SH-EP: 0.3 million; SK-N-BE: 0.5 million; IMR-5, IMR-32: 1.5-2 million per 10 cm dish). Before infection the frozen lentiviral supernatant was thawed by putting the cryo vials in 15 ml Falcon tubes into a 37 °C water bath (∼5 min). Subsequently the medium was removed from dishes plated for infection, then 5 ml of Basal medium were added together with 0.02-2 ml of thawed virus (as well as control without virus!) and 4 µg/ml polybrene (5 µl of 4 mg/ml stock solution) onto each dish. After 14–16 h the medium was changed to 10 ml Basal medium and 38–40 h post infection selection of infected cells was started using the appropriate cytostatic. Successful selection was controlled by a control dish without virus addition, ∼24 h after adding the cytostatic all control cells should have died. Selection was interrupted by washing the infected cells once with PBS and adding Basal medium without cytostatic. After successful selection infected cells were used for experiments.

3.2.6   Generation of cell clones

After successful Lipofectamine™ 2000 transfection and retro- or lentiviral infection, cell clones could be isolated from the genetically modified pool to generate a stable cell line. The pool of cells was split before or after selection with the appropriate antibiotic in different ratios ranging from 1:500–1:20 on 15 cm dishes and the singularised cells were cultivated on the dish with medium changes (with or without antibiotic) every three days until a clonal colony was formed, which was visible without the microscope. Each colony was marked on the dish bottom and then transferred to one well on a 96-Well plate either by scraping it off using a 200 µl pipette or by trypsinisation using an autoclaved metal ring, which was dipped in vaseline and placed onto the colony.

3.3   Protein biochemistry methods

3.3.1   Harvesting of cells for Western Blot or RNA isolation

Protein extraction or RNA isolation was performed on ice. First medium was removed from cells cultured on 10 cm dishes and afterwards cells were washed in ice cold PBS. Then cells were scraped of the cell culture dish in 700 µl ice cold PBS and transferred into a reaction tube (cells cultured on one 10 cm dish were usually used for protein and RNA extraction). After spinning down scraped cells (1500 rpm, 5 min, 4 °C), the supernatant was removed and the cell pellet was either resuspended in 1 ml TriFast reagent for RNA extraction or frozen as pellet for protein extraction. Samples were frozen in liquid nitrogen to be stored at -80 °C or directly subjected to lysis or RNA extraction (see methods, section 3.1.10).

3.3.2   Protein extraction (NP40 cell lysis)

To isolate total protein cell pellets were resuspended in 25-200 µl NP40 lysis buffer with freshly added protease inhibitor mix (1:1000) (25 µl if low density, 200 µl if high density). Subsequently the cells were shock frozen in liquid nitrogen for 30 s and then incubated for 1 min at 37 °C in a water bath using swimming rack. This freezing/thawing step was repeated twice. Afterwards the samples were incubated for 10 min on ice, then the cell debris were pelleted (13,000 rpm, 5 min, 4 °C) and the supernatant was transferred into new reaction tube. Samples were used for SDS-PAGE or frozen in liquid nitrogen and stored at –80 °C.

3.3.3   Determination of protein concentration by the Bradford method

Protein concentrations were determined according to Bradford [1976]. Water and Bradford solution was mixed in a 1:1 ration and 1 ml was pipetted into each Semi-Cuvette. Subsequently 1 µl of the protein sample was added, each sample was measured in triplicate. After mixing by pipetting up and down, the absorption was measured at a wavelength of 595 nm using an appropriate reference. The mean absorption from each sample was calculated and this was compared to a previously obtained standard curve to calculate the protein concentration.

3.3.4   Harvest and protein extraction for immunoprecipitation (IP)

Harvest, protein extraction and IP were performed on ice. For harvesting culture medium was removed, cells were washed once with ice cold PBS and scraped in 700 µl or 1-2 ml (15 cm dish) ice cold PBS, equivalent cells were pooled in 15 ml falcons. After pelleting cells for 10 min at 1500 rpm and 4 °C, the supernatant was aspirated and samples were frozen in liquid nitrogen to be stored at -80 °C or directly subjected to lysis. Cell lysis for IP was performed in 1 ml of 1x HEGN lysis buffer with 140 mM KCl (including protease inhibitor mix at 1:100 and phosphatase inhibitor I and II each at 1:1000 dilution). Following resuspension in 1x HEGN lysis buffer samples were sonified on ice supplemented with ethanol 4x 5 s at 20% amplitude with a pause of 10 s between each sonification. If cell density was high, the sonification procedure was performed twice with 1 min pause in between. Samples were incubated on ice for 30 min and then centrifuged 10 min at 4700 rpm and 4 °C. Supernatants were transferred from the 15 ml falcons into reaction tubes and centrifuged 10 min at 13,000 rpm and 4 °C to clear lysates from insoluble cell debris. This step was repeated until lysates were cleared, then the Bradford assay was performed to determine protein concentrations (see methods, section 3.3.3).

IP using Protein A/G sepharose

For IP 1-2 mg lysate was prepared in 1 ml 1x HEGN lysis buffer with 140 mM KCl, (including protease inhibitor mix at 1:100 and phosphatase inhibitor I and II each at 1:1000 dilution). An input sample was taken for each IP sample (e.g. 20 µl of 1 mg/ml lysate solution = 2%)

and 1/3 volume 3x SDS sample buffer was added. Input control samples were heated for 10 min at 95 °C, cooled down 90 s on ice and stored at -20 °C until SDS-PAGE was performed. To each IP sample 2-4 µg of antibody (IP antibody or control IP antibody from same species, or even same subtype) were added and samples were incubated circulating O/N at 4 °C. For IPs with ethidium bromide treatment 1 µg/ml of ethidium bromide solution were added. The next day sepharose beads were washed twice with 1 ml 1x HEGN lysis buffer with 140 mM KCl (5 min, 1700 rpm, 4 °C). For each IP sample 50 µl of protein A or G (depends on the species antibodies were derived from) sepharose suspension (contains 50% beads = 25 µl) were prepared. During washing steps supernatant was removed using a 0.5 mm needle and a vacuum pump. After washing, sepharose beads are resuspended in the IP sample containing antibody and lysate and incubated circulating for 2-3 h at 4 °C. Then IP samples are centrifuged 5 min at 1700 rpm and the same volume like the input control sample the day before is taken from the supernatant and further processed like input control. Remaining supernatant was sucked off completely and samples were washed three times with 1 ml 1x HEGN lysis buffer with 140 mM KCl (2 min, 1700 rpm, 4 °C) (0.5 mm needle). To elute immunoprecipitated proteins sepharose beads were resuspended in 50 µl of 3x SDS sample buffer and IP samples were boiled for 10 min at 95 °C, cooled down on ice for 90 s and stored at − 20 °C until SDS-PAGE. Before performing SDS-PAGE samples were boiled another 5 min at 95 °C.

IP using Anti-HA agarose

First 1-2 mg protein lysate was prepared in 1 ml 1x HEGN lysis buffer with 140 mM KCl (including protease inhibitor mix at 1:100 and phosphatase inhibitor I and II each at 1:1000 dilution) for each IP and an input control sample was taken (1-2%). Second for each sample 40 µl of Anti-HA Agarose suspension were prepared by washing twice with 1 ml 1x HEGN lysis buffer with 140 mM KCl as described before (see methods, section 3.3.4). Then the agarose was resuspended in the prepared 1 ml of lysate HEGN-solution and incubated circulating for 4 h or O/N at 4 °C. Afterwards the supernatant control sample was taken and the IP samples were washed as described before. For elution Anti-HA agarose was resuspended in 30 µl HA-peptide solution (including protease inhibitor mix at 1:300 dilution) and incubated 15 min at 30 °C with flipping the reaction tubes 3-5 times during the incubation time. To remove the agarose, samples were centrifuged 5 s at 12,000 rpm at RT and the supernatant was carefully transferred to Micro Bio-Spin Chromatography Columns (BioRad #732-6204), which were spun 4 min at 3263 rpm at RT. Then 1/3 volume of 3x SDS sample buffer was added to the eluat and 50 µl of 2x SDS sample buffer to the agarose. IP samples were boiled for 10 min at 95 °C, cooled down on ice for 90 s and stored at −20 °C until SDS-PAGE. Before performing SDS-PAGE samples were boiled another 5 min at 95 °C.

IP for mass spectrometry (MS) using Anti-HA agarose

HA-tagged N-MYC variants and interacting proteins were purified via Anti-HA agarose and HA-peptide elution for mass spectrometric analysis similar to the protocol described before. To avoid keratin contaminations all solutions were used fresh and filtered sterile and sterile, plugged pipette tips and pipettes were used. The sonification procedure was carried out 3x with 1 min pause in between. For each IP 10 mg of protein were used, 100 µl Anti-HA agarose and 50 µl HA-peptide solution (including protease inhibitor mix at 1:25 dilution). After elution 37 µl eluat were obtained, 33 µl were supplemented with 11 µl 4x NuPAGE® LDS sample buffer from Life Technologies for MS and the remaining 3 µl were loaded on an SDS-gel to verify that the IP was successful. MS was carried out in the group of Andreas Schlosser at the Rudolf Virchow Center (RVZ) at the University of Würzburg. The samples for MS were reduced by adding NuPAGE® Reducing Agent (DTT) to a final concentration of ∼50 mM and proteins were denatured for 10 min at 70 °C. After cooling the samples down to RT the alkylating reagent Iodoacetamide (IAA) was added to a final concentration of ∼120 mM and samples were incubated for 20 min in the dark at RT before they were loaded on ready-made NuPAGE® Novex 4-12% Bis-Tris gels (Life Technologies) with MOPS buffer. The Gel was placed under a sterile workbench and run according to manufacturer's instructions. Afterwards the gel was stained for 45 min with Simply Blue™ Safe Stain (Life Technologies) and each gel lane was cut into 15 bands. Cut gel bands were chopped and destained with 70% acetonitrile in 100 mM NH_4HCO_3 (pH 8.0). Then destained gel bands were shrunk with 100% acetonitrile and dried in a vacuum concentrator (Concentrator 5301, Eppendorf). Dried gel pieces were resuspended and digested in 100 mM NH_4HCO_3 (pH 8.0) containing 0.1 µg trypsin (Trypsin Gold, Mass Spectrometry Grade, Promega) overnight at 37 °C. NanoLC-MS/MS analysis was performed on an LTQ-Orbitrap Velos Pro (Thermo Scientific) equipped with an EASY-Spray Ion Source and coupled to an EASY-nLC1000 (Thermo Scientific). After the peptides were loaded on a trapping column (2 cm x 75 µm ID. PepMap C18 3 µm particles, 100 Å pore size), they were separated on an EASY-Spray column (25 cm x 75 µm ID, PepMap C18 2 µm particles, 100 Å pore size) with a 30 min linear gradient from 3% to 30% acetonitrile and 0.1% formic acid. First, MS scans were acquired in the Orbitrap analyser with a resolution of 30,000 at m/z 400 and second, MS/MS scans were acquired in the Orbitrap analyser with a resolution of 7,500 at m/z 400 using HCD fragmentation with 30% normalised collision energy. A TOP5 data-dependent MS/MS method was used and lock mass option was applied for internal calibration in all runs. For calibration background ions from protonated decamethylcyclopentasiloxane (m/z 371.10124) were used. For raw data processing and for generating peak lists Mascot Distiller 2.4 (Matrix Science) was utilised with standard settings for the Orbitrap Velos (high/high settings). For database searching Mascot Server 2.4 was used with the following parameters: a peptide mass tolerance of 8 ppm, an MS/MS mass tolerance of 0.02 Da, an enzyme setting of "trypsin" with 3 missed cleavage sites allowed for trypsin, a fixed modification of carbamidomethyl (C) and the following variable modifications: Gln->pyroGlu (N-term. Q)

and oxidation (M). Afterwards, database searching was performed against UniProt human database and results were imported into Scaffold Viewer 4.0, in which identified peptides and proteins were filtered using a peptide probability threshold and a protein probability threshold of 95%.

IP using Dynabeads® Protein A/G or MyOne^{TM} Streptavidin C1

First for each IP Dynabeads® (10 µl of Dynabeads® per µg antibody) were washed twice with 1 ml of 5 mg/ml BSA in PBS. Then beads were resuspended in 500 µl of 5 mg/ml BSA in PBS, antibodies were added (usually 2 µg per IP) and samples were incubated for ~6 h rotating at 4 °C. Afterwards the supernatant was removed, beads were washed twice with 1 ml of 5 mg/ml BSA in PBS and resuspended in 100 µl of lysis buffer. Then the lysate was added (usually 1 mg protein lysate in 1 ml of lysis buffer including protease inhibitor mix at 1:100 and phosphatase inhibitor I and II each at 1:1000 dilution) and samples were incubated O/N rotating at 4 °C. The next day beads were washed 3x with 1 ml of lysis buffer, resuspended in 50 µl of 2x SDS sample buffer boiled for 10 min at 95 °C for elution, cooled down on ice for 90 s and stored at –20 °C until SDS-PAGE. Before performing SDS-PAGE samples were boiled another 5 min at 95 °C.

Peptide pull-down using Dynabeads® MyOne^{TM} Streptavidin C1

For each pull-down 10 µl MyOne^{TM} Streptavidin C1 Dynabeads® were transferred into a low binding reaction tube and washed 4x with 500 µl PBS containing 0.01% Tween-20 using a magnetic rack. Beads were resuspended in 190 µl TBS with 2% BSA (10% stock in TBS) and 0.05% NP40 (0.5% stock in TBS) and 20 µg biotinylated peptide were added. After an incubation of 30 min circulating at RT, samples were washed 4x with 500 µl PBS containing 0.01% Tween-20 and resuspended in 1x HEGN lysis buffer with 140 mM KCl (including protease inhibitor mix at 1:100 and phosphatase inhibitor I and II each at 1:300 dilution). For each pull-down 1-2 mg protein lysate was added leading to a total volume of 500 µl and an input control sample was prepared from the same lysate (2% lysate amount used for pull-down) as described before. Samples were incubated 2.5 h circulating at 4 °C and subsequently washed 4x with 500 µl lysis buffer (1x HEGN with 140 mM KCl and protease inhibitor mix 1:100 and phosphatase inhibitors I and II 1:300). Elution was performed in 40 µl 1x SDS sample buffer by boiling the samples at 95 °C for 10 min. Then samples were cooled down on ice for 90 s and stored at – 20 °C until SDS-PAGE. Before performing SDS-PAGE samples were boiled another 5 min at 95 °C.

3.3.5   SDS polyacrylamide/Bis-Tris gel electrophoresis (SDS-PAGE)

Discontinuous SDS-PAGE (Sodium dodecyl sulfate polyacrylamide gel electrophoresis) was used to separate proteins according to size [Laemmli, 1970]. Protein lysates were filled up with lysis buffer to an equal volume and mixed with half the volume of 3x SDS sample

buffer. Then samples were incubated 5 min at 95 °C, cooled down on ice for 90 s and spun down as were eluats of immunoprecipitations and peptide pull-downs. The protein samples were loaded into the wells of an SDS polyacrylamide or a Bis-Tris gel consisting of a 7.5-15% stacking gel and a 4% resolving gel. The PageRuler Pre-Stained Protein Ladder or the HiMark$^{\text{TM}}$ Pre-Stained HMW Protein Standard was used as a size marker. The electrophoresis was carried out using a Bio-Rad SDS-PAGE chamber with SDS or MES 1x running buffer, first at 80 V for 30 min, then at 120 V for 90–120 min.

3.3.6 Western blot

After separating via SDS-PAGE proteins were transferred by electroblotting onto a PVDF membrane using a tank blot system. A PVDF membrane the size of the SDS/Bis-Tris gel was incubated in methanol or isopropanol for 1 min and then equilibrated in tank blot buffer or Bis-Tris blot buffer 1x for another 2 min. Gel and membrane were neatly layered on top of each other and fixed between Whatman filter papers and one sponge on each side in a Western blot transfer chamber (PeQlab) filled with 1x Tank blot buffer or Bis-Tris blot buffer. The electrophoretic protein transfer was carried out at 250 mA for 2-4 h depending on protein size. The membrane with immobilised proteins was blocked in blocking solution gently shaking for at least 30 min, then cut into pieces if several proteins from the same membrane were to be visualised. The membrane pieces were incubated overnight with a dilution of primary antibody in blocking solution in 50 ml falcon tubes on a roller conveyor at 4 °C, then washed 5x 10 min gently shaking in TBS-T and incubated with secondary antibody in blocking solution in 50 ml falcon tubes for 90 min on a roller conveyor at RT. After washing 5x 5 min gently shaking in TBS-T, the proteins of interest were visualised via chemiluminescence, induced by the horseradish peroxidase coupled to the secondary antibody. To trigger a specific chemiluminescent signal the Immobilon Western Chemiluminescent HRP Substrate from Millipore was used according to the manufacturer's instructions, the signal was detected with the ImageQuant LAS 4000 imager (Fujifilm Global).

3.3.7 Stripping antibodies from PVDF membranes

To release antibodies from a PVDF membrane covered with immobilised proteins, the membrane was washed once with TBS-T after protein visualisation and then incubated in stripping buffer for 30 min in a glass chamber placed in a 60 °C water bath with rocking. The membrane was washed 3x 10 min with TBS-T, blocked and incubated with primary and secondary antibodies as described in section 3.3.6.

3.3.8 TNT® in vitro translation, recombinant protein expression and GST-Assay

For in vitro translation of cDNA constructs cloned into the pcDNA3 plasmid the TNT® Quick Coupled Transcription/Translation Systems kit from Promega was used following the manufacturers manual for "Standard Reaction" and supplementing the missing methionine.

From each reaction 1–10 µl were boiled with 1/3 of volume of 3x SDS sample buffer for 5-10 Min at 95 °C, cooled down on ice for 90 s and stored at –20 °C until SDS-PAGE. For GST-Assay 10 µl from each reaction were directly added to 200 µl of GST-Aurora-A or GST-control coupled to Glutathione Sepharose^{TM} 4B beads and incubated for 2 h rotating at 4 °C in 500 µl 1x HEGN lysis buffer with 200 mM KCl and 0.5 mg/ml BSA. Afterwards samples were washed 3x with 1 ml of 1x HEGN lysis buffer with 200 mM KCl, resuspended in 50 µl 2x SDS sample buffer, boiled for 5-10 Min at 95 °C, cooled down on ice for 90 s and directly loaded on an SDS gel for SDS-PAGE.

For coupling GST-tagged proteins to Glutathione Sepharose^{TM} 4B beads proteins are cloned into bacterial expression plasmids (pGEX-6P-1) and expressed in competent BL21 bacteria (recombinant protein expression). First a 20 ml clonal pre-culture was inoculated and incubated shaking O/N at 37 °C, then a main-culture (1 l for GST-Aurora-A and 200 ml for empty control vector (pGEX-6P-1) was inoculated with 10 ml of pre-culture and incubated shaking at 37 °C until an OD of 600 nm was reached. GST-protein expression was induced via addition of 1 µM Isopropyl-β-D-thiogalactopyranosid (IPTG), before a pre-induction test-aliquot was taken (P0). GST-Aurora-A expression was induced over night shaking at 16 °C, GST-control expression was induced for 3 h shaking at 37 °C. Afterwards a post-induction test-aliquot was taken (P1) and samples were transferred into tubes for centrifugation for 10 min at 4000 rpm and 4 °C. Pellets were resuspended in 5 ml PBS (including protease inhibitor mix at 1:1000 and 200 µg/ml lysozyme) and divided into 4 ml aliquots in 15 ml Falcon tubes for sonification. Samples were sonified on ice supplemented with ethanol 8x 15 s at 20% amplitude with a pause of 59.9 s between each sonification, 40 µl Triton X-100 was added to each tube and tubes were incubated 50 min rotating at 4 °C. Then another test-aliquot was taken (P2) and samples were transferred into tubes for ultra-centrifugation. After centrifugation (13,000 rpm at 4 °C for 10 min) supernatants were pooled in one 50 ml Falcon tube for each sample, a test-aliquot was taken (P3) and the pellets were resuspended in PBS and pooled in one 15 ml Falcon tube for each sample (GST-Aurora-A 12.5 ml and GST-control 5 ml), a test-aliquot was taken as well (P4). Then Glutathione Sepharose^{TM} 4B beads were prepared. For each sample 300 µl bead suspension were washed twice with 1 ml of PBS (3000 rpm, 3 min, 4 °C) and resuspended in 300 µl PBS. After another centrifugation (4700 rpm, 10 min, 4 °C) GST-Aurora-A and GST-control supernatants were added to washed Glutathione Sepharose^{TM} 4B beads and incubated O/N rotating at 4 °C. The next day a test-aliquot was taken (P5) and samples were centrifuged at 3000 rpm at 4 °C for 3 min, supernatant was removed. Each sample was resuspended in 1 ml PBS, transferred to a 1.5 ml reaction tube and washed 3x with 1 ml PBS (3000 rpm, 3 min, 4 °C) rotating 5 min at 4 °C in between washing steps. After each washing step a test-aliquot was taken (P6–8). After washing samples were resuspended in 1 ml of 1x HEGN lysis buffer with 200 mM KCl and frozen at -20 °C in 100 µl aliquots. P0 - P8 test –aliquots were supplemented with 3x SDS sample buffer, boiled for 5 - 10 Min at 95 °C, cooled down on ice for 90 s and stored at -20 °C until SDS-PAGE, which was performed

before using GST-Aurora-A or GST-control coupled to Glutathione Sepharose^{TM} 4B beads with in vitro translated proteins.

3.3.9   Staining Protein gels with Coomassie Blue

To visualise proteins obtained by recombinant expression (see methods, section 3.3.8) or purified in IP samples were subjected to SDS-PAGE and the gel was stained in Coomassie solution for 2 h shanking gently at RT. To remove excess dye the gel was incubated in Coomassie destain solution with gentle shaking until a clear background was obtained

3.3.10   Chromatin immunoprecipitation (ChIP)

To IP DNA bound proteins together with their target DNA sequences the proteins are crosslinked to the DNA via formaldehyde. Cells for ChIP were cultured on 15 cm dished treated according to the experimental design and before harvest 1% formaldehyde was added to the medium, then dished were incubated shaking for 10 min at RT. Formaldehyde was quenched by adding 20 mM glycine and incubating for 5 min shaking at RT. Afterwards medium was removed, dishes were washed twice with ice cold PBS, cells were scraped off in 1 ml PBS containing 1:1000 protease inhibitor mix and pooled in 15 ml Falcon tubes. Harvested cells were pelleted at 1200 rpm and 4 °C for 5 min and either first shock frozen in liquid nitrogen before being stored at -80 °C or directly lysed. For lysis two different lysis buffers were used, first cells were swelled in 3 ml ChIP lysis buffer I including 1:1000 protease inhibitor mix dilution incubating for 20 min on ice and in a second step after centrifuging at 1200 rpm and 4 °C for 5 min cells were resuspended in ChIP lysis buffer II including 1:1000 protease inhibitor mix dilution and incubated on ice for 10 min to destroy all cellular membranes. Afterwards samples were sonified, sonification time and conditions varied according to the cell line. For IMR-5 cells total sonification time was 20 min with a sonification interval of 10 s at 20% amplitude followed by 30 s pause. To verify proper DNA fragmentation, every 5 min a 25 µl aliquot was taken. Sonified samples were stored on ice at 4 °C, while sonification aliquots were supplemented with 475 µl TE buffer, 160 mM NaCl and 20 µg/ml RNase to revert the crosslinking. After 1 h incubation at 37 °C and over night shaking at 65 °C, 5 mM EDTA and 200 µg/ml Proteinase K were added and samples were incubated for 2 h at 45 °C to digest proteins. Subsequently DNA was isolated performing a phenol/chloroform extraction (see methods, section 3.1.14) and DNA pellets were resuspended in 25 µl TE buffer. To check DNA fragment size 10 µl of sample was supplemented with 2 µl of 6x DNA loading buffer and loaded on a 2% agarose gel. When all DNA was fragmented to ˜200 bp fragments, ChIP was started. For each ChIP 15 µl of Protein A and 15 µl of Protein G Dynabeads® were prepared by washing 3x with 1 ml of PBS containing 5 mg/ml BSA using a magnetic rack. Washed Dynabeads® for each ChIP sample were resuspended in 1 ml PBS containing 5 mg/ml BSA, 3 µg of antibodies were added and samples were incubated O/N rotating at 4 °C. The next day sonified samples were cleared by centrifugation, first at 4700 rpm and 4 °C for 15 min, then supernatants

were transferred into 1.5 ml reaction tubes and samples were centrifuged at 13000 rpm and 4 °C for 15 min (this centrifugation step was repeated once). Afterwards Dynabeads® were washed like the day before and resuspended in 30 µl PBS containing 5 mg/ml BSA. Cleared chromatin was added to the Dynabeads® (~300 µl of a sample obtained from 80% confluent 6x 15 cm dishes). If different samples were prepared, concentration was determined for each condition by NanoDrop measurement of the DNA extracted from the 20 min sonification aliquot and the higher concentrated samples were adjusted according to the lowest using ChIP lysis buffer II including 1:1000 protease inhibitor mix dilution. For each sample two 1% input samples were taken as a control and kept at 4 °C until DNA extraction together with ChIP samples. Chromatin was incubated with antibody-coupled Dynabeads® for 6 h or O/N rotating at 4 °C. ChIP samples were washed using a magnetic rack first 3x with 1 ml ChIP wash buffer I, second 3x with 1 ml ChIP wash buffer II and third 3x with 1 ml ChIP wash buffer III (during the third wash step samples were incubated rotating at 4 °C in between each wash step). Afterwards samples were washed once with 1 ml TE buffer and transferred into a new 1.5 ml reaction tube during this wash step. Elution was conducted by resuspending the Dynabeads® in 150 µl ChIP elution buffer and incubating them rotating at RT for 15 min. Elution procedure was repeated once and eluates were pooled in one fresh 1.5 ml reaction tube. Eluats and input samples (with the same amount of ChIP elution buffer like ChIPs) were supplemented with 160 mM NaCl and 20 µg/ml RNase and incubated 1 h at 37 °C, then O/N shaking at 65 °C to revert the cross-linking, The next morning 5 mM EDTA and 200 µg/ml Proteinase K were added and samples were incubated for 2 h at 45 °C to digest proteins. Subsequently DNA was isolated performing a phenol/chloroform extraction (see methods, section 3.1.14) and DNA pellets were resuspended in 500 µl Ampuwa water. DNA was stored at -20 °C until qRT-PCR.

3.3.11   ChIP-sequencing library preparation

For ChIP-sequencing ChIPs were performed as described in section 3.3.10 using 50 million cells per IP. Cells were harvested and frozen cross-linked. For lysis all aliquots were pooled together and then redistributed (50 million cells/tube). Cells were pooled in ChIP lysis buffer II and redistributed for sonification (50 million cells/tube in 1.6 ml). During sonification it was taken care of the fact that the sonification needle is not touching the falcon tube containing the cell lysate. The amount of Dynabeads® and antibodies was increased to 100 µl of Dynabeads® (total) and 10 µg antibodies per ChIP. Chromatin concentrations were determined by Bradford Assay and NanoDrop measurement of sonification aliquots taken after total sonification time and concentrations and volumes were adjusted accordingly. Chromatin was incubated over night with Dynabeads® and antibodies and washing was performed as usual, except for 15 instead of 5 min incubation on the wheel in ChIP wash buffer III. Elution was performed using twice 250 µl elution buffer and phenol/chloroform extraction was performed with one additional washing step. Extracted DNA was resuspended in 30 µl Ampuwa water and 3 µl (5 µl for IgG) were diluted 1:40 to use in a control

qRT-PCR. Concentration of extracted DNA was determined via Quant-iT^{TM} PicoGreen$^{®}$ dsDNA assay from Invitrogen. Two different protocols were used for ChIP-Seq. library preparation. The first one utilises magnetic beads to bind DNA fragments, the second one is based on column purification (MinElute$^{®}$/QIAquick$^{®}$ PCR Purification Kits from Qiagen) and separation of DNA fragments on an agarose gel with subsequent cutting and purification of the $\sim$200 bp fragment (Qiagen Gel extraction Kit). Both methods were performed according to the NEBNext$^{®}$ ChIP-Seq Library Prep Master Mix Set for Illumina protocol. After the post-PCR purification step purity of samples was analysed using an Experion DNA 1 k Chip according to the manufacturers instructions. Samples for sequencing were adjusted to an equimolare concentration and denatured before loading on an Illumina flow cell according to the manufacturers instructions. First analysis of obtained ChIP-sequencing data showed that the first protocol used for library preparation yielded much less reads, which could be mapped to the human genome (version: hg19), than the second protocol for library preparation (see methods, section 3.4.1). Accordingly, only results from ChIP-sequencing of the samples generated using the second protocol described above were further taken into account for further analyses.

ChIP-sequencing data generated in this thesis are available at GEO under GSE78957.

3.4   Bioinformatic and statistical analysis

Bioinformatic and statistical analyses were performed in Microsoft Excel and R. Data were presented as mean + standard deviation (SD) or standard error of the mean (SEM) of at least three biological replicates, unless stated otherwise. In order to test for statistical significance, first a Shapiro-Wilk-test was conducted to test for normal-distribution of data at hand. Afterwards a two-sided student´s t-test was applied, if data were distributed normally. If the data did not fulfill the assumption of normality, non-parametric two-sided Wilcoxon rank sum tests were applied. Paired data was analysed using a paired t-test (parametric) or a Wilcoxon signed-rank test (non-parametric). Applied tests are indicated in the figure legends.

3.4.1   Bioinformatic analysis of ChIP-sequencing data

Bioinformatic analysis of ChIP-sequencing data was performed by Susanne Walz (Comprehensive Cancer Center Mainfranken, Core Unit Bioinformatics). Sequencing read data were processed with the standard Illumina software pipeline CASAVA for base calling and sequencing quality was assessed using the FastQC script. Only high quality reads (PF-Cluster) were taken into account. Fastq files from 3 out of 4 sequenced input samples were merged to create a mixed input control as reference. Bowtie v1.1.1 with default parameters was used to map the reads to the human genome (version: hg19) and resulting data was normalised to the sample with the smallest number of mapped reads. For peak calling MACS v1.4.2 was used and a p-value cut-off of 1.0×10^{-6} was applied. The input sample served as control. Published ChIP-sequencing data for CTCF and RAD21 were obtained from ENCODE (CTCF:

ENCFF001HXM, RAD21: ENCFF000RFT, control: ENCFF000RCC) and normalised to $1.0x10^7$ mapped reads. Wiggle files from normalised ChIP-sequencing data were generated in MACS v1.4.2. For visualisation of wiggle files the Integrated Genome Browser was used and for heat map generation SeqMINER with default options. To determine overlapping N-MYC/TFIIIC5 binding sites the intersectBed function from BEDTools was applied with a minimum overlap of 1 bp and corresponding p-values were calculated using a permutation test with $1.0x10^6$ iterations and considering only promoter regions for random picking. To assigne genes to be bound by N-MYC or TFIIIC5, a region of +/-1 kb around a transcriptional start site (TSS) was taken into account and analysed for the existence of called N-MYC or TFIIIC5 peaks. For calculation of changes in N-MYC and TFIIIC5 occupancy upon CD532 treatment at N-MYC/TFIIIC5 peaks tags in a region of 25/250 bp around the N-MYC peak were counted and p-values were calculated using a two-tailed one-sample Wilcoxon Signed-rank test. Occupancy changes are illustrated by box and whisker plots. The horizontal line of the box and whisker plots reflects the median, the boxes span the first and third quartile and whiskers expand to 1.5x interquartile range of the first and third quartile, respectively, outliers are shown as individual dots. *De novo* motif analyses of N-MYC and TFIIIC5 peaks was performed with the MEME Suite using MEME and DREME algorithms with an input region of +/- 50 bp around the peak summit and default parametres. The CentriMo tool from the MEME Suite was used to compute occurrences of pre-defined motifs (E-box: CACGTG, CTCF: MA0139.1 (JASPAR), AP2a: MA0003.2 (JASPAR)) and the frequency of a motif at a certain position was normalised to the number of input sequences. To smooth the resulting curves a rolling mean of 20 bp was applied.

4   Results

4.1   N-MYC interacts directly with Aurora-A

Neuroblastoma with an amplification of the N-MYC encoding gene, *MYCN*, often show high expression of Aurora-A [Berwanger et al., 2002]. This suggests a potential functional relationship between the two proteins, which was validated by Otto et al. [2009] (see introduction, section 1.5). They showed that N-MYC interacts with Aurora-A in exogenous and endogenous Co-immunoprecipitations (Co-IPs) and that Aurora-A overexpression can stabilise N-MYC and rescue it from FBXW7-mediated proteasomal degradation. Furthermore, Otto et al. [2009] discovered that the N-MYC T58A/S62A mutant (hereafter called N-MYC mut), which lacks the phospho-recognition motif essential for FBXW7 interaction and subsequent ubiquitination, was not stabilised by Aurora-A overexpression and showed a reduced interaction with Aurora-A.

However, there were several open questions on the functional relationship between N-MYC and Aurora-A in *MYCN*-amplified neuroblastoma. It was not known, whether their interaction is direct or indirect and whether the Aurora-A interaction domain in N-MYC comprises the FBXW7 phospho-recognition motif in MBI. Also, the questions about the physiological function of the N-MYC/Aurora-A complex and most importantly, about the underlying mechanism of the Aurora-A mediated stabilisation of N-MYC remained open.

To address the basic question about the direct interaction of N-MYC and Aurora-A, *in vitro* assays were performed utilising recombinant GST-tagged Aurora-A and *in vitro* translated N-MYC wt and N-MYC mut (Fig. 4.1 A). In GST pull-down assays N-MYC wt and N-MYC mut both interacted to the same extend with recombinant Aurora-A, suggesting that the N-MYC - Aurora-A interaction is direct and independent of other interacting proteins (Fig. 4.1 B). Since *in vitro* translated N-MYC wt was phosphorylated at T58 and S62, the phosphorylation at these sites appears to be irrelevant for the interaction with Aurora-A *in vitro* (Fig. 4.1 A).

In contrast, in neuroblastoma cell lines N-MYC interaction with Aurora-A is decreased, when N-MYC phosphorylation at T58 and S62 is blocked via displacement of the two residues with alanine (N-MYC mut) [Otto et al., 2009]. This indicates that there are additional components in the N-MYC/Aurora-A complex *in vivo*, which preferentially interact with N-MYC wt, which can be phosphorylated at T58 and S62.

The *in vitro* studies on the N-MYC/Aurora-A complex were continued in the laboratory of Richard Bayliss (University of Leeds, UK), while the composition and the physiological function of the complex *in vivo* was further investigated.
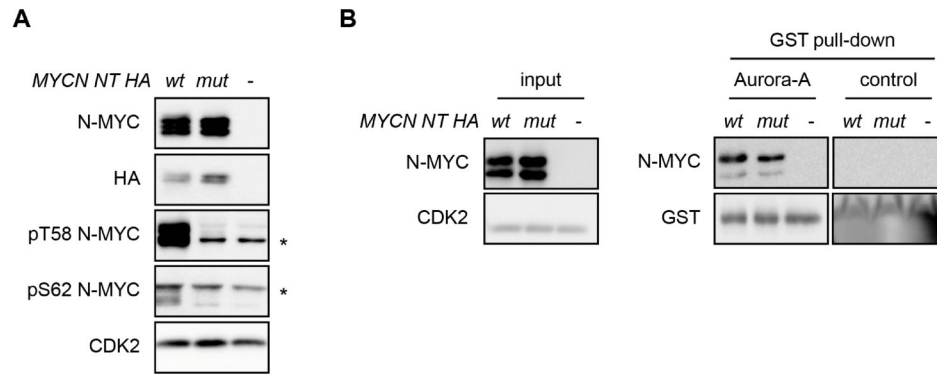
Figure 4.1
N-MYC wt and mut directly interact with Aurora-A
(A) Immunoblots of *in vitro* translated HA-tagged N-MYC wt or T58A/S62A (mut) constructs in pcDNA3 and empty control vector (-). CDK2 was used as a loading control. Asterisk indicates unspecific bands.
(B) GST pull-down of recombinant GST-tagged Aurora-A. *In vitro* translated N-MYC proteins and empty control samples from (A) were incubated with purified recombinant GST-tagged Aurora-A or an GST-only control bound to Glutathione sepharose. 20% input and eluates of GST-Aurora-A and control pull-downs were analysed by immunoblotting and probed with the indicated antibodies. CDK2 was used as a loading control.

4.2   Mass spectrometry (MS) on N-MYC protein complexes

To identify additional components in the N-MYC/Aurora-A complex, which mediate N-MYC stabilisation by Aurora-A *in vivo*, a mass spectrometric analysis of N-MYC complexes was conducted. One functional proteomic analysis is published on N-MYC, which was performed on exogenous FLAG-tagged N-MYC in HeLa cells [Choi et al., 2010]. The list of N-MYC interacting proteins in this publication comprised 33 proteins, including some components of the ubiquitin-system, for example HUWE1 and RUVBL1/2, as well as the deubiquitinating enzyme USP11. Components of the ubiquitin-system are of special interest for N-MYC interaction, since Aurora-A prevents degradation of N-MYC mediated via the ubiquitin ligase SCF$^{\text{FBXW7}}$ (see introduction, section 1.5).

4.2.1   Establishment and procedure of MS experiment

The aim of the proteomic analysis was the identification of novel N-MYC interacting proteins, which interact preferentially with N-MYC wt and could be responsible for Aurora-A-mediated stabilisation. To compare N-MYC wt and N-MYC mut interacting proteins, three SH-EP cell lines were generated. SH-EP is a neuroblastoma cell line, which does not express N-MYC, as it has only one silenced copy of the N-MYC encoding gene, but expresses C-MYC. Accordingly, exogenous N-MYC accounts for all N-MYC expressed in these cells. For MS one cell line was engineered expressing N-MYC wt and one expressing N-MYC mut, both tagged with an HA-tag in the N-terminus (NT), and one empty control cell line (Fig. 4.2 A). From generated cell pools clones were selected, which had similar N-MYC expression levels compared to *MYCN*-amplified neuroblastoma cells, shown here for IMR-32 cells (Fig.

4.2 A). This created an experimental setting, which was similar compared to conditions in *MYCN*-amplified neuroblastoma. To purify N-MYC complexes, N-MYC and interacting proteins were immunoprecipitated via the HA-tag and eluted with HA-peptides (Fig. 4.2 B). Conditions for purification were established by assessment of Aurora-A Co-IP in order to make sure that the conditions chosen enable the purification of proteins, which could be involved in Aurora-A-mediated stabilisation of N-MYC (Fig. 4.2 C). Test experiments showed that mild buffers with physiological salt concentration yielded higher amounts of purified N-MYC and co-purified Aurora-A protein than buffers with higher salt concentrations (Fig. 4.2 C, condition 2 and 4).

*conditions for IP washing: 1: 5x with TNN lysis buffer, 3rd step +80 mM NaCl; + last step 1x with PBS
2: 3x with TNN lysis buffer
3: 3x with HEGN lysis buffer, 3rd step +150 mM NaCl
4: 3x with HEGN lysis buffer
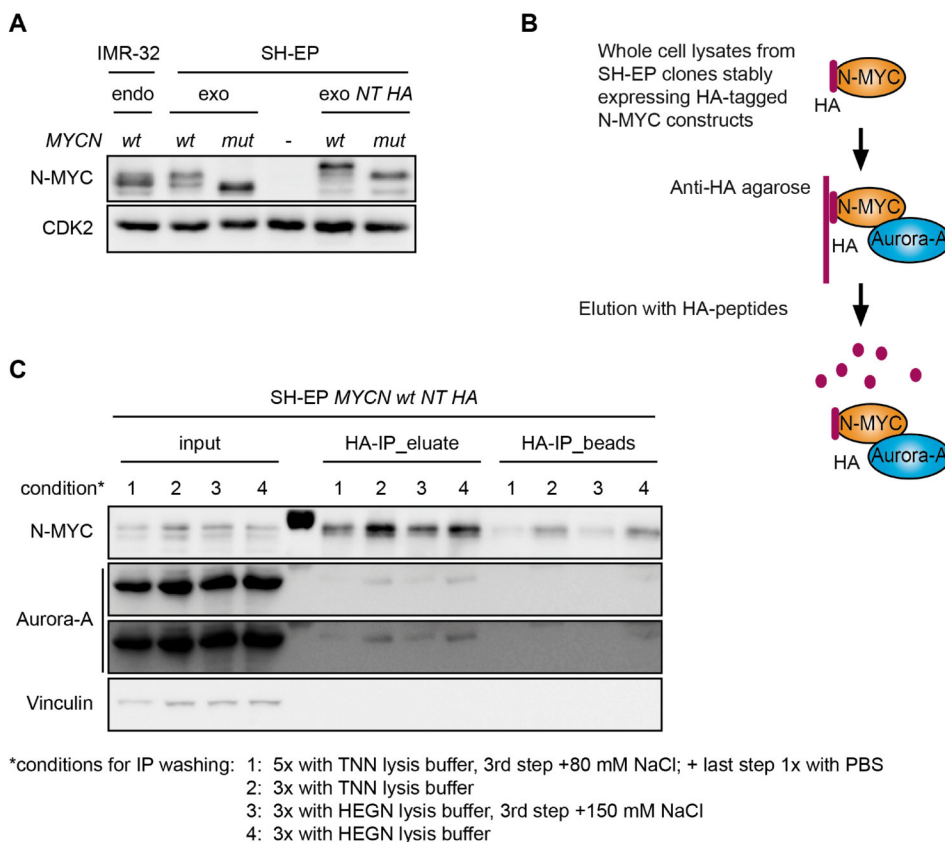
Figure 4.2
Purification of N-MYC protein complexes for MS
(A) Immunoblot of stable cell lines used for MS. Cell clones were generated and selected according to N-MYC expression levels being comparable to levels in *MYCN*-amplified neuroblastoma cells. HA-tagged N-MYC levels are shown in comparison to *MYCN*-amplified IMR-32 cells and SH-EP pools expressing untagged N-MYC. CDK2 was used as a loading control. endo: endogenous; exo: exogenous; - : empty vector expressing control cell line
(B) Scheme of N-MYC protein complex purification for MS. HA-tagged N-MYC and interacting proteins (represented by Aurora-A) are purified via HA-agarose beads and subsequently eluted with HA-peptides.
(C) Immunoprecipitation (IP) of N-MYC protein complexes using different conditions for washing. N-MYC complexes were purified from SH-EP cells shown in (A) expressing HA-tagged N-MYC wt. Aurora-A Co-IP was assayed using 4 different conditions. Purified proteins were eluted (eluate) and beads were subsequently boiled in loading buffer (beads). 1% input and IP samples were analysed by immunoblotting and probed with N-MYC and Aurora-A antibodies. Vinculin was used as a loading control.

After establishment of the purification method, the experiment was performed in a large scale for MS analysis, which was carried out in the group of Andreas Schlosser at the

Rudolf Virchow Center (RVZ) at the University of Würzburg. Eluted N-MYC complexes were reduced and alkylated before purified proteins were separated according to their size via SDS-Gel electrophoresis. Subsequent Coomassie staining revealed no obvious difference in the band-pattern of stained proteins for all three samples (Fig. 4.3 A). Nevertheless, western blot analysis from small aliquots of the samples for MS showed the N-MYC IP and Aurora-A and MAX Co-IPs, verifying the experiment was successful (Fig. 4.3 B). Accordingly, the samples were further processed and used for NanoLC-MS/MS analysis. Therefore, the lanes on the dried Coomassie-stained gel were cut into small pieces, the proteins in the gel were digested by trypsinisation and the resulting peptides were further cleaved yielding single amino acids. Obtained spectra from peptides and amino acids allowed the identification of proteins present in MS samples. Processed data was fed into the Scaffold Viewer illustrating the information on identified peptides and proteins.
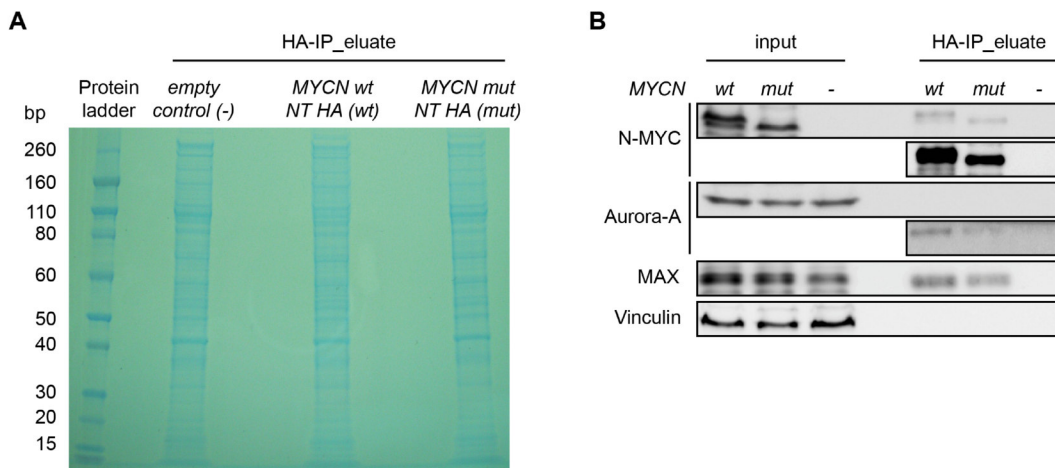
Figure 4.3
HA-IP samples for MS of N-MYC complexes
(A) Coomassie-stained SDS-gel loaded with eluates from HA-IPs of SH-EP cell clones expressing empty control vector, HA-tagged *MYCN wt* or *mut*. For MS each lane was cut into 15 pieces, which were further processed and analysed by NanoLC-MS/MS.
(B) Immunoblots of remaining HA-IP eluates from (A) and 1% input (100 μg) showing Aurora-A and MAX Co-IP with N-MYC wt and mut. Vinculin was used as a loading control.

4.2.2   Results of MS analysis on N-MYC protein complexes

MS analysis of N-MYC complexes resulted in a total number of 2515 identified proteins when all parameters for analysis were set most stringent (Fig. 4.4 A). N-MYC wt and mut proteins were identified with 125 and 207 total spectra (Fig. 4.4 A) and there was no N-MYC peptide identified in the empty control sample (data not shown). One feature of the applied MS technique (see methods, section 3.3.4) is that not only the amino acids of all peptides are identified, but also modifications of amino acids. Since N-MYC is stabilised by Aurora-A in mitosis when it is phosphorylated at T58 and S62 [Brockmann et al., 2013, Otto et al., 2009] (see introduction, section 1.5), the phosphorylation at these residues was quantified for all N-MYC wt peptides comprising this motif. Interestingly, most peptides identified

were phosphorylated on both residues (Fig. 4.4 B). The identification of several known C-MYC interacting proteins, like MAX, TRRAP and p400 [Blackwood and Eisenman, 1991, McMahon et al., 1998, Fuchs et al., 2001] (Fig. 4.4 A and Appendix A.1), confirmed that N-MYC IP and subsequent MS analysis were performed successfully. Additionally, a large number of previously unknown C-MYC interacting proteins was identified (see appendix A.1). To select for highly confident interaction partners, a list of proteins was generated, that fulfilled the following two criteria: 1. identification in N-MYC wt or mut sample with the number of exclusive unique peptides being 3-fold enriched compared to empty control sample; 2. identification of >4 exclusive unique peptides in N-MYC wt or mut sample. Application of these criteria yielded a list of 224 N-MYC interacting proteins (see appendix A.1), which was used to perform Functional Annotation Clustering. This analysis identified 10 clusters with an enrichment score (ES) >3 and a Benjamini-value <0.05 (Table 4.1). As a control for specificity, the analysis was performed with a list of proteins identified in the empty control sample and fulfilling the same two criteria described above. The resulting list comprised only 65 proteins and Functional Annotation Clustering yielded no cluster with an enrichment score (ES) >3 and a Benjamini-value <0.05 confirming the reliability of the previous analysis (not shown).

A

Analysis settings:
Protein threshold: 99.0%
Min # of peptides: 2
Peptide threshold: 95%

Total # of identified proteins: 2515

	total spectra	excl. un. peptides
N-MYC wt	125	17
N-MYC mut	207	15
MAX (wt/mut)	30/23	8/7

B

T58 (P)   (P) S62
N-MYC   56 peptides

T58 (P)   S62
N-MYC   9 peptides

T58   (P) S62
N-MYC   17 peptides

T58   S62
N-MYC   7 peptides
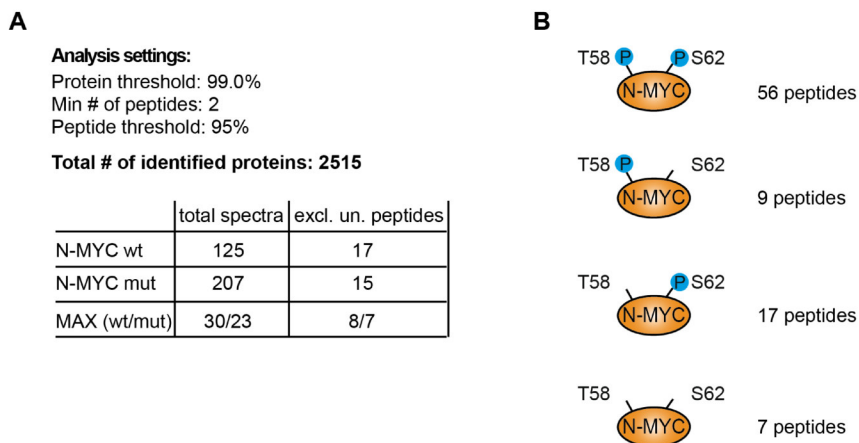
Figure 4.4
Summary of N-MYC MS results
(A) Experimental overview of N-MYC MS. Shown are settings for analysis using the Scaffold Viewer (version 4.0) and corresponding total number of identified proteins, as well as the number of total spectra and exclusive unique peptides (excl. un. peptides) for N-MYC wt and mut protein and for the known C-MYC interacting protein MAX.
(B) Scheme illustrating N-MYC wt phosphorylation at T58 and S62 in MS experiment. Shown are total numbers of peptides identified with the indicated phosphorylation status.

While the identified clusters for Ribosome biogenesis (#3), Chromatin/acetylation (#4), Helicase (#8) and RNA transcription, localisation and processing (#6,7,9) are likely to come up for a POL II transcription factor, the cluster for POL III/TFIIIC was not expected to be enriched. The transcription factor protein complex TFIIIC is known to be involved in POL III transcription and consists of 6 subunits, TFIIIC1-6, and there were 5 subunits

identified in the N-MYC MS (TFIIIC1-5) (see discussion, section 5.4). All TFIIIC subunits identified were present in the list of the 224 N-MYC interacting proteins described before (see appendix A.1), except for TFIIIC4, which was identified with 4 peptides in the N-MYC wt sample and with no peptides in the other two samples.

For selection of candidates to validate the N-MYC interaction, the list of 224 interacting proteins was shortened by setting more stringent criteria: 1. identification in N-MYC wt or mut sample with the number of exclusive unique peptides being 4-fold enriched compared to empty control sample; 2. identification of >7 exclusive unique peptides in N-MYC wt or mut sample.

Annotation Cluster	ES	identified proteins
1./2. Cellular localisation	26.92/17.96	SMCHD1, POLA1, WDR75
3. Ribosome biogenesis	5.38	GNL2, DDX56, GEMIN5, GNL3L
4. Chromatin/acetylation	5.22	TRRAP, EP400, DMAP1, EPC1
5. WD repeat	4.68	HERC2, WDR43, WDR33, WDR75
6. RNA transcription	4.37	CEBPZ, TFIIIC1, SUPT5H, POLR3A
7. RNA localisation	4.20	THOC1, RANBP2, NUP85, NUP188
8. Helicase/ATPase	3.84	CHD7, RFC1, TOP2A, TOP2B
9. RNA processing	3.76	RBM14, SRRM2, UTP20, DDX46
10. POL III/TFIIIC	3.67	TFIIIC subunit 1-5

Table 4.1
Functional Annotation Clustering for N-MYC interacting proteins identified in MS
For Functional Annotation Clustering a list of 224 N-MYC interacting proteins (shown in Appendix A.1) was fed into the Functional Annotation Tool from DAVID (Bioinformatics Resources 6.7, NIAID/NIH). Analysis was performed with check default parameters and medium stringency. Shown are all annotated clusters with an enrichment score (ES) >3 and Benjamini-value <0.05, as well as examples of identified proteins for each cluster.

Application of these criteria yielded a list of 82 proteins ("Top 82-List", see appendix A.2), which still included known MYC interacting proteins, like TRRAP, p400 and HCFC1 [McMahon et al., 1998, Fuchs et al., 2001, Furrer et al., 2010], as well as many proteins not published to interact with MYC proteins. TFIIIC subunits 1-3 and 5 were still present in this more stringent list and peptide counts are shown in Table 4.2. Aurora-A was not present in neither of the two lists generated. It was identified with 2 peptides in empty control and N-MYC mut sample and three peptides in the N-MYC wt sample. The discrepancy between western blot results and MS peptide counts for Aurora-A could be due to the hydrophobic nature of the Aurora-A peptides, which can lead to retardation of peptide detection in MS or lack of detection (Andreas Schlosser, personal communication).

Among the proteins in the "Top 82-List" were several proteins from the ubiquitin-system, for example MYCBP2, BIRC6 and USP7 (see appendix A.2). The identification of the deubiquitinating enzyme USP7 (Table 4.2) as an N-MYC interacting protein was highly interesting, since it is known that C-MYC degradation via SCF^{FBXW7} is inhibited by USP28, another deubiquitinating enzyme [Popov et al., 2007]. Deubiquitinating enzymes

can rescue proteins from degradation by cleaving attached ubiquitin chains targeting the proteasome. For N-MYC no deubiquitinating enzyme is published to regulate its degradation via SCF^{FBXW7}. As N-MYC stabilisation by Aurora-A interaction was shown not be caused by displacement of N-MYC from FBXW7 or the catalytic activity of Aurora-A [Otto et al., 2009], the mechanism for Aurora-A-mediated protection of N-MYC from degradation via SCF^{FBXW7} remained elusive and the interaction of USP7 with N-MYC represented a possible explanation for this open question.

rank	gene symbol	M.W.	number of peptides		
			-	mut	wt
3	GTFIIIC1	239 kDa	4	27	52
11	USP7	126 kDa	4	21	19
13	GTFIIIC5	60 kDa	0	7	19
20	GTFIIIC3	101 kDa	1	12	17
25	TOP2A	179 kDa	0	6	15
26	TOP2B	183 kDa	1	11	14
27	TOP1	91 kDa	3	7	13
32	CTR9	134 kDa	1	4	13
44	GTFIIIC2	101 kDa	0	2	11
54	ELP3	61 kDa	1	2	9
56	SUPT5H	120 kDa	0	4	9
58	CDC73	61 kDa	0	5	9

Table 4.2
Peptide counts for selected identified N-MYC interacting proteins in "Top 82-List"
The list represents a selection of identified proteins included in the "Top 82-List" (shown in Appendix A.2). Shown are rank number, official gene symbol, Molecular Weight (M.W.) and exclusive unique peptide counts in empty control, mut and wt sample. The "Top 82-List" is ranked according to the number of exclusive unique peptides first in N-MYC wt sample and second in N-MYC mut sample.

4.2.3 USP7/11 - candidates for Aurora-A mediated stabilisation of N-MYC

USP7 is a deubiquitinating enzyme belonging to the ubiquitin-specific protease family (USP), the largest family of deubiquitinating enzymes [Quesada et al., 2004]. It is published to be involved in various cellular processes, including the protection of several proteins from degradation by removal of ubiquitin chains targeting the proteasome, e.g. from TIP60 [Dar et al., 2013]. Additionally, USP7 was shown to interact with USP11 and the two USPs were described to stabilise the polycomb repressive complex 1 components BMI-1 and MEL-18 via deubiquitination [Maertens et al., 2010]. Furthermore, as mentioned in section 4.2, USP11 was identified in MS as an N-MYC interacting protein by Choi et al. [2010]. Accordingly, the interaction of N-MYC with both, USP7 and USP11, was investigated in immunoprecipitation experiments from neuroblastoma cell lines.

To validate USP7 interaction with N-MYC, HA-IPs were performed utilising the HA-tagged N-MYC expressing cell lines used in MS. USP7 was specifically eluted with N-MYC wt and mut, but there was also a weak USP7 signal detected in the empty control sample, reflecting the USP7 peptide counts in MS (Fig. 4.5 A). *Vice versa*, N-MYC was co-purified with USP7 in exogenous IPs from transiently transfected SH-EP cells (Fig. 4.5 B). Furthermore, endogenous IPs from *MYCN*-amplified IMR-5 cells showed the USP7 interaction with N-MYC, confirming the interaction of endogenous N-MYC with endogenous USP7 (Fig. 4.5 C).
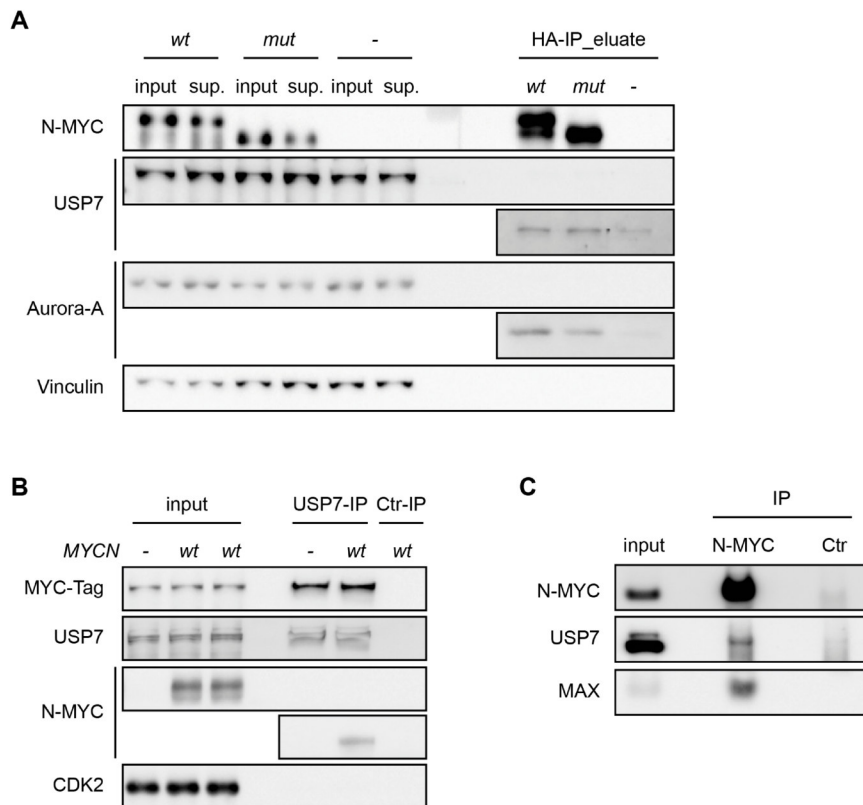
Figure 4.5
USP7 interacts with N-MYC
(A) Immunoprecipitation of N-MYC protein complexes from the stable SH-EP cell lines used for MS, expressing either N-terminally HA-tagged *MYCN wt* (*wt*) or *mut (mut)* or empty control vector (-). The experiment was performed in the same way as for MS, but in a smaller scale. 1.3% input, the same amount of supernatant (sup.) and eluate were analysed by immunoblotting and probed with the indicated antibodies. Vinculin was used as a loading control.
(B) Immunoprecipitation from SH-EP cells transfected with Myc-tagged USP7 and *MYCN wt* (*wt*) or empty control expression (-) plasmids. Cells were harvested after 48 h and USP7 protein complexes were immunoprecipitated with USP7 antibodies, precipitation with IgG was used as a control (Ctr). 1% input and IP samples were analysed by immunoblotting and probed with the indicated antibodies. CDK2 was used as a loading control.
(C) Immunoprecipitation from *MYCN*-amplified IMR-5 cells. N-MYC protein complexes were immunoprecipitated with N-MYC antibodies, precipitation with IgG was used as a control (Ctr). 0.75% input and IP samples were analysed by immunoblotting and probed with the indicated antibodies.

After successful validation of the the N-MYC - USP7 interaction, first, USP7 interaction with USP11 was confirmed in *MYCN*-amplified neuroblastoma cells [Maertens et al., 2010] (Fig. 4.6 A). Second, USP11 interaction with N-MYC was shown in transient transfection

experiments in SH-EP cells (Fig. 4.6 B). Surprisingly, N-MYC mut showed a much stronger interaction than N-MYC wt and this hold true in both directions, in N-MYC and USP11 IPs (Fig. 4.6 B). Third, endogenous IPs in *MYCN*-amplified neuroblastoma cells treated with or without ethidium bromide were performed. Ethidium bromide intercalates in double-stranded DNA and interferes with protein-binding to the DNA. Accordingly, treatment with ethidium bromide can clarify, if interactions observed in Co-IP experiments are due to the fact that the proteins in question bind close to each other to DNA or if the interaction is mediated via protein-protein contacts [Schroter et al., 1985]. Here, USP11 was co-purified with endogenous N-MYC regardless of ethidium bromide treatment, showing that contacts between N-MYC and USP11 are mediated via protein-protein interactions and that the endogenous proteins interact with each other in *MYCN*-amplified neuroblastoma cells (Fig. 4.6 C).
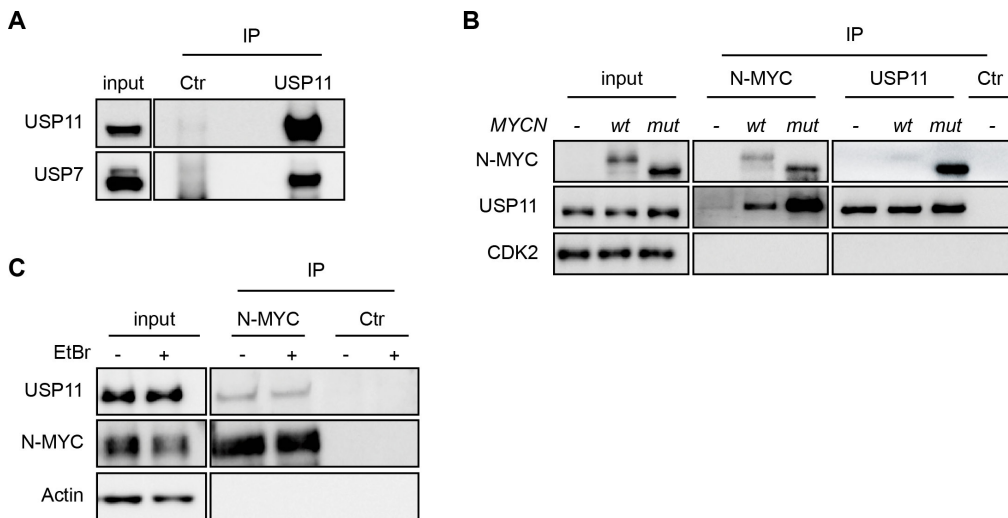
Figure 4.6
USP11 interacts with N-MYC
(A) Immunoprecipitation from *MYCN*-amplified IMR-5 cells. USP11 protein complexes were immunoprecipitated with USP11 antibodies, precipitation with IgG was used as a control (Ctr). 0.75% input and IP samples were analysed by immunoblotting and probed with the indicated antibodies.
(B) Immunoprecipitation from SH-EP cells transfected with *USP11* and either *MYCN wt (wt)* or *mut (mut)* expression plasmids or an empty control vector (-). Cells were harvested after 48 h and protein complexes were immunoprecipitated with USP11 or N-MYC antibodies, precipitation with IgG was used as a control (Ctr). 1% input and IP samples were analysed by immunoblotting and probed with the indicated antibodies. CDK2 was used as a loading control.
(C) Immunoprecipitation from *MYCN*-amplified IMR-32 cells treated with or without ethidium bromide (EtBr). N-MYC protein complexes were immunoprecipitated with N-MYC antibodies, precipitation with IgG was used as a control (Ctr). 1% input and IP samples were analysed by immunoblotting and probed with the indicated antibodies. Actin was used as a loading control.

Both, USP7 and USP11, showed no preference for interaction with N-MYC wt. USP7 was co-purified equally well with N-MYC wt and N-MYC mut (Fig 4.5.A), whereas USP11 immunoprecipitation experiments revealed a preference for interaction with N-MYC mut (Fig. 4.6 B). These findings indicate that USP7 and USP11 are not recruited by Aurora-A to deubiquitinate and stabilise N-MYC wt.

Indeed knockdown experiments showed, that *USP7* knockdown via three different shRNAs

had no clear effect on N-MYC levels, although all three shRNAs tested, decreased *USP7* mRNA expression and protein levels (Fig. 4.7 A,B). With *shUSP7-3*, N-MYC levels decreased compared to control cells, but since *MYCN* mRNA levels were decreased to more than 50%, the reduction of N-MYC was likely to be caused by a regulation of *MYCN* mRNA expression, instead of a regulation on protein level (Fig. 4.7 A,B). Also, *shUSP7-3* induced the least pronounced decrease of USP7, on protein and mRNA level, indicating an off-target effect of this specific shRNA (see discussion, section 5.3). Aurora-A was not affected upon *USP7* knockdown, except for *shUSP7-2*, which showed a decrease of Aurora-A protein and mRNA levels compared to control cells, accordingly, N-MYC levels were slightly decreased as well (Fig. 4.7 A,B). In shScr treated cells N-MYC protein decreased, whereas *MYCN*, *AURKA* and *USP7* mRNA expression increased (see discussion, section 5.3) (Fig. 4.7 A,B). While *USP7* depletion had no clear effect on N-MYC levels, it strongly affected cell proliferation and induced cleaved PARP levels, suggesting cell cycle arrest and apoptosis induction (Fig. 4.7 A,C). The cellular effects of *USP7* knockdown were further investigated by Johannes Dirks [Thesis from J. Dirks, soon to be published].
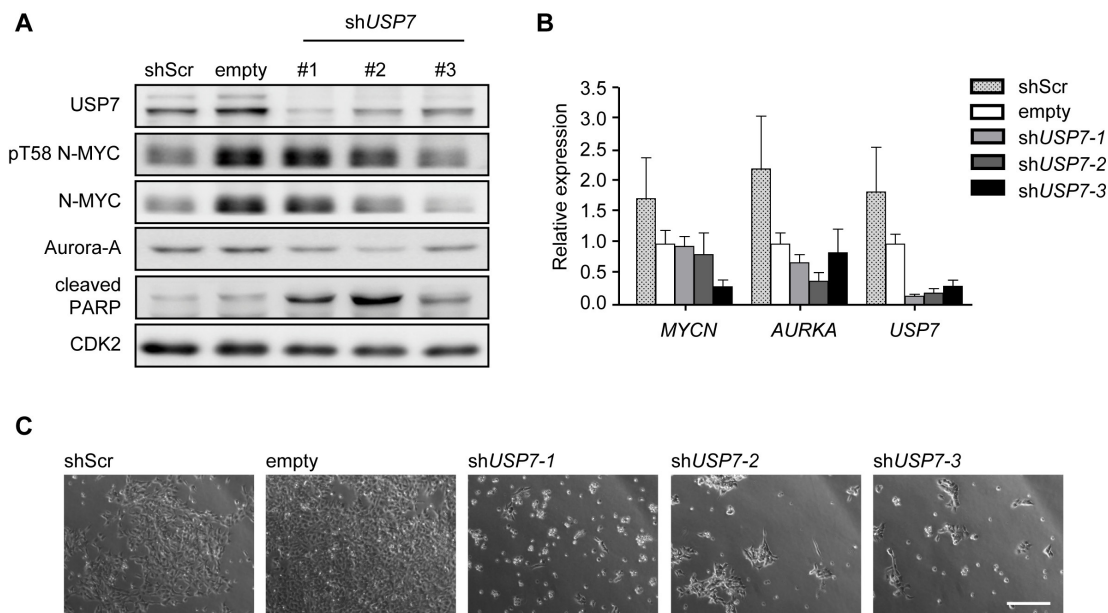
Figure 4.7
USP7 knockdown does not directly affect N-MYC protein levels
(A) Immunoblots of *MYCN*-amplified IMR-32 cells expressing three different shRNAs targeting *USP7* mRNA (sh*USP7* #1,2,3), empty pLKO vector (empty) or an scrambled shRNA (shScr) as non-targeting control. Cells were selected for shRNA expression and harvested 7 days after infection. Immunoblots were probed with the indicated antibodies. CDK2 was used as a loading control.
(B) *MYCN, AURKA* and *USP7* mRNA expression from cells in (A) was analysed by qRT-PCR. Expression was normalised to beta-2-microglobulin. Data are represented as mean of technical triplicates. Error bars indicate standard deviation.
(C) Phase contrast images from cells in (A). Scale bar represents 200 µm.

To exclude an USP7-independent role of USP11 in Aurora-A-mediated stabilisation of N-MYC, USP11 overexpression and knockdown experiments were performed.

Transfection of different amounts of USP11 expression plasmids in SH-EP cells together with

N-MYC wt or mut resulted in a concentration-dependent increase in N-MYC wt and N-MYC mut protein, suggesting N-MYC stabilisation via USP11-mediated deubiquitination (Fig. 4.8 A). But, side-by-side comparison of transfection effects of USP11 wt and the catalytically inactive mutant of USP11 C318S [Al-Salihi et al., 2012] revealed that exogenous N-MYC protein levels increased independently of the catalytic activity of USP11 (Fig. 4.8 B). *USP11* knockdown using specific siRNAs did not decrease N-MYC levels of *MYCN*-amplified neuroblastoma cells, although USP11 protein levels were clearly decreased 48 h post transfection (Fig. 4.8 C). Extension of the time from 48 to 72 h post transfection or increase of the amount of siRNA, did not result in a reduction of N-MYC as well (Fig. 4.8 C, D). Knockdown experiments using three different shRNAs targeting *USP11* confirmed that *USP11* depletion does not regulate N-MYC levels (data not shown). In summary, the increase of ectopically expressed N-MYC upon USP11 overexpression, indicating N-MYC stabilisation by USP11, was not confirmed in *USP11* knockdown experiments.
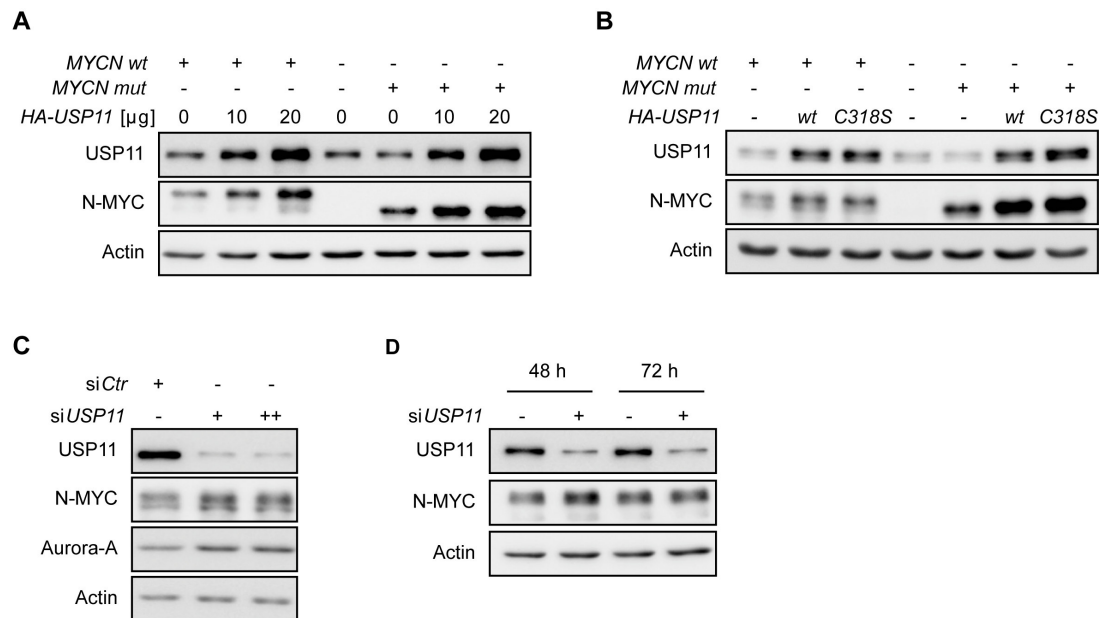
Figure 4.8
USP11 overexpression increases exogenous N-MYC levels, but siRNA-mediated knockdown of *USP11* does not affect endogenous N-MYC
(A), (B) Transient overexpression of USP11 in SH-EP cells. In (A) cells were transfected with indicated amounts of *USP11 wt* expression plasmids together with *MYCN wt*, *MYCN mut* or empty control plasmids. In (B) Cells were transfected with *USP11 wt* or catalytic inactive mutant *USP11 C318S* expression plasmid together with *MYCN wt*, *MYCN mut* or empty control plasmids. Cells were harvested 48 h after transfection. Immunoblots were probed with the indicated antibodies. Actin was used as a loading control.
(C), (D) Knockdown of *USP11* in IMR-5 cells using specific siRNAs. In (C) cells were transfected with two different concentrations of si*USP11*, 20 μg (+) or 40 μg (++), or non-targeting control (si*Ctr*) and harvested after 48 h. In (B) cells were transfected with 20 μg of si*USP11* or si*Ctr* and harvested 48 h or 72 h after transfection. Immunoblots were probed with the indicated antibodies. Actin was used as a loading control.

To conclude, although N-MYC interaction with USP7 and USP11 was validated, a direct involvement of USP7/11 in Aurora-A-mediated stabilisation of N-MYC wt could not be shown. The argument of USP7/11 showing no preference for interaction with N-MYC wt,

which, in contrast to N-MYC mut, can be stabilised by Aurora-A (Fig. 4.5 and 4.6), was strengthened in *USP7/11* knockdown experiments. Knockdown of *USP7* and *USP11* did not clearly affect N-MYC protein levels. Accordingly, the functional relevance of the N-MYC - USP7/11 interaction was not further investigated. It remains open, if there is a deubiquitinating enzyme, which is recruited by Aurora-A to mediate N-MYC stabilisation.

4.2.4 Validation of a novel group of N-MYC interacting proteins identified in MS

In addition to USP7, other novel N-MYC interacting proteins were identified in MS and validated in IP experiments. Proteins selected for validation were involved in structural organisation of chromatin or transcriptional elongation and showed a clear preference for interaction with N-MYC wt, suggesting a possible role for Aurora-A-mediated stabilisation of N-MYC (peptide counts are shown in section 4.2.2, Table 4.2).

The decision to focus the validation on structural chromatin-binding proteins was due to the identification of 5 out of 6 subunits of the TFIIIC POL III transcription factor (see results, section 4.2.2). Several more recent publications on TFIIIC show that the complex plays a role in chromatin organisation (see discussion, section 5.4). Importantly, there was no existing record on C- or N-MYC function in architectural organisation of chromatin and on interaction of C- and N-MYC with TFIIIC. The interaction of another POL III transcription factor, TFIIIB, and C-MYC was reported before [Gomez-Roman et al., 2003] (see introduction, section 1.3.2).

In order to validate the interaction of TFIIIC with N-MYC, immunoprecipitation experiments from neuroblastoma cell lines were performed. On the one hand the same cell lines as in the MS experiment (see results, section 4.2.1) were used (not shown) and on the other hand the interaction was tested in endogenous IPs from *MYCN*-amplified neuroblastoma cells (Fig. 4.9 A, C). TFIIIC subunit 5 (TFIIIC5) was chosen for validation experiments, since in comparison to subunit 1 and 2, antibodies directed against this subunit yielded the best results in immunoprecipitation experiments and subsequent western blotting. N-MYC IPs from *MYCN*-amplified IMR-5 cells confirmed the interaction of endogenous N-MYC with TFIIIC5 (Fig. 4.9 A). Interestingly, TFIIIC5 was also co-purified in Aurora-A IPs (Fig. 4.9 A). Since most N-MYC wt peptides identified in MS were phosphorylated at T58 and S62 (Fig. 4.4), it was assumed that proteins like TFIIIC5, detected with higher peptide counts in the N-MYC wt sample, preferentially interact with pT58/pS62 N-MYC. To test, whether this assumption hold true, SH-EP cells were transiently transfected with N-MYC wt, N-MYC mut or empty control vector and N-MYC was immunoprecipitated from transfected cells (Fig. 4.9 B). In line with TFIIIC5 peptide counts in MS, TFIIIC5 was co-purified from N-MYC wt expressing cells, whereas there was no enrichment in IPs from N-MYC mut expressing cells compared to control cells (Fig. 4.9 B). As expected, the same was true for Aurora-A, which showed a strong preference for interaction with N-MYC wt like TFIIIC5 (Fig. 4.9 B). To ensure that the co-purification of TFIIIC5 in N-MYC IPs was not a result of binding of the two proteins to adjacent DNA sequences, endogenous

IPs were performed in the presence or absence of ethidium bromide (described in results, section 4.2.3) (Fig. 4.9 C). Ethidium bromide treatment did not influence TFIIIC5 Co-IP with N-MYC, confirming IP results were based on protein-protein interactions (Fig. 4.9 C). Furthermore, TFIIIC5 IPs from *MYCN*-amplified IMR-32 cells showed that also N-MYC was co-purified with TFIIIC5 regardless of ethidium bromide treatment (Fig. 4.9 C). In summary, IP experiments clearly confirmed N-MYC´s interaction with TFIIIC subunit 5.
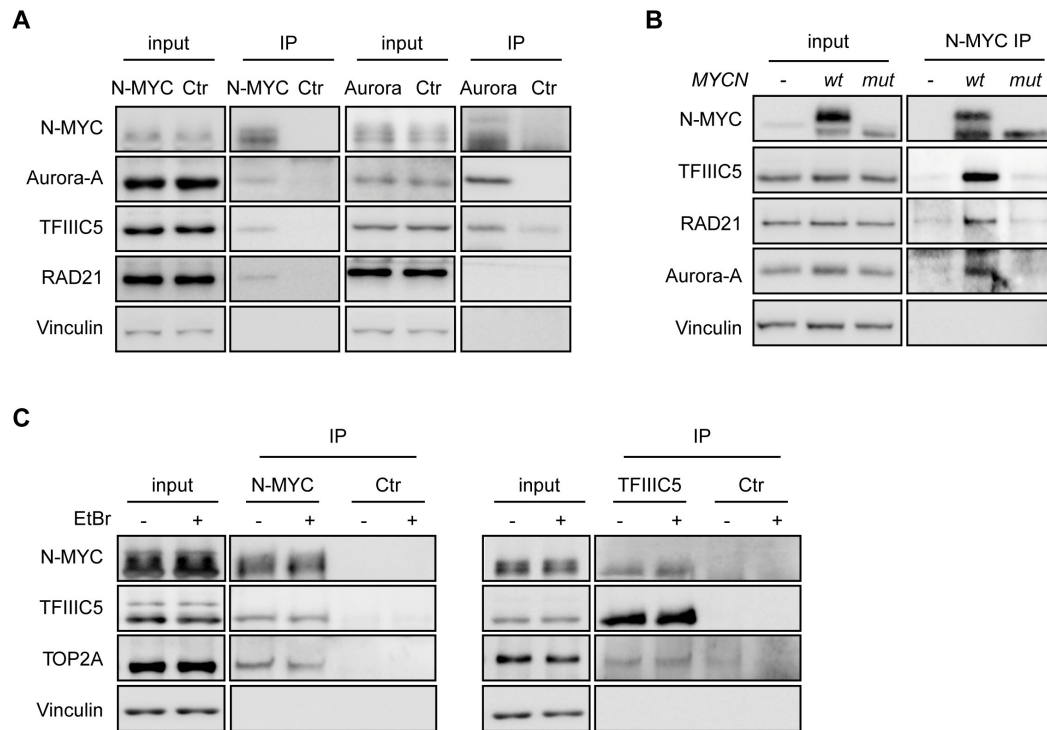
Figure 4.9
N-MYC interacts with a novel group of proteins involved in architectural organisation of chromatin
(A) Immunoprecipitation from *MYCN*-amplified IMR-5 cells. N-MYC and Aurora-A protein complexes were immunoprecipitated with N-MYC or Aurora-A antibodies, precipitation with IgG was used as a control (Ctr). 0.67% input and IP samples were analysed by immunoblotting and probed with the indicated antibodies. Vinculin was used as a loading control.
(B) Immunoprecipitation from SH-EP cells transfected with either *MYCN wt* (*wt*) or *mut* (*mut*) expression plasmids or an empty control vector (-). Cells were harvested 48 h after transfection and protein complexes were immunoprecipitated with N-MYC antibodies. 3% input and IP samples were analysed by immunoblotting and probed with the indicated antibodies. Vinculin was used as a loading control.
(C) Immunoprecipitation from *MYCN*-amplified IMR-5 cells (left panel) and IMR-32 cells (right panel) treated with or without ethidium bromide (EtBr). N-MYC and TFIIIC5 protein complexes were immunoprecipitated with N-MYC or TFIIIC5 antibodies, precipitation with IgG was used as a control (Ctr). 1% input and IP samples were analysed by immunoblotting and probed with the indicated antibodies. Vinculin was used as a loading control.

Besides TFIIIC5 the interaction of N-MYC with two DNA topoisomerases detected in N-MYC MS, TOP2A and TOP2B (Table 4.2), was assayed in IP experiments. Topoisomerases catalyse the process of winding DNA and for example are able to release the tension, which occurs upon transcription of DNA [Kouzine et al., 2014]. An interaction of MYC proteins with topoisomerases was not reported before, but would be highly interesting, for example in regard of MYC´s function as a "general amplifier" (see introduction, section 1.2). To confirm the interaction of N-MYC and TOP2A/B, immunoblots from endogenous N-MYC

IPs from *MYCN*-amplified IMR-5 cells treated with or without ethidium bromide were probed with TOP2A/B antibodies. Immunoblotting showed that TOP2A (Fig. 4.9 C) and TOP2B (not shown) are co-purified with N-MYC independent of ethidium bromide treatment. In addition, TOP2A was co-purified in TFIIIC5 IPs regardless of ethidium bromide treatment (Fig. 4.9 C). The third topoisomerase listed in the "Top 82-List", TOP1 (see appendices A.1, A.2 and Table 4.2), was not validated for N-MYC interaction, since in all experiments high background signals were detected with TOP1 antibodies in control IPs (data not shown). Thus, the interaction of N-MYC with TFIIIC5 and TOP2A/B was validated and suggests the existence of a quaternary complex of comprising N-MYC, Aurora-A, TFIIIC5 and TOP2A in neuroblastoma cells. A complex of N-MYC/Aurora-A with TFIIIC and topoisomerases was not described before and the function of this hypothetical complex remains to be determined.

Since TFIIIC was shown to be involved in the organisation of chromatin architecture (see discussion, section 5.4.1), the N-MYC/TFIIIC complex could function in chromatin-organisation. To test this hypothesis, N-MYC interaction with important regulators of chromatin compaction, cohesion and compartmentalisation [Jeppsson et al., 2014], namely condensins and cohesins, was assayed, since TFIIIC associates with condensin and cohesin (see discussion, section 5.4.1). While the interaction of N-MYC with the condensin II sub-unit hCAP-D3 (see appendix A.1, rank 212) and cohesin loading factor NIPBL (not detected in MS) was not observed in any of the performed immunoprecipitation experiments (not shown), the interaction with cohesin subunit RAD21 (identified with 0/3/3 exclusive unique peptide counts in empty/mut/wt MS sample) was clearly shown in endogenous N-MYC IPs (Fig. 4.9 A). Moreover, exogenous N-MYC IPs showed that RAD21 interacts, like TFIIIC5, preferentially with N-MYC wt (Fig. 4.9 B). An interaction of RAD21 and Aurora-A was not observed (Fig. 4.9 A). Hence, the N-MYC/TFIIIC complex could be associated with cohesin, which can tether two DNA strands together resulting in chromatin loops, which can for example separate an enhancer from its promoter or bring them close together [Wendt et al., 2008, Sofueva et al., 2013, Schaaf et al., 2013] (see discussion, section 5.4.1).

In addition, a second group of proteins was selected for validation comprising proteins involved in elongation of RNA transcripts. N-MYC interaction with ELP3, a catalytic sub-unit of the histone acetyltransferase elongator complex, the DRB sensitivity- inducing factor (DSIF) complex component SPT5 and the RNA polymerase II-associated factor (PAF1C) complex components CTR9 and CDC73 was assayed (Table 4.2). Neither N-MYC, nor C-MYC proteins are described to be associated with ELP3, DSIF or PAF1C, which all function in transcriptional elongation, while MYC proteins are known to function in tran-scriptional initiation of RNA POL II transcribed genes and in release of paused POL II (see introduction, section 1.3.1). In immunoprecipitation experiments from transiently transfec-ted SH-EP cells the interaction of N-MYC with overexpressed HA-tagged ELP3 was shown (Fig. 4.10). Furthermore, endogenous SPT5, CTR9 and CDC73 were co-purified with exo-genous N-MYC, validating MS results (Fig. 4.10). Importantly, also C-MYC associates

with SPT5, CTR9 and CDC73 (Laura Jaenicke, personal communication). The function of MYC together with DSIF and PAF1C was further investigated by Laura Jaenicke [Jaenicke et al., 2016].
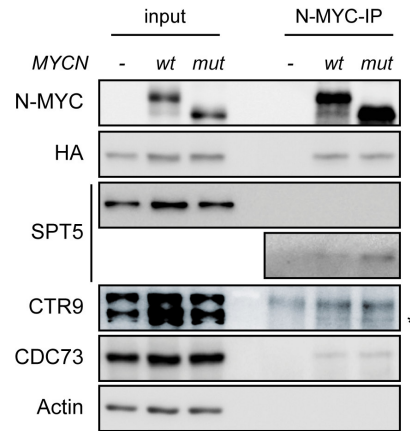
Figure 4.10
N-MYC interacts with a novel group of proteins involved in transcriptional elongation
Immunoprecipitation from SH-EP cells transfected with HA-tagged *ELP3* and either *MYCN wt* (*wt*) or *mut* (*mut*) expression plasmids or an empty control vector (-). Cells were harvested 48 h after transfection and protein complexes were immunoprecipitated with N-MYC antibodies. 1% input and IP samples were analysed by immunoblotting and probed with the indicated antibodies. Actin was used as a loading control. Asterisk marks band corresponding to CTR9 protein.

Since in exogenous N-MYC IPs TFIIIC5 was co-purified from N-MYC wt expressing cells and not from N-MYC mut expressing cells (Fig. 4.9 B) and MS peptide counts supported this observation showing a higher number of peptides recovered from N-MYC wt expressing cells than from N-MYC mut expressing cells (Table 4.2), it was likely that interaction of TFIIIC5 with N-MYC depends on its phosphorylation at T58 and S62.

To determine, if TFIIIC5 and also TOP2A interact with N-MYC MBI covering the residues T58 and S62 and if their interaction displays a preference for N-MYC phosphorylated at T58 and/or S62, pull-down assays with differently phosphorylated N-MYC peptides (aa28-89) were conducted. Indeed, TFIIIC5 interacted with MBI of N-MYC and showed, like Aurora-A, a preference for interaction with peptides phosphorylated at both residues, T58 and S62, confirming MS and IP results (Fig. 4.11 A, B). TOP2A was shown to interact with N-MYC peptides, but the preference for interaction with double phosphorylated peptides was not as clear as for TFIIIC5 (Fig. 4.11 A,B).

In summary, N-MYC interactions with a group of proteins involved in chromatin organisation and with proteins functioning in transcriptional elongation, which were identified in MS analysis of N-MYC complexes, were successfully validated. Furthermore, results of pull-down assays with N-MYC peptides clearly demonstrated that TFIIIC5 interacts with MBI in a phosphorylation-dependent manner, suggesting that N-MYC and TFIIIC interact directly. TFIIIC5 was also shown to interact with Aurora-A, which might suggest an involvement in N-MYC stabilisation by Aurora-A (see discussion, section 5.4).
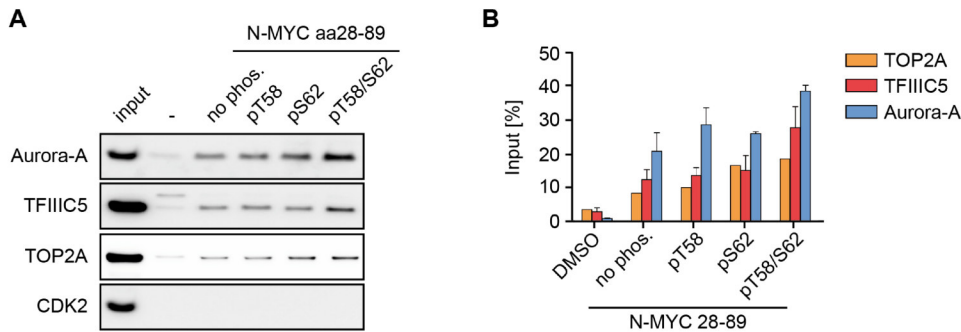
Figure 4.11
TFIIIC interacts preferentially with N-MYC peptides phosphorylated at T58 and S62
(A) Pull-down of indicated proteins with N-MYC peptides (aa28-89) covering MBI, which are not phosphorylated (no phos.), phosphorylated at T58 (pT58) or S62 (pS62) or on both sites (pT58/S62). Biotinylated peptides were coupled to streptavidin magnetic beads and incubated with whole cell lysates from SH-EP cells. Streptavidin beads without coupled MBI peptides were used as a control (DMSO). 1% input and pull-down samples were analysed by immunoblotting and probed with the indicated antibodies. CDK2 was used as a control for interaction specificity.
(B) Quantification of N-MYC peptide pull-down experiments as in (A). Shown is the quantification of two independent experiments as shown in (A) for TFIIIC5 and the quantification of the experiment shown in (A) for TOP2A. Binding of analysed proteins to the indicated N-MYC peptides was quantified and is given as relative binding compared to 1 % input, which was set as 100%. Error bars indicate standard error of the mean.

4.3 Global analysis of N-MYC and TFIIIC binding to chromatin

N-MYC and TFIIIC are transcription factors that bind to defined sites throughout the genome, regulating transcription of distinct groups of genes. N-MYC is known to occupy canonical and non-canonical E-box elements, as well as additional sites, which are characterised by histone marks for open chromatin (see introduction, section 1.2); TFIIIC binds to A- and B-box elements in the promoter of POL III transcribed genes and is essential for transcription of type I and II genes [Donze, 2012] (see discussion, section 5.4.1). More recently, TFIIIC was shown to bind to additional sites in the genome, termed ETC sites, which are not occupied by POL III and are characterised by a B-box motif or a motif similar to a B-box (ETC-motif) [Moqtaderi et al., 2010] (see discussion, section 5.4.1). To find out, if N-MYC and TFIIIC bind to joint sites throughout the genome, chromatin-immunoprecipitation coupled with high-throughput-sequencing (ChIP-sequencing) experiments were conducted using antibodies directed against N-MYC and TFIIIC5. In order to determine, whether N-MYC and TFIIIC binding to chromatin is dependent on N-MYC protein levels and/or Aurora-A, ChIP-sequencing was performed with IMR-5 cells treated with the Aurora-A inhibitor CD532, which does not only inhibit Aurora-A kinase activity, but also induces a decrease of N-MYC protein levels [Gustafson et al., 2014].

4.3.1 The Aurora-A inhibitor CD532 affects TFIIIC occupancy

Before preparing samples for ChIP-sequencing, the effect of CD532 treatment on protein levels and N-MYC and TFIIIC5 binding to their target genes was assessed in *MYCN*-amplified neuroblastoma cells. Therefore, samples from CD532 or DMSO treated IMR-5 cells were analysed by immunoblotting and in individual ChIP experiments.

CD532 treatment of *MYCN*-amplified IMR-5 cells resulted already after 4 h in a strong reduction of N-MYC levels and a concomitant decrease of Aurora-A levels (Fig. 4.12 A). The reason for the decrease of N-MYC is that CD532 binding to Aurora-A distorts the Aurora-A structure resulting in a conformation, which is incompatible with N-MYC binding and stabilisation [Gustafson et al., 2014]. The CD532-induced reduction of Aurora-A levels was not reported previously, but is consistent with the strong distortion of the Aurora-A conformation, which is likely to induce proteasomal degradation of Aurora-A after a certain period of time (Richard Bayliss, personal communication). After 4 h of CD532 treatment Aurora-A levels were obviously decreased, but not as strong as N-MYC levels (Fig. 4.12 A), while after 12 h of treatment there were only traces of detectable Aurora-A and N-MYC protein left (data not shown). TFIIIC protein levels were unaffected upon CD532 treatment and this was valid for all TFIIIC subunits tested (Fig. 4.12 A). On the contrary, CD532 induced changes in TFIIIC chromatin occupancy. ChIP experiments using antibodies directed against TFIIIC5 showed an enhancement of TFIIIC5 binding to POL III type II genes, namely tRNAs, in CD532 treated cells compared to DMSO treated cells (Fig. 4.12 B). As expected, in N-MYC ChIP experiments N-MYC binding to the transcriptional start site (TSS) of classical C-MYC target genes, shown here for *NPM1* and *NCL*, was decreased after CD532 treatment, although to a lesser extend than N-MYC protein levels were decreased (Fig. 4.12 A, B).
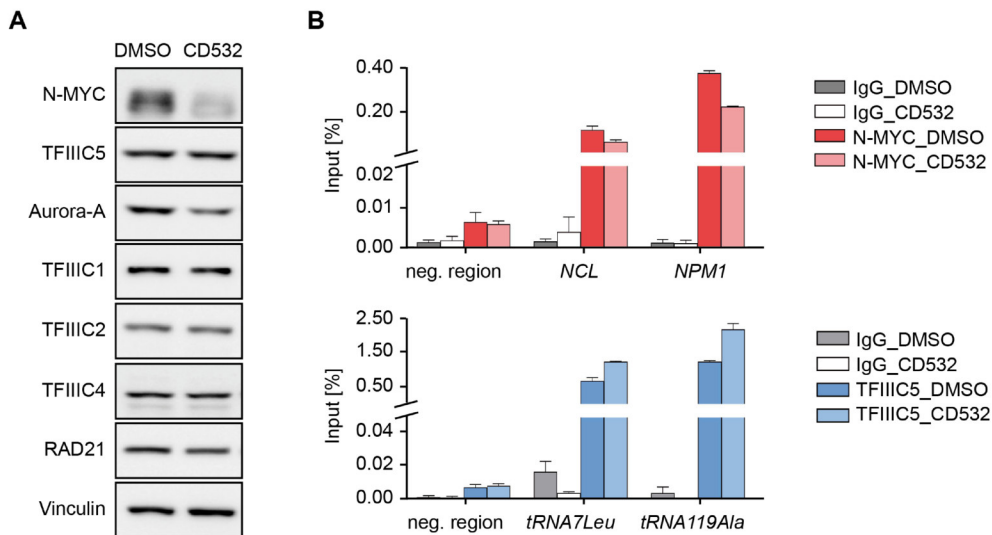
Figure 4.12
CD532 treatment leads to a reduction of N-MYC and an induction of TFIIIC occupancy
(A) Immunoblots from *MYCN*-amplified IMR-5 cells treated for 4 h with 1 μM CD532 or DMSO as a control. Immunoblots were probed with the indicated antibodies. Vinculin was used as a loading control.
(B) ChIP experiment using N-MYC, TFIIIC5 or IgG control antibodies. Precipitated and purified DNA was analysed by qRT-PCR, for N-MYC ChIPs using primers amplifying a region at the TSS of two C-MYC target genes, *NCL* and *NPM1*, and for TFIIIC5 ChIPs using primers amplifying two POL III target genes, *tRNA7Leu* and *tRNA119Ala*. Amplification of an intergenic control region (neg. region) is shown as a control for specificity. Cells were treated like in (A). Data are represented as mean of technical triplicates. Error bars indicate standard deviation.

4.3.2 N-MYC and TFIIIC bind to joint sites throughout the genome

For global analysis of N-MYC and TFIIIC occupancy in the presence or absence of CD532 IMR-5 cells were treated for 4 h with CD532 or DMSO as a control, creating a condition in which N-MYC levels were decreased to more than 50% and Aurora-A levels were only slightly decreased compared to DMSO control (Fig. 4.12 A). To this end, ChIPs with N-MYC, TFIIIC5 and control IgG antibodies were performed followed by deep sequencing. The bioinformatical analyses of deep-sequencing data were performed by Susanne Walz (Comprehensive Cancer Center Mainfranken, Core Unit Bioinformatics).

ChIP-sequencing of N-MYC and TFIIIC5 samples generated more than 1.5×10^7 reads and around 97% of reads could be mapped to the human genome, while input samples had less reads and were combined to yield around 1.08×10^7 reads (Table 4.3). Accordingly, all other samples were normalised to 1.08×10^7 reads for further analyses.

	total reads	aligned reads	% aligned	called peaks	FDR <0.25	FDR <0.1
Input	10,848,661	10,599,069	97.74	reference	n.a.	n.a.
N-MYC_DMSO	19,123,497	18,629,085	97.41	15,403	15,387	15,363
N-MYC_CD532	20,917,297	19,934,744	95.30	17,436	17,436	17,426
TFIIIC5_DMSO	15,711,908	15,234,044	96.96	7,273	7,273	7,273
TFIIIC5_CD532	18,892,914	18,421,768	97.51	35,736	35,736	35,736

Table 4.3
Statistics of ChIP-sequencing results
Statistical overview for N-MYC and TFIIIC5 ChIP-sequencing results. Shown are read numbers, aligned reads and % alignment to the human genome (hg19). Input samples were combined and all other samples were normalised to 1.08×10^7 reads. For peak calling with MACS, an equal mixture of 3 out of 4 input samples was taken as reference control. Called peak numbers for N-MYC peaks changed only slightly upon application of different false discovery rate (FDR) cut-offs, the number of called TFIIIC5 peaks did not change. Accordingly, all called peaks were taken into account for further analyses. n.a.: not applicable

First, N-MYC and TFIIIC5 occupancy within a window of 5 kb around the TSS of all annotated human POL II genes was assessed. Surprisingly, like N-MYC, TFIIIC5 was bound to the TSS of hundreds of POL II transcribed genes (Fig. 4.13 A). Peak calling identified 6,924 N-MYC-bound and 2,117 TFIIIC5-bound POL II promoters in DMSO treated cells (Fig. 4.13 B).

Upon CD532 treatment TFIIIC5 occupancy of POL II promoters was enhanced, confirming results from individual ChIPs and showing that CD532 effects on TFIIIC5 occupancy are not restricted to tRNA genes (Fig. 4.12 B, 4.13 A). The CD532-mediated increase of TFIIIC5 binding to POL II promoters was not only reflecting in tag density, but also in the number of called peaks (Fig. 4.13 A, B). Strikingly, not only the number of TFIIIC5 peaks in POL II promoters increased, but also the total number of TFIIIC5 binding sites increased around 5-fold with CD532 treatment. At tRNA genes TFIIIC5 binding displayed only minor changes in tag density and peak number upon CD532 treatment, since TFIIIC5 already occupied roughly all actively transcribed tRNAs in DMSO treated cells [Canella

et al., 2010, Dittmar et al., 2006] (Fig. 4.13 B, 4.14).

A

B

N-MYC
binding sites at POL II genes and tRNAs

CD532	all binding sites	peaks in POL II promoters	bound POL II genes	peaks in tRNA promoters	bound tRNA genes
-	15,403	9,125	6,924	156	129
+	17,436	8,831	6,645	165	128

TFIIIC5
binding sites at POL II genes and tRNAs

CD532	all binding sites	peaks in POL II promoters	bound POL II genes	peaks in tRNA promoters	bound tRNA genes
-	7,273	2,593	2,117	558	384
+	35,736	8,663	6,302	572	410

Figure 4.13
ChIP-sequencing identifies N-MYC and TFIIIC binding sites at POL II and POL III promoters
(A) Heat map documenting the distribution of tag densities obtained by ChIP-sequencing in a window of +/- 5 kb around all annotated human RefSeq TSS (hg19). Shown are normalised input, N-MYC and TFIIIC5 ChIP-sequencing samples from IMR-5 cells treated with 1 μM CD532 for 4 h or DMSO as a control. Tag densities of all samples are sorted according to N-MYC binding in DMSO treated cells (50 bp resolution).
(B) Localisation of 15,403 N-MYC and 7,273 TFIIIC5 binding sites in DMSO treated cells. Promoters are defined as +/- 1 kb around the TSS.

For N-MYC CD532 treatment induced no obvious decrease of occupancy at the TSS of POL II genes, although this was expected from individual ChIP experiments (Fig. 4.12, 4.13 A). The number of N-MYC peaks at POL II promoters was slightly lower in CD532 treated cells compared to DMSO treated cells (Fig. 4.13 B). Importantly, N-MYC peaks were also called at tRNA promoters, showing that like C-MYC, N-MYC also binds to POL III promoters [Gomez-Roman et al., 2003] (Fig. 4.13 B). N-MYC peaks displayed a lower tag density at tRNAs compared to TFIIIC5 and the number of called peaks for N-MYC was not as high as for TFIIIC5 (Fig. 4.13 B, 4.14). Nevertheless, the distribution of N-MYC tags at all TFIIIC5 peaks in tRNA promoters showed the same pattern as TFIIIC5, indicating that N-MYC, like TFIIIC5, binds to most tRNA promoters (Fig. 4.14).
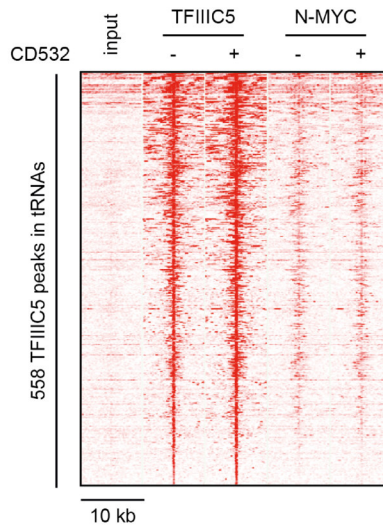
Figure 4.14
N-MYC binds together with TFIIIC to tRNA promoters
Heat map documenting the distribution of tag densities obtained by ChIP-sequencing in a window of +/- 5 kb around 558 TFIIIC5 peaks in tRNA promoters. Shown are normalised input, N-MYC and TFIIIC5 ChIP-sequencing samples from IMR-5 cells treated with 1 μM CD532 for 4 h or DMSO as a control. Tag densities of all samples are sorted according to TFIIIC5 binding in DMSO treated cells (50 bp resolution).

To identify joint N-MYC/TFIIIC binding sites the intersectBed function from BEDTools was used and binding sites were defined as overlapping, if N-MYC and TFIIIC5 peaks had a minimal overlap of 1 bp. This analysis identified 2,053 overlapping binding sites for N-MYC and TFIIIC5 in DMSO treated cells and the number of overlapping binding sites increased around 4-fold (7,994) in CD532 treated cells (Fig. 4.15 A).

A

B
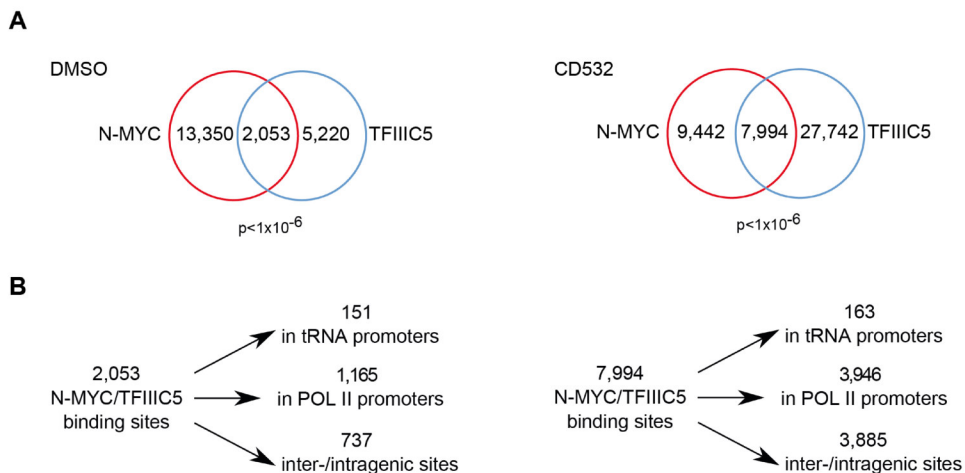
Figure 4.15
N-MYC and TFIIIC binding sites overlap at POL II and POL III promoters and inter-/intragenic sites
(A) Venn diagram showing the overlap of genome-wide N-MYC and TFIIIC5 binding sites in IMR-5 cells treated with 1 μM CD532 for 4 h or DMSO as a control. p-values were calculated using a permutation test with 1.0×10^6 iterations.
(B) Localisation of 2,053 N-MYC/TFIIIC5 binding sites in DMSO treated cells (left panel) and 7,994 binding sites in CD532 treated cells (right panel). Promoters are defined as +/- 1 kb around the TSS.

Permutation tests showed that the overlap of N-MYC and TFIIIC5 binding sites is highly significant in DMSO and CD532 treated cells (Fig. 4.15 A). To classify N-MYC/TFIIIC5 binding sites, a region of +/- 1 kb around the TSS of POL II transcribed genes and tRNA genes was taken into account and analysed for the existence of called N-MYC or TFIIIC5 peaks. Most overlapping N-MYC/TFIIIC5 binding sites were located either at POL II promoters (3,946) or at inter- and intragenic regions (3,885) and the number of tRNA genes identified to be bound by N-MYC and TFIIIC5 (163) was similar to the number bound by N-MYC alone (Fig. 4.13 B, 4.15 B). Hence, the localisation of overlapping N-MYC and TFIIIC5 binding sites revealed that not only tRNA promoters are occupied by both, N-MYC and TFIIIC transcription factors, but also a large number of POL II promoters. Furthermore, overlapping N-MYC and TFIIIC binding sites are located in intergenic regions, pointing to additional functions of N-MYC/TFIIIC complexes in other processes than transcription.

The knowledge that N-MYC and TFIIIC5 occupy overlapping sites raised the question, whether the two proteins bind to the same sites or whether binding occurs to adjacent sites. In order to visualise binding strength of N-MYC and TFIIIC5 at overlapping binding sites, the distribution of ChIP-sequencing tags from all samples were plotted in a window of 10 kb around all N-MYC or TFIIIC5 peaks in DMSO treated cells (Fig. 4.16). At both, N-MYC (Fig. 4.16, left panel) and TFIIIC5 (Fig. 4.16, right panel) peaks, tag density of all samples peaked in the center of the N-MYC/TFIIIC5 peak and tags were distributed +/- 1 kb around the peak center. The CD532-mediated increase in TFIIIC5 occupancy was clearly visible at N-MYC and TFIIIC5 peaks, resulting in higher tag number in the peak center and in the surrounding region of +/- 1 kb at N-MYC peaks and in an even broader region at TFIIIC5 peaks (Fig. 4.16). Given that N-MYC and TFIIIC5 interact with each other and N-MYC and TFIIIC5 peaks overlap, it is likely that they bind to the same sites as a complex (Fig. 4.9, 4.16).
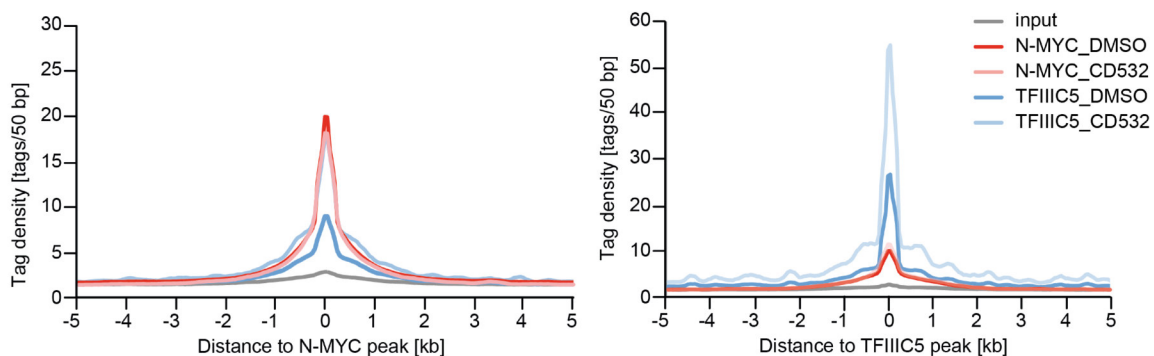
Figure 4.16
**N-MYC and TFIIIC binding sites largely overlap with each other**
Tag density plots centered to N-MYC (left panel) and TFIIIC5 (right panel) peaks. Tags were analysed for all peaks in DMSO treated cells, 15,403 peaks for N-MYC and 7,273 peaks for TFIIIC5. Tag densities were quantified with a resolution of 50 bp in regions of +/- 5 kb around the N-MYC or TFIIIC5 peak summits, respectively.

Since analysis of ChIP-sequencing data showed that N-MYC and TFIIIC5 bind to adjacent sites in POL II promoters (Fig. 4.15 B) and that the distribution of N-MYC and TFIIIC5 tag density shows the same pattern (Fig. 4.16), it was investigated, if N-MYC/TFIIIC5 binding sites have a certain orientation in respect of the TSS. Therefore, average tag density of N-MYC and TFIIIC5 around the TSS of all POL II transcribed genes, which were bound by N-MYC and TFIIIC5, was plotted in a resolution of 5 bp (Fig. 4.17). In this representation N-MYC was located close to the TSS of POL II promoters, while TFIIIC5 binding appeared broader and was shifted on average slightly 5' of N-MYC, suggesting that N-MYC/TFIIIC5 sites have a defined orientation in POL II promoters (Fig. 4.17).
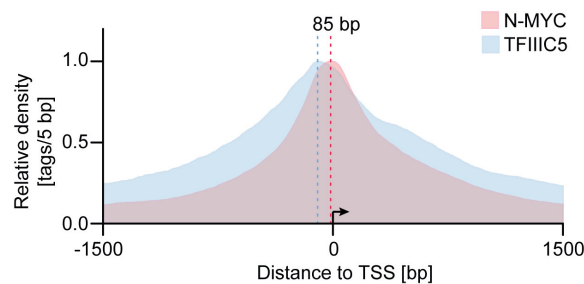
Figure 4.17
At POL II promoters N-MYC/TFIIIC binding sites have a defined orientation
Tag density distribution around the TSS of 3,946 POL II genes with N-MYC/TFIIIC5 binding sites in CD532 treated cells. Tag densities were quantified with a resolution of 5 bp in a region of +/- 1.5 kb around the TSS.

To quantify CD532-mediated effects on N-MYC and TFIIIC5 binding, first, changes in tag number in CD532 versus DMSO treated cells were plotted for all N-MYC and TFIIIC5 peaks. Whereas the previous analyses revealed no clear decrease for N-MYC, neither visually in tag density plots and heat maps, nor numerical in peak numbers, quantification of the overall N-MYC tag density at all N-MYC and TFIIIC5 peaks showed that CD532 treatment induced a significant decrease in N-MYC binding (Fig. 4.18 A). This indicates that although N-MYC occupancy changes significantly upon CD532 treatment, CD532-induced changes are not very strong and are not visible in non-quantitative representations, such as heat maps. In addition, in tag density plots, which show the average occupancy, strong CD532 effects on N-MYC occupancy at specific sites can be masked by weak effects on N-MYC occupancy at other sites. However, CD532 treatment does not result in a decrease of N-MYC binding below background, since the total number of N-MYC binding sites does not decrease with CD532 and the peak calling software MACS identifies peaks by calculating the significant local enrichment compared to background binding in input samples (see discussion, section 5.5.1). Also for TFIIIC5 changes in occupancy were highly significant at all N-MYC and TFIIIC5 peaks (Fig. 4.18 A). Quantification of N-MYC and TFIIIC5 tag density at overlapping binding sites showed similar results, CD532 treatment induced a significant decrease of N-MYC occupancy, while TFIIIC5 occupancy significantly

increased (Fig. 4.18 B). Importantly, the CD532-mediated decrease of N-MYC was even more prominent at N-MYC/TFIIIC5 binding sites and this hold true for binding sites in POL II promoters, tRNA promoters and intergenic regions (Fig. 4.18 B). The strongest increase of TFIIIC5 occupancy was evident at tRNA promoters with the median displaying a $\log_2FC > 1$ (Fig. 4.18 B).
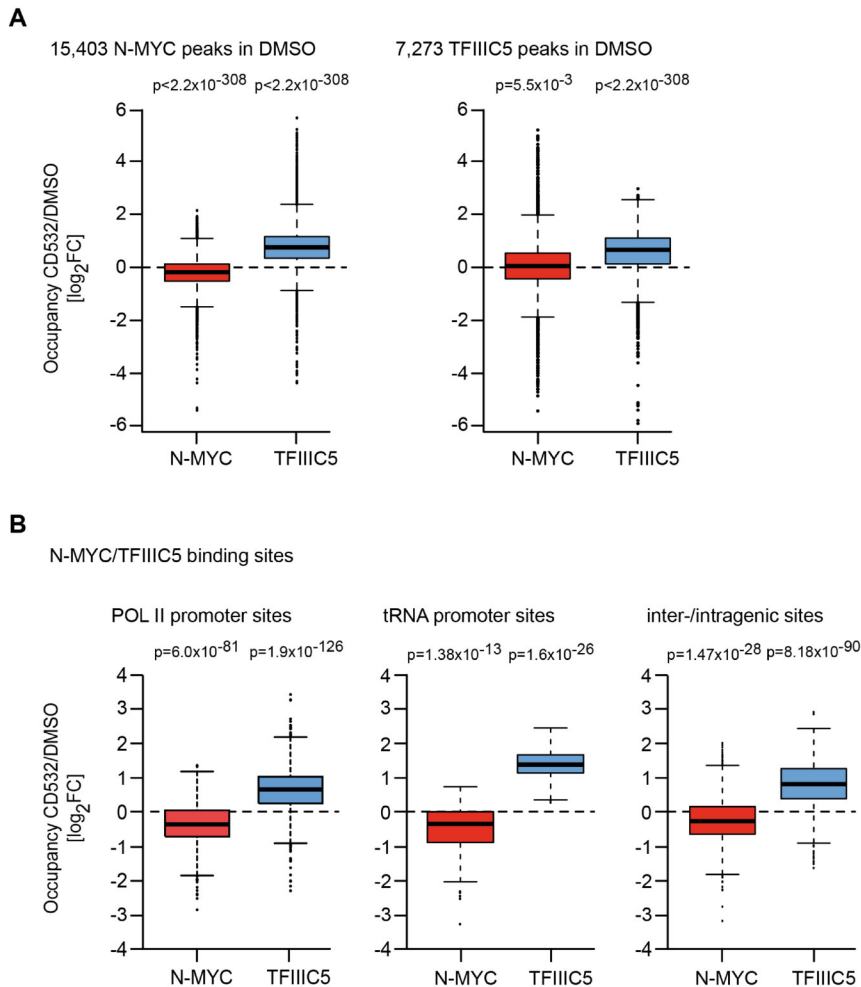
Figure 4.18
N-MYC and TFIIIC occupancy is significantly regulated upon CD532 treatment
(A) Box plots showing changes in N-MYC and TFIIIC5 occupancy in response to CD532 treatment. Fold changes ($\log_2FC$) of occupancy in CD532 versus DMSO treated cells were calculated for all N-MYC and TFIIIC5 peaks counting tags in a region of 250 bp around each peak. p-values were calculated using a two-tailed one-sample Wilcoxon Signed-rank test.
(B) Box plots showing changes in N-MYC and TFIIIC5 occupancy at overlapping binding sites located in POL II promoters (1,165 in DMSO treated cells), tRNA promoters (151 in DMSO treated cells) or inter-/intragenic regions (737 in DMSO treated cells) in response to CD532. Fold changes ($\log_2FC$) of occupancy in CD532 versus DMSO treated cells were calculated for all N-MYC/TFIIIC5 peaks counting tags in a region of 25 bp around each peak. p-values were calculated using a two-tailed one-sample Wilcoxon Signed-rank test.

In summary, analysis of ChIP-sequencing data on N-MYC and TFIIIC5 identified a large number of overlapping binding sites, which are located either at inter- and intragenic sites, or in promoters of POL II and POL III target genes. This shows that N-MYC and TFIIIC are bound to the same sites at their own target genes and *vice versa*, suggesting that

they form a complex at POL II and POL III promoters. TFIIIC binding to thousands of POL II promoters was not shown before and implicates additional, unknown functions of TFIIIC. Furthermore, the existence of overlapping binding sites at intergenic regions indicates that N-MYC/TFIIIC complexes could be involved in chromatin organisation, as it was shown for TFIIIC (see discussion, section 5.4) [Moqtaderi et al., 2010]. CD532 treatment appears to have opposing effects on N-MYC and TFIIIC occupancy, while N-MYC occupancy decreases, TFIIIC occupancy increases at sites, which are already occupied by TFIIIC, and at additional sites throughout the genome.

4.3.3 N-MYC/TFIIIC binding sites are enriched for the CTCF motif

For further characterisation of N-MYC/TFIIIC5 binding sites a *de novo* motif search was performed using MEME and DREME algorithms. Therefore, N-MYC/TFIIIC5 bound sequences from the three classes of binding sites were analysed individually, taking into account a region of +/- 50 bp around the peak summit. As expected, E-boxes were identified in N-MYC-only binding sites at POL II promoters and intergenic sites (see introduction, section 1.2) (Fig. 4.19 A). In TFIIIC5-only binding sites at POL III promoters A- and B-boxes were discovered in around 50% of binding sites and also at POL II promoters and intergenic sites TFIIIC5 binding sites often coincided with B-box elements, which was expected from what is published in literature (see discussion, section 5.4) (Fig. 4.19 A).
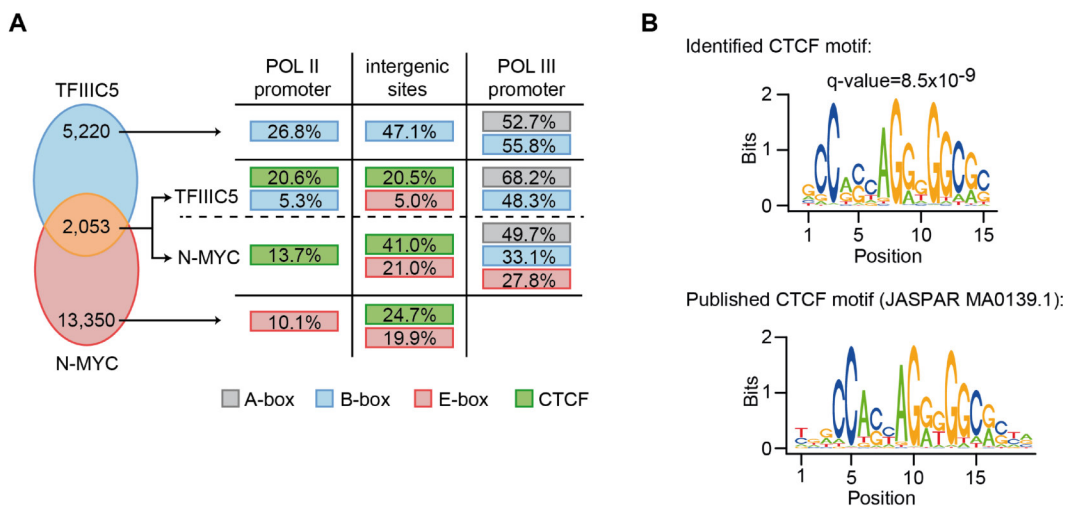
Figure 4.19
N-MYC/TFIIIC binding sites are characterised by the presence of a CTCF motif
(A) *De novo* motif search in N-MYC- and/or TFIIIC5-bound regions in DMSO treated cells. In N-MYC/TFIIIC5 binding sites both peak regions were analysed, for each peak a region of +/- 50 bp around the peak summit was taken into account. Promoters are defined as +/- 1 kb around the TSS. Percentages illustrate the number of sites in which the respective motif was found.
(B) The CTCF motif identified by *de novo* search shows a high similarity to a published CTCF binding motif (JASPAR MA0139.1). The identified motif was tested for similarity with motifs in the JASPAR database using the TOMTOM tool from the MEME Suite. The alignment with the CTCF motif from JASPAR yielded the smallest q-value [Gupta et al., 2007].

Interestingly, at N-MYC/TFIIIC5 binding sites in POL II promoters and intergenic sites

the most predominant motif was not an E-box or a B-box element, but a motif highly similar to the CTCF motif (Fig. 4.19 A ,B).

Next we asked, whether the CTCF motif was localised in the vicinity or the center of N-MYC/TFIIIC5 binding sites, since a central enrichment would strongly indicate that N-MYC and TFIIIC5 bind to this motif instead of binding to an E-box or a B-box element close by. Accordingly, the central enrichment of E-box and CTCF motifs was determined in N-MYC-only and N-MYC/TFIIIC5 binding sites using the CentriMo tool. The Ap2a motif was used as a control for specificity, since it is highly similar to the CTCF motif (JASPAR MA0003.2). Surprisingly, the CTCF motif was indeed enriched in the center of both, N-MYC-only peaks and N-MYC/TFIIIC5 binding sites, in POL II promoters and intergenic sites (Fig. 4.20). Interestingly, the enrichment varied between the two motifs for N-MYC-only and N-MYC/TFIIIC5 binding sites, in comparison to the CTCF motif the E-box element was less frequent at N-MYC/TFIIIC5 binding sites, while the CTCF motif was less frequent at N-MYC-only bound sites (Fig. 4.20). The differences in frequency were observed at POL II promoters and at intergenic binding sites (Fig. 4.20). These data imply, that there is either an E-box element or a CTCF motif located at N-MYC/TFIIIC5 binding sites and that they are enriched for CTCF motifs, whereas N-MYC-only bound sites are enriched for E-boxes.
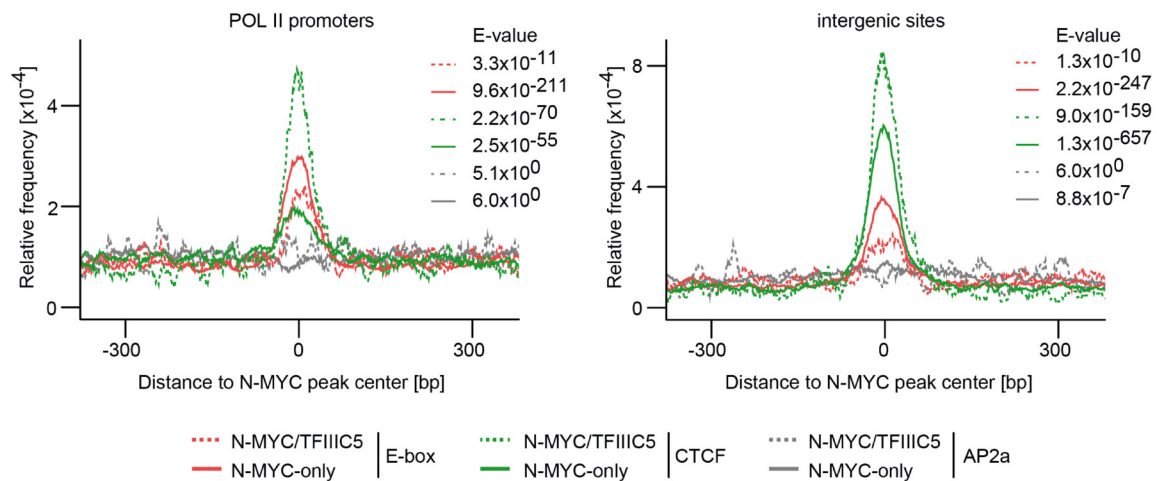
Figure 4.20
Both, E-box and CTCF motifs, are localised in the center of N-MYC peaks
Central enrichment of E-box and CTCF motifs. The CentriMo tool was used to calculate the occurrence of the predefined canonical E-box motif (CACGTG) and CTCF motif (MA0139.1) within a window of +/- 350 bp around the N-MYC peak center at N-MYC/TFIIIC5 binding sites and N-MYC-only binding sites in POL II promoters (left) or intergenic sites (right). The AP2a motif (MA0003.2) was used as a control for specificity. The frequency of a motif at a certain position was normalised to the number of input sequences and a rolling mean of 20 bp was applied for smoothing the curves. e-values were calculated using a binominal test and normalised to the number motifs in the database.

The CCCTC-binding factor (CTCF), a zinc finger transcription factor, is known to bind to the CTCF motif and to co-localise with cohesin complexes (see discussion, section 5.4), hence N-MYC/TFIIIC5 binding sites were aligned with published ChIP-sequencing data on CTCF and the cohesin subunit RAD21. Published data sets were obtained from the

ENCODE data base and selected ChIP-sequencing experiments were performed in another, non-*MYCN*-amplified neuroblastoma cell line, SK-N-SH. A heat map of N-MYC/TFIIIC5 binding sites revealed that CTCF occupies the same sites as N-MYC/TFIIIC5 and the cohesin subunit RAD21, which was shown to interact with N-MYC (Fig. 4.9, 4.21). CTCF and RAD21 binding strength was similar for sites, which showed strong (upper part of heat map in Fig. 4.21) or weak (lower part of heat map in Fig. 4.21) N-MYC/TFIIIC5 occupancy (Fig. 4.21). This results suggested that N-MYC/TFIIIC5 binding sites are also bound by CTCF/cohesin. At that time, it was unclear, whether N-MYC/TFIIIC5 and CTCF/cohesin bind together or whether either of two protein complexes binds to N-MYC/TFIIIC5 binding sites.
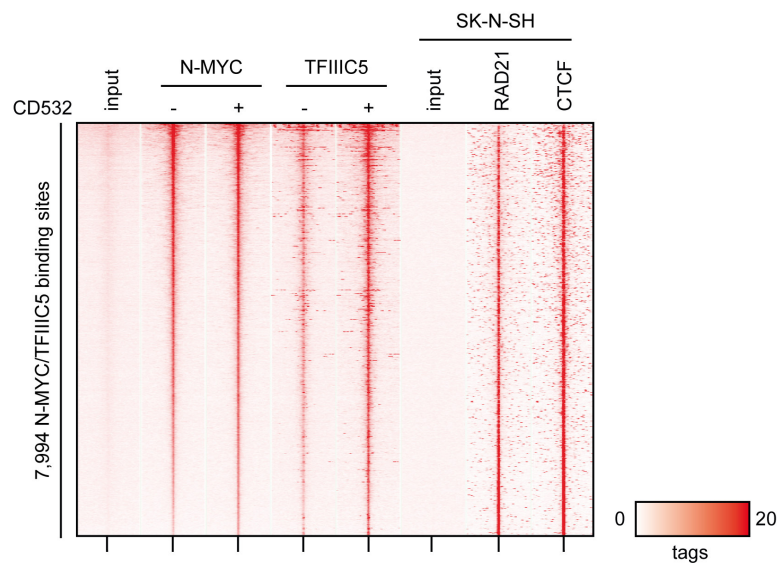
Figure 4.21
N-MYC/TFIIIC binding sites can be occupied by CTCF and cohesin
Heat map documenting occupancy of N-MYC, TFIIIC5, RAD21 and CTCF at 7,994 N-MYC/TFIIIC5 binding sites in CD532 treated cells. Samples were normalised to the same number of mapped reads, peaks were centered to the N-MYC peak and sorted according to N-MYC binding in DMSO treated cells. Shown are tag densities in a window of +/- 5 kb around the N-MYC peak summit (50 bp resolution). RAD21, CTCF and corresponding control ChIP-sequencing data from SK-N-SH cells were obtained from ENCODE (CTCF: ENCFF001HXM, RAD21: ENCFF000RFT, control: ENCFF000RCC).

Inspection of individual POL II genes (Fig. 4.22) and intergenic regions (data not shown) confirmed the co-localisation of N-MYC, TFIIIC5, CTCF and RAD21 peaks. Furthermore, most N-MYC/TFIIIC5 binding sites comprised a CTCF motif, but no E-box (Fig. 4.22), supporting the data from motif analyses (Fig. 4.19, 4.20).
Conclusively, the analysis of N-MYC and TFIIIC5 ChIP-sequencing data revealed that N-MYC/TFIIIC5 binding sites are enriched for a consensus CTCF binding motif and utilisation of published ChIP-sequencing data showed that CTCF and the cohesin subunit RAD21 can occupy N-MYC/TFIIIC5 bound sites.
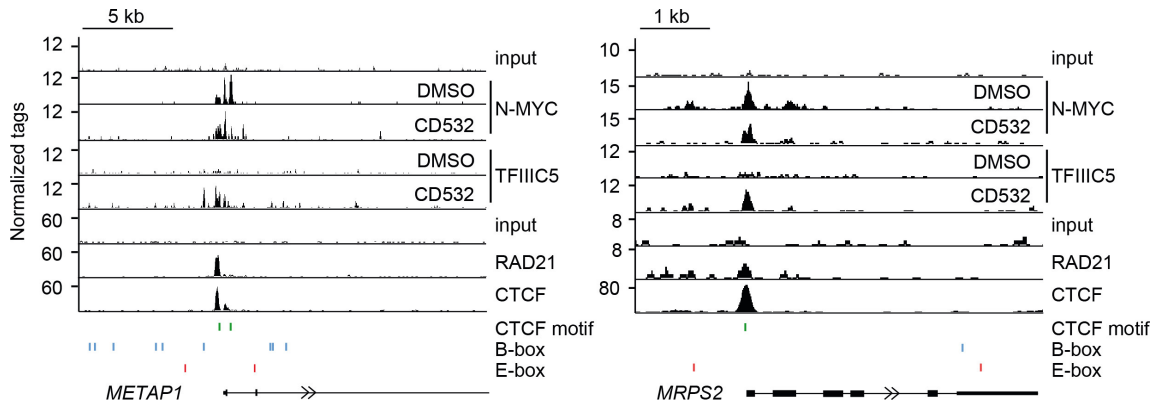
Figure 4.22
N-MYC/TFIIIC binding sites at POL II promoters show altered binding preference
Illustration of DNA-binding of indicated proteins at the TSS of the POL II genes *METAP1* and *MRPS2*. Reads from normalised ChIP-sequencing samples were visualised with the Integrated Genome Browser software. RAD21, CTCF and corresponding control ChIP-sequencing data is from the same source as in Fig. 4.21. The presence of CTCF (green), B-box (blue) and E-box (red) motifs is indicated by colored bars below the ChIP-sequencing tracks. The gene structure is indicated at the bottom of each panel, exons are represented by vertical lines and arrows indicate the direction of transcription.

4.3.4 Cohesin binds to N-MYC/TFIIIC occupied sites and its occupancy is regulated by CD532

N-MYC and TFIIIC binding to sites comprising a CTCF motif and potential co-binding of CTCF and cohesin to these sites represented an unexpected and interesting finding, as it suggests a role of the N-MYC/TFIIIC complex in regulation of chromatin architecture. CTCF was demonstrated to function as an insulator, separating actively transcribed from repressed areas of chromatin, and it was shown to exert its function in a complex with cohesin, which is a ring-shaped complex that holds together two DNA strands (see discussion, section 5.4). Moreover, TFIIIC was also implicated to act as an insulator when bound to tRNA genes [Raab et al., 2012]. In addition, intergenic TFIIIC binding sites, which are not co-occupied by POL III, were shown to be associated with cohesins and to be located close to CTCF binding sites (see discussion, section 5.4).

To substantiate the link between N-MYC/TFIIIC5 binding sites and CTCF/cohesin function, the interaction of the protein complexes was investigated. N-MYC interaction with cohesin subunit RAD21 was shown before (Fig. 4.9 A, B), but RAD21 interaction with TFIIIC was not tested and is also not shown in literature. Hence it was investigated, if TFIIIC5 and RAD21 interact with each other. Furthermore, the interaction of N-MYC and TFIIIC with CTCF was assessed. As for ChIP experiments, *MYCN*-amplified IMR-5 cells were treated for 4 h with CD532 or DMSO as a control and used for immunoprecipitation experiments. In endogenous TFIIIC5 IPs, RAD21 was co-purified regardless of CD532 treatment (Fig. 4.23 A). *Vice versa*, in RAD21 IPs TFIIIC5 was not co-purified, while the interaction of CTCF and RAD21 was verified (Fig. 23 A) [Rubio et al., 2008]. Importantly, neither TFIIIC5 (Fig. 23 A), nor N-MYC (not shown) IPs resulted in a co-purification of CTCF. These results indicate that CTCF motifs in N-MYC/TFIIIC5 binding sites are either bound by CTCF/cohesin complexes or by N-MYC/TFIIIC complexes that can interact with

cohesin.
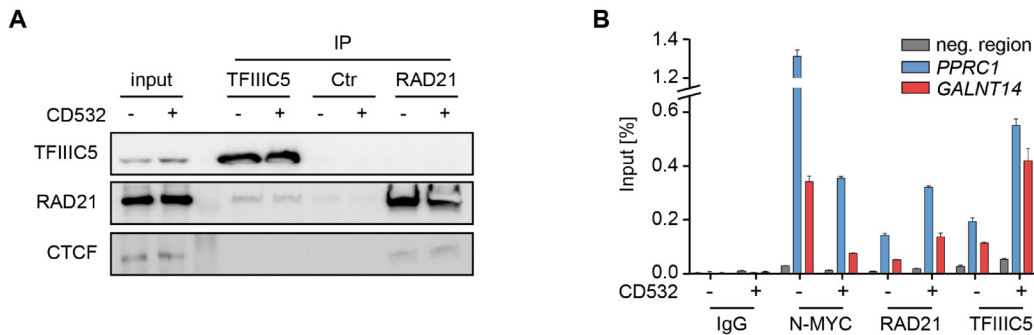
Figure 4.23
RAD21 interacts with N-MYC/TFIIIC independent of CD532 treatment and occupies N-MYC/TFIIIC binding sites in POL II promoters
(A) Immunoprecipitation from *MYCN*-amplified IMR-5 cells treated for 4 h with 1 µM CD532 or DMSO as a control. TFIIIC5 protein complexes were immunoprecipitated with TFIIIC5 antibodies, precipitation with IgG was used as a control (Ctr). 1% input and IP samples were analysed by immunoblotting and probed with the indicated antibodies.
(B) ChIP experiment using N-MYC, RAD21, TFIIIC5 or IgG control antibodies. Precipitated and purified DNA was analysed by qRT-PCR using primers amplifying a region at the TSS of two POL II target genes, *PPRC1* and *GALTN14*, and an intergenic control region (neg. region). IMR-5 cells were treated like in (A). Data are represented as mean of technical triplicates. Error bars indicate standard deviation.

In order to confirm that RAD21 binds to the same sites as N-MYC and TFIIIC in *MYCN*-amplified IMR-5 cells and to determine CD532-mediated effects on RAD21 occupancy, ChIP experiments were performed from IMR-5 cells treated with or without CD532. ChIP experiments did not only show that the three proteins were bound to the same region in the TSS of POL II genes, exemplified here by *PPRC1* and *GALNT14*, but also that CD532 treatment increased the occupancy of both, TFIIIC5 and RAD21, while N-MYC occupancy was decreased (Fig. 4.23 B). These results indicate a co-occupancy of cohesin and N-MYC/TFIIIC and a CD532-dependent regulation of cohesin occupancy. This observation was validated in additional ChIP experiments using primers for binding sites in promoters of several POL II genes and of tRNA119Ala, as well as in an intergenic region (Fig. 4.24 B). All sites investigated showed the same trend for TFIIIC5, RAD21 and N-MYC changes in occupancy upon CD532 treatment, except for RAD21 occupancy at tRNAs (Fig. 4.24 B). Since it is known that cohesin does not bind to tRNA genes, it was expected that RAD21 occupancy remained unchanged upon CD532 treatment.

In agreement with literature, CD532 did not only affect N-MYC and Aurora-A protein levels, but also inhibited the kinase activity of Aurora-A, which is indicated by the decrease of Aurora-A autophosphorylation at T288 [Gustafson et al., 2014] (Fig. 4.24 A). To determine the relevance of Aurora-A kinase function for TFIIIC, RAD21 and N-MYC binding, IMR-5 cells were treated with two additional Aurora-A inhibitors, MK-5108 and MLN8237. MK-5108 is a purely catalytic Aurora-A inhibitor, which does not change the Aurora-A conformation upon binding [Shimomura et al., 2010]. MLN8237 is a catalytic Aurora-A inhibitor, which slightly distorts the Aurora-A conformation upon binding, preventing the N-MYC interaction and stabilisation [Brockmann et al., 2013] (see introduction,

section 1.5).
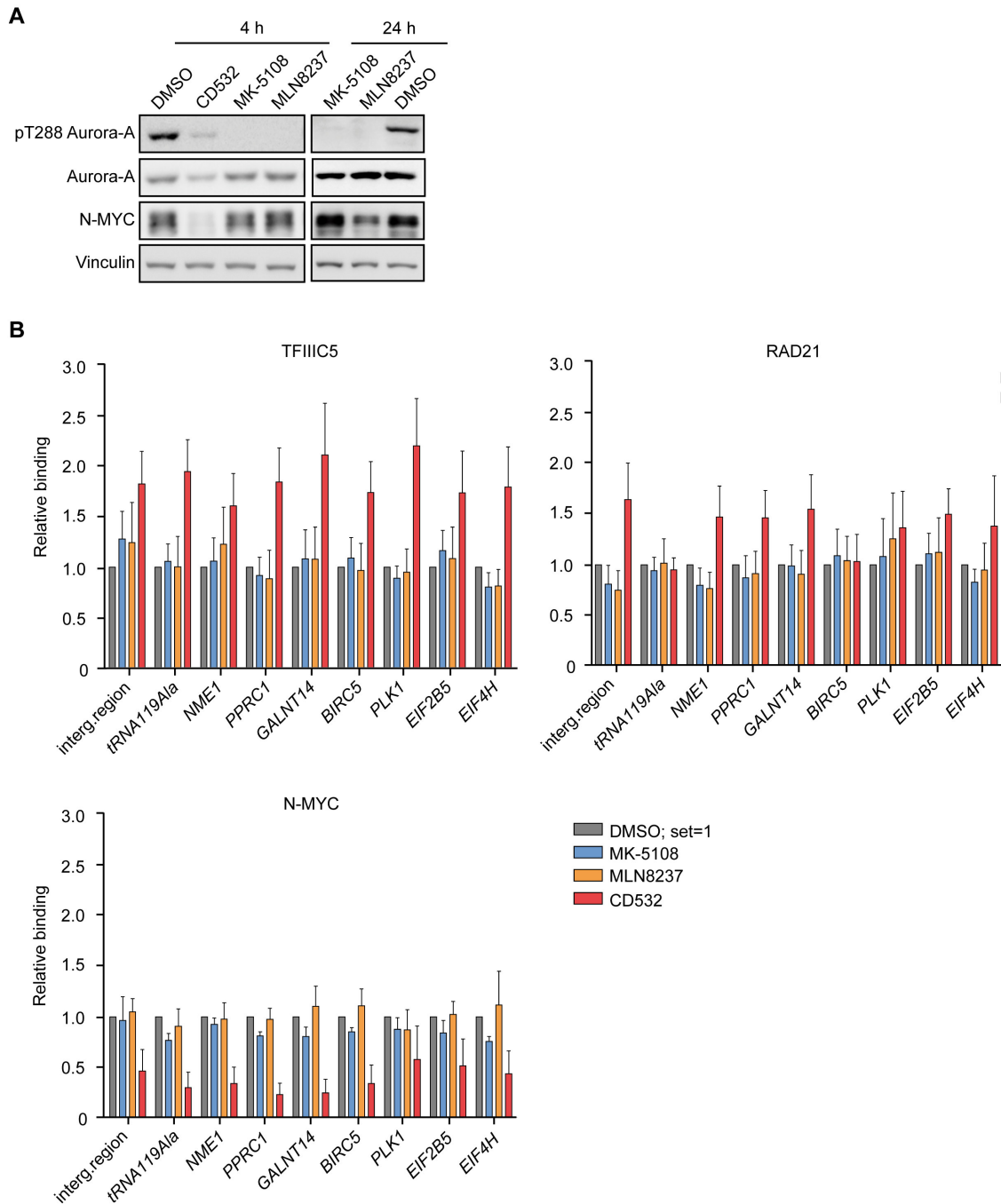
Figure 4.24
In contrast to Aurora-A inhibitors MK-5108 and MLN8237, CD532 increases RAD21 and TFIIIC occupancy
(A) Immunoblots of IMR-5 cells treated with CD532 for 4 h, and MK-5108 or MLN8237 for 4 h and 24 h and DMSO as a control. Vinculin was used as a loading control.
(B) Summary of ChIP experiments performed with cells shown in (A), documenting changes of occupancy for TFIIIC5, RAD21 and N-MYC at the indicated loci. Data are normalised to DMSO treated control cells and are represented as mean of 3 or 4 (targets of TFIIIC5 and RAD21 ChIPs in CD532 treated cells) independent experiments. Error bars indicate standard error of the mean.

MK-5108 and MLN8237 treatment completely abolished Aurora-A autophosphorylation at T288 already after 4 h, while there was still residual Aurora-A kinase activity left upon 4 h of CD532 treatment (Fig. 4.24 A). After 24 h of MLN8237 treatment N-MYC levels decreased as published by Brockmann et al. [2013] (Fig. 4.24 A). For ChIP experiments the 24 h period of treatment was chosen for MK-5108 and MLN8237 to include the effect of MLN8237 on N-MYC. Surprisingly, neither MK-5108, nor MLN8237 led to an increase of TFIIIC5 and RAD21 occupancy and both had no strong effect on N-MYC occupancy at all sites tested (Fig. 4.24 B).

In summary, ChIP results for the three different Aurora-A inhibitors led to the conclusion that neither the inhibition of Aurora-A kinase activity, nor the decrease of N-MYC levels is the sole determinant that induces an increase of TFIIIC and RAD21 occupancy upon CD532 treatment, suggesting that the change of Aurora-A levels is a relevant factor.

5   Discussion

MYC proteins are involved in a large variety of cellular processes, ranging from protein synthesis and cell-cycle progression to induction of apoptosis and metabolic reprogramming upon certain stimuli [Dang et al., 2006]. N-MYC belongs to the human MYC protein family and is a *bona fide* oncogene that is overexpressed in several tumour entities. Importantly, *MYCN* expression levels correlate with a poor prognosis for patients [Beltran, 2014]. In many cases amplification of the N-MYC encoding gene is the reason for high expression levels, for example in neuroblastoma [Huang and Weiss, 2013]. For *MYCN*-amplified neuroblastoma it was shown that N-MYC interacts with the protein kinase Aurora-A and that interaction with Aurora-A interferes with proteasomal degradation of N-MYC by an unknown mechanism [Otto et al., 2009]. Accordingly, the objective of this thesis was to unravel the mechanism of Aurora-A-mediated stabilisation of N-MYC. Therefore, a proteomic analysis of N-MYC protein complexes was conducted, aiming to identify novel N-MYC interaction partners. The identification of N-MYC interacting proteins does not only enable the determination of proteins, which could be involved in N-MYC stabilisation by Aurora-A, but also allows the detection of interacting proteins that could be targets for therapy of tumours with high N-MYC protein levels. In addition, a proteomic analysis always bears the potential to find novel interaction partners of a protein of interest, enabling the identification of previously unknown protein functions.

5.1   Characterisation of the N-MYC/Aurora-A complex

Otto *et al.* discovered the interaction of N-MYC and Aurora-A in a synthetic lethal screen aiming to identify potential therapeutic targets for *MYCN*-amplified neuroblastoma [Otto et al., 2009]. They showed that Aurora-A rescues N-MYC from proteasomal degradation via the SCF^{FBXW7} ubiquitin ligase complex, but how Aurora-A prevents degradation of N-MYC remained unclear. Importantly, they found that neither displacement of N-MYC from the F-box protein FBXW7, which is the part of the SCF^{FBXW7} complex that recognises N-MYC, nor the catalytic activity of Aurora-A play a role in Aurora-A-mediated stabilisation of N-MYC [Otto et al., 2009]. Ubiquitination assays indicated an Aurora-A-mediated change in N-MYC-attached ubiquitin chains from K48- to K11- or K63-linked polyubiquitin chains that do not target the proteasome [Otto et al., 2009]. However, N-MYC interaction with a candidate ubiquitin-conjugating enzyme, UBE2N, which was shown to interact with Aurora-A and which directs the synthesis of K63-linked polyubiquitin chains, was not detected in immunoprecipitation experiments [Ewart-Toland et al., 2003, Otto et al., 2009]. Furthermore, the structure of the N-MYC/Aurora-A complex was not solved and it was unclear whether N-MYC and Aurora-A interact directly and whether interaction is mediated via a specific domain of N-MYC and/or Aurora-A. The only information about the interaction of the two proteins present at that time originated from an N-MYC mutant, which displayed a decrease in interaction with Aurora-A and which was not stabilised by

Aurora-A [Otto et al., 2009]. This N-MYC mutant was mutated at T58 and S62 (N-MYC T58A/S62A=N-MYC mut), the two phosphorylation sites that have to be phosphorylated by cyclin B1/CDK1 and GSK-3ß in order to enable N-MYC recognition and degradation via the SCF^{FBXW7} ubiquitin ligase (see introduction, section 1.4).

In vitro binding assays with recombinant Aurora-A and *in vitro* translated N-MYC showed that N-MYC and Aurora-A interact directly (Fig. 4.1). In contrast to *in vivo* studies, *in vitro* pull-down assays with Aurora-A showed the same results for N-MYC wt and N-MYC mut (Fig. 4.1). *In vitro* studies utilising several N-terminal N-MYC peptides and recombinant Aurora-A (Aurora-A kinase domain, aa122-403) confirmed the direct interaction of N-MYC and Aurora-A and the N-MYC residues 28-89 were identified as the minimal Aurora-A binding region (Richards et al., in revision[1]). Furthermore, *in vitro* pull-down assays with differently phosphorylated N-MYC peptides confirmed that the N-MYC and Aurora-A interaction does not depend on phosphorylation of N-MYC on residues T58 and/or S62 *in vitro*[1], as it was shown in cellular immunoprecipitation experiments and pull-down assays *in vivo* [Otto et al., 2009] (Fig. 4.9, 4.11).

Recently, the laboratory of Richard Bayliss (University of Leeds, UK) accomplished the crystallography on an N-terminal region of N-MYC (aa61-89) with the Aurora-A kinase domain[1]. Since the N-terminal interaction surface between the N-MYC peptide used for crystallography (aa28-89) and Aurora-A was not observed in the crystal structure (aa28-60), the relevance of N-MYC residues T58 and S62 for the interaction with Aurora-A remains open. Nevertheless, solving a part of the structure of the N-MYC/Aurora-A complex is an important first step for the characterisation of the complex and represents a valuable tool for generating potent inhibitors, which disrupt the interaction of N-MYC and Aurora-A. The structure of Aurora-A when bound to the Aurora-A inhibitor MLN8054 was published before and provided a basis for the development of inhibitors specifically disrupting the N-MYC/Aurora-A complex [Dodson et al., 2010, Gustafson et al., 2014]. MLN8054 induces a twist in the conformation of Aurora-A and interferes with Aurora-A-mediated stabilisation of N-MYC [Brockmann et al., 2013] (see introduction, section 1.5). The crystal structure of the N-MYC/Aurora-A complex represents a structural basis for comparison of the Aurora-A structure when Aurora-A is bound to MLN8054 with the N-MYC-bound structure. Comparison revealed that in a complex with MLN8054 the Aurora-A affinity for N-MYC is reduced[1]. This explains why MLN8054 treatment results in both, Aurora-A inhibition and induction of N-MYC degradation, and the same was true for the improved variant MLN8237 [Brockmann et al., 2013]. The ability of MLN8054/8237 to disrupt the N-MYC/Aurora-A complex is even stronger for another drug, CD532, which was developed with the aim to disrupt the N-MYC/Aurora-A complex more efficiently then MLN8237 by inducing a stronger distortion of the Aurora-A structure [Gustafson et al., 2014]. Whereas phase II clinical trials for MLN8237 have been successfully accomplished, initial studies in

---

[1] Data on N-MYC - Aurora-A interaction obtained from *in vitro* assays and crystallography was submitted for publication in PNAS and the publication is currently in revision, see also the following pages.

mice showed that the CD532 compound is highly toxic and needs to be optimised to enable use in clinical trials (Clay W. Gustafson, personal communication). The crystal structure of the N-MYC/Aurora-A complex at hand reveals N-MYC - Aurora-A contacts within the kinase domain and allows the development of optimised compounds disrupting selectively the N-MYC/Aurora-A interaction surface[1]. Interestingly, *in vitro* assays demonstrated that in a complex with N-MYC Aurora-A is kinetically active[1], but substrate specificity appears to be altered (Mark W. Richards, personal communication), indicating an additional, previously unknown biological function of the N-MYC/Aurora-A complex, presumably in cooperation with other interacting proteins.

5.2   N-MYC interacts with proteins involved in diverse cellular processes

The identity of proteins that are co-purified with a protein of interest can be revealed by mass spectrometric analysis. The principle of mass spectrometry (MS) was discovered in the second half of the 19th century and is based on the separation of ions in a magnetic or electric field according to their mass to charge ratio. Today´s mass spectrometers are still based on the same principle, but recent advances in technology have increased specificity and potency of proteomic analysis, enabling specific detection of multiple protein modifications, a more reliable and quantifiable identification of recovered peptides, as well as multidimensional analysis of selected proteomes by combining information on several parameters [Larance and Lamond, 2015]. While there is a lot of information available on the human C-MYC interactome originating from several MS analyses [Agrawal et al., 2010, Dominguez-Sola et al., 2007, Koch et al., 2007], only one proteomic analysis of N-MYC complexes is published until now [Choi et al., 2010]. The existing MS analysis of N-MYC protein complexes was performed in HeLa cells, a cancer cell line, which displays very high C-MYC levels, but lacks endogenous N-MYC expression. Since HeLa cells do not originate from neuronal precursor cells [Scherer et al., 1953], the list of identified proteins might lack cell-type specific proteins that are for example important regulators of N-MYC stability. Furthermore, the published list of N-MYC interacting proteins included only 33 proteins [Choi et al., 2010]. Thus, judging from what is known on N-MYC protein function (see introduction, section 1.2) and published C-MYC interaction data [Agrawal et al., 2010, Choi et al., 2010, Koch et al., 2007], it reflects only a small fraction of N-MYC interacting proteins.
Therefore, a new proteomic analysis was conducted in a neuroblastoma cell line that was engineered to express N-MYC wt and N-MYC mut at levels similar to oncogenic N-MYC levels in *MYCN*-amplified neuroblastoma (see results, section 4.2). In neuroblastoma cells N-MYC wt is stabilised by Aurora-A, while N-MYC mut is not stabilised by Aurora-A [Otto et al., 2009]. Hence, the comparison of the N-MYC wt interactome with N-MYC mut interaction partners allows the identification of proteins exclusively or preferentially interacting with N-MYC wt. These N-MYC wt specific interaction partners are candidates for functional components in the mechanism that leads to Aurora-A-mediated stabilisation of N-MYC wt. Proteomic analysis identified hundreds of proteins specifically interacting

with N-MYC wt and/or N-MYC mut, but yielded very low peptide counts for Aurora-A, showing no enrichment compared to the empty control cell line (see results, section 4.2). On the contrary, Aurora-A Co-IP with N-MYC was detected by western blotting in the identical samples, which were subjected to MS analysis (Fig. 4.3), and Aurora-A was listed among the 33 proteins identified to interact with N-MYC in HeLa cells, though also with a low number of peptides [Choi et al., 2010]. There are several reasons for the discrepancy between results from western blotting and MS analysis of N-MYC complexes from neuroblastoma cells. One reason for the low number of identified Aurora-A peptides and the lack of specific enrichment in the sample of N-MYC wt expressing cells could be the hydrophobic nature of Aurora-A peptides, leading to retardation of peptide detection in MS or lack of detection (Andreas Schlosser, personal communication) (see results, section 4.2). In addition, in comparison to western blotting MS analysis is a multi-step process that encompasses several reactions, which could change the amount of detected peptides of a specific protein (see methods, section 3.3.4).

Besides Aurora-A, a large number of proteins was detected in MS analysis, in total 2515 proteins were identified. Setting a threshold for the number of detected peptides and the enrichment over empty control cells yielded a list of 224 highly confident interaction partners (see results, section 4.2 and appendix A.1). Functional Annotation Clustering revealed that these N-MYC interacting proteins were functional components of several cellular processes, which are among the processes known to involve MYC protein function (see introduction, section 1.2). The most significantly enriched functional clusters included for example clusters for proteins involved in chromatin acetylation and POL II transcription (Table 4.1). In contrast, the identification of a cluster for the POL III transcription factor complex TFIIIC among the most significantly enriched clusters was very surprising, since N-MYC was not known to interact with TFIIIC (see discussion, section 5.4). The relevance of N-MYC interaction with TFIIIC and additional novel N-MYC interaction partners and implications for MYC biology will be discussed in section 5.4.

The MS detection of three different peptides that are specific for a certain protein (exclusive unique peptides) is sufficient for reliable identification of a protein (Andreas Schlosser, personal communication). However, in case of MS analysis of samples from immunoprecipitation experiments the identification of proteins that were co-purified with a protein of interest needs to be validated in additional immunoprecipitation experiments to ensure reliability of the discovered specific interaction. There are two experimental reasons why validation is required: on the one hand side, although IP samples were eluted, samples can be contaminated with proteins that were unspecifically co-purified, on the other hand side, proteins from previous runs can contaminate the MS instrument and be detected in later runs. The detection of a large number of proteins in the empty control cell line, which is devoid of specific N-MYC interaction partners, since it does not express any N-MYC, undermines the need of validation (see appendix A.1, A.2).

Accordingly, the identity of selected N-MYC interacting proteins identified by MS analysis

was validated by immunoprecipitation experiments and subsequent immunoblotting. There-fore, more stringent criteria were applied to the list of 224 proteins identified to interact with N-MYC, yielding a list of 82 proteins, which was used to select novel interaction partners for validation (see results, section 4.2, and appendix A.2).

5.3   Two deubiquitinating enzymes, USP7 and USP11, interact with N-MYC

Since proteomic analysis of N-MYC complexes aimed to find components of the N-MYC/ Aurora-A complex that play a role in Aurora-A-mediated stabilisation of N-MYC, the list of identified interaction partners was searched for proteins belonging to the ubiquitin system. Components from the ubiquitin system, which are known to have the ability to rescue a tar-get protein from proteasomal degradation are deubiquitinating enzymes (see results, section 4.2). For example, the deubiquitinating enzyme USP28 removes ubiquitin chains targeting the proteasome, which were attached to C-MYC via the ubiquitin ligase SCF^{FBXW7} [Popov et al., 2007]. In contrast to C-MYC, N-MYC does not interact with USP28 and there is no deubiquitinating enzyme known to prevent degradation via SCF^{FBXW7} (Nikita Popov, personal communication). In order to identify deubiquitinating enzymes targeting N-MYC, an siRNA screen was performed in parallel to MS analysis. In the siRNA screen all known human deubiquitinating enzymes were targeted by 4 individual siRNAs and the effect of knockdown on N-MYC protein levels was monitored by measuring immunofluorescence (IF) intensity from N-MYC, which was detected using IF-labeled secondary antibodies. Screen-ing was performed by Ursula Eilers und Christina Schülein-Völk using a Operetta High Content Imaging System in the Microscopy Core Unit of the Biocenter at the University of Würzburg. Evaluation of two independent experiments identified 5 candidates: USP7, USP17, USP37, USP39 and PSMD14. Among these the three deubiquitinating enzymes USP7, USP17 and USP37 represented potential candidates to regulate N-MYC stability, as they are known to be localised in the cytoplasm and/or nucleus and to be involved in several cellular processes [Fraile et al., 2012]. The other two candidates were unlikely to be involved in the mechanism of Aurora-A-mediated N-MYC stabilisation, given that, although USP39 is classified as a deubiquitinating enzyme, it is deprived of its enzymatic activity, playing a role in mRNA splicing [van Leuken et al., 2008], and PSMD14 is a component of the 26S proteasome [Spataro et al., 1997]. MS analysis identified one out of these 5 candid-ates, USP7, which represented the only deubiquitinating enzyme in the "Top 82-List" of N-MYC interacting proteins (see appendix A.2). In addition to USP7, USP11 was selected for validation, since it interacts with USP7, sharing common targets for deubiquitination [Maertens et al., 2010]. A second reason was that USP11 was included in the published list of 33 proteins from MS analysis on N-MYC complexes in HeLa cells [Choi et al., 2010]. Immunoprecipitation experiments confirmed the interaction of exogenous N-MYC, as well as endogenous N-MYC proteins with USP7 and USP11 (Fig. 4.5, 4.6). If N-MYC would be stabilised by a mechanism, which involves Aurora-A-mediated recruitment of USP7 and/or

USP11 and subsequent N-MYC deubiquitination, knockdown of USP7 and USP11 should decrease N-MYC levels (Fig. 5.1). However, in contrast to results from the siRNA screen, shRNA-mediated knockdown of *USP7* mRNA in *MYCN*-amplified neuroblastoma cells did not result in a clear decrease of N-MYC on protein level (Fig. 4.7). *USP7* mRNA was targeted by three different shRNAs that induced a decrease of USP7 to more than 50% on mRNA and protein level. While *shUSP7-1* was most efficient, *shUSP7-3* showed the least pronounced decrease of USP7 mRNA and protein, though levels were still decreased to more than 50% (Fig. 4.7). Only expression of the least efficient shRNA, *shUSP7-3*, resulted in a clear reduction of N-MYC protein levels compared to controls. This observation could indicate that secondary effects play a role for USP7-mediated stabilisation of N-MYC, which include mechanisms that are only relevant if a certain USP7 protein level is reached. A similar mechanism was demonstrated to play a role in USP28-mediated stabilisation of C-MYC. USP28 does not only prevent SCF^{FBXW7}-mediated degradation of C-MYC and additional substrates of SCF^{FBXW7}, but also interferes with degradation of the SCF^{FBXW7} component FBXW7. Until a certain USP28 protein level is reached FBXW7 is preferentially deubiquitinated and stabilised by USP28, above this level USP28 also stabilises FBXW7 substrates [Schuelein-Voelk et al., 2014]. What contradicts this interpretation of *USP7* knockdown experiments, is the concomitant decrease of N-MYC mRNA levels to more than 50% upon knockdown of *USP7* by *shUSP7-3* (Fig. 4.7). The decrease of *MYCN* mRNA could be the reason for the decrease of N-MYC protein and could be due to off-target effects from this specific shRNA. Knockdown of a selected target mRNA via transfection of siRNAs or expression of shRNAs can trigger off-target effects that can be sequence-specific, for example caused by imperfect hybridisation with unintended target mRNAs, or non-specific, inducing immune or toxicity related cellular responses [Singh et al., 2011]. Since shRNAs are delivered as cDNA sequences in expression plasmids, expressed in the nucleus and processed by the endogenous miRNA machinery, they are less likely to trigger non-specific off-target effects compared to siRNAs. The induction of sequence-specific off-target effects by imperfect hybridisation of *shUSP7-3* with *MYCN* mRNA was tested by sequence alignment using the BLAST tool from NIH and yielded a maximal overlap with the human transcriptome of 8 from 19 nucleotides in the shRNA sequence. Although this corresponds to a sequence similarity of less than 50%, it is possible that *shUSP7-3* targets *MYCN* mRNA, as shRNAs with even less than 7 complementary nucleotides were demonstrated to induce off-target effects by suppressing unintended target mRNAs [Jackson et al., 2006]. The *USP7* knockdown effects were controlled by transfection of an empty control plasmid, as well as a non-targeting control sequence (shScr) (Fig. 4.7). Even though the selected non-targeting control showed no effects in several experiments in other neuroblastoma cell lines (Jiajia Xu, personal communication), shScr led to a decrease of N-MYC protein levels in *MYCN*-amplified IMR-5 (not shown) and IMR-32 cells (Fig. 4.7), whereas *MYCN*, *AURKA* and *USP7* mRNA expression increased. The increase of *MYCN* mRNA levels in contrast to the decrease of N-MYC protein levels and the increased expression of

all assayed mRNAs, compared to cells transfected with empty control plasmid, indicated non-sequence specific effects upon transcription and expression of sequences in the backbone of the shRNA expression vector used (pLKO.1). Expression of shScr also resulted in effects on proliferation, though these effects were much weaker compared to the effects upon *USP7* knockdown (Fig. 4.7). Knockdown of *USP7* resulted in a strong decrease of proliferation of *MYCN*-amplified neuroblastoma cells, in an arrest of cells in G1 phase of the cell cycle and in induction of neuronal differentiation (Fig. 4.7 and Thesis from J. Dirks, soon to be published). However, the effects of *USP7* knockdown on N-MYC remained unclear and revealed no direct connection between N-MYC protein levels and USP7 function.
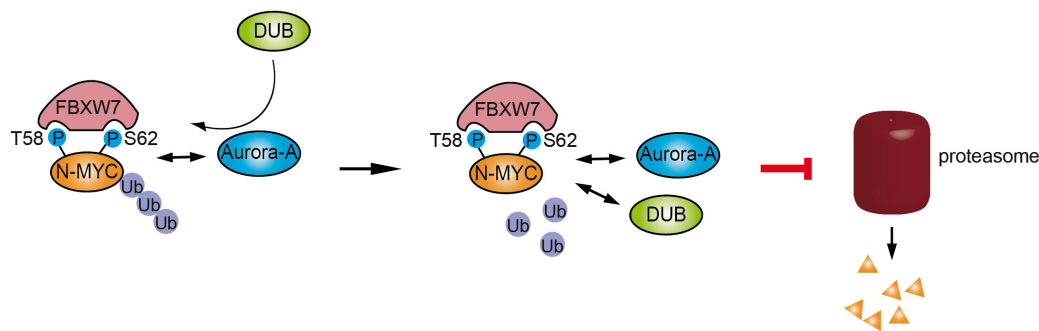
Figure 5.1
Proposed mechanism of Aurora-A-mediated stabilisation of N-MYC
Scheme illustrating a possible mechanism for Aurora-A-mediated N-MYC stabilisation. Aurora-A interacts with N-MYC and recruits a deubiquitinating enzyme (DUB). The DUB cleaves off ubiquitin chains, which were conjugated to N-MYC via the ubiquitin ligase complex SCF^{FBXW7}. Removal of attached ubiquitin chains targeting the proteasome inhibits N-MYC recognition and degradation via the proteasome system.

USP11 knockdown experiments did not induce a decrease of N-MYC, neither upon siRNA-mediated knockdown using a pool of 4 siRNAs (Fig. 4.8), nor with three different shRNAs (not shown). On the contrary, USP11 overexpression in SH-EP cells affected levels of co-transfected N-MYC. Transfection of different amounts of *USP11* expression plasmids induced levels of exogenous N-MYC wt and N-MYC mut in a concentration-dependent manner (Fig. 4.8). Overexpression experiments were performed in SH-EP cells that do not endogenously express N-MYC, because N-MYC levels in *MYCN*-amplified neuroblastoma cells are already extremely high. For this reason N-MYC levels of *MYCN*-amplified IMR-5 and IMR-32 cells were not increased upon USP11 overexpression (not shown). It was demonstrated in several studies that overexpression of a deubiquitinating enzyme can enhance deubiquitination and stabilisation of a target protein, as it was shown for example for USP7-mediated deubiquitination of TIP60 [Dar et al., 2013]. Accordingly, USP11 over-expression results indicate USP11-mediated deubiquitination of N-MYC. However, results were the same for N-MYC wt and N-MYC mut, whereas Aurora-A-mediated stabilisation was shown to be specific for N-MYC wt, suggesting an Aurora-A-independent function of USP11. Whether deubiquitination by USP11 induces the observed increase in N-MYC levels

was tested in additional overexpression experiments. Since deubiquitination is a catalytic reaction that involves the proteolytic cleavage of covalently attached ubiquitin moieties from a target protein, the integrity of the catalytic domain of deubiquitinating enzymes is vital for catalysing the proteolytic cleavage reaction [Hu et al., 2002]. USP7 and USP11 both belong to the USP protein family of deubiquitinating enzymes, which is characterised by a conserved three domain architecture and a catalytic triad of three amino acids, which is essential for their catalytic activity [Hu et al., 2002, Quesada et al., 2004]. Mutation of the cysteine residue in the catalytic triad abolishes the catalytic function of USP proteins [Dar et al., 2013, Hu et al., 2002, Maertens et al., 2010]. For USP11 it was shown that mutation of the cysteine (C) residue 318 to serine (S) (C318S) inhibits its catalytic activity [Al-Salihi et al., 2012]. Overexpression of catalytically inactive USP11 C318S resulted in a similar increase of N-MYC levels than overexpression of USP11 wt (Fig. 4.8). This observation is not in agreement with a catalytic role of USP11 in N-MYC stabilisation and hints to an indirect mechanism, which results in an increase of N-MYC levels upon USP11 overexpression. Transient overexpression experiments create a non-physiological condition and can show unspecific effects, as for example a general increase of expression of all co-transfected proteins (Björn von Eyss, personal communication). To exclude this possibility, as well as promoter effects from the *MYCN* expression plasmid, the effect of USP11 overexpression on levels of co-transfected green fluorescent protein (GFP) integrated into the same expression plasmid was determined. GFP levels remained constant with increasing amounts of USP11 protein levels, showing that the increase of N-MYC levels was specific (not shown). For USP7 overexpression effects on N-MYC were similar as for USP11. Ectopic N-MYC wt and N-MYC mut levels increased in a concentration-dependent manner upon overexpression of USP7 wt, but overexpression of catalytically inactive USP7 C223S had only minor effects on N-MYC levels [Thesis from J. Dirks, soon to be published].

Taken together, there is little evidence for a catalytic role of USP7 and USP11 in the regulation of N-MYC stability and no evidence for an involvement in the mechanism of Aurora-A-mediated stabilisation of N-MYC. Nevertheless, N-MYC interaction with both, USP7 and USP11, was revealed by MS analysis of N-MYC complexes and verified in multiple immunoprecipitation experiments on exogenous and endogenous proteins. Importantly, the interaction with USP11 appeared to be stronger for N-MYC mut than for N-MYC wt, supporting an Aurora-A-independent mechanism (Fig. 4.6). It is possible that members of the USP protein family have a redundant function in N-MYC stabilisation. Although USP7 and USP11 show no obvious similarities in their primary sequence apart from the catalytic domains, which are common in all USP protein family members, they were both shown to deubiquitinate the polycomb repressive complex 1 components BMI-1 and MEL-18 [Maertens et al., 2010, Nijman et al., 2005]. To ensure that redundancy of USP7 and USP11 function is not the reason for missing effects on N-MYC protein levels upon knockdown, both proteins should be targeted in parallel using specific shRNA sequences expressed under promoters with different selection markers. However, the results have to be regarded with

caution, since knockdown of either protein already severely effects proliferation (for cellular effects upon *USP11* knockdown see master thesis from Svenja Wolf, 2015), making it hard to distinguish direct knockdown effects from secondary cellular effects.

To this end, the functional relationship of N-MYC and USP7/11 remained open and was further investigated by RNA-sequencing of neuroblastoma cells that were depleted either of N-MYC or of USP11. RNA-sequencing was performed in order to test the hypothesis that N-MYC and USP7/11 interact with each other to regulate the expression of polycomb repressive complex 1/2 target genes. N-MYC function is connected with polycomb repressive complexes, as it was shown to interact with polycomb repressive complex 2 component EZH2 and to induce transcriptional repression together with polycomb complexes [Corvetta et al., 2013]. Accordingly, N-MYC could interact with USP7/11 in order to induce deubiquitination and stabilisation of polycomb repressive complex 1 components BMI-1 and MEL-18, supporting the repression of common target genes [Maertens et al., 2010]. But since RNA-sequencing did not identify more than 10 genes, which were regulated upon knockdown of both, N-MYC and USP11, analysis was not continued, leaving the question about the functional relevance for N-MYC interaction with USP7 and USP11 open.

5.4   Identification of novel N-MYC interaction partners implicates previously undefined MYC protein functions

Besides known interaction partners of MYC proteins, such as TRRAP [McMahon et al., 1998], MS analysis revealed N-MYC interactions with several proteins that were not shown to interact with MYC proteins previously (see appendices, A.1, A.2). Importantly, some of these novel N-MYC interacting proteins displayed higher peptide counts for N-MYC wt compared to N-MYC mut, which carries two alanine mutations in MBI, at T58 and S62, preventing phosphorylation at these residues. Accordingly, MS recovery of more peptides in the N-MYC wt sample than in the N-MYC mut sample suggests that the interaction with N-MYC depends on the integrity of MBI and indicates that identified N-MYC interacting proteins interact with N-MYC in a phosphorylation-dependent manner. There are several proteins known to interact with MBI, such as FBXW7 and TRUSS, which represent the substrate recognition subunits of the E3 ubiquitin ligase complexes SCF^{FBXW7} and DBB1-CUL4, respectively, as well as several kinases and phosphatases, for example GSK-3ß and PP2A (Fig. 1.1). Apart from its role in regulating MYC protein stability, MBI is also important for MYC function as a transcription factor. MBI and MBII are both located in the transregulatory domain (TRD) in the N-terminus of MYC proteins and were shown to be required for transformation by MYC, forming a platform for the interaction with proteins involved in transcriptional activation and repression by MYC transcription factors [Dang, 2012, Kato et al., 1990, Lee et al., 1996]. The importance of this domain for MYC biology is undermined by the finding that most mutations occur in this domain, specifically the T58 residue in MBI is often mutated in several cancer entities. The mutation of T58 to alanine results not only in higher MYC protein stability, but also in increased transforming

capacity, disabling MYC-induced apoptosis [Tansey, 2014]. In addition, in neuroblastoma cells a preferential interaction of identified N-MYC interacting proteins with N-MYC wt is a prerequisite for participation in the mechanism of Aurora-A-mediated stabilisation of N-MYC, which is specific for N-MYC wt [Otto et al., 2009]. Several novel N-MYC interacting proteins with higher peptide counts in the N-MYC wt sample were chosen for validation experiments. The most promising candidates for validation were components of the TFIIIC complex, which is a GTF for POL III-mediated transcription, since 5 out of 6 subunits were identified and all subunits showed higher peptide counts for N-MYC wt. Furthermore, one of the most significant clusters in a functional annotation clustering analysis of identified N-MYC interacting proteins was a cluster for POL III/TFIIIC (see results, section 4.2.2 and Table 4.1).

5.4.1   N-MYC interacts with TFIIIC that functions not only in POL III transcription, but also in organisation of chromatin structure

The TFIIIC complex is not published to interact with MYC proteins, but 4 TFIIIC subunits have been identified in a previous MS analysis of C-MYC protein complexes from transformed human cell lines [Koch et al., 2007]. Whereas the interaction of C-MYC and TFIIIC subunits was not validated in immunoprecipitation experiments, the interaction of C-MYC with TFIIIB, another POL III GTF, was shown in immunoprecipitations from HeLa cells [Gomez-Roman et al., 2003].

TFIIIC represents a large protein complex and comprises 6 subunits, which are conserved from yeast to human [Dumay-Odelot et al., 2007, Geiduschek and Kassavetis, 2001]. The mechanism of POL III-mediated transcription differs among its target genes, which are classified into three distinct groups (see introduction, section 1.3.2). TFIIIC was demonstrated to be required for transcription of type I and type II genes, which, compared to type III genes, do not have a promoter sequence upstream of the TSS and lack a TATA box [Dumay-Odelot et al., 2007, Geiduschek and Kassavetis, 2001, Willis, 1993]. At type I target genes TFIIIC binding is mediated by TFIIIA, which binds first to the intermediate element (IE) in the internal control region (ICR) in the promoter and then recruits the TFIIIC complex that induces recruitment of TFIIIB and POL III [Lassar et al., 1983, Schramm and Hernandez, 2002]. At type II genes, which comprise mainly tRNA encoding genes, TFIIIC binds directly to A- and B-box elements in the promoter and initiates assembly of the pre-initiation complex for POL III-mediated transcription [Geiduschek and Kassavetis, 2001, Schramm and Hernandez, 2002, Willis, 1993]. Importantly, the TFIIIC complex has HAT activity and is able to relieve nucleosome-mediated repression of POL III transcription [Hsieh et al., 1999, Kundu et al., 1999]. Although no specific functional relationship is reported for MYC proteins and TFIIIC, a more general connection of POL III-mediated transcription and MYC transcription factors was demonstrated in multiple studies, showing that MYC induces POL III transcription by several mechanisms (see introduction, section 1.3.2).

Here, N-MYC interaction with TFIIIC was validated in numerous immunoprecipitation experiments, which showed the interaction of TFIIIC subunit 5 (TFIIIC5) with endogenous N-MYC, as well as with exogenous N-MYC, displaying a clear preference for N-MYC wt compared to N-MYC mut (Fig. 4.9). Furthermore, TFIIIC5 also interacts with Aurora-A, indicating that N-MYC functions with TFIIIC in a complex with Aurora-A (Fig. 4.9). Whether TFIIIC and N-MYC interact directly was not investigated so far, but N-MYC peptide pull-down assays demonstrated the interaction of TFIIIC5 with short N-MYC peptides covering aa28-89 (Fig. 4.11). These peptides comprised MBI with the residues T58 and S62 that have to be phosphorylated to enable N-MYC recognition by the SCF$^{\text{FBXW7}}$ E3 ligase complex, which mediates N-MYC degradation in mitosis and which is opposed by Aurora-A (see introduction, section 1.5). Pull-down assays with N-MYC peptides that were not phosphorylated or phosphorylated at T58 and/or S62 revealed a preference of TFIIIC5 interaction with N-MYC peptides, which are phosphorylated at both residues, supporting the results from immunoprecipitation experiments with exogenous N-MYC wt and N-MYC mut (Fig. 4.9, 4.11). Like TFIIIC5, Aurora-A interacts preferentially with N-MYC peptides phosphorylated at T58 and S62 and it was shown that in comparison to N-MYC mut Aurora-A stabilises selectively N-MYC wt, which can be phosphorylated at T58 and S62 (see introduction, section 1.5). These findings indicate that both, Aurora-A and the TFIIIC complex, interact with N-MYC in a phosphorylation-dependent manner, making contacts with MBI. Resolving the crystal structure of the N-MYC/TFIIIC complex, would enable the identification of the interaction surface between N-MYC and TFIIIC. Combined with the knowledge from the structure of the N-MYC/Aurora-A complex the resolution of the N-MYC/TFIIIC structure could answer the question, whether N-MYC, Aurora-A and TFIIIC can form a trimeric complex. Further studies need to be performed in order to determine, if a trimeric complex of N-MYC, Aurora-A and TFIIIC could function in Aurora-A mediated stabilisation of N-MYC, such as knockdown and overexpression experiments (see discussion, section 5.3). But conduction of these experiments would be difficult due to the fact that TFIIIC is a complex consisting of multiple subunits.

TFIIIC is involved in several additional mechanisms apart from its essential role in POL III transcription. Importantly, TFIIIC binds to thousands of genomic sites that are not bound by POL III and are characterised by the presence of a B-box element or a similar motif, which was named "extra TFIIIC" (ETC) loci [Moqtaderi et al., 2010] (Fig. 5.2). These TFIIIC-only binding sites were first discovered in yeast and were given different names, the term ETC (extra TFIIIC) site will be used in the following [Donze, 2012, Moqtaderi and Struhl, 2004, Noma et al., 2006]. Most research on TFIIIC was performed in yeast, but more recently several studies have been conducted in mammals, mainly using human cell lines. The first study demonstrating a function of TFIIIC besides its role in POL III-mediated transcription was performed in yeast and revealed that transposon integration is directed by tDNAs and requires binding of TFIIIC and TFIIIB, whereas the process is inhibited by POL III [Chalker and Sandmeyer, 1990, Connolly and Sandmeyer, 1997, Kirchner et al.,

1995] (Fig. 5.2). The integration of retrotransposons is promoted by HDACs, which interact with TFIIIC [Mou et al., 2006, Venters et al., 2011]. One class of retrotransposons are SINEs, which are bound by POL III and general POL III transcription factors in yeast and human, since they display similar features as a tRNA promoter, comprising an A- and a B-box element [Carriere et al., 2012, Roy-Engel, 2012]. The function of SINEs is poorly understood [Roy-Engel, 2012]. Interestingly, in cells from the murine somatosensory cortex it was demonstrated that TFIIIC binding to SINE elements induces relocation of activity-dependent neuronal genes to transcription factories, where their transcription is enhanced, while knockdown of TFIIIC induced differentiation, linking TFIIIC function with neuronal differentiation [Crepaldi et al., 2013]. TFIIIC binds DNA with very high affinity and remains bound to DNA in all phases of the cell cycle, inducing exclusion of nucleosomes from TFIIIC-bound sites [Jansen and Verstrepen, 2011, Jourdain et al., 2003, Roberts et al., 2003] (Fig. 5.2). In addition, the nucleosome-remodeling complex RSC was shown to associate with tDNAs [Ng et al., 2002] (Fig. 5.2). Different classes of TFIIIC binding sites, tDNAs, SINEs and ETC sites, have been implicated to function in spatial organisation of chromatin [Kirkland et al., 2013]. TFIIIC-bound sites separate actively transcribed from repressed areas of chromatin (insulation/barrier function) and bring together areas of actively transcribed chromatin [Crepaldi et al., 2013, Kirkland et al., 2013, Van Bortle et al., 2014]. First evidence for a barrier function of TFIIIC originates from studies in yeast, which revealed that TFIIIC occupied loci prevent the spread of heterochromatin [Donze et al., 1999, Donze and Kamakaka, 2001]. Furthermore, in yeast and in human cells tDNAs were shown to function in insulation, interfering with enhancer-promoter interactions in a TFIIIC-dependent manner [Raab et al., 2012, Simms et al., 2008]. Analysis of the three-dimensional organisation of an exemplary genomic locus, comprising several tDNAs and ETC sites, by circular chromosome conformation capture (4C) identified intra-chromosomal interactions among tDNAs and ETC-sites [Raab et al., 2012]. Another protein, which is well known to function as an insulator in vertebrates, is the transcriptional repressor CTCF. CTCF binds to boundaries of different chromatin domains and induces loop formation, which is stabilised by the cohesin complex, separating actively transcribed from repressed areas [Cuddapah et al., 2009, Handoko et al., 2011, Parelho et al., 2008, Vietri Rudan and Hadjur, 2015, Wendt et al., 2008]. Cohesin is a ring-shaped protein complex that comprises two structural maintenance of chromosomes (SMC) complexes, SMC1a and SMC3, which can encompass one or two DNA stands, forming a ring that is closed by two additional subunits, RAD21 and SA1/2 [Jeppsson, Kanno, Shirahige, and Sjogren, 2014]. Importantly, the function of TFIIIC in three-dimensional organisation of chromatin domains appears to be analogous to the function of CTCF, since cohesin was shown to co-localise with TFIIIC [Carriere et al., 2012]. In yeast, TFIIIC binding sites are associated with the cohesin-related condensin complex [D'Ambrosio et al., 2008]. Genome-wide mapping of TFIIIC, CTCF, cohesin and condensin binding sites uncovered the co-localisation of all 4 protein complexes at the border of distinct topological associated domains, connecting the different complexes in their

function in organisation of chromatin architecture [Van Bortle et al., 2014].
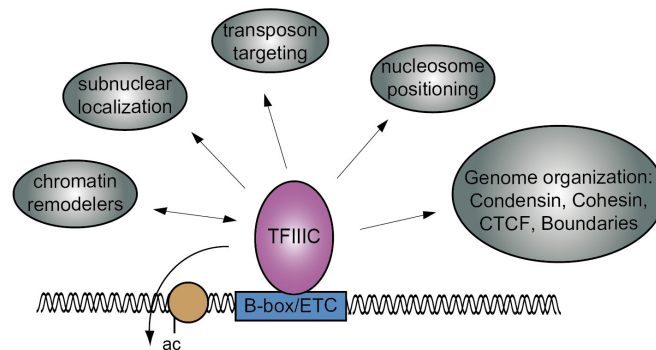
Figure 5.2
Extra-transcriptional functions of TFIIIC
Scheme illustrating additional processes involving TFIIIC function besides its role in POL III transcription. TFIIIC exerts these extra-transcriptional functions upon binding to B-box elements and to a motif similar to a B-box, named "extra TFIIIC" (ETC) motif. TFIIIC itself has HAT activity and induces histone (brown circle) acetylation (ac). Adapted from Donze, 2012.

Judging from what is known about extra-transcriptional functions of TFIIIC, validation of N-MYC interaction with TFIIIC not only implicates a role of TFIIIC in MYC-mediated induction of POL III transcription in addition to TFIIIB, but also suggests that MYC proteins could function in the spatial organisation of actively transcribed and repressed chromatin domains in the nucleus. Importantly, validation experiments did not only confirm N-MYC interaction with TFIIIC, but also with the topoisomerases TOP2A and TOP2B. In addition, immunoprecipitation experiments revealed that TFIIIC5 also interacts with TOP2A (Fig 4.9). Furthermore, TOP2A displayed a preference for the interaction with phosphorylated N-MYC peptides, though less pronounced compared to TFIIIC5 (Fig. 4.11). The interaction of DNA topoisomerases with members of the MYC transcription factor family was not shown before, but is in agreement with their function in facilitating transcription by releasing the tension, which occurs upon transcription of DNA [Kouzine et al., 2014]. Hence, it is possible that N-MYC function in transcription is supported by its interaction with topoisomerases. The phosphorylation-dependent interaction of both, TFIIIC5 and TOP2A, with MBI of N-MYC, opens the possibility that TFIIIC and TOP2A form a complex with Aurora-A and N-MYC that is phosphorylated at T58 and S62. This hypothesis is supported by the finding that TFIIIC5 also interacts with Aurora-A (Fig. 4.9). Since N-MYC, TFIIIC and TOP2A are DNA-binding proteins, it is likely that the complex comprises N-MYC as a heterodimer with MAX and is bound to DNA. However, the functional relevance of this complex remains to be elucidated (Fig. 5.3). To assess a participation of the complex in spatial organisation of chromatin, N-MYC interaction with components known to be involved in this process was determined in immunoprecipitation experiments (see results, section 4.2.2). Strikingly, N-MYC interaction with the cohesin subunit RAD21 was shown in exogenous N-MYC IPs, as well as in endogenous N-MYC IPs, revealing a preferential interaction of

RAD21 with N-MYC wt, as it was shown for TFIIIC5 and Aurora-A (Fig. 4.9). Though, in contrast to TFIIIC5, RAD21 was not co-purified with Aurora-A (Fig. 4.9). The discovery of an interaction of N-MYC with the cohesin subunit RAD21 strengthens the theory that N-MYC protein complexes comprising TFIIIC could function in the organisation of specific areas of chromatin, as it was shown for TFIIIC.
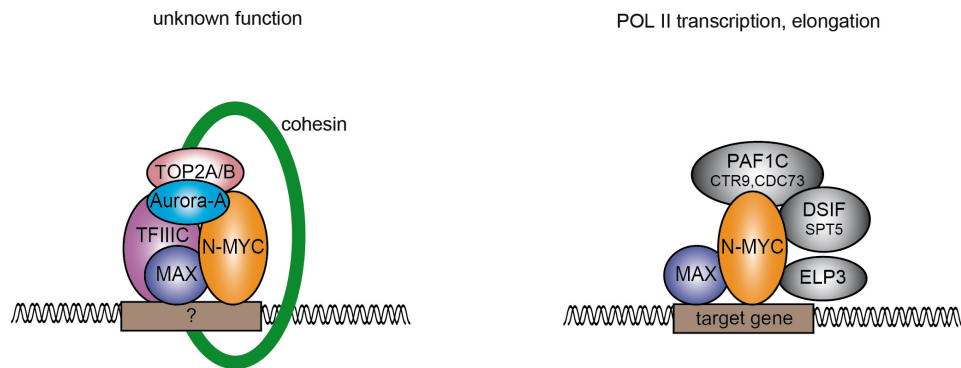
Figure 5.3
N-MYC protein complexes identified by MS analysis
Scheme summarising N-MYC interactions with proteins identified in MS analysis of N-MYC protein complexes. On the one hand side, proteins validated for interaction with N-MYC are involved in structural organisation of chromatin, but their function with N-MYC remains to be elucidated (left). On the other hand side, novel N-MYC interacting proteins suggest an extension of MYC protein functions in transcription to the step of elongation (right).

5.4.2 N-MYC interacts with elongation factors for POL II transcription

Among the novel N-MYC interacting proteins, which were identified in MS analysis and displayed higher peptide counts for N-MYC wt, were several proteins that are known to function at the step of elongation of POL II-mediated transcription (see results, section 4.2.2). Although MYC proteins exert multiple functions in induction of transcription by POL II and are involved in pause-release of promoter proximal paused POL II (see introduction, section 1.3.1), an interaction with the elongation factors ELP3, DSIF and PAF1C was not reported. MS analysis of N-MYC protein complexes identified peptides from ELP3, the DSIF component SPT5 and two subunits of the PAF1C complex, CTR9 and CDC73. Importantly, the interaction with N-MYC was validated in subsequent immunoprecipitation experiments, suggesting a previously unknown function of MYC transcription factors in elongation (Fig. 4.10). The interaction of SPT5, CTR9 and CDC73 with MYC proteins was shown for C-MYC as well [Thesis from L.A. Jaenicke, 2015], supporting the theory of a novel and conserved function of MYC proteins together with DSIF and PAF1C (Fig. 5.2). DSIF comprises two subunits, SPT4 and SPT5, and has a dual role in the regulation of transcriptional elongation. Initially it functions as a negative elongation factor stimulating promoter proximal pausing of POL II, but upon phosphorylation by p-TEFb it is transformed into a positive elongation factor [Kwak and Lis, 2013, Yamada et al., 2006]. PAF1C is a multiprotein complex and is involved not only in elongation, but also in RNA processing

and modification of histones [Sims et al., 2004]. Like for DSIF, a dual role in the regulation of transcriptional elongation was suggested for PAF1C, being converted from a negative factor, which inhibits pause-release of POL II, into a positive elongation factor [Bai et al., 2010, Chen et al., 2015a]. Studies on C-MYC function with PAF1C revealed a homology of MBI with the CTD of POL II, which is bound by PAF1C when the CTD is phosphorylated at S2 and S5 residues, and suggested that MYC proteins can form a platform for transient recruitment of PAF1C, regulating the assembly of elongation-competent POL II [Jaenicke et al., 2016, Qiu et al., 2012]. Furthermore, C-MYC interaction with the PAF1C subunits CTR9 and CDC73, as well as the DSIF subunit SPT5 is induced by phosphorylation of the MBI residues T58 and S62 and complex formation is enhanced upon proteasomal inhibition, leading to an accumulation of C-MYC phosphorylated at T58 and S62. Accumulation of C-MYC/PAF1C complexes negatively regulates elongation and decreases transcription of MYC target genes [Jaenicke et al., 2016]. A proposed mechanism for C-MYC/PAF1C function involves the recruitment of the co-activator complex TRRAP that interacts with MBII and induces histone acetylation, which is required for recruitment of p-TEFb (see introduction, section 1.3.1). The phosphorylation of the repetitive CTD of POL II at S2 residues by p-TEFb is necessary in order to enable the transfer of PAF1C from C-MYC onto POL II, turning it into a positive elongation factor. Inhibition of C-MYC degradation can result in the accumulation of C-MYC complexes bound to ubiquitin ligases. Since ubiquitin ligases that interact with MBII prevent C-MYC interaction with TRRAP, histone acetylation and POL II CTD phosphorylation can be blocked and disable PAF1C binding to POL II, freezing PAF1C in its state as a negative elongation factor [Jaenicke et al., 2016].

Although counts for ELP3, SPT5, CDC73 and CTR9 recovered in MS analysis of N-MYC complexes suggested a preference for the interaction with N-MYC wt (Table 4.2), validation experiments using SH-EP cells transfected with either N-MYC wt or N-MYC mut did not confirm a stronger interaction with N-MYC wt compared to N-MYC mut (Fig. 4.10). In contrast, endogenous C-MYC immunoprecipitation experiments and peptide pull-down assays using the same N-MYC peptides as in Fig. 4.11, which comprise aa28-89 that are conserved for C- and N-MYC, did show a phosphorylation-dependent interaction of SPT5, CDC73 and CTR9 [Thesis from L.A. Jaenicke, 2015, Jaenicke et al., 2016]. On the one hand side, these findings indicate that results display a high variability among different experiments and several validation experiments are needed to confirm a relative statement about the interaction of proteins with one another. On the other hand side, the discrepancy of results highlights the fact that the MS analysis performed here is not quantitative and can only reveal protein interactions, which have to be confirmed in further experiments. In addition, the peptide counts, which were taken as a measurement to evaluate the discovered interactions, are exclusive unique peptide counts that only reflect reliability of protein identification and do not represent a quantitative statement. In order to improve MS analysis, enabling a quantitative statement, immunoprecipitation experiments for MS samples would have to be performed at least in triplicates. Another approach, which allows quantifica-

tion of MS results, is the metabolic labeling of proteins by a method called "stable isotope labeling by amino acids in cell culture" (SILAC) [Carneiro et al., 2016]. In a SILAC experiment different samples are labeled in cell culture by supplementing an unique stable isotope to the medium, enabling mixing of different samples for MS analysis in order to analyse the samples in the same run. However, this method does not resolve differences that arise from purification of a protein complex for MS analysis. Purification needs to be performed previous to the combination of different samples in order to distinguish the composition of protein complexes of cells differing in expression of a certain protein, as it is the case for comparison of N-MYC wt and N-MYC mut interacting proteins.

5.5   ChIP-sequencing reveals joint N-MYC/TFIIIC binding sites

The discovery of the interaction between N-MYC and the POL III GTF TFIIIC opens several questions, including the questions, whether the N-MYC/TFIIIC complex is bound to DNA and whether certain DNA elements exist that are bound by both, N-MYC and TFIIIC (Fig. 5.3). In order to answer these questions and to get information about a possible function of the complex, N-MYC and TFIIIC binding to chromatin was analysed by ChIP-sequencing using antibodies directed against N-MYC and TFIIIC5.
ChIP-sequencing analyses revealed hundreds of overlapping N-MYC and TFIIIC5 binding sites throughout the genome. Classification of N-MYC/TFIIIC5 binding sites according to their localisation in respect of their proximity to POL II target genes and tDNAs, showed that N-MYC and TFIIIC5 occupied both, POL II and POL III target genes, as well as inter- and intragenic regions (Fig. 4.15). Strikingly, a large number of N-MYC/TFIIIC5 binding sites was localised in the promoter region of POL II target genes (Fig. 4.13, 4.15), which was not expected from literature on TFIIIC (see discussion, section 5.4). In contrast, it was shown before that MYC transcription factors bind to the promoter of tDNAs, inducing their transcription (see introduction, section 1.3.2). A connection of POL II and POL III transcription has been suggested in several studies, showing that actively transcribed POL II and POL III target genes are often in adjacent or overlapping chromatin areas, sharing histone marks for open chromatin and proteins involved in induction of transcription, such as the transcription factors ETS1 and STAT1 [Alla and Cairns, 2014, Barski et al., 2010, Oler et al., 2010, Raha et al., 2010]. Tag density profiles of N-MYC and TFIIIC5 indicated that their binding sites are indeed overlapping and not only in close proximity to one another, as the tag density pattern was similar and binding peaked in the same region (Fig. 4.16). Analysis of N-MYC and TFIIIC5 tag density using a higher resolution and taking into account only N-MYC/TFIIIC5 binding sites in POL II promoters supported the observation that N-MYC and TFIIIC5 binding sites largely overlap and revealed that on average N-MYC occupancy peaks close to the TSS, whereas TFIIIC5 occupancy peaks not at the TSS, but slightly 5' of N-MYC (Fig. 4.17). The results from tag density plots indicate that N-MYC and TFIIIC5 can bind together to the same sites and that N-MYC/TFIIIC5 binding sites at POL II promoters have a defined orientation. However, these findings have to be regarded

with caution, since tag density of all binding sites are averaged in order to create such plots and variations in the distance of N-MYC and TFIIIC5 peaks to one another and to the TSS can remain unrecognised. Inspection of individual binding sites in POL II promoters revealed differences in the proximity of N-MYC and TFIIIC5 peaks, ranging from largely overlapping peaks to a distance of 100-200 bp in between, but N-MYC binding was rarely observed 5' of TFIIIC5 (not shown).

5.5.1 N-MYC and Aurora-A regulate TFIIIC binding to chromatin

Samples for ChIP-sequencing were prepared from *MYCN*-amplified neuroblastoma cells, which were treated with or without the Aurora-A inhibitor CD532 for 4 h, in order to investigate, whether the TFIIIC interaction partners N-MYC and Aurora-A regulate TFIIIC binding to chromatin. CD532 interferes with Aurora-A mediated stabilisation of N-MYC and in contrast to MLN8237 it bears the advantage of inducing a strong decrease in N-MYC protein levels already after a short time of treatment, reducing the chance to cause secondary effects [Gustafson et al., 2014]. In addition, CD532 binding to the Aurora-A kinase domain not only inhibits the kinase activity of Aurora-A, but also changes the Aurora-A conformation leading to a strong distortion of the three-dimensional structure, presumably inducing degradation of Aurora-A (see results, section 4.3.1 and discussion, section 5.1). Accordingly, DMSO treated control samples from *MYCN*-amplified neuroblastoma cells, which have high N-MYC and Aurora-A levels, were compared to samples, which were treated with CD532, inducing a strong decreases of N-MYC levels, a less pronounced decrease in Aurora-A levels and inhibition of Aurora-A kinase activity.

Upon CD532 treatment the total number of TFIIIC5 peaks obtained from analysis of ChIP-sequencing data on TFIIIC5 was increased around 5-fold (Table 4.3). Furthermore, an increase of TFIIIC5 occupancy was obvious in a heat map displaying N-MYC and TFIIIC5 occupancy of all annotated genes, as well as in tag density plots and box plots, visualising average changes in occupancy upon CD532 treatment (Fig. 4.13, 4.16, 4.18). These findings reveal an overall increase of TFIIIC5 occupancy when N-MYC and Aurora-A levels are decreased and Aurora-A kinase activity is inhibited, indicating that N-MYC and/or Aurora-A negatively regulate TFIIIC5 binding to chromatin. The increased number of TFIIIC5 binding sites and inspection of individual binding sites, not only confirmed a global increase of TFIIIC5 occupancy, but also revealed that TFIIIC5 binds to additional sites upon CD532 treatment that are not occupied in DMSO treated cells. Most novel TFIIIC5 binding sites were located in intergenic regions, though also the number of TFIIIC5 binding sites in POL II promoters increased around 2-fold, while TFIIIC5 binding sites in POL III promoters displayed only small changes, since in DMSO treated cells nearly all actively transcribed tDNAs are already occupied by TFIIIC5 (Fig. 4.13).

As expected from the CD532-mediated decrease of N-MYC protein levels, N-MYC occupancy decreased with CD532. Interestingly, the decrease of N-MYC binding was most pronounced at N-MYC/TFIIIC5 binding sites (Fig. 4.18). However, the total number of

called N-MYC peaks did not change much and the CD532-induced decrease was not apparent in tag density plots and heat maps (Fig. 4.13, 4.14, 4.16). Accordingly, N-MYC occupancy changes did not reflect the strong decrease of N-MYC protein levels, which were decreased to more than 50% upon CD532 treatment (Fig. 4.12). On the one hand side, this has a technical reason, since CD532-induced changes on N-MYC occupancy are not very strong, N-MYC binding does not decrease below background and effects are not obvious in non-quantitative representations, such as heat maps (see results, section 4.3.1). In addition, ChIP experiments for sequencing have not been performed in triplicates and efficiency of individual ChIPs were not controlled by using an internal spiking control [Bonhoure et al., 2014]. Hence, it can not be excluded that the N-MYC ChIP from CD532 treated cells was more efficient compared to the ChIP from DMSO treated cells. On the other hand side, the different degree of N-MYC reduction on protein level compared to the decrease in DNA occupancy can be explained by the fact that *MYCN*-amplified neuroblastoma cells have oncogenic N-MYC levels. Overexpression of MYC proteins can not only induce MYC binding to low affinity sites and invasion of sites with open chromatin marks, but also lead to saturation of all binding sites, leaving a free nuclear pool of MYC proteins, which is not bound to DNA and could compensate a decrease in MYC protein levels [Fernandez et al., 2003, Lin et al., 2012, Nie et al., 2012].

Interestingly, the number of N-MYC/TFIIIC5 binding sites increased significantly upon CD532 treatment, showing a strong increase of overlapping N-MYC and TFIIIC5 peaks in POL II promoters and intergenic regions (Fig. 4.15). Nevertheless, CD532 induces a decrease of N-MYC occupancy at joint binding sites, whereas TFIIIC5 occupancy is increased (Fig. 4.18). These findings hint to a more complex functional relationship of N-MYC, TFIIIC and Aurora-A, which is not explained simply by antagonistic binding of N-MYC and TFIIIC. Comparison of CD532 effects on N-MYC and TFIIIC5 occupancy with effects of two additional Aurora-A inhibitors revealed a clear difference in their influence on N-MYC and TFIIIC5 binding to DNA and this was consistent for all sites tested (Fig. 4.24). In contrast to CD532, the purely catalytic Aurora-A inhibitor MK-5108, which does not affect Aurora-A-mediated stabilisation of N-MYC, did not lead to an increase of TFIIIC5 occupancy and did not clearly affect N-MYC occupancy. The same was true for the second Aurora-A inhibitor, MLN8237, which does not only inhibit Aurora-A kinase activity, but also interferes with N-MYC stabilisation by Aurora-A [Brockmann et al., 2013]. These observations clearly indicate that inhibition of Aurora-A kinase activity alone does not regulate TFIIIC5 and/or N-MYC occupancy, especially, since with MK-5108 and MLN8237 Aurora-A kinase activity was not detectable, indicated by the lack of Aurora-A autophosphorylation at T288, whereas with CD532 residual kinase activity remained (Fig. 4.24). Compared to CD532, MLN8237 treatment decreased N-MYC protein levels to a lesser extend. However, this small difference in N-MYC levels does not explain the strong difference for CD532 and MLN8237 in their effects on N-MYC and TFIIIC5 occupancy. Conclusively, these observations suggest that the decrease of Aurora-A protein levels upon CD532 treatment plays a

role in CD532-mediated changes in TFIIIC5 and N-MYC binding to chromatin. The combination of Aurora-A inhibition and the decrease of N-MYC and Aurora-A protein levels appears to account for CD532-specific effects on N-MYC and TFIIIC5, but the underlying mechanism remains to be elucidated. Since CD532 was developed only recently and its effects have not been studied extensively, it is possible that CD532 has unknown secondary effects, which influence N-MYC and TFIIIC5 occupancy. Importantly, for ChIP-sequencing a 4 h time point of CD532 treatment was chosen, at which no changes in cell morphology were observed, while at later time points cells showed morphological changes. First cells were flatting and developed protrusions, and after 10-12 h of CD532 treatment most cells died (Olga Sumara, personal communication). In contrast, upon MLN8237 treatment, using the same concentration as for CD532, cells did not show such strong changes in morphology and instead of dying, most cells displayed a delay in progression through G1 and G2 phase of the cell cycle [Brockmann et al., 2013]. Apart from direct inhibition of Aurora-A kinase activity, MLN8237 effects became obvious only after 24 h, when cells completed one round of the cell cycle and N-MYC protein levels were decreased (Fig. 4.24). The MLN8237-induced delay in G2 phase is specific for Aurora-A inhibition, since Aurora-A is required for multiple steps in mitosis (see introduction, section 1.5). A delay in G1 phase of the cell cycle can be explained by the MLN8237-mediated decrease of N-MYC protein levels, which induces expression of the negative cell cycle regulator p21 [Brockmann et al., 2013]. Why N-MYC protein levels decrease much more rapidly with CD532 is not completely clear, as with MLN8237 it was shown that most N-MYC is degraded via the E3 ubiquitin ligase SCF^{FBXW7}, which recognises N-MYC only in mitosis when it is phosphorylated at T58 and S62 (see introduction, section 1.4).

5.5.2   N-MYC/TFIIIC binding sites overlap with CTCF/cohesin binding sites

In order to find out, whether N-MYC/TFIIIC binding sites are characterised by the presence of a distinct DNA element, *de novo* motif analysis was conducted on N-MYC- and TFIIIC5-only and N-MYC/TFIIIC5 binding sites (Fig. 4.19). Apart from the motifs, which are known to be bound by N-MYC and TFIIIC, such as E- and A-/B-box elements, respectively, an additional motif was identified that has not been described to be bound by MYC transcription factors or TFIIIC (see introduction, section 1.2 and discussion, section 5.4). Surprisingly, this motif was the predominant motif for N-MYC/TFIIIC5 binding sites in POL II promoters and at intergenic regions, as well as at intergenic N-MYC-only binding sites (Fig. 4.19). Based on the similarity to a published motif, it was identified as a CTCF motif, which is a motif known to be bound by the CTCF zinc finger transcription factor (Fig. 4.19). Strikingly, CTCF motifs and E-box elements, have been both identified at N-MYC-only and N-MYC/TFIIIC5 binding sites, although displaying a different frequency. Therefore, the localisation of the respective motif within the N-MYC peak was determined using the peak summit of all N-MYC peaks in POL II promoters and intergenic sites (Fig. 4.20). Like E-box elements, the CTCF motif occurs in the center of N-MYC peaks,

suggesting that either an E-box element or a CTCF motif is present at N-MYC binding sites. Indeed, further analysis revealed that CTCF motifs and E-boxes in N-MYC peaks are mutually exclusive (Susanne Walz, personal communication). Interestingly, E-box elements were more frequent at N-MYC-only binding sites, whereas CTCF motifs were more frequent at N-MYC/TFIIIC5 binding sites, hinting to a specific enrichment of N-MYC/TFIIIC5 at sites that comprise a CTCF motif (Fig. 4.20). Binding of MYC proteins to E-box sequences requires dimerisation with MAX, resulting in formation of stable heterodimers, which make base-specific contacts with E-box motifs located within the major groove of DNA [Blackwell et al., 1990, Blackwood and Eisenman, 1991, Nair and Burley, 2003]. Unlike CTCF, MYC transcription factors do not comprise zinc finger motifs, which mediate CTCF binding to DNA [Liu et al., 2015]. Accordingly, N-MYC binding to the CTCF motif suggests the interaction of N-MYC with another protein that recognises the CTCF motif in the DNA. Although TFIIIC is a multiprotein complex, it does not comprise a protein with a zinc finger recognition motif, indicating that an additional protein is present at N-MYC/TFIIIC5 binding sites comprising a CTCF motif. For N-MYC/TFIIIC5 binding sites at intergenic regions the structural maintenance of chromosomes flexible hinge domain-containing protein 1 (SMCHD1) could mediate binding to the CTCF motif, since the epigenetic regulator was shown to bind to cis-regulatory elements, which coincide with CTCF binding sites [Chen et al., 2015b]. Additionally, SMCHD1 was identified as an N-MYC interacting protein in MS analysis (see appendices A.1, A.2).

The identification of a CTCF motif in N-MYC/TFIIIC5 binding sites supports the idea that N-MYC and TFIIIC could function together in spatial organisation of chromatin domains, as it was shown for TFIIIC (see discussion, section 5.4). TFIIIC binding sites were shown to co-localise with cohesin binding sites, as it was shown for the majority of intergenic CTCF binding sites [Carriere et al., 2012, Ong and Corces, 2014, Van Bortle et al., 2014]. Furthermore, some binding sites of CTCF located near tDNAs, SINEs and ETC sites, suggesting that TFIIIC and CTCF cooperate in chromatin organisational processes [Ong and Corces, 2014]. Alignment of ChIP-sequencing data of N-MYC/TFIIIC5 binding sites with published ChIP-sequencing data on CTCF and the cohesin subunit RAD21 from ChIPs in another neuroblastoma cell line, revealed that CTCF and RAD21 are bound to N-MYC/TFIIIC5 binding sites (Fig. 4.21, 4.22). Inspection of individual sites uncovered a large number of sites, which were occupied by N-MYC, TFIIIC5, CTCF and RAD21 and did not comprise an E-box, but a CTCF motif, confirming results from motif analyses of N-MYC/TFIIIC5 binding sites (Fig. 4.22). Immunoprecipitation experiments in *MYCN*-amplified neuroblastoma cells demonstrated that both, N-MYC and TFIIIC5 interact with the cohesin subunit RAD21 and the interaction of RAD21 with CTCF was confirmed (Fig. 4.9, 4.23) [Rubio et al., 2008]. In contrast, neither N-MYC, nor TFIIIC5 showed an interaction with CTCF (not shown), indicating that cohesin forms a complex either with N-MYC/TFIIIC5 or with CTCF. This theory is supported by the finding that SMCHD1 and CTCF can act in opposing ways: while SMCHD1 binding was shown to induce repression of the transcription

of *clustered protocadherin* (*Pcdh*) genes, CTCF binding is associated with transcriptional activation [Chen et al., 2015b]. Combining this information leads to a hypothetical model, in which CTCF motifs are either bound by CTCF/cohesin or by N-MYC/TFIIIC/cohesin, exhibiting different effects on chromatin structure.

Cohesin binding to N-MYC/TFIIIC5 binding sites was validated in individual ChIP experiments, showing that the cohesin subunit RAD21 binds to the same sites as N-MYC and TFIIIC5 in POL II promoters and in intergenic regions (Fig. 4.23, 4.24). Interestingly, CD532 treatment induced an increase of RAD21 occupancy at all sites tested, as it was shown for TFIIIC5. This observation indicates that N-MYC and Aurora-A are functionally connected with cohesin and that TFIIIC and cohesin function together.

The picture emerging from these findings suggests a functional connection of N-MYC/Aurora-A with TFIIIC/cohesin, which was not described so far. The architecture of the complex of N-MYC/Aurora-A together with TFIIIC/cohesin remains to be determined. On the one hand side, the complex could assemble at CTCF motifs upstream of the TSS of POL II genes and in intergenic regions (Fig. 5.4 A). On the other hand side, the components of the complex could bind to different DNA strands, which could be linked together by cohesin (Fig. 5.4 B). The enrichment of the CTCF motif in N-MYC binding sites can be due to loop formation and connection of two separate DNA strands, as it was shown for enhancer-promoter interactions [Van Bortle and Corces, 2012]. Transcription factors, such as MYC proteins, are known to bind to enhancer regions distant from promoters, which induce activation of transcription of target promoters upon interaction by recruitment of additional transcription factors and opening of the chromatin [Tansey, 2014]. Importantly, cohesin assists both, activating enhancer-promoter interactions and transcription inhibiting insulator interactions mediated by CTCF [Raab and Kamakaka, 2010]. Several genome-wide studies investigated enhancer-promoter and insulator interactions via chromatin interaction analysis with paired-end-tag sequencing (ChIA-PET), but the results are hardly reproducible, as ChIA-PET experiments are difficult to analyse and to interpret due to very high background signals [Handoko et al., 2011, Kieffer-Kwon et al., 2013, Li et al., 2010, 2012]. Accordingly, the existing picture of short- and long-range interactions is still largely incomplete.
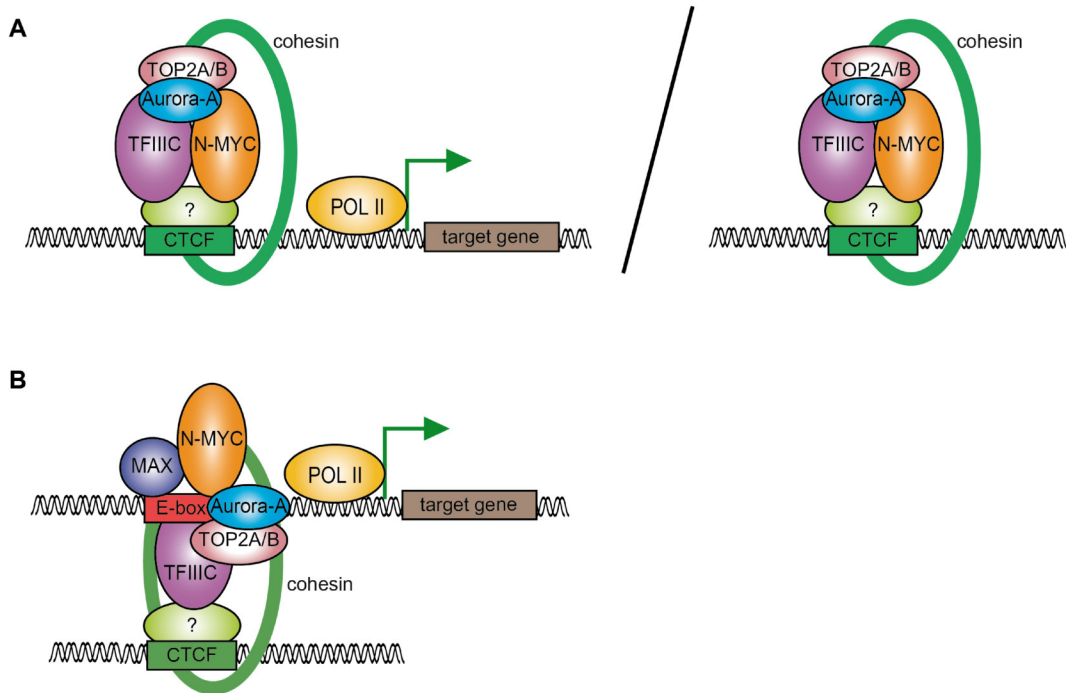
Figure 5.4
Proposed models for the architecture of N-MYC/TFIIIC binding sites
(A) Scheme illustrating the proposed composition of N-MYC/TFIIIC binding sites at POL II promoters (left) and intergenic sites (right).
(B) Scheme illustrating an alternative architecture of N-MYC/TFIIIC binding sites. N-MYC binds to a POL II promoter region and TFIIIC binds to an intergenic region. N-MYC/TFIIIC interaction induces loop formation of chromatin, which is supported by cohesin interaction.

5.6 Cell cycle-dependent organisation of transcription by regulation of chromatin architecture - a novel function of MYC proteins?

The DNA-binding complex consisting of N-MYC, TFIIIC and cohesin discovered here, which associates presumably with Aurora-A and topoisomerases, such as TOP2A, could be bound to POL II promoters and/or intergenic sites that make contacts with promoter regions (Fig. 5.4). In order to obtain a clearer picture of composition and hierarchy of this novel MYC protein complex, single or multiple components should be removed using specific shRNAs or siRNA pools targeting a certain component. Subsequently, sh/siRNA treated *MYCN*-amplified neuroblastoma cells should be analysed in immunoprecipitation and ChIP experiments using antibodies that recognise individual complex components and subunits, for example different subunits of TFIIIC. Information obtained from these experiments would shed light on the complex composition and the questions about dependency and hierarchy of interactions: which interaction depends on the interaction of another protein, which protein recruits another complex component and which component mediates DNA-binding?

Initial ChIP experiments with *MYCN*-amplified IMR-5 cells expressing an inducible shRNA targeting *TFIIIC5* demonstrated that N-MYC binding to N-MYC/TFIIIC5 binding sites at POL II promoters and intergenic regions was unaffected when TFIIIC5 binding was de-

creased to around 50%, whereas at the same sites RAD21 binding clearly decreased upon knockdown of *TFIIIC5* (Cathy Mak, personal communication). These results indicate that RAD21 is recruited in a TFIIIC5-dependent manner to N-MYC/TFIIIC5 binding sites, while N-MYC binding is independent of TFIIIC5. The functional relationship of two proteins can be specific for distinct DNA binding sites, therefore, a global analysis of DNA binding profiles by ChIP-sequencing is required to determine how DNA occupancy of a protein of interest is affected in certain conditions, such as knockdown of a specific protein. ChIP-sequencing on N-MYC, TFIIIC5 and RAD21 upon depletion of one out of the three proteins at once, would allow to distinguish the effects caused by knockdown of one protein and to get to know how they affect each other in terms of chromatin occupancy. In general the interpretation of knockdown effects is difficult when the depletion of a protein is not complete, as it was the case here for *TFIIIC5* knockdown, since it remains open, whether a certain level of the protein is sufficient to induce a distinct function or whether the protein is not required. Accordingly, it can not be ruled out that N-MYC binding to distinct genomic regions depends on TFIIIC5, but requires only a low level of TFIIIC5. Utilisation of the clustered, regularly interspaced, short palindromic repeat (CRISPR) technology, a more recent approach than shRNA technology, would circumvent the drawbacks of residual protein translation upon shRNA-mediated knockdown. Since the CRISPR technique enables depletion of the encoding DNA sequence of a protein of interest via RNA-guided nucleases, such as Cas9 [Sander and Joung, 2014]. However, deletion of the TFIIIC5 encoding locus using CRISPR technology should be lethal, since TFIIIC function is essential for POL III-mediated transcription of type I and II genes, including tDNAs that are needed for translation of all mRNAs (see discussion, section 5.4.1). Since cohesin plays an important role during mitosis, mediating sister chromatid cohesion, depletion of a cohesin subunit is likely to cause severe mitotic defects [Nasmyth and Haering, 2009]. Accordingly, depletion of RAD21 has been studied only in non-cycling cells to investigate non-mitotic functions in three-dimensional organisation of chromatin [Seitan et al., 2013, Sofueva et al., 2013]. Depletion of the DNA-unloading factor of cohesin, WAPL, has been studied in cycling cells and was shown to induce chromatin condensation in interphase and severe mitotic defects [Tedeschi et al., 2013]. N-MYC depletion would strongly affect proliferation and cell viability, since *MYCN*-amplified tumours depend on N-MYC expression [Otto et al., 2009]. But due to the high N-MYC expression levels in *MYCN*-amplified neuroblastoma cells, it is hard to achieve a good knockdown with si/shRNAs. Short-term treatment with an inhibitor that specifically targets a distinct protein, for example CD532, which is specific for Aurora-A compared to Aurora-B and -C, circumvents secondary effects upon knockdown of an essential protein [Gustafson et al., 2014]. Since it can not be excluded that treatment with the small molecule inhibitor CD532 induces unspecific effects, for example on proteins that were not included in tests for specificity during drug development, the best approach would be to reproduce ChIP-sequencing studies on short-term CD532-treated cells and to analyse N-MYC, TFIIIC5 and RAD21 DNA binding profiles from cells expressing an inducible shRNA

targeting *MYCN*, *TFIIIC5* or *RAD21*.

To elucidate the function of the N-MYC/Aurora-A complex with TFIIIC/cohesin in transcription, RNA-sequencing experiments were performed on *MYCN*-amplified IMR-5 cells, which have been transfected either with siRNAs targeting *AURKA*, *TFIIIC5* or *RAD21*, or which were treated with CD532 for 4 or 8 h. Upon siRNA-mediated knockdown Aurora-A, TFIIIC5 and RAD21 protein levels were decreased to more than 50%, but residual protein was detected for all three proteins (Gabriele Buechel, personal communication). Since TFIIIC is required for transcription of tRNA encoding genes, severe defects were expected upon *TFIIIC5* knockdown in proliferating cells (see discussion, section 5.4). Surprisingly, cells treated with si*TFIIIC5* were vital and showed no morphological changes (Gabriele Buechel, personal communication). In contrast, cells treated with si*AURKA* and si*RAD21* mostly detached and started to die 48 h post transfection, which is expected from what is known about their important roles during mitosis [Nasmyth and Haering, 2009] (for Aurora-A functions, see introduction, section 1.5). Strikingly, analysis of the transcriptome of cells depleted of Aurora-A, TFIIIC5 or RAD21 and of CD532 treated cells uncovered a high similarity in expression changes. Most genes whose expression was downregulated in one condition, also decreased in the other 4 conditions. Notably, CD532 treatment resulted in a strong increase of expression of a large set of genes, which was not observed for cells treated with the three different siRNA pools. Gene set enrichment analysis (GSEA) showed that in comparison to control cells genes involved in DNA replication, S phase progression, as well as E2F target genes were downregulated in all 5 conditions (Susanne Walz, personal communication). Importantly, utilisation of ChIP-sequencing data on N-MYC and TFIIIC5 uncovered that these genes were bound by N-MYC and TFIIIC5 and that their occupancy was regulated upon CD532 treatment as shown before (see discussion, section 5.5.1). Furthermore, comparison with published expression data on N-MYC depleted neuroblastoma cells revealed that the same sets of genes were downregulated upon *MYCN* knockdown [Valentijn et al., 2012] (Susanne Walz, personal communication). In addition, GSEA revealed that the group of genes, which showed an upregulation of transcription upon CD532 treatment, encoded proteins involved in POL I-dependent transcription and protein translation. Although the genes encoding transcripts that were upregulated by CD532 displayed N-MYC and TFIIIC5 binding in ChIP-sequencing analysis, they were not identified upon alignment with genes regulated by N-MYC depletion (Susanne Walz, personal communication). While the transcripts upregulated by CD532 are known to be transcribed in G1 phase of the cell cycle, downregulated transcripts of E2F target genes and genes encoding proteins involved in DNA replication and S phase progression are mainly transcribed in early S phase of the cell cycle [Bertoli et al., 2013, Chaudhry et al., 2002]. The CD532-mediated increase of transcription in G1 phase was not surprising, since BrdU propidium iodide (PI) fluorescence activated cell sorting (FACS) analysis of unsynchronised cells that were treated for 4 or 12 h with CD532 led to a decrease in BrdU-positive cells and an accumulation of BrdU-negative cells in S phase, showing that CD532 arrests cells in S phase and pre-

vents progression in S phase (Gabriele Buechel, personal communication). The inhibition of S phase entry by CD532 was shown before, and supports the strong decreasing effect of CD532 on N-MYC protein levels, which prevents S phase entry, inducing a G1 arrest in the cell cycle [Brockmann et al., 2013, Gustafson et al., 2014]. Proximity ligation assays (PLAs) of *MYCN*-amplified IMR-5 cells, which were synchronised via a double-thymidine block, demonstrated that N-MYC and Aurora-A interact preferentially in S phase, whereas N-MYC and TFIIIC5 interact with each other throughout the cell cycle (Evon Poon, personal communication). Interestingly, N-MYC interaction with RAD21 is specific for G1 phase of the cell cycle (Isabelle Röschert, personal communication).

Putting together the information obtained by ChIP-sequencing, RNA-sequencing and interaction studies yields a flexible model, which is based on an equilibrium between two distinct complexes that assemble in a cell cycle-dependent manner (Fig. 5.5). In G1 phase of the cell cycle N-MYC forms a complex together with TFIIIC and cohesin that binds to promoter-close regions, inducing transcription via multiple mechanisms. N-MYC alone can enhance transcription, for example by recruitment of positive co-factors (see introduction, section 1.3.1). In addition, recruitment of TOP2A/B releases the tension in the DNA, enabling progression of transcription. TFIIIC can acetylate histones and recruit cohesin, which can mediate loop formation with an enhancer region (see discussion, section 5.4). However, there are several transcription factors and co-factors that induce transcription in G1 phase in a similar manner and it is likely that upon depletion of N-MYC, TFIIIC5 or RAD21 an alternative mechanism takes over. On the contrary, in S phase of the cell cycle cohesin gets acetylated and becomes less flexible, which leads to specific changes in chromatin architecture [Gerlich et al., 2006, Seitan et al., 2013, Sofueva et al., 2013]. The S phase-specific interaction of N-MYC and Aurora-A and the specific downregulation of transcription of genes transcribed in S phase upon knockdown of *MYCN*, *TFIIIC5*, *RAD21* and *AURKA* indicates a functional relationship, which is important specifically in S phase. Since cohesin is more stably associated with DNA in S phase, it is likely that transcription is inhibited upon stable binding of cohesin close to promoters. In a hypothetical model association of Aurora-A with N-MYC would lead to dissociation of the N-MYC/TFIIIC complex from the DNA and interfere with TFIIIC-mediated cohesin recruitment to promoter-close sites, allowing transcription in S phase (Fig. 5.5). The observation that the TFIIIC2 subunit of TFIIIC is phosphorylated by Aurora-A could represent a mechanistic explanation for the question of how Aurora-A prevents DNA binding of the N-MYC/TFIIIC complex (Mark W. Richards, personal communication). The effects of CD532 treatment support this idea, since the CD532-mediated decrease of N-MYC and Aurora-A, as well as inhibition of Aurora-A kinase activity would result in an increase of TFIIIC binding to chromatin and cohesin recruitment. Importantly, Aurora-A is kinetically active when it is bound to N-MYC (see discussion, section 5.1), whereas it is in an inactive conformation when it is not in a complex with N-MYC or another activating protein, such as TPX2 [Bayliss et al., 2003] (Fig. 5.5). However, it remains open, why TFIIIC5 occupancy was not affected upon treatment with

the catalytic Aurora-A inhibitor MK-5108 and with MLN8237 (Fig. 4.24). Additionally, it is unclear, why a large number of genes transcribed in G1 phase of the cell cycle is selectively induced upon CD532 treatment.

In order to support the hypothesis of a dual function of the N-MYC/TFIIIC complex, immunoprecipitation and ChIP experiments from synchronised cells should be performed to confirm cell cycle-specific interactions and chromatin associations. In addition, reproducing the results for different TFIIIC subunits, would support the observations. Importantly, the N-MYC/Aurora-A-dependent results should be confirmed using an N-MYC mutant deficient in Aurora-A interaction instead of CD532. Furthermore, it should be assessed, whether the findings can be reproduced for C-MYC. While the interaction of N-MYC with DSIF and PAF1C was validated for C-MYC (see discussion, section 5.4.2), the interaction of C-MYC with TFIIIC was not tested yet. It has been proposed previously that MYC proteins can induce loop formation of chromatin, for example by linking rDNA promoters with terminator sequences, enhancing re-initiation of transcription [Shiue et al., 2009, Zeller et al., 2006]. ChIA-PET analysis for N-MYC, TFIIIC5 and RAD21 from cells depleted of one of the three proteins, would help to understand how N-MYC functions together with TFIIIC/cohesin complex in the three-dimensional organisation of chromatin. Initial analysis of N-MYC- and TFIIIC5-mediated looping by ChIA-PET experiments not only confirmed TFIIIC-mediated looping, especially among tDNAs [Raab et al., 2012], but also identified several loops emerging from N-MYC binding sites (Chia-Lin Wei, personal communication).
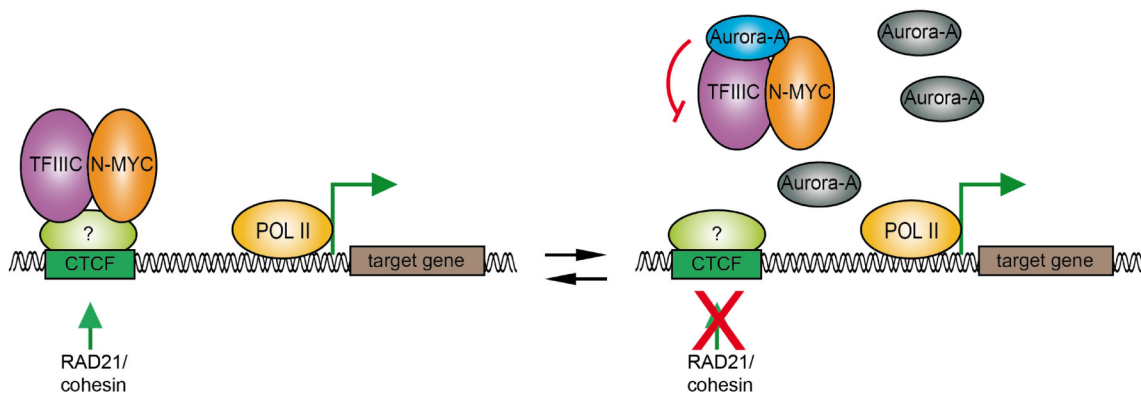
Figure 5.5
Proposed model for N-MYC/TFIIIC complex function
Scheme illustrating a proposed dual function of N-MYC/TFIIIC in regulating transcription of POL II target genes. Before S phase the equilibrium is shifted to an DNA-binding N-MYC/TFIIIC complex, which binds to promoter-close regions (left). The N-MYC/TFIIIC complex can induce transcription for example by recruiting cohesin complexes, which can stabilise enhancer-promoter interactions. In S phase N-MYC/TFIIIC associates with Aurora-A and dissociates from the DNA, inhibiting recruitment of cohesin to promoter-close regions (right). Aurora-A is kinetically active (indicated by the blue color), since it adopts an active conformation in a complex with N-MYC. It is possible that Aurora-A phosphorylates TFIIIC and this could prevent TFIIIC binding to chromatin. In order to allow transcription in S phase the equilibrium has to be shifted to the right, or otherwise cohesin binding to promoter-close regions would prevent transcription.

The picture emerging from the results presented here suggests a novel function of MYC proteins together with TFIIIC/cohesin in cell cycle-dependent organisation of transcription

by regulating chromatin architecture. The functional role of Aurora-A in the complex needs to be studied in more detail and it has to be determined, whether Aurora-A-mediated stabilisation of N-MYC is a secondary effect of N-MYC/TFIIIC complex formation and whether N-MYC phosphorylation is relevant for its function with TFIIIC.

Bibliography

References

P. Agrawal, K. Yu, A. R. Salomon, and J. M. Sedivy. Proteomic profiling of Myc-associated proteins. *Cell Cycle*, 9(24):4908–4921, Dec 2010.

M. A. Al-Salihi, L. Herhaus, T. Macartney, and G. P. Sapkota. USP11 augments TGF-beta signalling by deubiquitylating ALK5. *Open Biol*, 2(6):120063, Jun 2012.

R. K. Alla and B. R. Cairns. RNA polymerase III transcriptomes in human embryonic stem cells and induced pluripotent stem cells, and relationships with pluripotency transcription factors. *PLoS ONE*, 9(1):e85648, 2014.

E. Alvarez, I. C. Northwood, F. A. Gonzalez, D. A. Latour, A. Seth, C. Abate, T. Curran, and R. J. Davis. Pro-Leu-Ser/Thr-Pro is a consensus primary sequence for substrate protein phosphorylation. Characterization of the phosphorylation of c-myc and c-jun proteins by an epidermal growth factor receptor threonine 669 protein kinase. *J. Biol. Chem.*, 266 (23):15277–15285, Aug 1991.

A. Arabi, S. Wu, K. Ridderstrale, H. Bierhoff, C. Shiue, K. Fatyol, S. Fahlen, P. Hydbring, O. Soderberg, I. Grummt, L. G. Larsson, and A. P. Wright. c-Myc associates with ribosomal DNA and activates RNA polymerase I transcription. *Nat. Cell Biol.*, 7 (3):303–310, Mar 2005.

X. Bai, J. Kim, Z. Yang, M. J. Jurynec, T. E. Akie, J. Lee, J. LeBlanc, A. Sessa, H. Jiang, A. DiBiase, Y. Zhou, D. J. Grunwald, S. Lin, A. B. Cantor, S. H. Orkin, and L. I. Zon. TIF1gamma controls erythroid cell fate by regulating transcription elongation. *Cell*, 142 (1):133–143, Jul 2010.

T. L. Bailey, M. Boden, F. A. Buske, M. Frith, C. E. Grant, L. Clementi, J. Ren, W. W. Li, and W. S. Noble. MEME SUITE: tools for motif discovery and searching. *Nucleic Acids Res.*, 37(Web Server issue):W202–208, Jul 2009.

A. Barski, I. Chepelev, D. Liko, S. Cuddapah, A. B. Fleming, J. Birch, K. Cui, R. J. White, and K. Zhao. Pol II and its associated epigenetic marks are present at Pol III-transcribed noncoding RNA genes. *Nat. Struct. Mol. Biol.*, 17(5):629–634, May 2010.

R. Bayliss, T. Sardon, I. Vernos, and E. Conti. Structural basis of Aurora-A activation by TPX2 at the mitotic spindle. *Mol. Cell*, 12(4):851–862, Oct 2003.

H. Beltran. The N-myc Oncogene: Maximizing its Targets, Regulation, and Therapeutic Potential. *Mol. Cancer Res.*, 12(6):815–822, Jun 2014.

H. Beltran, D. S. Rickman, K. Park, S. S. Chae, A. Sboner, T. Y. MacDonald, Y. Wang, K. L. Sheikh, S. Terry, S. T. Tagawa, R. Dhir, J. B. Nelson, A. de la Taille, Y. Allory,

M. B. Gerstein, S. Perner, K. J. Pienta, A. M. Chinnaiyan, Y. Wang, C. C. Collins, M. E. Gleave, F. Demichelis, D. M. Nanus, and M. A. Rubin. Molecular characterization of neuroendocrine prostate cancer and identification of new drug targets. *Cancer Discov*, 1 (6):487–495, Nov 2011.

R. Beroukhim, C. H. Mermel, D. Porter, G. Wei, S. Raychaudhuri, J. Donovan, J. Barretina, J. S. Boehm, J. Dobson, M. Urashima, K. T. Mc Henry, R. M. Pinchback, A. H. Ligon, Y. J. Cho, L. Haery, H. Greulich, M. Reich, W. Winckler, M. S. Lawrence, B. A. Weir, K. E. Tanaka, D. Y. Chiang, A. J. Bass, A. Loo, C. Hoffman, J. Prensner, T. Liefeld, Q. Gao, D. Yecies, S. Signoretti, E. Maher, F. J. Kaye, H. Sasaki, J. E. Tepper, J. A. Fletcher, J. Tabernero, J. Baselga, M. S. Tsao, F. Demichelis, M. A. Rubin, P. A. Janne, M. J. Daly, C. Nucera, R. L. Levine, B. L. Ebert, S. Gabriel, A. K. Rustgi, C. R. Antonescu, M. Ladanyi, A. Letai, L. A. Garraway, M. Loda, D. G. Beer, L. D. True, A. Okamoto, S. L. Pomeroy, S. Singer, T. R. Golub, E. S. Lander, G. Getz, W. R. Sellers, and M. Meyerson. The landscape of somatic copy-number alteration across human cancers. *Nature*, 463(7283):899–905, Feb 2010.

C. Bertoli, J. M. Skotheim, and R. A. de Bruin. Control of cell cycle transcription during G1 and S phases. *Nat. Rev. Mol. Cell Biol.*, 14(8):518–528, Aug 2013.

B. Berwanger, O. Hartmann, E. Bergmann, S. Bernard, D. Nielsen, M. Krause, A. Kartal, D. Flynn, R. Wiedemeyer, M. Schwab, H. Schafer, H. Christiansen, and M. Eilers. Loss of a FYN-regulated differentiation and growth arrest pathway in advanced stage neuroblastoma. *Cancer Cell*, 2(5):377–386, Nov 2002.

T. K. Blackwell, L. Kretzner, E. M. Blackwood, R. N. Eisenman, and H. Weintraub. Sequence-specific DNA binding by the c-Myc protein. *Science*, 250(4984):1149–1151, Nov 1990.

T. K. Blackwell, J. Huang, A. Ma, L. Kretzner, F. W. Alt, R. N. Eisenman, and H. Weintraub. Binding of myc proteins to canonical and noncanonical DNA sequences. *Mol. Cell. Biol.*, 13(9):5216–5224, Sep 1993.

E. M. Blackwood and R. N. Eisenman. Max: a helix-loop-helix zipper protein that forms a sequence-specific DNA-binding complex with Myc. *Science*, 251(4998):1211–1217, Mar 1991.

N. Bonhoure, G. Bounova, D. Bernasconi, V. Praz, F. Lammers, D. Canella, I. M. Willis, W. Herr, N. Hernandez, M. Delorenzi, N. Hernandez, M. Delorenzi, B. Deplancke, B. Desvergne, N. Guex, W. Herr, F. Naef, J. Rougemont, U. Schibler, T. Andersin, P. Cousin, F. Gilardi, P. Gos, F. Lammers, S. Raghav, D. Villeneuve, R. Fabbretti, V. Vlegel, I. Xenarios, E. Migliavacca, V. Praz, F. David, Y. Jarosz, D. Kuznetsov, R. Liechti, O. Martin, J. Delafontaine, J. Cajan, K. Gustafson, I. Krier, M. Leleu, N. Molina, A. Naldi, L. Rib, L. Symul, and G. Bounova. Quantifying ChIP-seq data: a spiking method providing an

internal reference for sample-to-sample normalization. *Genome Res.*, 24(7):1157–1168, Jul 2014.

C. Bouchard, J. Marquardt, A. Bras, R. H. Medema, and M. Eilers. Myc-induced proliferation and transformation require Akt-mediated phosphorylation of FoxO proteins. *EMBO J.*, 23(14):2830–2840, Jul 2004.

M. M. Bradford. A rapid and sensitive method for the quantitation of microgram quantities of protein utilizing the principle of protein-dye binding. *Anal. Biochem.*, 72:248–254, May 1976.

C. Brenner, R. Deplus, C. Didelot, A. Loriot, E. Vire, C. De Smet, A. Gutierrez, D. Danovi, D. Bernard, T. Boon, P. G. Pelicci, B. Amati, T. Kouzarides, Y. de Launoit, L. Di Croce, and F. Fuks. Myc represses transcription through recruitment of DNA methyltransferase corepressor. *EMBO J.*, 24(2):336–346, Jan 2005.

M. Brockmann, E. Poon, T. Berry, A. Carstensen, H. E. Deubzer, L. Rycak, Y. Jamin, K. Thway, S. P. Robinson, F. Roels, O. Witt, M. Fischer, L. Chesler, and M. Eilers. Small molecule inhibitors of aurora-a induce proteasomal degradation of N-myc in childhood neuroblastoma. *Cancer Cell*, 24(1):75–89, Jul 2013.

G. M. Brodeur and R. Bagatell. Mechanisms of neuroblastoma regression. *Nat Rev Clin Oncol*, 11(12):704–713, Dec 2014.

G. M. Brodeur, R. C. Seeger, M. Schwab, H. E. Varmus, and J. M. Bishop. Amplification of N-myc in untreated human neuroblastomas correlates with advanced disease stage. *Science*, 224(4653):1121–1124, Jun 1984.

K. J. Campbell and R. J. White. MYC regulation of cell growth through control of transcription by RNA polymerases I and III. *Cold Spring Harb Perspect Med*, 4(5), May 2014.

D. Canella, V. Praz, J. H. Reina, P. Cousin, and N. Hernandez. Defining the RNA polymerase III transcriptome: Genome-wide localization of the RNA polymerase III transcription machinery in human cells. *Genome Res.*, 20(6):710–721, Jun 2010.

D. G. Carneiro, T. Clarke, C. C. Davies, and D. Bailey. Identifying novel protein interactions: Proteomic methods, optimisation approaches and data analysis pipelines. *Methods*, 95:46–54, Feb 2016.

L. Carriere, S. Graziani, O. Alibert, Y. Ghavi-Helm, F. Boussouar, H. Humbertclaude, S. Jounier, J. C. Aude, C. Keime, J. Murvai, M. Foglio, M. Gut, I. Gut, M. Lathrop, J. Soutourina, M. Gerard, and M. Werner. Genomic binding of Pol III transcription machinery and relationship with TFIIS transcription factor distribution in mouse embryonic stem cells. *Nucleic Acids Res.*, 40(1):270–283, Jan 2012.

D. L. Chalker and S. B. Sandmeyer. Transfer RNA genes are genomic targets for de Novo transposition of the yeast retrotransposon Ty3. *Genetics*, 126(4):837–850, Dec 1990.

D. W. Chang, G. F. Claassen, S. R. Hann, and M. D. Cole. The c-Myc transactivation domain is a direct modulator of apoptotic versus proliferative signals. *Mol. Cell. Biol.*, 20(12):4309–4319, Jun 2000.

J. Charron, B. A. Malynn, P. Fisher, V. Stewart, L. Jeannotte, S. P. Goff, E. J. Robertson, and F. W. Alt. Embryonic lethality in mice homozygous for a targeted disruption of the N-myc gene. *Genes Dev.*, 6(12A):2248–2257, Dec 1992.

M. A. Chaudhry, L. A. Chodosh, W. G. McKenna, and R. J. Muschel. Gene expression profiling of HeLa cells in G1 or G2 phases. *Oncogene*, 21(12):1934–1942, Mar 2002.

G. M. Cheetham, R. M. Knegtel, J. T. Coll, S. B. Renwick, L. Swenson, P. Weber, J. A. Lippke, and D. A. Austen. Crystal structure of aurora-2, an oncogenic serine/threonine kinase. *J. Biol. Chem.*, 277(45):42419–42422, Nov 2002.

F. X. Chen, A. R. Woodfin, A. Gardini, R. A. Rickels, S. A. Marshall, E. R. Smith, R. Shiekhattar, and A. Shilatifard. PAF1, a Molecular Regulator of Promoter-Proximal Pausing by RNA Polymerase II. *Cell*, 162(5):1003–1015, Aug 2015a.

K. Chen, J. Hu, D. L. Moore, R. Liu, S. A. Kessans, K. Breslin, I. S. Lucet, A. Keniry, H. S. Leong, C. L. Parish, D. J. Hilton, R. J. Lemmers, S. M. van der Maarel, P. E. Czabotar, R. C. Dobson, M. E. Ritchie, G. F. Kay, J. M. Murphy, and M. E. Blewitt. Genome-wide binding and mechanistic analyses of Smchd1-mediated epigenetic regulation. *Proc. Natl. Acad. Sci. U.S.A.*, 112(27):E3535–3544, Jul 2015b.

S. S. Chen, P. C. Chang, Y. W. Cheng, F. M. Tang, and Y. S. Lin. Suppression of the STK15 oncogenic activity requires a transactivation-independent p53 function. *EMBO J.*, 21(17):4491–4499, Sep 2002.

S. H. Choi, J. B. Wright, S. A. Gerber, and M. D. Cole. Myc protein is stabilized by suppression of a novel E3 ligase complex in cancer cells. *Genes Dev.*, 24(12):1236–1241, Jun 2010.

P. Cohen and S. Frame. The renaissance of GSK3. *Nat. Rev. Mol. Cell Biol.*, 2(10):769–776, Oct 2001.

M. D. Cole and V. H. Cowling. Transcription-independent functions of MYC: regulation of translation and DNA replication. *Nat. Rev. Mol. Cell Biol.*, 9(10):810–815, Oct 2008.

M. Conacci-Sorrell, L. McFerrin, and R. N. Eisenman. An overview of MYC and its interactome. *Cold Spring Harb Perspect Med*, 4(1):a014357, Jan 2014.

C. M. Connolly and S. B. Sandmeyer. RNA polymerase III interferes with Ty3 integration. *FEBS Lett.*, 405(3):305–311, Apr 1997.

D. Corvetta, O. Chayka, S. Gherardi, C. W. D'Acunto, S. Cantilena, E. Valli, I. Piotrowska, G. Perini, and A. Sala. Physical interaction between MYCN oncogene and polycomb repressive complex 2 (PRC2) in neuroblastoma: functional and therapeutic implications. *J. Biol. Chem.*, 288(12):8332–8341, Mar 2013.

L. Crepaldi, C. Policarpi, A. Coatti, W. T. Sherlock, B. C. Jongbloets, T. A. Down, and A. Riccio. Binding of TFIIIC to sine elements controls the relocation of activity-dependent neuronal genes to transcription factories. *PLoS Genet.*, 9(8):e1003699, 2013.

S. Cuddapah, R. Jothi, D. E. Schones, T. Y. Roh, K. Cui, and K. Zhao. Global analysis of the insulator binding protein CTCF in chromatin barrier regions reveals demarcation of active and repressive domains. *Genome Res.*, 19(1):24–32, Jan 2009.

C. D'Ambrosio, C. K. Schmidt, Y. Katou, G. Kelly, T. Itoh, K. Shirahige, and F. Uhlmann. Identification of cis-acting sites for condensin loading onto budding yeast chromosomes. *Genes Dev.*, 22(16):2215–2227, Aug 2008.

C. V. Dang. MYC on the path to cancer. *Cell*, 149(1):22–35, Mar 2012.

C. V. Dang and W. M. Lee. Identification of the human c-myc protein nuclear translocation signal. *Mol. Cell. Biol.*, 8(10):4048–4054, Oct 1988.

C. V. Dang, K. A. O'Donnell, K. I. Zeller, T. Nguyen, R. C. Osthus, and F. Li. The c-Myc target gene network. *Semin. Cancer Biol.*, 16(4):253–264, Aug 2006.

A. Dar, E. Shibata, and A. Dutta. Deubiquitination of Tip60 by USP7 determines the activity of the p53-dependent apoptotic pathway. *Mol. Cell. Biol.*, 33(16):3309–3320, Aug 2013.

D. Dauch, R. Rudalska, G. Cossa, J. C. Nault, T. W. Kang, T. Wuestefeld, A. Hohmeyer, S. Imbeaud, T. Yevsa, L. Hoenicke, T. Pantsar, P. Bozko, N. P. Malek, T. Longerich, S. Laufer, A. Poso, J. Zucman-Rossi, M. Eilers, and L. Zender. A MYC-aurora kinase A protein complex represents an actionable drug target in p53-altered liver cancer. *Nat. Med.*, May 2016.

A. C. Davis, M. Wims, G. D. Spotts, S. R. Hann, and A. Bradley. A null c-myc mutation causes lethality before 10.5 days of gestation in homozygotes and reduced fertility in heterozygous female mice. *Genes Dev.*, 7(4):671–682, Apr 1993.

G. Dieci, G. Fiorino, M. Castelnuovo, M. Teichmann, and A. Pagano. The expanding RNA polymerase III transcriptome. *Trends Genet.*, 23(12):614–622, Dec 2007.

G. Dieci, A. Conti, A. Pagano, and D. Carnevali. Identification of RNA polymerase III-transcribed genes in eukaryotic genomes. *Biochim. Biophys. Acta*, 1829(3-4):296–305, 2013.

J. Dirks. Charakterisierung der Wechselwirkung zwischen N-Myc und Aurora-A im MYCN-amplifizierten Neuroblastom. *Doctoral thesis*, soon to be published.

K. A. Dittmar, J. M. Goodenbour, and T. Pan. Tissue-specific differences in human transfer RNA expression. *PLoS Genet.*, 2(12):e221, Dec 2006.

C. A. Dodson, M. Kosmopoulou, M. W. Richards, B. Atrash, V. Bavetsias, J. Blagg, and R. Bayliss. Crystal structure of an Aurora-A mutant that mimics Aurora-B bound to MLN8054: insights into selectivity and drug design. *Biochem. J.*, 427(1):19–28, Apr 2010.

D. Dominguez-Sola, C. Y. Ying, C. Grandori, L. Ruggiero, B. Chen, M. Li, D. A. Galloway, W. Gu, J. Gautier, and R. Dalla-Favera. Non-transcriptional control of DNA replication by c-Myc. *Nature*, 448(7152):445–451, Jul 2007.

D. Donze. Extra-transcriptional functions of RNA Polymerase III complexes: TFIIIC as a potential global chromatin bookmark. *Gene*, 493(2):169–175, Feb 2012.

D. Donze and R. T. Kamakaka. RNA polymerase III and RNA polymerase II promoter complexes are heterochromatin barriers in Saccharomyces cerevisiae. *EMBO J.*, 20(3): 520–531, Feb 2001.

D. Donze, C. R. Adams, J. Rine, and R. T. Kamakaka. The boundaries of the silenced HMR domain in Saccharomyces cerevisiae. *Genes Dev.*, 13(6):698–708, Mar 1999.

S. G. DuBois, Y. Kalika, J. N. Lukens, G. M. Brodeur, R. C. Seeger, J. B. Atkinson, G. M. Haase, C. T. Black, C. Perez, H. Shimada, R. Gerbing, D. O. Stram, and K. K. Matthay. Metastatic sites in stage IV and IVS neuroblastoma correlate with age, tumor biology, and survival. *J. Pediatr. Hematol. Oncol.*, 21(3):181–189, 1999.

H. Dumay-Odelot, C. Marck, S. Durrieu-Gaillard, O. Lefebvre, S. Jourdain, M. Prochazkova, A. Pflieger, and M. Teichmann. Identification, molecular cloning, and characterization of the sixth subunit of human transcription factor TFIIIC. *J. Biol. Chem.*, 282(23): 17179–17189, Jun 2007.

S. R. Eberhardy and P. J. Farnham. Myc recruits P-TEFb to mediate the final step in the transcriptional activation of the cad promoter. *J. Biol. Chem.*, 277(42):40156–40162, Oct 2002.

R. Edgar, M. Domrachev, and A. E. Lash. Gene Expression Omnibus: NCBI gene expression and hybridization array data repository. *Nucleic Acids Res.*, 30(1):207–210, Jan 2002.

M. Eilers and R. N. Eisenman. Myc's broad reach. *Genes Dev.*, 22(20):2755–2766, Oct 2008.

I. Ernens, S. J. Goodfellow, F. Innes, N. S. Kenneth, L. E. Derblay, R. J. White, and P. H. Scott. Hypoxic stress suppresses RNA polymerase III recruitment and tRNA gene transcription in cardiomyocytes. *Nucleic Acids Res.*, 34(1):286–294, 2006.

A. Ewart-Toland, P. Briassouli, J. P. de Koning, J. H. Mao, J. Yuan, F. Chan, L. MacCarthy-Morrogh, B. A. Ponder, H. Nagase, J. Burn, S. Ball, M. Almeida, S. Linardopoulos, and A. Balmain. Identification of Stk6/STK15 as a candidate low-penetrance tumor-susceptibility gene in mouse and human. *Nat. Genet.*, 34(4):403–412, Aug 2003.

Z. A. Felton-Edkins, N. S. Kenneth, T. R. Brown, N. L. Daly, N. Gomez-Roman, C. Grandori, R. N. Eisenman, and R. J. White. Direct regulation of RNA polymerase III transcription by RB, p53 and c-Myc. *Cell Cycle*, 2(3):181–184, 2003.

P. C. Fernandez, S. R. Frank, L. Wang, M. Schroeder, S. Liu, J. Greene, A. Cocito, and B. Amati. Genomic targets of the human c-Myc protein. *Genes Dev.*, 17(9):1115–1129, May 2003.

J. M. Fraile, V. Quesada, D. Rodriguez, J. M. Freije, and C. Lopez-Otin. Deubiquitinases in cancer: new functions and therapeutic options. *Oncogene*, 31(19):2373–2388, May 2012.

S. R. Frank, T. Parisi, S. Taubert, P. Fernandez, M. Fuchs, H. M. Chan, D. M. Livingston, and B. Amati. MYC recruits the TIP60 histone acetyltransferase complex to chromatin. *EMBO Rep.*, 4(6):575–580, Jun 2003.

M. Fuchs, J. Gerber, R. Drapkin, S. Sif, T. Ikura, V. Ogryzko, W. S. Lane, Y. Nakatani, and D. M. Livingston. The p400 complex is an essential E1A transformation target. *Cell*, 106(3):297–307, Aug 2001.

M. Furrer, M. Balbi, M. Albarca-Aguilera, M. Gallant, W. Herr, and P. Gallant. Drosophila Myc interacts with host cell factor (dHCF) to activate transcription and control growth. *J. Biol. Chem.*, 285(51):39623–39636, Dec 2010.

P. Gallant. Myc function in Drosophila. *Cold Spring Harb Perspect Med*, 3(10):a014324, Oct 2013.

P. Gallant, Y. Shiio, P. F. Cheng, S. M. Parkhurst, and R. N. Eisenman. Myc and Max homologs in Drosophila. *Science*, 274(5292):1523–1527, Nov 1996.

A. L. Gartel, X. Ye, E. Goufman, P. Shianov, N. Hay, F. Najmabadi, and A. L. Tyner. Myc represses the p21(WAF1/CIP1) promoter and interacts with Sp1/Sp3. *Proc. Natl. Acad. Sci. U.S.A.*, 98(8):4510–4515, Apr 2001.

E. P. Geiduschek and G. A. Kassavetis. The RNA polymerase III transcription apparatus. *J. Mol. Biol.*, 310(1):1–26, Jun 2001.

D. Gerlich, B. Koch, F. Dupeux, J. M. Peters, and J. Ellenberg. Live-cell imaging reveals a stable cohesin-chromatin interaction after but not before DNA replication. *Curr. Biol.*, 16(15):1571–1578, Aug 2006.

N. Gomez-Roman, C. Grandori, R. N. Eisenman, and R. J. White. Direct activation of RNA polymerase III transcription by c-Myc. *Nature*, 421(6920):290–294, Jan 2003.

C. Grandori, N. Gomez-Roman, Z. A. Felton-Edkins, C. Ngouenet, D. A. Galloway, R. N. Eisenman, and R. J. White. c-Myc binds to human ribosomal DNA and stimulates transcription of rRNA genes by RNA polymerase I. *Nat. Cell Biol.*, 7(3):311–318, Mar 2005.

M. A. Gregory and S. R. Hann. c-Myc proteolysis by the ubiquitin-proteasome pathway: stabilization of c-Myc in Burkitt's lymphoma cells. *Mol. Cell. Biol.*, 20(7):2423–2435, Apr 2000.

M. A. Gregory, Y. Qi, and S. R. Hann. Phosphorylation by glycogen synthase kinase-3 controls c-myc proteolysis and subnuclear localization. *J. Biol. Chem.*, 278(51):51606–51612, Dec 2003.

S. S. Grewal, L. Li, A. Orian, R. N. Eisenman, and B. A. Edgar. Myc-dependent regulation of ribosomal RNA synthesis during Drosophila development. *Nat. Cell Biol.*, 7(3):295–302, Mar 2005.

I. Grummt. Regulation of mammalian ribosomal gene transcription by RNA polymerase I. *Prog. Nucleic Acid Res. Mol. Biol.*, 62:109–154, 1999.

E. Guccione, F. Martinato, G. Finocchiaro, L. Luzi, L. Tizzoni, V. Dall' Olio, G. Zardo, C. Nervi, L. Bernard, and B. Amati. Myc-binding-site recognition in the human genome is determined by chromatin context. *Nat. Cell Biol.*, 8(7):764–770, Jul 2006.

J. Guo, T. Li, J. Schipper, K. A. Nilson, F. K. Fordjour, J. J. Cooper, R. Gordan, and D. H. Price. Sequence specificity incompletely defines the genome-wide occupancy of Myc. *Genome Biol.*, 15(10):482, 2014.

S. Gupta, J. A. Stamatoyannopoulos, T. L. Bailey, and W. S. Noble. Quantifying similarity between motifs. *Genome Biol.*, 8(2):R24, 2007.

W. C. Gustafson, J. G. Meyerowitz, E. A. Nekritz, J. Chen, C. Benes, E. Charron, E. F. Simonds, R. Seeger, K. K. Matthay, N. T. Hertz, M. Eilers, K. M. Shokat, and W. A. Weiss. Drugging MYCN through an allosteric transition in Aurora kinase A. *Cancer Cell*, 26(3):414–427, Sep 2014.

K. Haglund and I. Dikic. Ubiquitylation and cell signaling. *EMBO J.*, 24(19):3353–3359, Oct 2005.

L. Handoko, H. Xu, G. Li, C. Y. Ngan, E. Chew, M. Schnapp, C. W. Lee, C. Ye, J. L. Ping, F. Mulawadi, E. Wong, J. Sheng, Y. Zhang, T. Poh, C. S. Chan, G. Kunarso, A. Shahab, G. Bourque, V. Cacheux-Rataboul, W. K. Sung, Y. Ruan, and C. L. Wei. CTCF-mediated functional chromatin interactome in pluripotent cells. *Nat. Genet.*, 43 (7):630–638, Jul 2011.

K. M. Hannan, E. Sanij, L. I. Rothblum, R. D. Hannan, and R. B. Pearson. Dysregulation of RNA polymerase I transcription during disease. *Biochim. Biophys. Acta*, 1829(3-4): 342–360, 2013.

K. S. Hatton, K. Mahon, L. Chin, F. C. Chiu, H. W. Lee, D. Peng, S. D. Morgenbesser, J. Horner, and R. A. DePinho. Expression and activity of L-Myc in normal mouse development. *Mol. Cell. Biol.*, 16(4):1794–1804, Apr 1996.

M. Henriksson, A. Bakardjiev, G. Klein, and B. Luscher. Phosphorylation sites mapping in the N-terminal domain of c-myc modulate its transforming potential. *Oncogene*, 8(12): 3199–3209, Dec 1993.

A. Herbst, S. E. Salghetti, S. Y. Kim, and W. P. Tansey. Multiple cell-type-specific elements regulate Myc protein stability. *Oncogene*, 23(21):3863–3871, May 2004.

S. Herold, M. Wanzel, V. Beuger, C. Frohme, D. Beul, T. Hillukkala, J. Syvaoja, H. P. Saluz, F. Haenel, and M. Eilers. Negative regulation of the mammalian UV response by Myc through association with Miz-1. *Mol. Cell*, 10(3):509–521, Sep 2002.

Y. J. Hsieh, T. K. Kundu, Z. Wang, R. Kovelman, and R. G. Roeder. The TFIIIC90 subunit of TFIIIC interacts with multiple components of the RNA polymerase III machinery and contains a histone-specific acetyltransferase activity. *Mol. Cell. Biol.*, 19(11):7697–7704, Nov 1999.

M. Hu, P. Li, M. Li, W. Li, T. Yao, J. W. Wu, W. Gu, R. E. Cohen, and Y. Shi. Crystal structure of a UBP-family deubiquitinating enzyme in isolation and in complex with ubiquitin aldehyde. *Cell*, 111(7):1041–1054, Dec 2002.

d. a. W. Huang, B. T. Sherman, and R. A. Lempicki. Bioinformatics enrichment tools: paths toward the comprehensive functional analysis of large gene lists. *Nucleic Acids Res.*, 37 (1):1–13, Jan 2009a.

d. a. W. Huang, B. T. Sherman, and R. A. Lempicki. Systematic and integrative analysis of large gene lists using DAVID bioinformatics resources. *Nat Protoc*, 4(1):44–57, 2009b.

M. Huang and W. A. Weiss. Neuroblastoma and MYCN. *Cold Spring Harb Perspect Med*, 3(10):a014415, Oct 2013.

P. J. Hurlin. N-Myc functions in transcription and development. *Birth Defects Res. C Embryo Today*, 75(4):340–352, Dec 2005.

P. Hydbring, F. Bahram, Y. Su, S. Tronnersjo, K. Hogstrand, N. von der Lehr, H. R. Sharifi, R. Lilischkis, N. Hein, S. Wu, J. Vervoorts, M. Henriksson, A. Grandien, B. Luscher, and L. G. Larsson. Phosphorylation by Cdk2 is required for Myc to repress Ras-induced senescence in cotransformation. *Proc. Natl. Acad. Sci. U.S.A.*, 107(1):58–63, Jan 2010.

A. L. Jackson, J. Burchard, J. Schelter, B. N. Chau, M. Cleary, L. Lim, and P. S. Linsley. Widespread siRNA "off-target" transcript silencing mediated by seed region sequence complementarity. *RNA*, 12(7):1179–1187, Jul 2006.

L. A. Jaenicke. Regulation of MYC Activity by the Ubiquitin-Proteasome System. *Doctoral thesis*, 2015.

L. A. Jaenicke, B. von Eyss, A. Carstensen, E. Wolf, W. Xu, A. K. Greifenberg, M. Geyer, M. Eilers, and N. Popov. Ubiquitin-Dependent Turnover of MYC Antagonizes MYC/PAF1C Complex Accumulation to Drive Transcriptional Elongation. *Mol. Cell*, 61(1):54–67, Jan 2016.

A. Jansen and K. J. Verstrepen. Nucleosome positioning in Saccharomyces cerevisiae. *Microbiol. Mol. Biol. Rev.*, 75(2):301–320, Jun 2011.

K. Jeppsson, T. Kanno, K. Shirahige, and C. Sjogren. The maintenance of chromosome structure: positioning and functioning of SMC complexes. *Nat. Rev. Mol. Cell Biol.*, 15 (9):601–614, Sep 2014.

H. Ji, G. Wu, X. Zhan, A. Nolan, C. Koh, A. De Marzo, H. M. Doan, J. Fan, C. Cheadle, M. Fallahi, J. L. Cleveland, C. V. Dang, and K. I. Zeller. Cell-type independent MYC target genes reveal a primordial signature involved in biomass accumulation. *PLoS ONE*, 6(10):e26057, 2011.

L. A. Johnston, D. A. Prober, B. A. Edgar, R. N. Eisenman, and P. Gallant. Drosophila myc regulates cellular growth during development. *Cell*, 98(6):779–790, Sep 1999.

S. Jourdain, J. Acker, C. Ducrot, A. Sentenac, and O. Lefebvre. The tau95 subunit of yeast TFIIIC influences upstream and downstream functions of TFIIIC.DNA complexes. *J. Biol. Chem.*, 278(12):10450–10457, Mar 2003.

J. H. Kang, P. G. Rychahou, T. A. Ishola, J. Qiao, B. M. Evers, and D. H. Chung. MYCN silencing induces differentiation and apoptosis in human neuroblastoma cells. *Biochem. Biophys. Res. Commun.*, 351(1):192–197, Dec 2006.

D. Karolchik, A. S. Hinrichs, T. S. Furey, K. M. Roskin, C. W. Sugnet, D. Haussler, and W. J. Kent. The UCSC Table Browser data retrieval tool. *Nucleic Acids Res.*, 32(Database issue):D493–496, Jan 2004.

D. Karthigeyan, S. B. Prasad, J. Shandilya, S. Agrawal, and T. K. Kundu. Biology of Aurora A kinase: implications in cancer manifestation and therapy. *Med Res Rev*, 31(5): 757–793, Sep 2011.

H. Katayama, K. Sasai, H. Kawai, Z. M. Yuan, J. Bondaruk, F. Suzuki, S. Fujii, R. B. Arlinghaus, B. A. Czerniak, and S. Sen. Phosphorylation by aurora kinase A induces Mdm2-mediated destabilization and inhibition of p53. *Nat. Genet.*, 36(1):55–62, Jan 2004.

G. J. Kato, J. Barrett, M. Villa-Garcia, and C. V. Dang. An amino-terminal c-myc domain required for neoplastic transformation activates transcription. *Mol. Cell. Biol.*, 10(11): 5914–5920, Nov 1990.

N. S. Kenneth, B. A. Ramsbottom, N. Gomez-Roman, L. Marshall, P. A. Cole, and R. J. White. TRRAP and GCN5 are used by c-Myc to activate RNA polymerase III transcription. *Proc. Natl. Acad. Sci. U.S.A.*, 104(38):14917–14922, Sep 2007.

A. M. Kenney, M. D. Cole, and D. H. Rowitch. Nmyc upregulation by sonic hedgehog signaling promotes proliferation in developing cerebellar granule neuron precursors. *Development*, 130(1):15–28, Jan 2003.

A. M. Kenney, H. R. Widlund, and D. H. Rowitch. Hedgehog and PI-3 kinase signaling converge on Nmyc1 to promote cell cycle progression in cerebellar neuronal precursors. *Development*, 131(1):217–228, Jan 2004.

K. R. Kieffer-Kwon, Z. Tang, E. Mathe, J. Qian, M. H. Sung, G. Li, W. Resch, S. Baek, N. Pruett, L. Gr?ntved, L. Vian, S. Nelson, H. Zare, O. Hakim, D. Reyon, A. Yamane, H. Nakahashi, A. L. Kovalchuk, J. Zou, J. K. Joung, V. Sartorelli, C. L. Wei, X. Ruan, G. L. Hager, Y. Ruan, and R. Casellas. Interactome maps of mouse gene regulatory domains reveal basic principles of transcriptional regulation. *Cell*, 155(7):1507–1520, Dec 2013.

J. Kirchner, C. M. Connolly, and S. B. Sandmeyer. Requirement of RNA polymerase III transcription factors for in vitro position-specific integration of a retroviruslike element. *Science*, 267(5203):1488–1491, Mar 1995.

J. G. Kirkland, J. R. Raab, and R. T. Kamakaka. TFIIIC bound DNA elements in nuclear organization and insulation. *Biochim. Biophys. Acta*, 1829(3-4):418–424, 2013.

P. S. Knoepfler, P. F. Cheng, and R. N. Eisenman. N-myc is essential during neurogenesis for the rapid expansion of progenitor cell populations and the inhibition of neuronal differentiation. *Genes Dev.*, 16(20):2699–2712, Oct 2002.

H. B. Koch, R. Zhang, B. Verdoodt, A. Bailey, C. D. Zhang, J. R. Yates, A. Menssen, and H. Hermeking. Large-scale identification of c-MYC-associated proteins using a combined TAP/MudPIT approach. *Cell Cycle*, 6(2):205–217, Jan 2007.

N. E. Kohl, N. Kanda, R. R. Schreck, G. Bruns, S. A. Latt, F. Gilbert, and F. W. Alt. Transposition and amplification of oncogene-related sequences in human neuroblastomas. *Cell*, 35(2 Pt 1):359–367, Dec 1983.

F. Kouzine, D. Levens, and L. Baranello. DNA topology and transcription. *Nucleus*, 5(3): 195–202, 2014.

C. Kramps, V. Strieder, A. Sapetschnig, G. Suske, and W. Lutz. E2F and Sp1/Sp3 Synergize but are not sufficient to activate the MYCN gene in neuroblastomas. *J. Biol. Chem.*, 279 (7):5110–5117, Feb 2004.

T. K. Kundu, Z. Wang, and R. G. Roeder. Human TFIIIC relieves chromatin-mediated repression of RNA polymerase III transcription and contains an intrinsic histone acetyl-transferase activity. *Mol. Cell. Biol.*, 19(2):1605–1615, Feb 1999.

J. F. Kurland and W. P. Tansey. Myc-mediated transcriptional repression by recruitment of histone deacetylase. *Cancer Res.*, 68(10):3624–3629, May 2008.

H. Kwak and J. T. Lis. Control of transcriptional elongation. *Annu. Rev. Genet.*, 47: 483–508, 2013.

U. K. Laemmli. Cleavage of structural proteins during the assembly of the head of bacterio-phage T4. *Nature*, 227(5259):680–685, Aug 1970.

B. Langmead. Aligning short sequencing reads with Bowtie. *Curr Protoc Bioinformatics*, Chapter 11:Unit 11.7, Dec 2010.

M. Larance and A. I. Lamond. Multidimensional proteomics for cell biology. *Nat. Rev. Mol. Cell Biol.*, 16(5):269–280, May 2015.

A. B. Lassar, P. L. Martin, and R. G. Roeder. Transcription of class III genes: formation of preinitiation complexes. *Science*, 222(4625):740–748, Nov 1983.

L. A. Lee, C. Dolde, J. Barrett, C. S. Wu, and C. V. Dang. A link between c-Myc-mediated transcriptional repression and neoplastic transformation. *J. Clin. Invest.*, 97(7):1687–1695, Apr 1996.

G. Li, M. J. Fullwood, H. Xu, F. H. Mulawadi, S. Velkov, V. Vega, P. N. Ariyaratne, Y. B. Mohamed, H. S. Ooi, C. Tennakoon, C. L. Wei, Y. Ruan, and W. K. Sung. ChIA-PET tool for comprehensive chromatin interaction analysis with paired-end tag sequencing. *Genome Biol.*, 11(2):R22, 2010.

G. Li, X. Ruan, R. K. Auerbach, K. S. Sandhu, M. Zheng, P. Wang, H. M. Poh, Y. Goh, J. Lim, J. Zhang, H. S. Sim, S. Q. Peh, F. H. Mulawadi, C. T. Ong, Y. L. Orlov, S. Hong, Z. Zhang, S. Landt, D. Raha, G. Euskirchen, C. L. Wei, W. Ge, H. Wang, C. Davis, K. I. Fisher-Aylor, A. Mortazavi, M. Gerstein, T. Gingeras, B. Wold, Y. Sun, M. J. Fullwood, E. Cheung, E. Liu, W. K. Sung, M. Snyder, and Y. Ruan. Extensive promoter-centered chromatin interactions provide a topological basis for transcription regulation. *Cell*, 148 (1-2):84–98, Jan 2012.

H. Li, B. Handsaker, A. Wysoker, T. Fennell, J. Ruan, N. Homer, G. Marth, G. Abecasis, and R. Durbin. The Sequence Alignment/Map format and SAMtools. *Bioinformatics*, 25 (16):2078–2079, Aug 2009.

Y. Li, P. S. Choi, S. C. Casey, D. L. Dill, and D. W. Felsher. MYC through miR-17-92 suppresses specific target genes to maintain survival, autonomous proliferation, and a neoplastic state. *Cancer Cell*, 26(2):262–272, Aug 2014.

Z. Li and S. R. Hann. Nucleophosmin is essential for c-Myc nucleolar localization and c-Myc-mediated rDNA transcription. *Oncogene*, 32(15):1988–1994, Apr 2013.

C. Y. Lin, J. Loven, P. B. Rahl, R. M. Paranal, C. B. Burge, J. E. Bradner, T. I. Lee, and R. A. Young. Transcriptional amplification in tumor cells with elevated c-Myc. *Cell*, 151 (1):56–67, Sep 2012.

A. Lindqvist, V. Rodriguez-Bravo, and R. H. Medema. The decision to enter mitosis: feedback and redundancy in the mitotic entry network. *J. Cell Biol.*, 185(2):193–202, Apr 2009.

L. Liu, R. C. Wade, and D. W. Heermann. A multiscale approach to simulating the conformational properties of unbound multi-C_2H_2 zinc finger proteins. *Proteins*, 83(9):1604–1615, Sep 2015.

C. Lorenzo, Q. Liao, M. A. Hardwicke, and B. Ducommun. Pharmacological inhibition of aurora-A but not aurora-B impairs interphase microtubule dynamics. *Cell Cycle*, 8(11): 1733–1737, Jun 2009.

L. Y. Lu, J. L. Wood, L. Ye, K. Minter-Dykhouse, T. L. Saunders, X. Yu, and J. Chen. Aurora A is essential for early embryonic development and tumor suppression. *J. Biol. Chem.*, 283(46):31785–31790, Nov 2008.

B. Lutterbach and S. R. Hann. Hierarchical phosphorylation at N-terminal transformation-sensitive sites in c-Myc protein is regulated by mitogens and in mitosis. *Mol. Cell. Biol.*, 14(8):5510–5522, Aug 1994.

W. Lutz and M. Schwab. In vivo regulation of single copy and amplified N-myc in human neuroblastoma cells. *Oncogene*, 15(3):303–315, Jul 1997.

G. N. Maertens, S. El Messaoudi-Aubert, S. Elderkin, K. Hiom, and G. Peters. Ubiquitin-specific proteases 7 and 11 modulate Polycomb regulation of the INK4a tumour suppressor. *EMBO J.*, 29(15):2553–2565, Aug 2010.

B. A. Malynn, I. M. de Alboran, R. C. O'Hagan, R. Bronson, L. Davidson, R. A. DePinho, and F. W. Alt. N-myc can functionally replace c-myc in murine development, cellular growth, and differentiation. *Genes Dev.*, 14(11):1390–1399, Jun 2000.

M. G. Manfredi, J. A. Ecsedy, K. A. Meetze, S. K. Balani, O. Burenkova, W. Chen, K. M. Galvin, K. M. Hoar, J. J. Huck, P. J. LeRoy, E. T. Ray, T. B. Sells, B. Stringer, S. G. Stroud, T. J. Vos, G. S. Weatherhead, D. R. Wysong, M. Zhang, J. B. Bolen, and C. F. Claiborne. Antitumor activity of MLN8054, an orally active small-molecule inhibitor of Aurora A kinase. *Proc. Natl. Acad. Sci. U.S.A.*, 104(10):4106–4111, Mar 2007.

C. F. Manohar, M. L. Short, A. Nguyen, N. N. Nguyen, D. Chagnovich, Q. Yang, and S. L. Cohn. HuD, a neuronal-specific RNA-binding protein, increases the in vivo stability of MYCN RNA. *J. Biol. Chem.*, 277(3):1967–1973, Jan 2002.

F. Martinato, M. Cesaroni, B. Amati, and E. Guccione. Analysis of Myc-induced histone modifications on target chromatin. *PLoS ONE*, 3(11):e3650, 2008.

H. Matsushima and E. Bogenmann. Expression of trkA cDNA in neuroblastomas mediates differentiation in vitro and in vivo. *Mol. Cell. Biol.*, 13(12):7447–7456, Dec 1993.

K. K. Matthay, C. P. Reynolds, R. C. Seeger, H. Shimada, E. S. Adkins, D. Haas-Kogan, R. B. Gerbing, W. B. London, and J. G. Villablanca. Long-term results for children with high-risk neuroblastoma treated on a randomized trial of myeloablative therapy followed by 13-cis-retinoic acid: a children's oncology group study. *J. Clin. Oncol.*, 27(7):1007–1013, Mar 2009.

S. B. McMahon, H. A. Van Buskirk, K. A. Dugan, T. D. Copeland, and M. D. Cole. The novel ATM-related protein TRRAP is an essential cofactor for the c-Myc and E2F oncoproteins. *Cell*, 94(3):363–374, Aug 1998.

S. B. McMahon, M. A. Wood, and M. D. Cole. The essential cofactor TRRAP recruits the histone acetyltransferase hGCN5 to c-Myc. *Mol. Cell. Biol.*, 20(2):556–562, Jan 2000.

Z. Moqtaderi and K. Struhl. Genome-wide occupancy profile of the RNA polymerase III machinery in Saccharomyces cerevisiae reveals loci with incomplete transcription complexes. *Mol. Cell. Biol.*, 24(10):4118–4127, May 2004.

Z. Moqtaderi, J. Wang, D. Raha, R. J. White, M. Snyder, Z. Weng, and K. Struhl. Genomic binding profiles of functionally distinct RNA polymerase III transcription complexes in human cells. *Nat. Struct. Mol. Biol.*, 17(5):635–640, May 2010.

Z. Mou, A. E. Kenny, and M. J. Curcio. Hos2 and Set3 promote integration of Ty1 retrotransposons at tRNA genes in Saccharomyces cerevisiae. *Genetics*, 172(4):2157–2167, Apr 2006.

S. Mueller and K. K. Matthay. Neuroblastoma: biology and staging. *Curr Oncol Rep*, 11 (6):431–438, Nov 2009.

K. Mullis, F. Faloona, S. Scharf, R. Saiki, G. Horn, and H. Erlich. Specific enzymatic amplification of DNA in vitro: the polymerase chain reaction. *Cold Spring Harb. Symp. Quant. Biol.*, 51 Pt 1:263–273, 1986.

S. K. Nair and S. K. Burley. X-ray structures of Myc-Max and Mad-Max recognizing DNA. Molecular bases of regulation by proto-oncogenic transcription factors. *Cell*, 112(2):193–205, Jan 2003.

M. Nakagawa and S. Yamanaka. Reprogramming of somatic cells to pluripotency. *Adv. Exp. Med. Biol.*, 695:215–224, 2010.

A. Nakagawara and G. M. Brodeur. Role of neurotrophins and their receptors in human neuroblastomas: a primary culture study. *Eur. J. Cancer*, 33(12):2050–2053, Oct 1997.

A. Nakagawara, M. Arima-Nakagawara, N. J. Scavarda, C. G. Azar, A. B. Cantor, and G. M. Brodeur. Association between high levels of expression of the TRK gene and favorable outcome in human neuroblastoma. *N. Engl. J. Med.*, 328(12):847–854, Mar 1993.

K. Nara, T. Kusafuka, A. Yoneda, T. Oue, S. Sangkhathat, and M. Fukuzawa. Silencing of MYCN by RNA interference induces growth inhibition, apoptotic activity and cell differentiation in a neuroblastoma cell line with MYCN amplification. *Int. J. Oncol.*, 30 (5):1189–1196, May 2007.

K. Nasmyth and C. H. Haering. Cohesin: its roles and mechanisms. *Annu. Rev. Genet.*, 43:525–558, 2009.

M. M. Nau, B. J. Brooks, J. Battey, E. Sausville, A. F. Gazdar, I. R. Kirsch, O. W. McBride, V. Bertness, G. F. Hollis, and J. D. Minna. L-myc, a new myc-related gene amplified and expressed in human small cell lung cancer. *Nature*, 318(6041):69–73, 1985.

H. H. Ng, F. Robert, R. A. Young, and K. Struhl. Genome-wide location and regulated recruitment of the RSC nucleosome-remodeling complex. *Genes Dev.*, 16(7):806–819, Apr 2002.

J. W. Nicol, G. A. Helt, S. G. Blanchard, A. Raja, and A. E. Loraine. The Integrated Genome Browser: free software for distribution and exploration of genome-scale datasets. *Bioinformatics*, 25(20):2730–2731, Oct 2009.

Z. Nie, G. Hu, G. Wei, K. Cui, A. Yamane, W. Resch, R. Wang, D. R. Green, L. Tessarollo, R. Casellas, K. Zhao, and D. Levens. c-Myc is a universal amplifier of expressed genes in lymphocytes and embryonic stem cells. *Cell*, 151(1):68–79, Sep 2012.

S. M. Nijman, M. P. Luna-Vargas, A. Velds, T. R. Brummelkamp, A. M. Dirac, T. K. Sixma, and R. Bernards. A genomic and functional inventory of deubiquitinating enzymes. *Cell*, 123(5):773–786, Dec 2005.

A. S. Nikonova, I. Astsaturov, I. G. Serebriiskii, R. L. Dunbrack, and E. A. Golemis. Aurora A kinase (AURKA) in normal and pathological cell division. *Cell. Mol. Life Sci.*, 70(4): 661–687, Feb 2013.

H. Niu, M. Manfredi, and J. A. Ecsedy. Scientific Rationale Supporting the Clinical Development Strategy for the Investigational Aurora A Kinase Inhibitor Alisertib in Cancer. *Front Oncol*, 5:189, 2015.

K. Noguchi, C. Kitanaka, H. Yamana, A. Kokubu, T. Mochizuki, and Y. Kuchino. Regulation of c-Myc through phosphorylation at Ser-62 and Ser-71 by c-Jun N-terminal kinase. *J. Biol. Chem.*, 274(46):32580–32587, Nov 1999.

K. Noma, H. P. Cam, R. J. Maraia, and S. I. Grewal. A role for TFIIIC transcription factor complex in genome organization. *Cell*, 125(5):859–872, Jun 2006.

A. J. Oler, R. K. Alla, D. N. Roberts, A. Wong, P. C. Hollenhorst, K. J. Chandler, P. A. Cassiday, C. A. Nelson, C. H. Hagedorn, B. J. Graves, and B. R. Cairns. Human RNA polymerase III transcriptomes and relationships to Pol II promoter chromatin and enhancer-binding factors. *Nat. Struct. Mol. Biol.*, 17(5):620–628, May 2010.

C. T. Ong and V. G. Corces. CTCF: an architectural protein bridging genome topology and function. *Nat. Rev. Genet.*, 15(4):234–246, Apr 2014.

T. Otto, S. Horn, M. Brockmann, U. Eilers, L. Schuttrumpf, N. Popov, A. M. Kenney, J. H. Schulte, R. Beijersbergen, H. Christiansen, B. Berwanger, and M. Eilers. Stabilization of N-Myc is a critical function of Aurora A in human neuroblastoma. *Cancer Cell*, 15(1): 67–78, Jan 2009.

V. Parelho, S. Hadjur, M. Spivakov, M. Leleu, S. Sauer, H. C. Gregson, A. Jarmuz, C. Canzonetta, Z. Webster, T. Nesterova, B. S. Cobb, K. Yokomori, N. Dillon, L. Aragon, A. G. Fisher, and M. Merkenschlager. Cohesins functionally associate with CTCF on mammalian chromosome arms. *Cell*, 132(3):422–433, Feb 2008.

F. Parisi, S. Riccardo, M. Daniel, M. Saqcena, N. Kundu, A. Pession, D. Grifoni, H. Stocker, E. Tabak, and P. Bellosta. Drosophila insulin and target of rapamycin (TOR) pathways regulate GSK3 beta activity to control Myc stability and determine Myc expression in vivo. *BMC Biol.*, 9:65, 2011.

A. Pession and R. Tonelli. The MYCN oncogene as a specific and selective drug target for peripheral and central nervous system tumors. *Curr Cancer Drug Targets*, 5(4):273–283, Jun 2005.

K. Peukert, P. Staller, A. Schneider, G. Carmichael, F. Hanel, and M. Eilers. An alternative pathway for gene regulation by Myc. *EMBO J.*, 16(18):5672–5686, Sep 1997.

C. M. Pickart and M. J. Eddins. Ubiquitin: structures, functions, mechanisms. *Biochim. Biophys. Acta*, 1695(1-3):55–72, Nov 2004.

G. Poortinga, M. Wall, E. Sanij, K. Siwicki, J. Ellul, D. Brown, T. P. Holloway, R. D. Hannan, and G. A. McArthur. c-MYC coordinately regulates ribosomal gene chromatin

remodeling and Pol I availability during granulocyte differentiation. *Nucleic Acids Res.*, 39(8):3267–3281, Apr 2011.

N. Popov, M. Wanzel, M. Madiredjo, D. Zhang, R. Beijersbergen, R. Bernards, R. Moll, S. J. Elledge, and M. Eilers. The ubiquitin-specific protease USP28 is required for MYC stability. *Nat. Cell Biol.*, 9(7):765–774, Jul 2007.

N. Popov, C. Schulein, L. A. Jaenicke, and M. Eilers. Ubiquitylation of the amino terminus of Myc by SCF(β-TrCP) antagonizes SCF(Fbw7)-mediated turnover. *Nat. Cell Biol.*, 12 (10):973–981, Oct 2010.

E. N. Pugacheva, S. A. Jablonski, T. R. Hartman, E. P. Henske, and E. A. Golemis. HEF1-dependent Aurora A activation induces disassembly of the primary cilium. *Cell*, 129(7): 1351–1363, Jun 2007.

B. J. Pulverer, C. Fisher, K. Vousden, T. Littlewood, G. Evan, and J. R. Woodgett. Site-specific modulation of c-Myc cotransformation by residues phosphorylated in vivo. *Oncogene*, 9(1):59–70, Jan 1994.

H. Qiu, C. Hu, N. A. Gaur, and A. G. Hinnebusch. Pol II CTD kinases Bur1 and Kin28 promote Spt5 CTR-independent recruitment of Paf1 complex. *EMBO J.*, 31(16):3494–3505, Aug 2012.

V. Quesada, A. Diaz-Perales, A. Gutierrez-Fernandez, C. Garabaya, S. Cal, and C. Lopez-Otin. Cloning and enzymatic analysis of 22 novel human ubiquitin-specific proteases. *Biochem. Biophys. Res. Commun.*, 314(1):54–62, Jan 2004.

A. R. Quinlan and I. M. Hall. BEDTools: a flexible suite of utilities for comparing genomic features. *Bioinformatics*, 26(6):841–842, Mar 2010.

J. R. Raab and R. T. Kamakaka. Insulators and promoters: closer than we think. *Nat. Rev. Genet.*, 11(6):439–446, Jun 2010.

J. R. Raab, J. Chiu, J. Zhu, S. Katzman, S. Kurukuti, P. A. Wade, D. Haussler, and R. T. Kamakaka. Human tRNA genes function as chromatin insulators. *EMBO J.*, 31 (2):330–350, Jan 2012.

D. Raha, Z. Wang, Z. Moqtaderi, L. Wu, G. Zhong, M. Gerstein, K. Struhl, and M. Snyder. Close association of RNA polymerase II and many transcription factors with Pol III genes. *Proc. Natl. Acad. Sci. U.S.A.*, 107(8):3639–3644, Feb 2010.

P. B. Rahl and R. A. Young. MYC and transcription elongation. *Cold Spring Harb Perspect Med*, 4(1):a020990, Jan 2014.

P. B. Rahl, C. Y. Lin, A. C. Seila, R. A. Flynn, S. McCuine, C. B. Burge, P. A. Sharp, and R. A. Young. c-Myc regulates transcriptional pause release. *Cell*, 141(3):432–445, Apr 2010.

D. N. Roberts, A. J. Stewart, J. T. Huff, and B. R. Cairns. The RNA polymerase III transcriptome revealed by genome-wide localization and activity-occupancy relationships. *Proc. Natl. Acad. Sci. U.S.A.*, 100(25):14695–14700, Dec 2003.

A. M. Roy-Engel. LINEs, SINEs and other retroelements: do birds of a feather flock together? *Front Biosci (Landmark Ed)*, 17:1345–1361, 2012.

S. Rozen and H. Skaletsky. Primer3 on the WWW for general users and for biologist programmers. *Methods Mol. Biol.*, 132:365–386, 2000.

E. D. Rubio, D. J. Reiss, P. L. Welcsh, C. M. Disteche, G. N. Filippova, N. S. Baliga, R. Aebersold, J. A. Ranish, and A. Krumm. CTCF physically links cohesin to chromatin. *Proc. Natl. Acad. Sci. U.S.A.*, 105(24):8309–8314, Jun 2008.

J. Russell and J. C. Zomerdijk. The RNA polymerase I transcription machinery. *Biochem. Soc. Symp.*, (73):203–216, 2006.

A. Sabo, T. R. Kress, M. Pelizzola, S. de Pretis, M. M. Gorski, A. Tesi, M. J. Morelli, P. Bora, M. Doni, A. Verrecchia, C. Tonelli, G. Faga, V. Bianchi, A. Ronchi, D. Low, H. Muller, E. Guccione, S. Campaner, and B. Amati. Selective transcriptional regulation by Myc in cellular growth control and lymphomagenesis. *Nature*, 511(7510):488–492, Jul 2014.

J. D. Sander and J. K. Joung. CRISPR-Cas systems for editing, regulating and targeting genomes. *Nat. Biotechnol.*, 32(4):347–355, Apr 2014.

K. Sasai, J. M. Parant, M. E. Brandt, J. Carter, H. P. Adams, S. A. Stass, A. M. Killary, H. Katayama, and S. Sen. Targeted disruption of Aurora A causes abnormal mitotic spindle assembly, chromosome misalignment and embryonic lethality. *Oncogene*, 27(29): 4122–4127, Jul 2008.

C. A. Schaaf, H. Kwak, A. Koenig, Z. Misulovin, D. W. Gohara, A. Watson, Y. Zhou, J. T. Lis, and D. Dorsett. Genome-wide control of RNA polymerase II activity by cohesin. *PLoS Genet.*, 9(3):e1003382, Mar 2013.

W. F. Scherer, J. T. Syverton, and G. O. Gey. Studies on the propagation in vitro of poliomyelitis viruses. IV. Viral multiplication in a stable strain of human malignant epithelial cells (strain HeLa) derived from an epidermoid carcinoma of the cervix. *J. Exp. Med.*, 97 (5):695–710, May 1953.

I. Schlosser, M. Holzel, M. Murnseer, H. Burtscher, U. H. Weidle, and D. Eick. A role for c-Myc in the regulation of ribosomal RNA processing. *Nucleic Acids Res.*, 31(21): 6148–6156, Nov 2003.

L. Schramm and N. Hernandez. Recruitment of RNA polymerase III to its target promoters. *Genes Dev.*, 16(20):2593–2620, Oct 2002.

H. Schroter, G. Maier, H. Ponstingl, and A. Nordheim. DNA intercalators induce specific release of HMG 14, HMG 17 and other DNA-binding proteins from chicken erythrocyte chromatin. *EMBO J.*, 4(13B):3867–3872, Dec 1985.

C. Schuelein-Voelk, E. Wolf, J. Zhu, W. Xu, L. Taranets, A. Hellmann, L. A. Jaenicke, M. E. Diefenbacher, A. Behrens, M. Eilers, and N. Popov. Dual regulation of Fbw7 function and oncogenic transformation by Usp28. *Cell Rep*, 9(3):1099–1109, Nov 2014.

M. Schwab, K. Alitalo, K. H. Klempnauer, H. E. Varmus, J. M. Bishop, F. Gilbert, G. Brodeur, M. Goldstein, and J. Trent. Amplified DNA with limited homology to myc cellular oncogene is shared by human neuroblastoma cell lines and a neuroblastoma tumour. *Nature*, 305(5931):245–248, 1983.

R. C. Seeger, G. M. Brodeur, H. Sather, A. Dalton, S. E. Siegel, K. Y. Wong, and D. Hammond. Association of multiple copies of the N-myc oncogene with rapid progression of neuroblastomas. *N. Engl. J. Med.*, 313(18):1111–1116, Oct 1985.

V. C. Seitan, A. J. Faure, Y. Zhan, R. P. McCord, B. R. Lajoie, E. Ing-Simmons, B. Lenhard, L. Giorgetti, E. Heard, A. G. Fisher, P. Flicek, J. Dekker, and M. Merkenschlager. Cohesin-based chromatin interactions enable regulated gene expression within preexisting architectural compartments. *Genome Res.*, 23(12):2066–2077, Dec 2013.

R. Serra, R. W. Pelton, and H. L. Moses. TGF beta 1 inhibits branching morphogenesis and N-myc expression in lung bud organ cultures. *Development*, 120(8):2153–2161, Aug 1994.

J. Shandilya and S. G. Roberts. The transcription cycle in eukaryotes: from productive initiation to RNA polymerase II recycling. *Biochim. Biophys. Acta*, 1819(5):391–400, May 2012.

D. Sheiness, L. Fanshier, and J. M. Bishop. Identification of nucleotide sequences which may encode the oncogenic capacity of avian retrovirus MC29. *J. Virol.*, 28(2):600–610, Nov 1978.

T. Shimomura, S. Hasako, Y. Nakatsuru, T. Mita, K. Ichikawa, T. Kodera, T. Sakai, T. Nambu, M. Miyamoto, I. Takahashi, S. Miki, N. Kawanishi, M. Ohkubo, H. Kotani, and Y. Iwasawa. MK-5108, a highly selective Aurora-A kinase inhibitor, shows antitumor activity alone and in combination with docetaxel. *Mol. Cancer Ther.*, 9(1):157–166, Jan 2010.

C. N. Shiue, R. G. Berkson, and A. P. Wright. c-Myc induces changes in higher order rDNA structure on stimulation of quiescent cells. *Oncogene*, 28(16):1833–1842, Apr 2009.

T. A. Simms, S. L. Dugas, J. C. Gremillion, M. E. Ibos, M. N. Dandurand, T. T. Toliver, D. J. Edwards, and D. Donze. TFIIIC binding sites function as both heterochromatin

barriers and chromatin insulators in Saccharomyces cerevisiae. *Eukaryotic Cell*, 7(12): 2078–2086, Dec 2008.

R. J. Sims, R. Belotserkovskaya, and D. Reinberg. Elongation by RNA polymerase II: the short and long of it. *Genes Dev.*, 18(20):2437–2468, Oct 2004.

S. Singh, A. S. Narang, and R. I. Mahato. Subcellular fate and off-target effects of siRNA, shRNA, and miRNA. *Pharm. Res.*, 28(12):2996–3015, Dec 2011.

S. K. Sjostrom, G. Finn, W. C. Hahn, D. H. Rowitch, and A. M. Kenney. The Cdk1 complex plays a prime role in regulating N-myc phosphorylation and turnover in neural precursors. *Dev. Cell*, 9(3):327–338, Sep 2005.

S. Sofueva, E. Yaffe, W. C. Chan, D. Georgopoulou, M. Vietri Rudan, H. Mira-Bontenbal, S. M. Pollard, G. P. Schroth, A. Tanay, and S. Hadjur. Cohesin-mediated interactions organize chromosomal domain architecture. *EMBO J.*, 32(24):3119–3129, Dec 2013.

V. Spataro, T. Toda, R. Craig, M. Seeger, W. Dubiel, A. L. Harris, and C. Norbury. Resistance to diverse drugs and ultraviolet light conferred by overexpression of a novel human 26 S proteasome subunit. *J. Biol. Chem.*, 272(48):30470–30475, Nov 1997.

P. Staller, K. Peukert, A. Kiermaier, J. Seoane, J. Lukas, H. Karsunky, T. Moroy, J. Bartek, J. Massague, F. Hanel, and M. Eilers. Repression of p15INK4b expression by Myc through association with Miz-1. *Nat. Cell Biol.*, 3(4):392–399, Apr 2001.

D. Steiger, M. Furrer, D. Schwinkendorf, and P. Gallant. Max-independent functions of Myc in Drosophila melanogaster. *Nat. Genet.*, 40(9):1084–1091, Sep 2008.

V. Strieder and W. Lutz. E2F proteins regulate MYCN expression in neuroblastomas. *J. Biol. Chem.*, 278(5):2983–2989, Jan 2003.

A. Subramanian, P. Tamayo, V. K. Mootha, S. Mukherjee, B. L. Ebert, M. A. Gillette, A. Paulovich, S. L. Pomeroy, T. R. Golub, E. S. Lander, and J. P. Mesirov. Gene set enrichment analysis: a knowledge-based approach for interpreting genome-wide expression profiles. *Proc. Natl. Acad. Sci. U.S.A.*, 102(43):15545–15550, Oct 2005.

W. P. Tansey. Mammalian MYC Proteins and Cancer. *New Journal of Science*, 2014:27, Feb 2014.

R. Taub, I. Kirsch, C. Morton, G. Lenoir, D. Swan, S. Tronick, S. Aaronson, and P. Leder. Translocation of the c-myc gene into the immunoglobulin heavy chain locus in human Burkitt lymphoma and murine plasmacytoma cells. *Proc. Natl. Acad. Sci. U.S.A.*, 79 (24):7837–7841, Dec 1982.

A. Tedeschi, G. Wutz, S. Huet, M. Jaritz, A. Wuensche, E. Schirghuber, I. F. Davidson, W. Tang, D. A. Cisneros, V. Bhaskara, T. Nishiyama, A. Vaziri, A. Wutz, J. Ellenberg,

and J. M. Peters. Wapl is an essential regulator of chromatin structure and chromosome segregation. *Nature*, 501(7468):564–568, Sep 2013.

S. Terry and H. Beltran. The many faces of neuroendocrine differentiation in prostate cancer progression. *Front Oncol*, 4:60, 2014.

C. J. Thiele, C. P. Reynolds, and M. A. Israel. Decreased expression of N-myc precedes retinoic acid-induced morphological differentiation of human neuroblastoma. *Nature*, 313 (6001):404–406, 1985.

L. R. Thomas, Q. Wang, B. C. Grieb, J. Phan, A. M. Foshage, Q. Sun, E. T. Olejniczak, T. Clark, S. Dey, S. Lorey, B. Alicie, G. C. Howard, B. Cawthon, K. C. Ess, C. M. Eischen, Z. Zhao, S. W. Fesik, and W. P. Tansey. Interaction with WDR5 promotes target gene recognition and tumorigenesis by MYC. *Mol. Cell*, 58(3):440–452, May 2015.

G. P. Tonini, A. Nakagawara, and F. Berthold. Towards a turning point of neuroblastoma therapy. *Cancer Lett.*, 326(2):128–134, Dec 2012.

L. J. Valentijn, J. Koster, F. Haneveld, R. A. Aissa, P. van Sluis, M. E. Broekmans, J. J. Molenaar, J. van Nes, and R. Versteeg. Functional MYCN signature predicts outcome of neuroblastoma irrespective of MYCN amplification. *Proc. Natl. Acad. Sci. U.S.A.*, 109 (47):19190–19195, Nov 2012.

K. Van Bortle and V. G. Corces. Nuclear organization and genome function. *Annu. Rev. Cell Dev. Biol.*, 28:163–187, 2012.

K. Van Bortle, M. H. Nichols, L. Li, C. T. Ong, N. Takenaka, Z. S. Qin, and V. G. Corces. Insulator function and topological domain border strength scale with architectural protein occupancy. *Genome Biol.*, 15(6):R82, 2014.

R. J. van Leuken, M. P. Luna-Vargas, T. K. Sixma, R. M. Wolthuis, and R. H. Medema. Usp39 is essential for mitotic spindle checkpoint integrity and controls mRNA-levels of aurora B. *Cell Cycle*, 7(17):2710–2719, Sep 2008.

N. V. Varlakhanova, R. F. Cotterman, W. N. deVries, J. Morgan, L. R. Donahue, S. Murray, B. B. Knowles, and P. S. Knoepfler. myc maintains embryonic stem cell pluripotency and self-renewal. *Differentiation*, 80(1):9–19, Jul 2010.

B. Vennstrom, D. Sheiness, J. Zabielski, and J. M. Bishop. Isolation and characterization of c-myc, a cellular homolog of the oncogene (v-myc) of avian myelocytomatosis virus strain 29. *J. Virol.*, 42(3):773–779, Jun 1982.

B. J. Venters, S. Wachi, T. N. Mavrich, B. E. Andersen, P. Jena, A. J. Sinnamon, P. Jain, N. S. Rolleri, C. Jiang, C. Hemeryck-Walsh, and B. F. Pugh. A comprehensive genomic binding map of gene and chromatin regulatory proteins in Saccharomyces. *Mol. Cell*, 41 (4):480–492, Feb 2011.

J. Vervoorts, J. Luscher-Firzlaff, and B. Luscher. The ins and outs of MYC regulation by posttranslational mechanisms. *J. Biol. Chem.*, 281(46):34725–34729, Nov 2006.

M. Vietri Rudan and S. Hadjur. Genetic Tailors: CTCF and Cohesin Shape the Genome During Evolution. *Trends Genet.*, 31(11):651–660, Nov 2015.

R. K. Wada, R. C. Seeger, C. P. Reynolds, T. Alloggiamento, J. M. Yamashiro, C. Ruland, A. C. Black, and J. D. Rosenblatt. Cell type-specific expression and negative regulation by retinoic acid of the human N-myc promoter in neuroblastoma cells. *Oncogene*, 7(4): 711–717, Apr 1992.

C. W. Walker, J. D. Boom, and A. G. Marsh. First non-vertebrate member of the myc gene family is seasonally expressed in an invertebrate testis. *Oncogene*, 7(10):2007–2012, Oct 1992.

S. Walz, F. Lorenzin, J. Morton, K. E. Wiese, B. von Eyss, S. Herold, L. Rycak, H. Dumay-Odelot, S. Karim, M. Bartkuhn, F. Roels, T. Wustefeld, M. Fischer, M. Teichmann, L. Zender, C. L. Wei, O. Sansom, E. Wolf, and M. Eilers. Activation and repression by oncogenic MYC shape tumour-specific gene expression profiles. *Nature*, 511(7510): 483–487, Jul 2014.

M. Wanzel, A. C. Russ, D. Kleine-Kohlbrecher, E. Colombo, P. G. Pelicci, and M. Eilers. A ribosomal protein L23-nucleophosmin circuit coordinates Mizl function with cell growth. *Nat. Cell Biol.*, 10(9):1051–1061, Sep 2008.

V. M. Weake and J. L. Workman. Inducible gene expression: diverse regulatory mechanisms. *Nat. Rev. Genet.*, 11(6):426–437, Jun 2010.

J. S. Wei, Y. K. Song, S. Durinck, Q. R. Chen, A. T. Cheuk, P. Tsang, Q. Zhang, C. J. Thiele, A. Slack, J. Shohet, and J. Khan. The MYCN oncogene is a direct target of miR-34a. *Oncogene*, 27(39):5204–5213, Sep 2008.

M. Welcker, A. Orian, J. Jin, J. E. Grim, J. A. Grim, J. W. Harper, R. N. Eisenman, and B. E. Clurman. The Fbw7 tumor suppressor regulates glycogen synthase kinase 3 phosphorylation-dependent c-Myc protein degradation. *Proc. Natl. Acad. Sci. U.S.A.*, 101(24):9085–9090, Jun 2004.

K. S. Wendt, K. Yoshida, T. Itoh, M. Bando, B. Koch, E. Schirghuber, S. Tsutsumi, G. Nagae, K. Ishihara, T. Mishiro, K. Yahata, F. Imamoto, H. Aburatani, M. Nakao, N. Imamoto, K. Maeshima, K. Shirahige, and J. M. Peters. Cohesin mediates transcriptional insulation by CCCTC-binding factor. *Nature*, 451(7180):796–801, Feb 2008.

R. J. White. RNA polymerases I and III, non-coding RNAs and cancer. *Trends Genet.*, 24 (12):622–629, Dec 2008.

I. M. Willis. RNA polymerase III. Genes, factors and transcriptional specificity. *Eur. J. Biochem.*, 212(1):1–11, Feb 1993.

M. Yada, S. Hatakeyama, T. Kamura, M. Nishiyama, R. Tsunematsu, H. Imaki, N. Ishida, F. Okumura, K. Nakayama, and K. I. Nakayama. Phosphorylation-dependent degradation of c-Myc is mediated by the F-box protein Fbw7. *EMBO J.*, 23(10):2116–2125, May 2004.

T. Yamada, Y. Yamaguchi, N. Inukai, S. Okamoto, T. Mura, and H. Handa. P-TEFb-mediated phosphorylation of hSpt5 C-terminal repeats is critical for processive transcription elongation. *Mol. Cell*, 21(2):227–237, Jan 2006.

T. Ye, A. R. Krebs, M. A. Choukrallah, C. Keime, F. Plewniak, I. Davidson, and L. Tora. seqMINER: an integrated ChIP-seq data interpretation platform. *Nucleic Acids Res.*, 39 (6):e35, Mar 2011.

K. I. Zeller, A. G. Jegga, B. J. Aronow, K. A. O'Donnell, and C. V. Dang. An integrated database of genes responsive to the Myc oncogenic transcription factor: identification of direct genomic targets. *Genome Biol.*, 4(10):R69, 2003.

K. I. Zeller, X. Zhao, C. W. Lee, K. P. Chiu, F. Yao, J. T. Yustein, H. S. Ooi, Y. L. Orlov, A. Shahab, H. C. Yong, Y. Fu, Z. Weng, V. A. Kuznetsov, W. K. Sung, Y. Ruan, C. V. Dang, and C. L. Wei. Global mapping of c-Myc binding sites and target gene networks in human B cells. *Proc. Natl. Acad. Sci. U.S.A.*, 103(47):17834–17839, Nov 2006.

Y. Zhang, T. Liu, C. A. Meyer, J. Eeckhoute, D. S. Johnson, B. E. Bernstein, C. Nusbaum, R. M. Myers, M. Brown, W. Li, and X. S. Liu. Model-based analysis of ChIP-Seq (MACS). *Genome Biol.*, 9(9):R137, 2008.

X. Zhao, J. I. Heng, D. Guardavaccaro, R. Jiang, M. Pagano, F. Guillemot, A. Iavarone, and A. Lasorella. The HECT-domain ubiquitin ligase Huwe1 controls neural differentiation and proliferation by destabilizing the N-Myc oncoprotein. *Nat. Cell Biol.*, 10(6):643–653, Jun 2008.

K. A. Zimmerman, G. D. Yancopoulos, R. G. Collum, R. K. Smith, N. E. Kohl, K. A. Denis, M. M. Nau, O. N. Witte, D. Toran-Allerand, and C. E. Gee. Differential expression of myc family genes during murine development. *Nature*, 319(6056):780–783, 1986.

Appendix A

Lists of proteins identified in N-MYC MS

Shown are rank number, official gene symbol, Molecular Weight (M.W.) and exclusive unique peptide counts in empty control (-), N-MYC mut (mut) and N-MYC wt (wt) sample. Lists are ranked according to the number of exclusive unique peptides, first in N-MYC wt sample and second in N-MYC mut sample.

A.1 List of 224 N-MYC interacting proteins

rank	gene symbol	M.W.	-	mut	wt
1	TRRAP	438 kDa	6	167	144
2	EP400	340 kDa	0	69	69
3	GTFIIIC1	239 kDa	4	27	52
4	UBR4	576 kDa	9	7	41
5	RAD50	155 kDa	10	13	30
6	SMCHD1	226 kDa	6	23	30
7	POLR2B	133 kDa	8	24	27
8	RANBP2	358 kDa	5	7	27
9	RANBP2	358 kDa	4	6	26
10	NUP153	154 kDa	7	15	23
11	ASPM	410 kDa	0	3	23
12	PARP1	113 kDa	6	25	22
13	NUP93	93 kDa	7	17	21
14	HCFC1	209 kDa	4	11	21
15	UTP20	318 kDa	2	5	21
16	OPA1	116 kDa	6	8	19
17	U2SURP	118 kDa	5	12	19
18	USP7	126 kDa	4	21	19
19	RBM14	69 kDa	4	4	19
20	GTFIIIC5	60 kDa	0	7	19
21	MYCN	50 kDa	0	15	19

rank	gene symbol	M.W.	-	mut	wt
22	DMAP1	53 kDa	0	11	19
23	NUP205	228 kDa	6	12	18
24	PBRM1	187 kDa	1	6	18
25	BPTF	325 kDa	0	11	18
26	MYCBP2	510 kDa	0	0	18
27	SLC25A13	74 kDa	4	9	17
28	CEBPZ	121 kDa	4	13	17
29	GEMIN5	169 kDa	3	8	17
30	GTFIIIC3	101 kDa	1	12	17
31	MYCN	50 kDa	0	15	17
32	NUP133	129 kDa	5	10	16
33	BIRC6	530 kDa	3	1	16
34	DDX46	117 kDa	2	5	16
35	ANLN	124 kDa	1	1	16
36	TOP2A	179 kDa	0	6	15
37	DDX23	96 kDa	4	3	14
38	TOP2B	183 kDa	1	11	14
39	TPO1	91 kDa	3	7	13
40	SRRM2	300 kDa	3	8	13
41	IQGAP3	179 kDa	1	13	13
42	PLK1	68 kDa	2	9	13
43	SRPR	70 kDa	2	8	13
44	CTR9	134 kDa	1	4	13
45	HERC2	527 kDa	0	0	13
46	NOL6	127 kDa	6	18	12
47	SQSTM1	48 kDa	4	9	12
48	TCOF1	152 kDa	4	1	12
49	ACIN1	147 kDa	3	4	12

rank	gene symbol	M.W.	-	mut	wt
50	ACACA	260 kDa	3	0	12
51	GNL2	84 kDa	3	3	12
52	LRPAP1	41 kDa	3	4	12
53	RAI14	107 kDa	0	45	12
54	DMAP1	53 kDa	0	9	12
55	BAZ1A	179 kDa	0	6	12
56	RFC1	128 kDa	0	6	12
57	UBR2	171 kDa	0	5	12
58	ATXN2L	110 kDa	3	6	11
59	SRSF9	26 kDa	3	4	11
60	ADNP	124 kDa	2	3	11
61	GTFIIIC2	101 kDa	0	2	11
62	HK2	99 kDa	3	8	10
63	WDHD1	126 kDa	3	6	10
64	UTP14A	82 kDa	3	6	10
65	PTPRF	212 kDa	2	4	10
66	BCR	143 kDa	0	9	10
67	MKI67	359 kDa	0	2	10
68	SACS	521 kDa	0	0	10
69	SAFB2	107 kDa	3	4	9
70	MTA1	79 kDa	3	5	9
71	LRRFIP2	82 kDa	3	4	9
72	MAPB1	271 kDa	3	15	9
73	MAPB1	271 kDa	3	15	9
74	GFPT1	77 kDa	3	4	9
75	EIF3M	43 kDa	3	5	9
76	LSG1	75 kDa	2	6	9
77	DDX56	62 kDa	2	2	9

rank	gene symbol	M.W.	-	mut	wt
78	CTBP2	56 kDa	1	5	9
79	HECTD1	289 kDa	1	1	9
80	ESF1	99 kDa	1	3	9
81	MCMBP	73 kDa	1	2	9
82	ELP3	61 kDa	1	2	9
83	POLR3A	154 kDa	0	9	9
84	SUPT5H	120 kDa	0	4	9
85	CHD7	336 kDa	0	1	9
86	CDC73	61 kDa	0	5	9
87	GNL3L	66 kDa	0	3	9
88	MYO9B	229 kDa	0	0	9
89	HDAC1	55 kDa	2	1	8
90	WDR43	75 kDa	2	5	8
91	RAB3GAP2	156 kDa	2	9	8
92	THOC1	76 kDa	2	2	8
93	DIMT1	35 kDa	2	4	8
94	POLA1	166 kDa	2	3	8
95	AP3B1	121 kDa	2	3	8
96	P4HA1	61 kDa	2	2	8
97	NUP85	75 kDa	2	6	8
98	PTPRF	212 kDa	2	4	8
99	NOL10	75 kDa	2	6	8
100	PAWR	37 kDa	1	4	8
101	WDR33	146 kDa	1	5	8
102	MAX	18 kDa	0	7	8
103	USF2	36 kDa	0	3	8
104	EPC1	91 kDa	0	3	8
105	TBL1XR1	41 kDa	2	5	7

rank	gene symbol	M.W.	-	mut	wt
106	PPIH	19 kDa	2	2	7
107	AXL	97 kDa	2	5	7
108	TBC1D4	140 kDa	2	4	7
109	SDAD1	80 kDa	2	2	7
110	SEC23IP	90 kDa	2	4	7
111	SUPT6H	199 kDa	2	3	7
112	CALU	38 kDa	1	2	7
113	TBL2	46 kDa	1	3	7
114	PHF6	41 kDa	1	2	7
115	FAR1	59 kDa	1	4	7
116	WDR75	95 kDa	1	3	7
117	TRIP12	226 kDa	1	4	7
118	AKAP8L	72 kDa	1	2	7
119	MRPS26	24 kDa	0	2	7
120	POGZ	154 kDa	0	6	7
121	NUP188	182 kDa	0	6	7
122	KIF14	186 kDa	0	5	7
123	UNC84A	108 kDa	0	5	7
124	PAF1	60 kDa	0	2	7
125	BRAT1	88 kDa	0	0	7
126	SREBF1	115 kDa	0	0	7
127	METAP2	53 kDa	0	0	7
128	THOC2	183 kDa	0	6	6
129	THOC2	183 kDa	0	0	6
130	SON	248 kDa	3	10	6
131	EPB41L2	42 kDa	3	14	6
132	IKBIP	43 kDa	2	3	6
133	RAB8A	24 kDa	1	1	6

rank	gene symbol	M.W.	-	mut	wt
134	ERLIN2	38 kDa	1	0	6
135	DDX41	70 kDa	2	3	6
136	ME2	65 kDa	2	5	6
137	TRMT1	69 kDa	2	1	6
138	MRPL17	20 kDa	2	2	6
139	CDC42BPB	194 kDa	2	8	6
140	AATF	63 kDa	2	6	6
141	CBX3	21 kDa	2	4	6
142	ZYX	52 kDa	2	5	6
143	XPOT	110 kDa	2	2	6
144	CCDC86	40 kDa	2	3	6
145	PUS1	42 kDa	2	2	6
146	NOC4L	58 kDa	2	0	6
147	POR	77 kDa	2	0	6
148	BRIX1	41 kDa	1	5	6
149	CHERP	104 kDa	1	4	6
150	COPS2	52 kDa	1	1	6
151	TXN	9 kDa	1	1	6
152	FUSIP1	21 kDa	1	1	6
153	CHORDC1	35 kDa	1	1	6
154	EIF3J	29 kDa	1	0	6
155	AP3M1	47 kDa	1	2	6
156	SMARCE1	39 kDa	1	1	6
157	NUP214	153 kDa	1	0	6
158	DKFZP586J0619	266 kDa	1	2	6
159	YME1L1	76 kDa	1	0	6
160	SMSC5	129 kDa	1	3	6
161	PDLIM5	64 kDa	0	5	6

rank	gene symbol	M.W.	-	mut	wt
162	MBTD1	71 kDa	0	3	6
163	RIF1	272 kDa	0	1	6
164	MED14	161 kDa	0	2	6
165	SAMD1	56 kDa	0	2	6
166	EDC4	152 kDa	0	3	6
167	CHAF1B	61 kDa	0	1	6
168	NOM1	96 kDa	0	2	6
169	USP19	150 kDa	0	1	6
170	WHSC1	152 kDa	0	1	6
171	PCM1	228 kDa	0	0	6
172	ZNF384	54 kDa	0	0	6
173	NBAS	255 kDa	0	0	6
174	SAP18	18 kDa	1	3	5
175	CTBP2	56 kDa	1	2	5
176	MRPS28	21 kDa	1	1	5
177	COX5B	14 kDa	1	1	5
178	WDR4	45 kDa	1	1	5
179	HSPBP1	39 kDa	1	2	5
180	DDX20	92 kDa	1	1	5
181	RPF2	36 kDa	1	1	5
182	STMN1	17 kDa	1	0	5
183	MRPS25	20 kDa	1	1	5
184	DPM1	30 kDa	1	2	5
185	MTHFD2	38 kDa	1	5	5
186	QKI	37 kDa	1	3	5
187	RCL1	41 kDa	1	1	5
188	AUP1	46 kDa	1	3	5
189	TWISTNB	37 kDa	1	0	5

rank	gene symbol	M.W.	-	mut	wt
190	DDX51	72 kDa	1	3	5
191	ZCCHC8	51 kDa	1	1	5
192	ANAPC1	217 kDa	1	1	5
193	TRMT2A	71 kDa	1	0	5
194	TOE1	57 kDa	1	2	5
195	DHX57	156 kDa	1	1	5
196	CD2AP	71 kDa	1	0	5
197	NOA1	78 kDa	1	0	5
198	LRRC40	68 kDa	1	0	5
199	DDX10	101 kDa	0	0	5
200	UTP15	58 kDa	0	2	5
201	IGF2R	274 kDa	0	3	5
202	YEATS4	27 kDa	0	4	5
203	RRP15	31 kDa	0	2	5
204	GALNT7	75 kDa	0	1	5
205	SDF4	42 kDa	0	0	5
206	FAM208A	171 kDa	0	2	5
207	NCAPG2	102 kDa	0	0	5
208	FIP1L1	66 kDa	0	0	5
209	CD3EAP	55 kDa	0	0	5
210	DNAJB6	29 kDa	0	5	4
211	LTN1	201 kDa	0	8	4
212	NCAPD3	169 kDa	0	7	4
213	MRPL44	38 kDa	2	7	3
214	JUP	82 kDa	2	9	0
215	IKBKAP	150 kDa	1	8	3
216	DSP	332 kDa	0	8	0
217	PELO	43 kDa	1	6	3

rank	gene symbol	M.W.	-	mut	wt
218	UFL1	90 kDa	2	6	2
219	PICALM	70 kDa	2	6	1
220	THOC2	183 kDa	0	6	0
221	DIAPH3	129 kDa	0	5	3
222	LAMC1	178 kDa	0	5	3
223	ASCC3	251 kDa	1	5	2
224	BRD8	95 kDa	0	5	2

A.2 "Top 82-List" of N-MYC interacting proteins

rank	gene symbol	M.W.	-	mut	wt
1	TRRAP	438 kDa	6	167	144
2	EP400	340 kDa	0	69	69
3	GTFIIIC1	239 kDa	4	27	52
4	UBR4	576 kDa	9	7	41
5	SMCHD1	226 kDa	6	23	30
6	RANBP2	358 kDa	4	6	26
7	ASPM	410 kDa	0	3	23
8	PARP1	113 kDa	6	25	22
9	HCFC1	209 kDa	4	11	21
10	UTP20	318 kDa	2	5	21
11	USP7	126 kDa	4	21	19
12	RBM14	69 kDa	4	4	19
13	GTFIIIC5	60 kDa	0	7	19
14	PBRM1	187 kDa	1	6	18
15	BPTF	325 kDa	0	11	18
16	MYCBP2	510 kDa	0	0	18
17	SLC25A13	74 kDa	4	9	17
18	CEBPZ	121 kDa	4	13	17
19	GEMIN5	169 kDa	3	8	17
20	GTFIIIC3	101 kDa	1	12	17
21	MYCN	50 kDa	0	15	17
22	BIRC6	530 kDa	3	1	16
23	DDX46	117 kDa	2	5	16
24	ANLN	124 kDa	1	1	16
25	TOP2A	179 kDa	0	6	15
26	TOP2B	183 kDa	1	11	14

rank	gene symbol	M.W.	-	mut	wt
27	TOP1	91 kDa	3	7	13
28	SRRM2	300 kDa	3	8	13
29	IQGAP3	179 kDa	1	13	13
30	PLK1	68 kDa	2	9	13
31	SRPR	70 kDa	2	8	13
32	CTR9	134 kDa	1	4	13
33	HERC2	527 kDa	0	0	13
34	ACIN1	147 kDa	3	4	12
35	ACACA	260 kDa	3	0	12
36	GNL2	84 kDa	3	3	12
37	LRPAP1	41 kDa	3	4	12
38	RAI14	107 kDa	0	45	12
39	DMAP1	53 kDa	0	9	12
40	BAZ1A	179 kDa	0	6	12
41	RFC1	128 kDa	0	6	12
42	UBR2	171 kDa	0	5	12
43	ADNP	124 kDa	2	3	11
44	GTFIIIC2	101 kDa	0	2	11
45	BCR	143 kDa	0	9	10
46	MKI67	359 kDa	0	2	10
47	SACS	521 kDa	0	0	10
48	MAP1B	271 kDa	3	15	9
49	LSG1	75 kDa	2	6	9
50	DDX56	62 kDa	2	2	9
51	HECTD1	289 kDa	1	1	9
52	ESF1	99 kDa	1	3	9
53	MCMBP	73 kDa	1	2	9
54	ELP3	61 kDa	1	2	9

rank	gene symbol	M.W.	-	mut	wt
55	POLR3A	154 kDa	0	9	9
56	SUPT5H	120 kDa	0	4	9
57	CHD7	336 kDa	0	1	9
58	CDC73	61 kDa	0	5	9
59	GNL3L	66 kDa	0	3	9
60	MYO9B	229 kDa	0	0	9
61	HDAC1	55 kDa	2	1	8
62	WDR43	75 kDa	2	5	8
63	RAB3GAP2	156 kDa	2	9	8
64	THOC1	76 kDa	2	2	8
65	DIMT1	35 kDa	2	4	8
66	POLA1	166 kDa	2	3	8
67	AP3B1	121 kDa	2	3	8
68	P4HA1	61 kDa	2	2	8
69	NUP85	75 kDa	2	6	8
70	PTPRF	212 kDa	2	4	8
71	NOL10	75 kDa	2	6	8
72	PAWR	37 kDa	1	4	8
73	WDR33	146 kDa	1	5	8
74	MAX	18 kDa	0	7	8
75	USF2	36 kDa	0	3	8
76	EPC1	91 kDa	0	3	8
77	EPB41L2	42 kDa	3	14	6
78	JUP	82 kDa	2	9	0
79	CDC42BPB	194 kDa	2	8	6
80	LTN1	201 kDa	0	8	4
81	IKBKAP	150 kDa	1	8	3
82	DSP	332 kDa	0	8	0

Appendix B

List of abbreviations

B.1 Prefixes

p Pico- (10^{-12})
n Nano- (10^{-9})
μ Micro- (10^{-6})
m Milli- (10^{-3})
c Centi- (10^{-2})
k Kilo- (10^{3})

B.2 Units

A ampere
Da dalton
g gram
h hour
l liter
m meter
M mol/l
min minute
OD optical density
s second
U unit
v/v volume per volume
w/v weight per volume
°C degree celsius

B.3 Proteins, protein domains and other biomolecules

A alanine
ATP adenosine-triphosphate
aa amino acid
AKT RAC-alpha serine/threonine-protein kinase
bp basepair(s)
C cytosine
cDNA complementary DNA
CDK cyclin-dependent kinase
CTD C-terminal domain
DNA deoxyribonucleic acid
dNTPs deoxyribonucleoside-5'-triphosphate (dATP, dCTG, dGTP, dTTP)

FBXW7 F-box and WD repeat domain containing 7

GFP green fluorescent protein

GST glutathione-S-transferase

GTF general transcription factor

HRP horseradish peroxidase

HUWE1 HECT, UBA and WWE domain containing 1

MB Myc-box

MIZ1 E3 SUMO-protein ligase PIAS2; old name: Msx-interacting zinc finger protein

mRNA messenger RNA

POL RNA polymerase

PP2A protein phosphatase 2A

PSMD14 proteasome 26S subunit, non-ATPase 14

pT58/S62 phosphorylated aa T58/S62

RNA ribonucleic acid

RUVBL1/2 RuvB-like 1/2

S serine

shRNA short hairpin RNA

SINE short interspersed nuclear element

siRNA small interfering RNA

T threonine

TF transcription factor

tRNA transfer RNA

TRRAP transactivation/ transformation-associated protein

TRUSS (TRPC4AP) transient receptor potential cation channel subfamily C member 4 associated protein

UBE2N Ubiquitin-conjugating enzyme E2 N

USP ubiquitin-specific-protease

B.4 Chemicals and solutions

APS ammoniumpersulfate

aqua dest destilled water

H$_2$O water

DMEM Dulbeccos Modified Eagle-Medium

DMSO dimethylsulfoxide

DTT dithiothreitol

EDTA ethylendiamintetraacetate

FBS fetal bovine serum

PBS phosphate-buffered saline

PVDF polyvinylidenfluoride

SCF SKP1-CUL1-F-box containing complex

SDS sodium dodecyl sulfate

TAE Tris-acetate-EDTA

TBS Tris-buffered saline

TBS-T Tris-buffered saline with Tween-20

TE Tris-EDTA-buffer

TEMED N,N,N',N'-tetramethylethylendiamine

Tris Tris-(hydroxymethyl)-aminomethan

TSS transcriptional start site

Ub ubiquitin

B.5 Other abbreviations

CID Collisional-induced Dissociation

ChIP Chromatin immunoprecipitation

Co-IP Co-precipitation of a protein interacting with the precipitated one

ECL enhanced chemoluminescence

E. coli Escherichia coli

FLAG polypeptide protein tag

G1/G2 phase Gap 1/2 phase of the cell cycle

HA polypeptide protein tag derived from the Human influenza hemagglutinin protein

HPLC high performance liquid chromatography

Fig. Figure

Inc. Incorporated

IP immunoprecipitation

LC liquid chromatography

M phase mitotic phase of the cell cycle

MS mass spectrometry

nt nucleotides

PAGE polyacrylamide-gelelectrophoresis

PCR polymerase chain reaction

qPCR quantitative PCR

qRT-PCR quantitative real time PCR

rpm rotations per minute

RT room temperature

S1 security level 1

S2 security level 1

S phase synthetic phase of the cell cycle

O/N over night; 16-20 h

UV ultraviolet

wt wild type

Appendix C

Acknowledgements

First of all, I would like to thank Prof. Dr. Martin Eilers for supervising this thesis and for the discussions and new models that helped shaping this thesis. I am very grateful for his advice and constant support and motivation throughout this project.

Second, I would like to thank Prof. Dr. Hermann Schindelin and Prof. Dr. Alexander Buchberger for their support and commitment as thesis committee members. I would also like to thank Prof. Dr. Manfred Gessler for chairing the defense.

I want to express my gratitude to Louis Chesler, Evon Poon, Richard Bayliss and Mark Richards for continuous and fruitful collaboration on this project.

I thank the Graduate School of Life Sciences (GSLS) for providing many useful courses and enabling my participation in the organisation of the yearly international symposium that allowed me to acquire multiple additional skills.

Furthermore, I want to thank all former and current members of the Eilers, Gallant, Popov, Schulze and Wiegering lab for the great working atmosphere and for always offering technical help and advice if needed. I especially thank Björn and Elmar for always answering my questions and giving me scientific advice, as well as Steffi H., Susanne, Gabriele and Olga for proof reading this thesis. Also, I want to especially thank the "N-MYC crew", Markus, Olga, Gabriele and Cathy, for the productive, fruitful and sympathetic work together.

In addition, I would like to thank Francesca D., Francesca L., Silvia, Jiajia, Eva, Oriel, Jenny, Giacomo, Irem, Laura, Maria, Sarah and Nathiya for the great time we had together, inside and outside the lab. I would also like to thank David, Lisa and Anup for the good working atmosphere and the fun we had in all the years during and around the organisation of the GSLS symposium.

Importantly, I want to express my gratitude to Francesca and Francesca for always being there for me during my time in the lab and to Oli for always being there for me outside the lab and never stopping to believe in me.

Finally, I want to thank my family for their continuous support and love.

Appendix D

Curriculum vitae

Personal data

> Anne Carstensen
> Frechengasse 19
> 53127 Bonn
>
> Born August 16th 1986 in Henstedt-Ulzburg

Education

1993-1997	"Grundschule Tangstedt" (PS), *25499 Tangstedt, Germany*
1997-2005	"Johannes-Brahms-Schule" (SS), *25421 Pinneberg, Germany*
	Abitur accomplished 06/2005
2005-2010	Studies of "Moleculare Biomedizin" at the
	"Rheinische Friedrich-Wilhelms -Universität", *53113 Bonn, Germany*
	Diploma accomplished in 03/2010
2010-2016	Graduate student of the Graduate School of Life Sciences,
	Julius-Maximillians-Universität Würzburg, *97070 Würzburg, Germany*

Bonn, Aug 15, 2016

Appendix E

Publications:

- Jaenicke LA, von Eyss B, **Carstensen A**, Wolf E, Xu W, Greifenberg AK, Geyer M, Eilers M, Popov N; Ubiquitin-Dependent Turnover of MYC Antagonizes MYC/PAF1C Complex Accumulation to Drive Transcriptional Elongation. *Molecular Cell*; 2016 Jan 7; 61(1):54-67

- Gosejacob D, Jäger PS, Dorp v. K, Frejno M, **Carstensen AC**, Köhnke M, Degen J, Dörmann P, Hoch M; Ceramide Synthase 5 Is Essential to Maintain $C_{16:0}$-Ceramide Pools and Contributes to the Development of Diet-induced Obesity. *J Biol Chem.*; 2016 Mar 25; 291(13):6989-7003

- **Carstensen A**, Brockmann M, Eilers M; Myc - Proteinstabilität als Angriffsziel für zielgerichtete Therapien.; *BIOspektrum*; 2013 Nov; 19(7):726- 729

- Brockmann M, Poon E, Berry T, **Carstensen A**, Deubzer HE, Rycak L, Jamin Y, Thway K, Robinson SP, Roels F, Witt O, Fischer M, Chesler L, Eilers M; Small molecule inhibitors of aurora-a induce proteasomal degradation of N-myc in childhood neuroblastoma. *Cancer Cell*; 2013 Jul 8; 24(1):75-89

Manuscripts in preparation/revision:

- Richards MW, Burgess SG, Poon E, **Carstensen A**, Eilers M, Chesler L, Bayliss R; Structural basis of N-MYC binding by Aurora-A and its destabilization by kinase inhibitors. *PNAS*; in revision

- **Carstensen A**, Richards MW, Büchel G, Walz S, Poon E, Burgess SG, Mak K-Y, Sumara O, Dardenne E, Chesler L, Rickman DS, Bayliss R, Eilers M; N-MYC and Aurora-A complex with TFIIIC to regulate cohesin association with chromatin and drive transcription in S phase. Manuscript in preparation

Appendix F

Affidavit

I hereby confirm that my thesis entitled "Identification of novel N-MYC interacting proteins reveals N-MYC interaction with TFIIIC" is the result of my own work. I did not receive any help or support from commercial consultants. All sources and/or materials applied are listed and specified in the thesis.

Furthermore, I confirm that this thesis has not yet been submitted as part of another examination process neither in identical nor in similar form.

Bonn, Aug 15, 2016

Eidesstattliche Erklärung

Hiermit erkläre ich an Eides statt, die Dissertation "Identifizierung von neuen N-MYC interagierenden Proteinen offenbart N-MYC´s Interaktion mit TFIIIC" eigenständig, d.h. insbesondere selbstständig und ohne Hilfe eines kommerziellen Promotionsberaters, angefertigt und keine anderen als die von mir angegebenen Quellen und Hilfsmittel verwendet zu haben.

Ich erkläre außerdem, dass die Dissertation weder in gleicher noch in ähnlicher Form bereits in einem anderen Prüfungsverfahren vorgelegen hat.

Bonn, Aug 15, 2016